Biochemical Investigation of Zinc Transporters to Discover their Functional Mechanism in Cells

A thesis submitted in accordance with the conditions governing candidates for the degree of:

Philosophiae Doctor in Cardiff University

by

Ahmed Alzahrani

July 2023

Cardiff School of Pharmacy and Pharmaceutical Sciences

Cardiff University

Summary

Zinc is one of the most abundant micronutrients in the human body and it plays a vital role in many normal cellular processes. The cellular zinc level is tightly controlled by zinc transporters, including the ZIP family, which function to increase cytosolic zinc levels. The alteration of this function has been associated with human diseases, including cancer.

ZIP7 belongs to the ZIP family of zinc transporters and resides on the endoplasmic reticulum store. It is responsible for releasing zinc from stores after it has been phosphorylated by CK2 on residues S275 and S276. This ZIP7-mediated zinc release inhibits tyrosine phosphatases and activates cellular tyrosine kinases, several of which are associated with progression of cancer.

Moreover, two other ZIP transporters, namely ZIP6 and ZIP10, have been demonstrated to be involved in cell growth and proliferation by importing zinc across biological membranes to cause cell rounding and detachment, essential for migration and the first step of mitosis. In order to achieve this, the N-terminus of ZIP6 has to be cleaved before these transporters relocate to the plasma membrane.

The present study generated novel constructs to understand the functional mechanisms of these transporters. Firstly, the activation of ZIP7 was investigated by mutating all four residues S275, S276, S293 and T294 predicted to be phosphorylated. This study found that all four of these residues were required for ZIP7 maximal activation. Secondly, the role of N-terminal cleavage of ZIP6 and ZIP10 was investigated by making chimera constructs replacing the usually cleaved N-terminus with the ZIP7 N-terminus, known not to be cleaved. This study found that the N-terminal cleavage of ZIP6 and ZIP10 was required to enable the cells to round up and detach, indicating a critical role for the N-terminus of ZIP6 and ZIP10 in this mechanism.

These findings not only help us to understand the mechanism for these transporters but also enable new tools to be discovered for diseases, such as cancer, that are exacerbated by these transporters.

Acknowledgment

Firstly, I would like to express my sincere gratitude to my supervisor Dr.Kathryn Taylor, for the continuous support and her patience, motivation, and immense knowledge. Her guidance was invaluable throughout the duration of this project, and she profoundly helped me in the writing of this thesis.

I am grateful to all my group members for their help and support. I want to extend a special thanks to Samuel for his continuous help, support and encouragement. Also, my deepest thanks go to Georgia for her help and endless support in the lab. I would like to thank my sponsor, Umm Al-Qura University, for offering me a full scholarship and granting me the opportunity to complete my higher degree at Cardiff University.

Moreover, I must express my very profound gratitude to my father and mother, for their love, prayers, and encouragement have consistently been my strength. Their patience and sacrifices will continue to inspire me throughout my life. A special thanks goes to all my brothers, sisters, and friends for their constant support during my PhD.

last but by no means least, my deepest gratitude belongs to my wife, Amani, who offers me unconditional love and spiritual support at every single stage of life. Her patience and sacrifices will never be forgotten. I am thankful to my lovely son, Nejad, and beloved daughter, Layan, who have offered unconditional love and have always been there for me. Everything that I am, I owe to you.

Table of Contents:

List of Figures:

List of Tables:

List of Abbreviations:

AKT: Protein Kinase B

BSA: Bovine Serum Albumin

BRCA: Breast invasive carcinoma

CICR: Calcium-induced calcium release

CK2: Protein kinase II

CTR1: Copper uptake transporter

CREB: cAMP response element-binding protein

DAPI: 4,6-diamino-2-phenylindol

DUB: Deubiquitinating enzyme

EGFR: Epidermal Growth Factor Receptor

EGA: European Genome- phenome Atlas

EMT: Epithelial mesenchymal transition

ER: Endoplasmic reticulum

ESCC: Esophageal squamous cell carcinoma

IF: immunofluorescence

FBS: Foetal bovine serum

FcεRI: High affinity immunoglobin E receptor

GEO: Gene Expression Omnibus

MT: Metallothionein

mRNA: messenger RNA

MAPK: Mitogen-activated protein kinase

NCBI: National Center for Biotechnology Information

OS: Overall survival

PSP: PhosphoSitePlus

PLA: Proximity ligation assay

PLK1: Polo-like kinase 1

pZIP7: Phospho-ZIP7 antibody

STAT3: Signal transducer and activator of transcription 3

TBST: Tris-buffered saline with Tween−20

TM: Transmembrane domains

TCGA: The Cancer Genome Atlas

Ub: Ubiquitin

RFS: Relapse-free survival

WB: Western blot

Zn: Zinc

Chapter 1

Introduction

1.1 The role of zinc in human health and disease

Zinc is the second most abundant micronutrient in the human body following iron that plays a vital role in the biological function of cellular processes (Hara et al., 2017). In the 1930s, zinc was found to be essential as a key nutrient for human growth and reproduction (Bafaro et al., 2017). A couple of decades later, the association of zinc deficiency and impaired nutrition gained increasing attention as many illnesses such as diarrhoea, alopecia, and compromised physical growth were attributed to inadequate zinc intake. Therefore, minimum dietary requirements were established for zinc and other trace elements for human consumption (Cummings and Kovacic, 2009).

Zinc is one of the most abundant biometals in the body. It is therefore not surprising that zinc has been known as a cofactor in over 300 enzymes that are required for carbohydrate, lipid, and protein metabolism. Moreover, approximately 10 % of the proteins encoded in the human genome need zinc for their appropriate function and structure (Takagishi et al., 2017) (Hara et al., 2022). Zinc is also involved in various processes such as cellular signalling, gene expression and membrane function and structure (Cummings and Kovacic, 2009)(Bafaro et al., 2017). Given the importance of zinc for many biological roles, its excess or deficiency can hugely impact human health.

1.1.1. The importance of zinc in human nutrition

Zinc plays a crucial role in human life. It is required for regulating a multitude of biological processes including the body's metabolism as well as modulating the redox state of the cell (Fukada and Kambe, 2014). The fundamental role of zinc in human health was identified as early as the 1960's when several clinical syndromes such as hypogonadism and dwarfism were attributed to zinc deficiency (Prasad et al., 1961). Indeed, zinc deficiency has since been associated with severe metabolic disease, immune system impairment, growth defects and skin disorders (Hambidge and Krebs, 2007). On the other hand, zinc excess has been recently involved in metabolic disorders (Tuncay et al., 2017) (Adulcikas et al., 2019), immune system defects (Miyai et al., 2014a), neurogenerative disorders (Grubman et al., 2014) and cancer (Taylor et al., 2008)(Sheng et al., 2017) (**Figure 1.1**). It is therefore clear that maintaining the zinc content in the body is essential for optimal human health.

The human body has roughly 2-3 g of zinc which exists as a divalent cation (Zn^{2+}). A small fraction of zinc is found in plasma and the remainder is distributed throughout all tissues in the body, mainly in skeletal muscle, bones, and skin (Hambidge, 2000)(Fukada et al., 2011). The highest concentration of zinc is seen in the prostatic fluid and the choroid region of the eye (Hambidge, 2000). Zinc is primarily obtained from the diet. It is ubiquitously available in sea foods such as oyster and also red meat (Hotz et al., 2003). Dairy products, nuts, potatoes, and fruits are also considered a source of zinc (Maret and Sandstead, 2006). However, zinc from vegetarian sources is less easily absorbed by the body compared to zinc from meat sources because vegetable-based foods contain compounds such as phosphate and phytate (phytic acid) that can inhibit zinc absorption (Maret and Sandstead, 2006). The recommended daily intake of zinc for women is 8 mg, for men it is 11 mg, for infants it is 2-3 mg, and for children it is 5-9 mg (Hambidge et al., 2008). The primary absorption site for dietary zinc is the small intestine, from where it is then transported throughout the body by the serum (Krebs, 2000) (**Figure 1.2**). In serum, which has a small part of the total body zinc (~0.1%), eighty percent of zinc is bound to albumin, around twenty percent bound to α-2 macroglobulin and the remainder is distributed between transferrin and ceruloplasmin (Barnett et al., 2013).

In contrast, the vast majority of zinc (~ 95%) is bound to intracellular proteins and cell membranes. Inside the cell, 50% of the zinc is found in the cytoplasm and its organelles, while the remaining amount is shared by the nucleus and the cell membrane (Cummings and Kovacic, 2009)(Kambe et al., 2015). Approximately, all intracellular zinc is bound to proteins or peptides such as metallothioneins (MTs), enzymes and gene regulatory proteins. Furthermore, bioinformatic analysis has revealed that zinc can bind up to 10% of all the proteins found in the human body (Andreini and Bertini, 2012)(Takagishi et al., 2017). The cytosol has an imperceptible pool of free zinc in nano to picomolar (10^{-9} – 10^{-12}) concentration compared with 0.2 mM of total cellular zinc, emphasising the indispensability of zinc in numerous physiological processes (Maret, 2003)(Hara et al., 2017) (Hara et al., 2022). Therefore, alterations in zinc concentration could induce specific pathophysiological conditions related to diseases.

Figure 1.1 Effect of zinc imbalance on human health

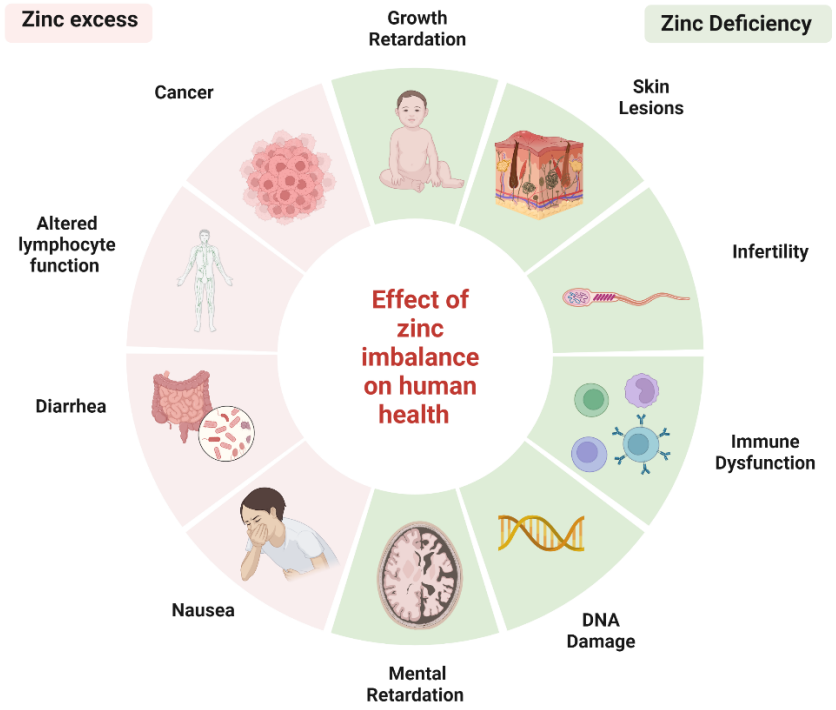

Changes in the balance of zinc in the body can lead to malfunctioning cells. Therefore, keeping the levels of zinc in the body within a healthy range is crucial for optimal health conditions.

Figure 1.2 Zinc storage and distribution in the body

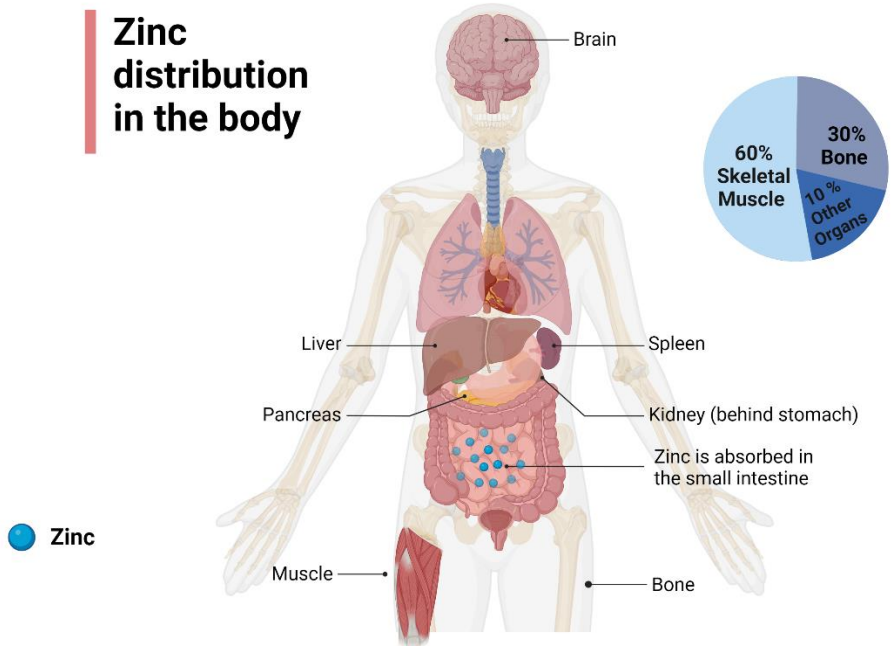

Zinc from dietary sources is primarily absorbed by the small intestine and distributed to various organs, with bones and muscles being major storage sites for zinc.

1.1.2. Biological function of zinc in the human body

The human body contains two types of zinc: labile zinc and zinc bound to proteins. A significant proportion of the zinc present in the human body is attached to proteins. Interestingly, nearly 10% of proteins that can be produced from the human genome have the ability to bind with zinc (Colvin et al., 2010)(Andreini and Bertini, 2012). For proper homeostatic function, zinc needs to be available at the appropriate concentration. Therefore, the zinc level in cells is well controlled to protect the body from excess as well as deficiency (Hambidge and Krebs, 2007). Zinc also helps the body to fight against infectious microorganisms through its major role in the immune system (Haase and Rink, 2014). Furthermore, it has been identified that zinc can protect cells from oxidative damage by exerting its pro-antioxidant properties (Maret, 2008). The role of zinc in proteins, as a catalyst, structural component, and regulator, makes it an essential nutrient and required for the proper functioning of various biological processes.

The importance of zinc in the body is now understood in relation to the structure and function of proteins, including enzymes, transcription factors, hormonal receptors, and biological membranes. Zinc plays a crucial role in DNA and RNA metabolism and is involved in the process of signal transduction, gene expression, and cell death (apoptosis)(Hambidge and Krebs, 2007)(Chasapis et al., 2012). Zinc also plays a critical role in the functioning of enzymes, which control many important cell processes, such as DNA synthesis, growth, brain development, reproduction, development of the fetus, stabilization of membranes, bone construction, and the process of wound healing (Fukada et al., 2011)(Chasapis et al., 2012). A major advancement in our understanding of zinc's role in biology was the discovery of proteins featuring zinc finger motifs. These motifs are recurring sequences of amino acids with consistent residues of cysteine and histidine that facilitate the specific binding of zinc (Hambidge and Krebs, 2007)(Andreini and Bertini, 2012). Many zinc finger motifs have been discovered and more are being identified. More than 10% of all human genes have zinc finger domains and may interact with zinc ion (Hambidge and Krebs, 2007)(Chasapis et al., 2012), which illustrates the wide range of zinc's role in modulating gene expression.

Intercellularly, a major advance in the field of zinc biology was the identification that zinc can work as a second messenger, much like calcium (Ca). A study in mast cells has shown that cellular zinc is capable of modulating cell signal transduction, activating some protein kinases and inhibiting phosphatases within two minutes (Yamasaki et al., 2007).

When the high affinity immunoglobin E receptor (FcεRI) on mast cells is activated, it triggers the release of zinc from the endoplasmic reticulum (ER) in a rapid "zinc wave" that occurs within minutes, in contrast to the slower process of transcription factor effects that take many hours. Additionally, this zinc wave from the ER is dependent on an influx of calcium and the activation of mitogen-activated protein kinase (Yamasaki et al., 2007)(Murakami and Hirano, 2008). This release of zinc inside the cell leads to the inhibition of tyrosine phosphatases and the subsequent activation of MAP kinases. This inhibition of tyrosine phosphatases prolongs the activation of tyrosine kinases, which are enzymes that need to be de-phosphorylated by phosphatases in order to be turned off. Inhibiting tyrosine phosphatases is particularly important in cancer, as many cancers are caused by the prolonged activation of tyrosine kinases (Östman et al., 2006). The fact that the level of zinc inside the cell can be changed by an external stimulus to influence a physiological response shows that zinc can act as a second messenger and emphasizes the significance of keeping the zinc levels inside the cell in balance.

Furthermore, cellular zinc plays a regulatory role in apoptosis through its involvement in the pathways that result in apoptosis and has a direct impact on the apoptotic regulators triggered by a decrease in intracellular zinc (Miyai et al., 2014a). The disruption of the normal process of cell death plays a crucial role in the development of many diseases such as neurodegenerative disorders, autoimmune diseases and cancer (Fernald and Kurokawa, 2013). Interestingly, a decline in the zinc levels within the cell in vivo may directly or indirectly result in increased cell death in living organisms (Chimienti et al., 2001). Additionally, research performed on living organisms has shown that a severe lack of zinc can lead to DNA damage due to increased oxidative stress and impaired DNA repair mechanisms, indicating that zinc plays a crucial role in preserving the integrity of DNA (Song et al., 2009).

Taken together, altering the amount of zinc in cells by either introducing more zinc or removing it through chelating agents can impact various signalling pathways that need zinc to be activated.

1.1.3. Cellular zinc transporter and homeostasis

The small fraction of free labile Zn^{2+} in cells plays a biologically significant role, particularly regarding its function in cell signalling. Therefore, the intracellular zinc concentration is tightly regulated in order to provide a normal homeostatic function (Cummings and Kovacic, 2009) (Lichten and Cousins, 2009). The general distribution of zinc within cells can vary depending on the cell type and its physiological state. Studies conducted on rat liver cells and human lung adenocarcinoma cells determined that 50% of zinc is found in the cytoplasm, 30–40% is found in the nucleus, and the remaining 10% is found in the plasma and organelle membranes (Haase and Beyersmann, 2002)(Yuan et al., 2012). It is thought that the cytosol concentration of zinc is quite low, possibly within the range of pico-molar to low nano-molar levels. This is due to zinc binding with a variety of functional proteins in the cytosol and organelles, and being found in vesicles in the cytosol such as mitochondria, Golgi and endoplasmic reticulum (Qin et al., 2013). However, significant variations in concentrations can occur, which may be caused by factors such as variations in the environment, protein folding, interactions between zinc and other proteins, and perhaps the techniques used for measurement (Chabosseau et al., 2014).

Zinc is unable to diffuse passively through cell membranes, so it requires transporter proteins for its mobilisation. There are three families of proteins that regulate cytosolic zinc homeostasis. They include the solute carrier family 30A (SLC30A) or ZnT exporters, solute carrier family 39A (SLC39A) or ZIP importers and zinc-binding proteins such as metallothionein (MT) and glutathione (Cummings and Kovacic, 2009)(Bafaro et al., 2017)(Lichten and Cousins, 2009).

SLC30A or ZnT transporters have 10 human members (ZnT1 to ZnT10), all of which have six transmembrane domains with both an N-terminus and C-terminus inside the cell (Kimura and Kambe, 2016)(Bowers and Srai, 2018). They have been shown to act as Zn2+/H+ exchangers that function to reduce the cytosolic concentration of zinc by mobilising it into the extracellular space or intracellular compartments (Bafaro et al., 2017). The ZnT1 protein is located on the plasma membrane of the cell, while the remaining members are found on intracellular membranes (Nishito and Kambe, 2019).

In contrast, the SLC39A or ZIP transporters family encompasses 14 human members (ZIP1 to ZIP14) that act to import zinc from either the extracellular space or cellular zinc stores into the cytoplasm. The majority of ZIP transporters are found on the plasma membrane and transport zinc from outside the cell.

However, some ZIP transporters have been identified as residing on other cellular membranes, such as intracellular storage vesicles (ZIP8, ZIP13, and ZIP14), the golgi apparatus (ZIP9, ZIP11 and ZIP13), or the endoplasmic reticulum (ZIP7), and these transporters release zinc from intracellular compartments (Kambe et al., 2015). Each transporter has eight transmembrane domains with N-terminus and C-terminus ends that are both located outside the cell (Fukada et al., 2011) (Hara et al., 2017) (**Figure 1.3)**. Finally, zinc-binding proteins such as MT and glutathione also participate in cellular zinc homeostasis through buffering cytosolic free zinc under physiological conditions and regulating the storage and release of intracellular zinc. MTs are able to bind up to seven zinc atoms through their cysteine residues in order to maintain cellular zinc levels within an appropriate concentration (Pinter and Stillman, 2014). Noteworthy that the specific way in which zinc is transported through ZIP transporters is not well understood.

1.2 ZIP transporters

Zinc transporters are responsible for regulating the cytosolic zinc level as well as the zinc concentration in cellular compartments (Kimura and Kambe, 2016). Zinc is unable to cross the cell membranes, and thus ZIP and ZnT are required to facilitate cellular zinc physiological function (Jeong and Eide, 2013)(Lichten and Cousins, 2009). ZIP transporters contain 14 human members that influx zinc into the cytoplasm either from the extracellular space or from cellular zinc stores. The underling mechanism for these transporters has not been fully elucidated yet, however, some studies have shown that ZIP7 and ZIP6 may be activated by phosphorylation (Taylor et al., 2012) and heterodimerisation (Taylor et al., 2016), respectively. Moreover, ZIP4 is abundantly present in enterocytes and plays a crucial role in the absorption of dietary zinc from the small intestine.

Figure 1.3 Regulation of Zinc homeostasis by the ZnT and ZIP transporters

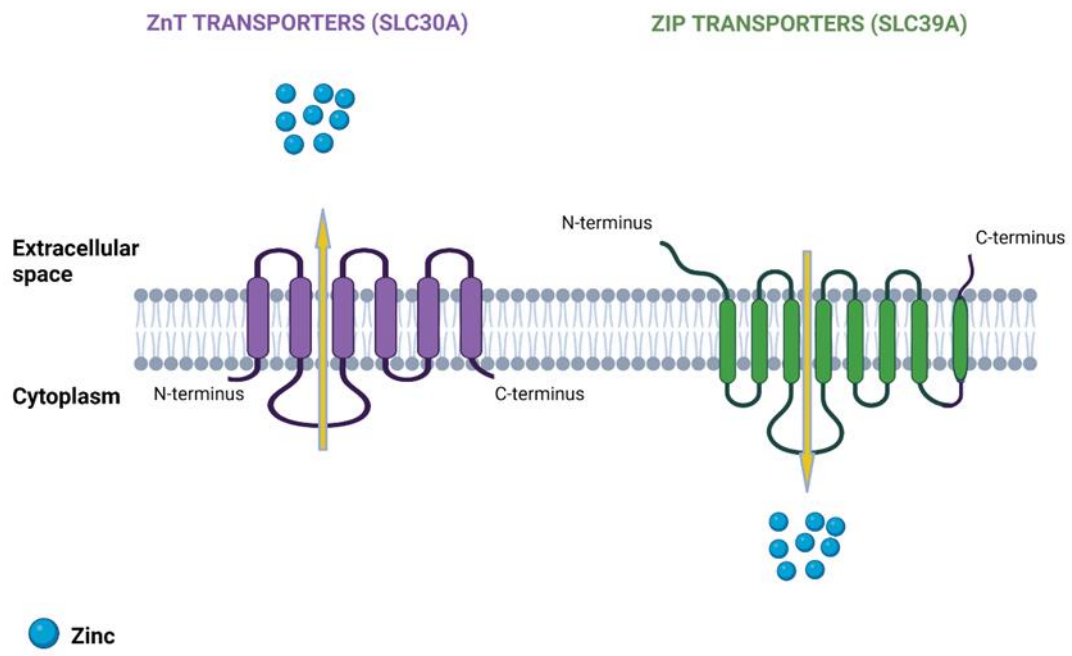

ZnT transporters (purple) have 6 transmembrane domains and are responsible for moving zinc out of the cell's cytoplasm. In contrast, ZIP transporters (green) transport zinc in a direction that is reverse to that of ZnT transporters. ZIP transporters have 8 transmembrane domains and a large intracellular loop between the third and fourth transmembrane domains.

Therefore, during zinc deficiency the expression of ZIP4 is upregulated on the membrane of the intestinal microvilli, and the opposite occurs when there is an abundance of zinc (Liuzzi et al. 2004).

ZIP transporters are categorised according to the phylogenetic tree into four subfamilies, including gufA, subfamily I, subfamily II, and the LIV−1 subfamily (Taylor et al., 2004)(Liu et al., 2015) (**Figure 1.4**). In the phylogenetic tree, if two members are located in the same branch of a tree, it indicates that they have a shared ancestor and are more closely related to each other. ZIP7 and ZIP13 are in the same branch of a family tree, indicating that they are closely related to one another. This is further supported by the fact that ZIP7 and ZIP13 are the members that are located on the membrane of intracellular storage, rather than the plasma membrane.

Additionally, ZIP6 and ZIP10 are found in the same category, suggesting that they are also closely related. This is strengthened by the fact that ZIP6 and ZIP10 form a heteromer to become functional (Taylor et al., 2016). Although ZIP5 is not known to be directly related to ZIP6 and ZIP10, it is believed to have a closer relationship to them than to other members of the family due to its more recent ancestry. Each transporter is predicted to have eight transmembrane domains (TM) that are accompanied by extracytoplasmic N and C termini (Jeong and Eide, 2013)(Adulcikas et al., 2018). Additionally, there is a long cytoplasmic loop between TM3 and TM4 containing various histidine residues, predicted to be involved in the region where metal binding occurs due to the binding of zinc to histidine, and thus their role in transporting zinc. It is also supposed to be a potential functional site for ZIP transporters (**Figure 1.5A**) (Guerinot, 2000)(Taylor et al., 2004). Although the intracellular loop of the transporters does not have many similarities, it indicates that each zinc transporter in the family may have distinct regulation mechanisms to be activated. Furthermore, there are additional histidine residues at the N-terminus and in the cytoplasmic loop between TM2 and TM3 (Taylor et al., 2004).

The LIV-1 subfamily has the most members amongst the ZIP family. Along with the features that are common to the entire family, the members of the LIV-1 subfamily also possess a CPALLY motif and a HEXPHEXGD consensus motif (Taylor et al., 2003)(Taylor et al., 2004)(Kambe et al., 2021).

The CPALLY motif (C=cystine, P=proline, A=alanine, L=leucine, Y=tyrosine) is located immediately preceding the first TM, with the exception of ZIP13 and ZIP7. These are the transporters that never localise to the plasma membrane (Taylor et al., 2003). This motif is thought to help maintain the tertiary structure of the protein and control zinc transport by creating a disulfide bond with the initial conserved cysteine in the metalloprotease-like motif (Taylor et al., 2007). The LIV-1 subfamily also contains a specific consensus motif HEXPHEXGD (H, histidine; E, glutamate; X, any amino acid; P, proline; D, aspartate; G, glycine). This region has highly conserved histidine residues and matches the motif in zinc metallopeptidases that is responsible for zinc binding. Therefore, it is predicted to be the main site for selective zinc transport in the LIV-1 ZIP transporters (**Figure 1.5 B**). (Taylor et al., 2003)(Taylor et al., 2004) (Taylor et al., 2007).

Figure 1.4 Phylogenetic tree of the human ZIP family of zinc transporters

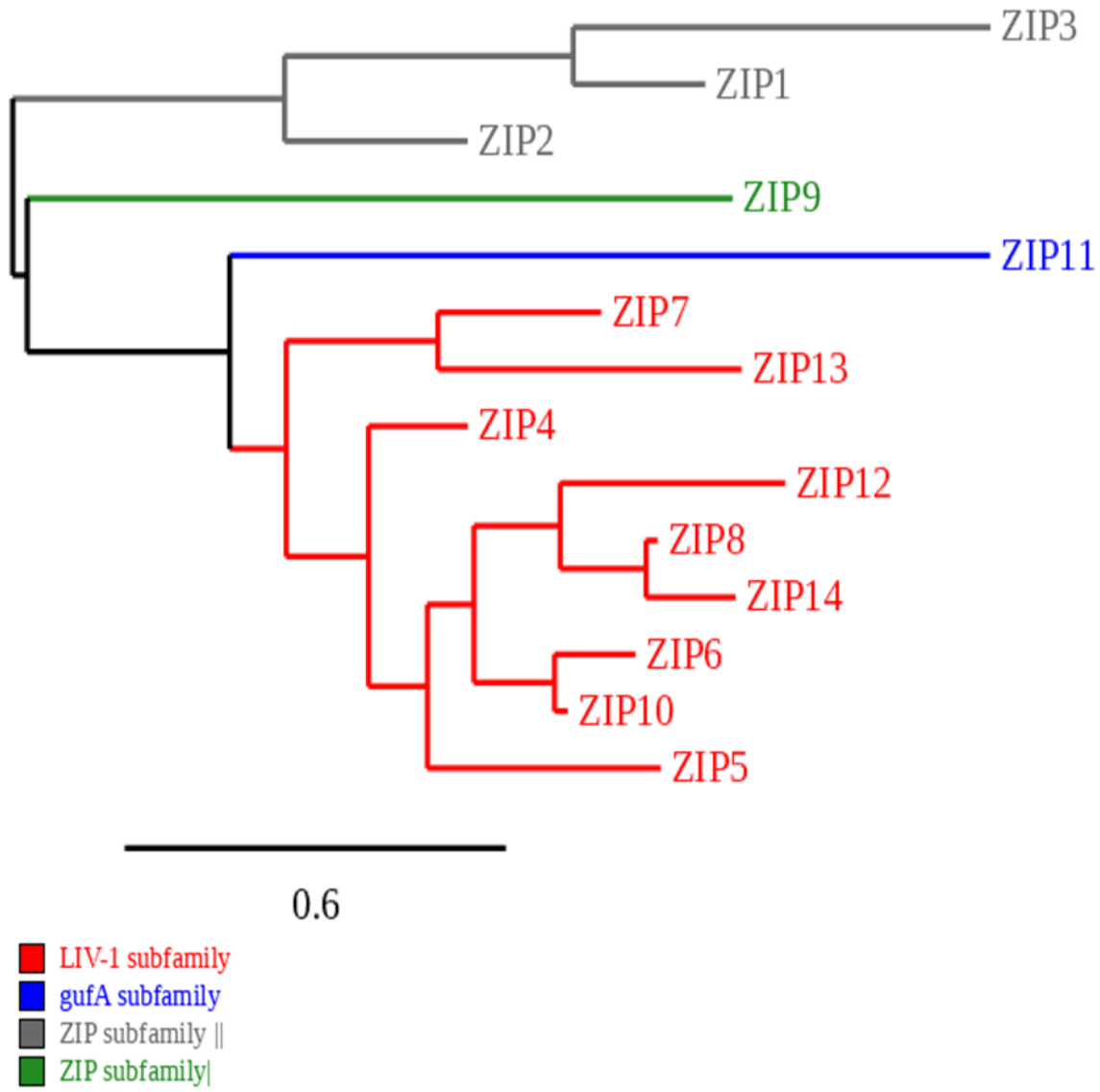

This diagram demonstrates the categorisation of ZIP transporters according to Phylogenetic tree (Larkin et al., 2007). The horizontal axis of the phylogram is measured by the genetic alterations, and the degree of these changes is illustrated by the scale shown at the bottom bar. The sequences of ZIP proteins were retrieved in FASTA format by using the NCBI database and then the tree was obtained by using the Phylogeny.fr web service (Dereeper et al., 2008).

Figure 1.5 The predicted structure of the ZIP transporters

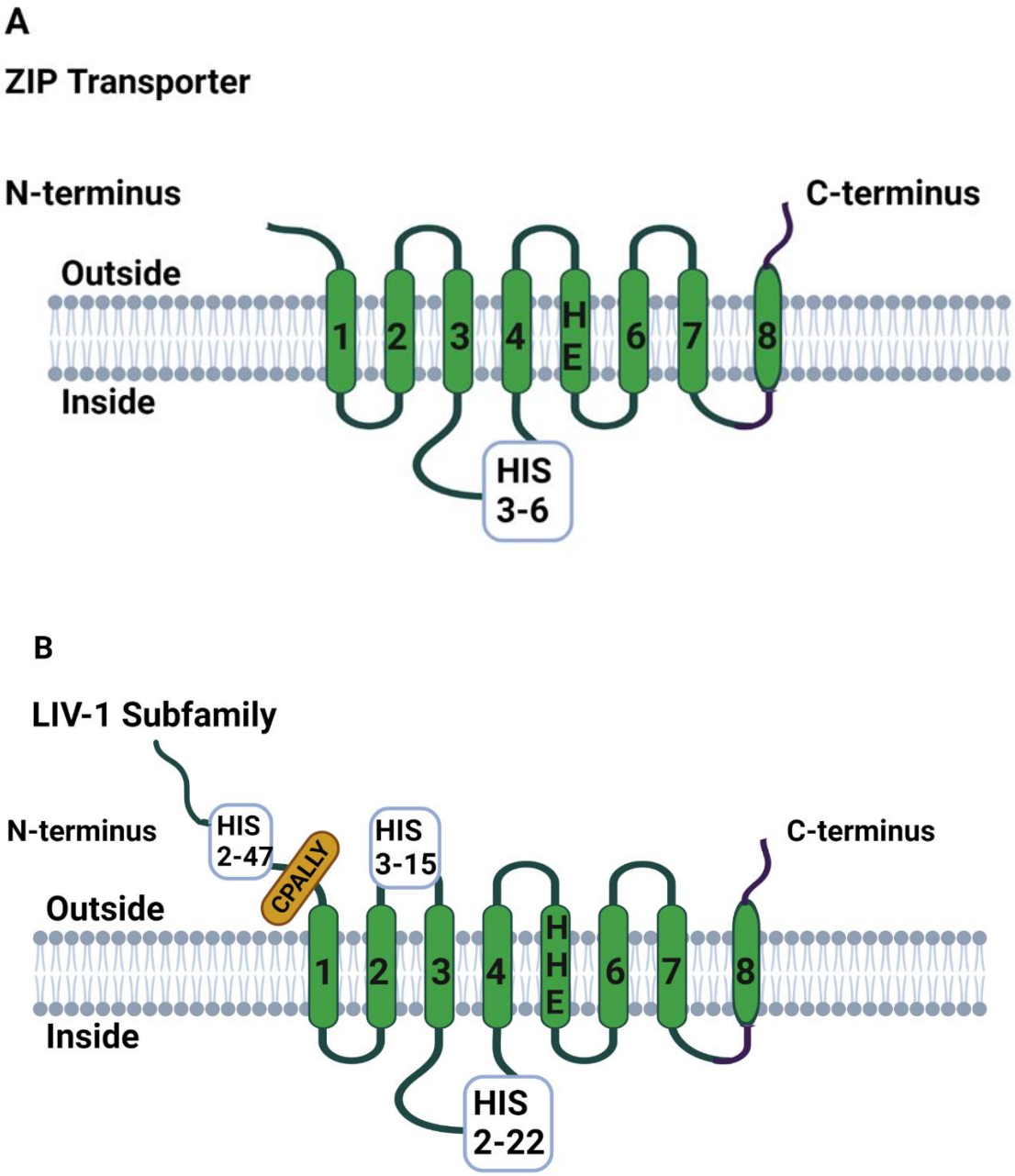

A) The ZIP transporters are predicted to have 8 TMs with extracellular N and C termini and 3 to 6 histidine residues in a long cytoplasmic loop between TM3 and TM4. **B**) The ZIP proteins in the LIV-1 subfamily are predicted to have 8 TM that are accompanied by an extra cytoplasmic N and C termini. Additionally, there is a long cytoplasmatic loop between TM3 and TM4 containing various histidine residues. Moreover, there are additional histidine residues in N-terminus and the cytoplasmatic loop between TM2 and TM3. It is also known for having an extended N terminus containing a CPALLY, and a metalloprotease motif, in the 5 TM. This is similar to the way that metalloproteinases bind zinc (Taylor et al., 2004).

1.3 Zinc handling in cells

Zinc plays a significant role in regulating various cellular processes, and disruptions in its balance can lead to various types of health issues in humans (Murakami and Hirano, 2008)(Chasapis et al., 2012)(Jie Wang et al., 2020)(Maywald and Rink, 2022). The level and distribution of zinc within cells is regulated by MT, as well as by transporters from the SLC39A/ZIP and SLC30A/ZnT families; these transporters raise and lower the amount of zinc in the cytosol respectively (Fukada et al., 2011)(Kimura and Kambe, 2016)(Takatani-Nakase, 2018) (Krężel and Maret, 2021). Zinc is then available in four forms. It can bind tightly to metalloproteins as a structural component or to metalloenzymes as a cofactor. The binding to MT can occupy 5-15% of the total cellular zinc pool (Colvin et al., 2010)(Kimura and Kambe, 2016). Additionally, it can be retained in intracellular compartments such as ER for storing zinc and providing it to zinc-dependent proteins, a process that is facilitated by zinc transporters (ZIP7) (Hennigar and Kelleher, 2012)(Nimmanon et al., 2017). Finally, the pool of cytosolic free zinc is maintained at very low concentrations (pM-low nM levels)(Kimura and Kambe, 2016). The maintenance of this cellular zinc homeostasis is crucial and is achieved through the actions of metalloproteins and two zinc transporter families, (ZIP, solute carrier 39A [SLC39A]) and Zn transporters (ZnT, SLC30A)(**Figure 1.6**)(Taylor et al., 2003)(Kimura and Kambe, 2016)(Takagishi et al., 2017).

1.4 Zinc and cancer

Several dietary compounds, including zinc, have been thought to aid in cancer prevention due to its crucial role in protecting against the onset and progression of various cancers (Chasapis et al., 2012). Altered zinc levels in the serum and tissues of cancer patients support the idea that zinc is involved in cancer development. Zinc concentrations in serum are commonly reduced in cancer patients, including breast, pancreatic and lung cancer compared to normal serum levels (Lichten and Cousins, 2009) (Gumulec et al., 2014) (Wang et al., 2019) (Feng et al., 2020). Interestingly, despite low serum zinc levels in most cancer patients, tumour tissues have higher zinc levels compared to normal tissue (Chasapis et al., 2012).

Figure 1.6 Homeostasis of intracellular zinc

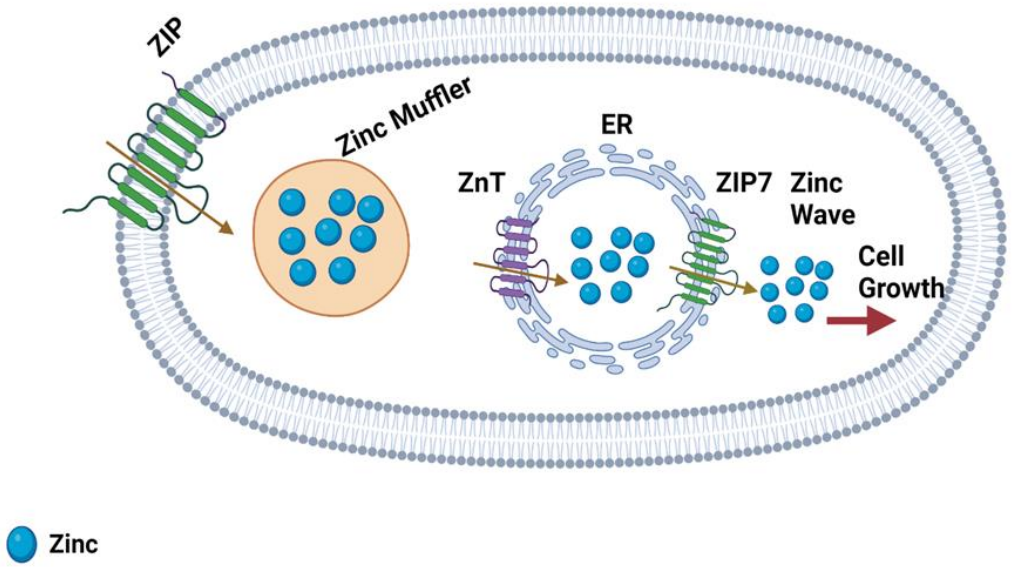

This model demonstrates intracellular zinc homeostasis. When zinc enters the cell by a ZIP transporter, zinc is rapidly buffered by zinc-binding proteins such as metallothionein through its cysteine−binding site and then transported to intracellular stores such as ER. After an activation, zinc releases from cellular stores and leads to zinc-mediated cellular responses.

Although there is restricted data on zinc levels in tumour tissue, the widespread recognition is that ZIP transporters are upregulated in many types of cancer, suggesting higher zinc concentrations in most tumours (Bafaro et al., 2017)(Jie Wang et al., 2020) (Jones et al., 2022). An exception to the findings is seen in prostate cancer, where zinc levels in prostate tumour tissue are lower compared to normal prostate tissue (Renty B Franklin, 2014). Upregulated zinc transporters in tumour tissues are associated with their growth and development, indicating that the dysregulation of cellular zinc homeostasis could lead to the severity of cancer (Taylor et al., 2012)(Jie Wang et al., 2020). This is supported by bioinformatic studies that reveal that the mRNA expression of most zinc transporters is upregulated in various cancers (Ding et al., 2019)(Hara et al., 2022)(Jones et al., 2022). It has been shown that, in vivo, overexpression of zinc transporters is consistent with the severity of breast cancer, colorectal and gastric cancer (Taylor et al., 2008)(Ziliotto et al., 2019)(Sheng et al., 2017)(Y. Zhang et al., 2020). This result suggests that cancer cells require a higher amount of zinc for their survival and proliferation.

1.4.1 The role of ZIP transporters in cancers

It has been reported that zinc is required for normal cell growth and proliferation. Any changes in free labile cellular zinc concentration in cells leads to an alteration of cell signalling pathways (Maret, 2017). In mast cells, cellular zinc was rapidly released into the cytoplasm after an extracellular stimulus of the IgE receptor (Yamasaki et al., 2007).

The released zinc, also called a zinc wave, activates signalling pathways such as mitogen-activated protein kinase (MAPK) pathways, mechanistic target of rapamycin mTOR pathway and the extra-cellular signal-related kinase (ERK) that are involved in controlling cell growth, and proliferation (Yamasaki et al., 2007). This zinc release from stores inhibits protein tyrosine phosphatases which explains the prolonged activation of tyrosine kinases (Nimmanon et al., 2017)(Bafaro et al., 2017). Using this mechanism, elevated cellular zinc levels are likely to drive cell growth and proliferation and must be regulated to avoid harmful levels that could lead to diseases of excessive growth, like cancer.

ZIP transporters are involved in regulating cellular zinc concentration; thus, members of this family especially the LIV-1 family have been implicated in different types of cancers (**Table 1.1**). For example, the normal human prostate has an increased level of zinc compared with other soft tissue cells. This elevated zinc in epithelial prostate cells is mainly attributed to ZIP1 expression and its ability to import zinc from the circulation (Renty B Franklin, 2014). In addition, ZIP2 and ZIP3 are also expressed in the prostate cells, and they are able to retain the zinc within such cells. Compared with normal prostate tissues, the malignant tissues show lower zinc levels simultaneously with reduced the expression levels of ZIP1,ZIP2 and ZIP3 (Bafaro et al., 2017)(Fong et al., 2018). The significant role of ZIP1 in prostate cells has been illustrated by the relationship between a reduction in metastatic ability and overexpression of ZIP1 (Fong et al., 2018). Additionally, the overexpression of ZIP4 has been linked to the progression and growth of pancreatic cancer (Unno et al., 2014)(Liu et al., 2015). This finding is supported by another study that showed the gene expression of all zinc transporters, excluding ZIP4, have reduced expression in malignant pancreatic tissue compared to non-malignant tissue (Yang et al., 2013). It has been shown that the overexpression of ZIP4 is linked to suppression of apoptosis, enhanced migration, and stimulation of the cell cycle (Jin et al., 2018)(Jie Wang et al., 2020).

The efficacy of this was demonstrated through the silencing of ZIP4 expression or the use of TPEN, a zinc chelator, which effectively diminished proliferation, migration, and tumour size in different pancreatic cancer cell lines when administered to these cells (Cui et al., 2014)(Yu et al., 2019).

Furthermore, ZIP5 and ZIP14 have been shown to be upregulated in hepatocellular cancer, confirmed by bioinformatic work and in vivo study (Bitirim, 2021). Their overexpression was negatively correlated with survival time, indicating the dysfunction of zinc homeostasis and the progression of liver cancer (Gartmann et al., 2018)(Bitirim, 2021). Collectively, the data indicated that there is an association between a disruption in the zinc transporter and cancer. Understanding how ZIP transporters and zinc signalling operate in various types of cancer has the potential to lead to the development of clinical biomarkers and treatments for numerous forms of cancer.

1.4.1.1 The role of ZIP transporters in breast cancer

As previously discussed, the intracellular zinc concentration is controlled by zinc transporters. Despite conflicting information regarding zinc levels in tumour tissue, it is widely acknowledged that zinc imbalances in tumours are primarily due to the abnormal expression of zinc transporters, particularly the LIV-1 family. Cancers in the prostate, pancreatic and liver have been demonstrated to have low levels of zinc in their tissue (Jie Wang et al., 2020). Interestingly, unlike these cancers, breast cancer has been found to possess elevated concentrations of zinc in the tumour compared to normal breast tissue (Gumulec et al., 2014) (Ziliotto et al., 2019) (Jie Wang et al., 2020). A study conducted by (Farquharson et al., 2009) used synchrotron radiation micro probe x-ray fluorescence to measure zinc levels in breast cancer tissues in 59 cases. This method facilitated the distinction between zinc levels in cancerous and non-cancerous regions within the same samples. The findings indicated a considerable elevation in zinc levels only in instances of estrogen receptor-positive breast cancer, showing a 1.5-fold increase. In contrast, estrogen receptor-negative cases exhibited no such increase, maintaining similar zinc levels to those found in the neighbouring non-cancerous breast tissue (Farquharson et al., 2009). Recently, an investigation of the zinc level in invasive human breast cancer tissues was determined in a series of 28 samples, using Laser Ablation Inductively Coupled Plasma Mass Spectrometry (LA-ICPMS). This study revealed a correlation between higher zinc levels and increase of the histopathological grade of malignancy (Rusch et al., 2021).

Collectively, an elevated zinc in breast cancer tissue may indicate a requirement for zinc to drive the cell growth and proliferation.

There has been growing indication of some ZIP transporter dysregulation and breast cancer progression. Both in clinical and in vitro researchers have shown the significant association between some LIV-1 subfamily such as ZIP6,7 and 10 and metastasis of breast cancer (Taylor et al. 2008) (Sheng et al. 2017) (Takatani-Nakase 2018). Due to the significance of zinc to the functioning of cancer cells, ZIP6 was the first ZIP transporter linked to tumour progression in estrogen receptor-positive breast cancer and in cases with regional lymph node metastasis (Tozlu et al., 2006). Similarly, ZIP10, which is the closest family member to ZIP6, has also been demonstrated to play a role in breast cancer, where its expression has been observed to have a positive association with the expression of estrogen receptor (Tozlu et al., 2006).

In order to act as a zinc transporter, both ZIP6 and ZIP10 must become dimerized. It also has been shown that these two family members have the capability to form a heteromer, which is crucial for the cell migration and proper development of zebrafish embryos (Taylor et al., 2016). The same was found to be true in breast cancer cells, with a strong correlation between ZIP6 and ZIP10 expression being seen in cells undergoing cell division, suggesting that ZIP6/ZIP10 heteromers play a role in facilitating zinc influx to initiate cell division (Nimmanon et al., 2020).

Accordingly, clinical studies have shown that increased expression of ZIP7 is commonly seen in breast cancer patients, especially those with a poor prognosis (Taylor et al., 2003). This pattern was also seen in patients who became resistant to the drug tamoxifen (Taylor et al., 2008). The heightened expression of ZIP7 is accompanied by a significant rise in the levels of activated ZIP7 compared to models that are sensitive to tamoxifen (Ziliotto et al., 2019). These findings suggest that tamoxifen-resistant cells require intracellular zinc to drive more aggressive cellular behaviour. Given the association between ZIP6, ZIP10, and ZIP7 with breast cancer, the mechanisms by which these three ZIP transporters play a role in breast cancer development will be discussed in greater detail in the subsequent sections.

Table 1.1 Human ZIP transporters and their location throughout the human body

ZIP proteins	Major location of protein expression	Subcellular location	Cancer	Reference
ZIP1	Kidney, Small intestine, and Prostate	Plasma membrane	Prostate cancer	(Renty B Franklin, 2014)
ZIP2	Widespread	Plasma membrane	Prostate cancer	(Fong et al., 2018)
ZIP3	Testis and Pancreatic cells	Plasma membrane	Prostate cancer	(Fong et al., 2018)
ZIP4	Small intestine, stomach and kidney	Apical surface of enterocyte	Pancreatic cancer and liver cancer	(Cui et al., 2014)(Gartmann et al., 2018)
ZIP5	Liver, kidney and colon	Plasma membrane	liver cancer	(Bitirim, 2021)
ZIP6	Widespread	Plasma membrane	Breast and pancreatic cancer	(Takatani-Nakase, 2018)(Liu et al., 2015)
ZIP7	Widespread	Endoplasmic reticulum	Breast cancer and colorectal cancer	(Taylor et al., 2008)(Sheng et al., 2017)
ZIP8	Testis, Erythroid and T-cells	Plasma membrane and lysosome	Neuroblastoma	(Mei et al., 2018)

Continued

ZIP9	Prostate	Golgi	Prostate cancer	(Bulldan et al., 2018)
ZIP10	Widespread	Plasma membrane	Breast cancer	(Kagara et al., 2007a) (Takatani-Nakase, 2018)
ZIP11	Mammary gland, stomach and Ileum	Golgi	Bladder cancer	(Wu et al., 2015)
ZIP12	Neurons, Endothelial and Muscle cells	Plasma membrane	Unknown	(Kambe et al., 2015)
ZIP13	Retinal pigment epithelial cell line	Endoplasmic reticulum	Ovarian cancer	(Cheng et al., 2021)
ZIP14	Widespread	Plasma membrane and lysosome	Colorectal cancer and Hepatocellular cancer	(Kambe et al., 2015)(Gartmann et al., 2018)

This table demonstrates the location of ZIP transporters throughout the human body and the types of cancer that are usually linked with the upregulation of these transporters.

1.5 Zinc transporters ZIP7

ZIP7, a member of the LIV-1 subfamily of ZIP transporters, is widespread throughout human tissues. ZIP7 has been suggested to play a vital role in releasing zinc from cellular stores and activating cellular tyrosine kinases, hence it localizes to the ER (Taylor et al., 2008). ZIP7-mediated zinc release from the ER results in activating the phosphorylation of EGFR, Src and IGF−1R, possibly due to the ability of zinc to inhibit protein tyrosine phosphatases (Taylor et al., 2012)(Bellomo et al., 2014). The activation of these kinases leads to the phosphorylation of target proteins such as ERK1/2 and AKT, which promote cell growth and migration (Taylor et al., 2008)(Hogstrand et al., 2009).

Importantly, ZIP7 is thought to be activated by protein kinase CK2 through phosphorylation of serine residues S275 and S276, which are located in the large cytoplasmic loop between TM3 and TM4 of the transporter. After exposure to extracellular stimuli, the CK2 activation of ZIP7 promotes zinc release from cellular stores into the cytoplasm (Taylor et al., 2012). The released zinc (also called zinc wave) then inhibits protein tyrosine phosphatases and activates cellular serine kinases such as MAPK, mTOR and PI3K-AKT, which together enhance cell growth and motility (**Figure 1.7**) (Nimmanon et al., 2017). The mechanism explains that zinc is recognised as a second messenger which is rapidly released from its stores in response to an extracellular stimulus. This leads to a rise in the amount of zinc in the cytosol, resulting in a range of effects on cell signalling pathways (Yamasaki et al., 2007).

A relationship between zinc dyshomeostasis and tamoxifen-resistant breast cancer has been recognised when these breast cancer cells have shown a twofold increase of intracellular zinc compared to tamoxifen-sensitive cells. ZIP7 has been found among 10 % of genes frequently upregulated in many breast cancers with poor prognosis (Hogstrand et al., 2009)(Kambe et al., 2015). Recently, bioinformatic database analysis revealed that upregulation of ZIP7 was strongly associated with poor outcomes in breast cancer (Jones et al., 2022).

Approximately 70% of breast cancer cells have the oestrogen receptor. Tamoxifen and other oestrogen receptor-targeting drugs are now used in clinical settings to obstruct the effects of oestrogen and have demonstrated promising initial results (Johnston, 2010)(Chang, 2012). However, their effectiveness is limited due to high rates of both innate and acquired resistance to hormonal therapy (Chang, 2012).

The exact molecular causes of resistance to tamoxifen are mainly obscure. Hence, it is vital to identify the factors responsible for this resistance in order to create new approaches for treating breast cancer.

Our group have demonstrated a relationship between cellular zinc and tamoxifen resistant cells, showing that ZIP7 is abundantly upregulated in tamoxifen-resistant MCF-7 breast cancer cells (Taylor et al., 2008). Moreover, tamoxifen-resistant cells have shown increased ZIP7 protein expression and upregulated mRNA level of ZIP7. Interestingly, it has been shown that the elevated intracellular zinc in vitro is a direct result of increased expression of ZIP7 protein, as a decrease in cytosolic zinc was seen in tamoxifen-resistant cells in which ZIP7 was silenced (Taylor et al., 2008)(Hogstrand et al., 2009) (Ziliotto et al., 2019). These results illustrate the importance of ZIP7-mediated zinc signalling as a potential strategy for controlling the progression of breast cancer and preventing drug resistance.

Based on this finding, our team created a monoclonal antibody that specifically recognizes ZIP7 when it is phosphorylated on residues S275 and S276, which indicates that it is in its activated state (Taylor et al., 2012). Given the function of activated ZIP7 in breast cancer development, especially in creating resistance to endocrine therapy, this antibody could be used to recognise higher grade breast cancer or as a predictor of tamoxifen treatment success (Ziliotto et al., 2019). These findings indicate the important position of ZIP7 as a vital regulator of cell growth and its suggestion as a therapeutic target in diseases where inhibiting tyrosine kinase-activated downstream pathways is essential.

Figure 1.7 Schematic model of ZIP7 mediated zinc release

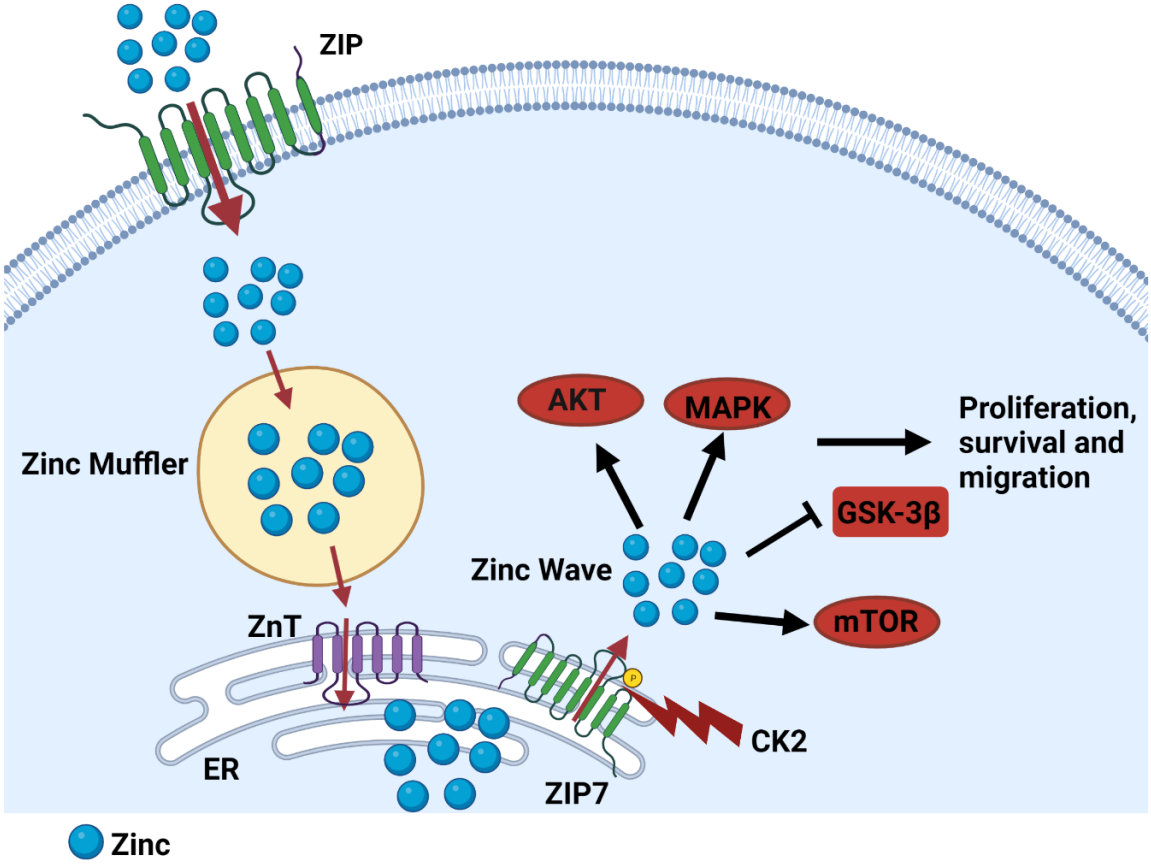

ZIP transporters import zinc from the extracellular space into the cytoplasm where zinc is immediately buffered by zinc muffler such as MT. Zinc then is stored in ER or/and Golgi by ZnTs. After phosphorylation by CK2, ZIP7 releases zinc into the cytoplasm. Subsequently, the released zinc inhibits some tyrosine phosphatases while leading to activate cell proliferation and migration (Nimmanon et al., 2017).

1.6 Zinc transporter ZIP6

ZIP6 (also called SLC39A6 or LIV-1) was the first member of the LIV-1 subfamily to be discovered (Taylor et al., 2003). ZIP6 has been recognised as an oestrogen-regulated gene since 1994 and associated with oestrogen receptor-positive breast cancer, particularly those that are able to metastasize to the lymph nodes (McClelland et al., 1998). However, the role of the LIV-1 protein in cells was unknown until its protein sequence was analysed at a later time. LIV-1 is now known as ZIP6 or SLC39A6, belonging to the SLC39A family of zinc transporters, and it is a member of the LIV-1 subfamily (Taylor et al., 2003). Unlike ZIP7, which has ubiquitous expression, ZIP6 is primarily expressed in tissues that are regulated by sex steroid hormones such as the breast, prostate, and placenta (Taylor et al., 2004).

ZIP6 was found to be more commonly associated with estrogen receptor-positive breast cancers spreading to lymph nodes (Taylor et al., 2003). Approximately, 92% of the breast cancer patients with metastasis to lymph nodes displayed ZIP6 expression (Grattan and Freake, 2012). Therefore, ZIP6 was proposed as a dependable tumour marker for identifying estrogen receptor positive breast cancers, as demonstrated by its correlation with the metastatic transformation of estrogen receptor positive MCF7 cells (Takatani-Nakase et al., 2016). Recently, the expression level of ZIP6 has been shown to be significantly elevated in tumour compared with normal breast tissue using the Cancer-specific database GEPIA (Tang et al., 2019)(Jones et al., 2022). Indeed, ZIP6 protein expression was found to be induced adherent breast cancer cells (MCF-7) to round up and detach, suggesting anoikis resistance, the first step in the progression of metastasis (Hogstrand et al., 2013).

ZIP6 was shown to have an involvement in the epithelial–mesenchymal transition (EMT) process where the epithelial phenotype of cells is replaced by a mesenchymal phenotype, thereby gaining the ability to migrate (Hogstrand et al., 2013) (Taylor et al., 2016b). The crucial step of EMT is the loss of intracellular adhesion and the increased cytoskeleton, resulting in an increased tendency for migration. The decline in intracellular adhesion is largely caused by the loss of E-cadherin, the primary component of adherens junctions, which maintains intracellular adhesion through a mechanism depending on Ca2+-dependent homophilic binding (Koen and Collier, 2010). During zebrafish gastrulation, ZIP6 has been found to be a downstream target of the signal transducer and activator of transcription 3 (STAT3), leading Snail, a zinc-finger transcription factor, to translocate to the nucleus and suppress the expression of the E-cadherin molecule responsible for epithelial adhesion (Yamashita et al., 2004).

Later on, the association between the ZIP6 and STAT3 was also shown in breast cancer, indicating the possibility of ZIP6 being involved breast cancer migration, which also requires EMT (Taylor et al., 2007). STAT3 is recognised to have a critical role in cancer progression (Li and Huang, 2017). Our group demonstrated that ZIP6 is transactivated by STAT3, leading ZIP6 to be produced as a pro−protein residing in the ER (Hogstrand et al., 2013). The ZIP6 pro-protein was activated by N-terminal cleavage at a predicted PEST cleavage site before relocation to the plasma membrane for zinc influx (Hogstrand et al., 2013).

The PEST sequence refers to a portion of a peptide sequence that is abundant in proline (P), glutamic acid (E), serine (S), and threonine (T), which explains its name. The influx of zinc causes an inhibitory phosphorylation of GSK-3ß either by directly effecting it or through the activation of AKT by zinc, which in turn phosphorylates GSK-3ß to inhibit it (Ohashi et al., 2015). Once GSK-3ß has been phosphorylated, Snail moves to the nucleus and inhibits the expression of E-cadherin, allowing cell detachment, migration and metastasis (**Figure 1.8**) (Hogstrand et al., 2013). This mechanism of how ZIP6 works in EMT clearly illustrates the direct link between ZIP6 and metastasis of breast cancer.

Figure 1.8 Role of ZIP6 in EMT and cancer progression

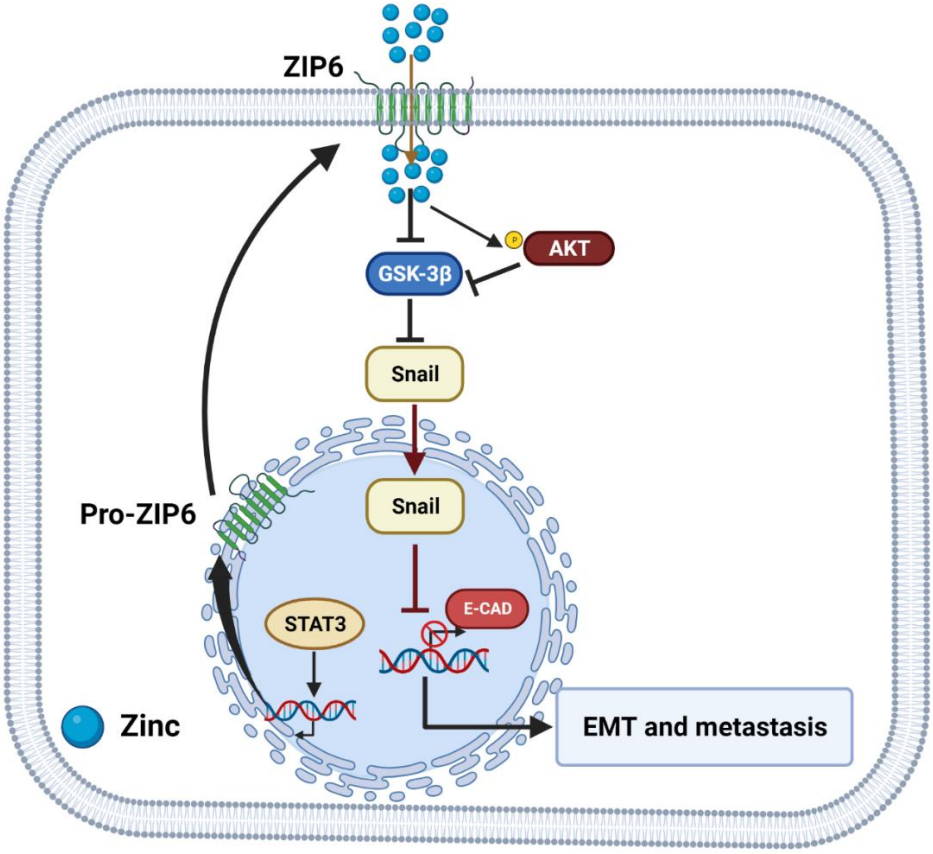

This schematic illustrates the role of ZIP6 in EMT. When triggered by STAT3, ZIP6 is transcribed and stored as a pro-protein in the ER. N-terminal proteolytic cleavage activates ZIP6, which is then moved to the plasma membrane resulting in an influx of zinc into the cytoplasm. This results in inhibitory phosphorylation of GSK-3ß, the accumulation of the transcriptional repressor Snail in the nucleus, the downregulation of E-cadherin, and cell migration and metastasis (Hogstrand et al., 2013).

1.7 Zinc transporter ZIP10

ZIP10, which is the closet LIV-1 family member to ZIP6, is another ZIP transporter with a potential role in breast cancer and it is localised mainly to the plasma membrane (Taylor et al., 2003)(Taylor et al., 2004). ZIP10 is recognised to have an indispensable role for B-cell development in early and mature stages. This is confirmed by a study of a ZIP10 knockout revealing a reduced humoral immune response (Miyai et al., 2014a). Moreover, a comparison of renal cell carcinoma with corresponding normal tissue revealed that ZIP10 expression was elevated in high-grade tumours, indicating its contribution to the progression of renal carcinoma (Pal et al., 2014). It is therefore not surprising that ZIP10 was seen to enhance survival by suppressing caspase activation, proteins which are required in the regulation of apoptosis (Miyai et al., 2014b).

Similarly to ZIP6, ZIP10 has been linked to aggressive breast cancer and its spread to the lymph nodes (Taylor et al., 2003). This is supported by the fact that the expression of the ZIP10 gene was noticeably elevated in breast cancer cell lines that had a high ability to invade and metastasise such as MDA−MB−435S and MDA−MB−231 compared with the less aggressive MCF-7 cells (Kagara et al., 2007b). Clinically, the expression of ZIP10 mRNA has been quantified in 177 surgical samples taken from patients with breast cancer. By using real-time quantitative PCR, ZIP10 mRNA expression was significantly higher in patients with breast cancer who had lymph node metastasis compared to those without (Kagara et al., 2007b).

Conversely, when ZIP10 was knocked out and zinc was depleted, the ability of cells to migrate was diminished, confirming the role of both ZIP10 and cellular zinc in the aggressiveness of breast cancer (Kagara et al., 2007a). Intriguingly, ZIP10 was discovered to form a heteromer with ZIP6, stimulating cells to round-up and detach, allowing cells to migrate (Taylor et al., 2016). Moreover, ZIP10 has been demonstrated to have a role in inducing EMT in human breast cancer cells and zebrafish embryos by inactivating GSK-3β and repressing the expression of E-cadherin, in a comparable manner to that previously observed with ZIP6 (Taylor et al., 2016). These results suggest that zinc transporters could work in conjunction to conduct biological function, highlighting the important role of zinc transporters in the development of tumours.

Given the importance of ZIP10 expression in various types of cancer, ZIP10 shows a propensity for a role in cancer progression similarly to ZIP6. Therefore, this could recognise ZIP10 as another potential biomarker to predict metastasis of breast cancer.

1.8 ZIP6 and ZIP10 are driving cell mitosis

ZIP6 and ZIP10 are two close homologues within the LIV-1 subfamily, sharing a sequence similarity of 43.5% and belong to the same branch of the ZIP family phylogenetic tree (Taylor et al., 2016). They have been independently implicated in various types of cancer including breast cancer (Saravanan et al., 2022). These transporters have been shown to be integrated to perform biological functions when they form a heteromer which promotes cell migration during embryonic development and carcinogenesis (Hogstrand et al., 2013) (Taylor et al., 2016). Additionally, ZIP6 knockdown increased ZIP10 levels, suggesting an important relationship between these two ZIP transporters (Nimmanon et al., 2020). Recently, our group has discovered the essential role of ZIP6 and ZIP10 heteromer in facilitating zinc influx to trigger mitosis (Nimmanon et al., 2020). The ZIP6/ZIP10 heteromer has to be relocated to the plasma membrane to begin mitosis, a process that requires the cleavage of the N-terminus of ZIP6. After it reaches the plasma membrane, the ZIP6/ZIP10 heteromer facilitates zinc uptake, which then attaches to the transcriptionally active form of STAT3, pSTAT3^{S705}, and changes it to pSTAT3^{S727}. This form of STAT3 remains bound to the ZIP6/ZIP10 heteromer throughout the cell division process (Nimmanon et al., 2020). During mitosis, the active form of STAT3 also binds to pS^{38}tathmin, the form of Stathmin that facilitates the rearrangement of microtubules needed for cell division (Silva and Cassimeris, 2013). After mitosis is completed, the C-terminal end of STAT3 is cleaved, which removes the S727 residue and enables the normal transcription-active form of STAT3 to start a new cell cycle (**Figure 1.9**) (Nimmanon et al., 2020). Interestingly, this mechanism can be inhibited by using a ZIP6 antibody that can recognize the extracellular N-termini of ZIP6, thus preventing zinc influx and halting the initiation of mitosis (Nimmanon et al., 2020). The ability of this promising antibody to block zinc influx by targeting ZIP6 N-terminus emphasises the critical role of the N-terminus region in ZIP6 function.

Figure 1.9 The role of ZIP6/ZIP10 heteromer in driving mitosis

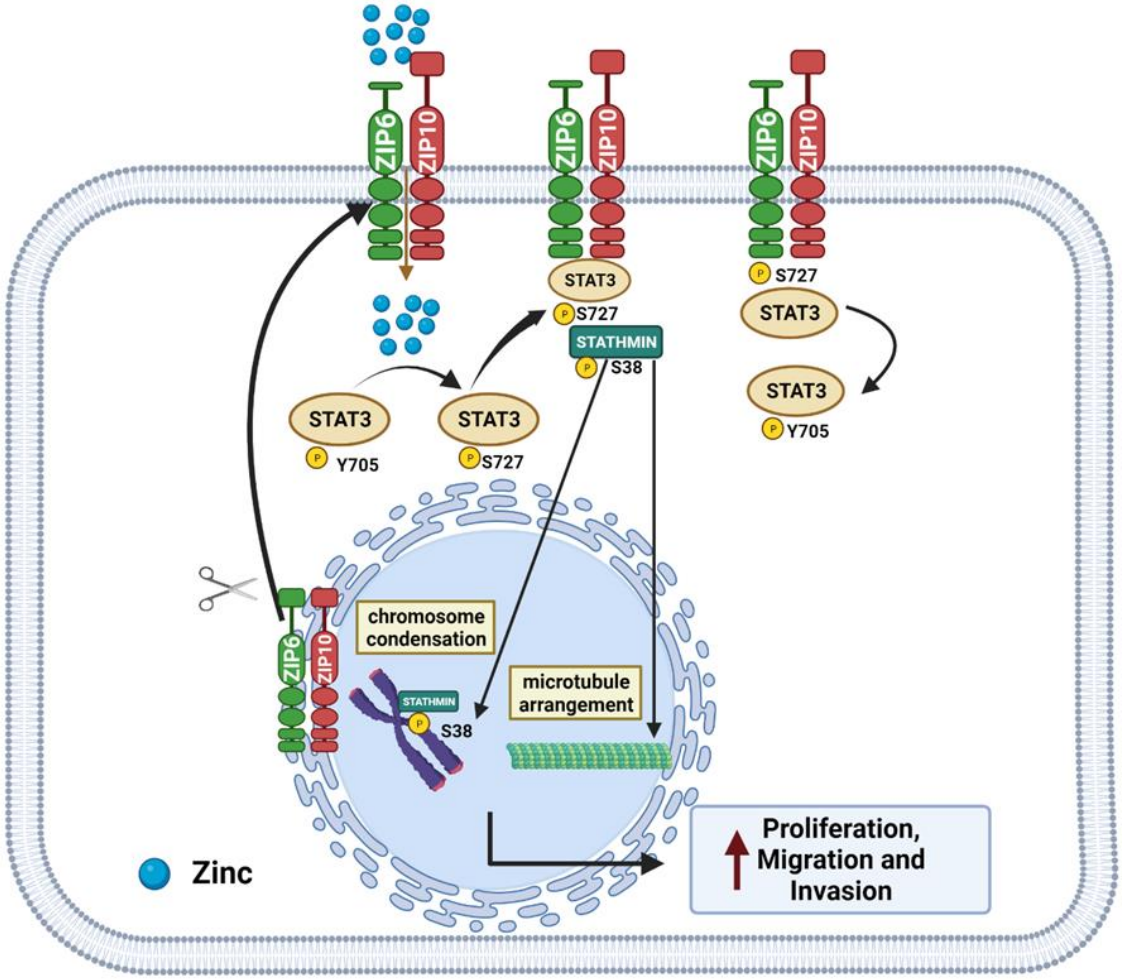

The ZIP6/ZIP10 heteromer has to be relocated to the plasma membrane to begin mitosis, a process that requires the cleavage of the N-terminus of ZIP6. After it reaches the plasma membrane, the ZIP6/ZIP10 heteromer facilitates zinc uptake, which then attaches to the transcriptionally active form of STAT3, $pSTAT3^{S705}$, and changes it to $pSTAT3^{S727}$. This form of STAT3 remains bound to the ZIP6/ZIP10 heteromer throughout the cell division process. During mitosis, the active form of STAT3 also binds to pStathmin, the form of $Stathmin^{P38}$. After mitosis is completed, the C-terminal end of STAT3 is cleaved, which removes the S727 residue and enables the normal transcription-active form of STAT3 to start a new cycle of the cell.

1.9. Post translational modification of ZIP transporters

ZIP transporters proteins are largely involved in cancer progression. Therefore, it is important to understand their post- translational modifications that are crucial for their function and regulation. It has been reported that ZIP transporter modification typically occurs through the addition of a phosphor group (phosphorylation) or degradation of proteins (proteolytic cleavage or ubiquitination). These processes have been observed in ZIP7 and ZIP6 respectively (Taylor et al., 2012b)(Hogstrand et al., 2013).

1.9.1. Phosphorylation of ZIP transporters

Phosphorylation is considered to be the most important process that regulates the function of several proteins including ZIP transporters. (Taylor et al., 2012)(Ardito et al., 2017). Phosphorylation is thought to take place in more than 90 percent of proteins encoded by the human genome. It is a mechanism involving the addition of a phosphate group to a protein and consequently, triggering a conformational change in that protein in order for it to interact with other molecules (Ardito et al., 2017). The attachment of a phosphoryl group usually derives from ATP to one of three different residues: serine (84%), threonine (15%), or tyrosine (less than 1%) (Roskoski, 2019). It is a fundamental process for cellular biological events such as signal transduction, development and the cell cycle (Ardito et al., 2017). Phosphorylation is mechanistically involved in nearly all biological processes. Phosphorylation is a modulator that controls enzyme activity as well as protein degradation, binding, conformation, and translocation (Humphrey et al., 2015)(Ardito et al., 2017). It also has biological interferences with other post-translational modifications such as ubiquitination, acetylation (Humphrey et al., 2015). In contrast, dephosphorylation is the opposite mechanism that stops phosphorylation by removing the phosphate group from the substrate. Given the importance of phosphorylation in regulating cellular transduction signalling, its hyperactivity or dysfunction is mostly seen in several diseases including cancer (Ardito et al., 2017).

It has been reported that ZIP7 is phosphorylated by CK2 on two adjacent serine residues S275 and S276, requiring for its activation. Moreover, the interaction between CK2 and ZIP7 has illustrated the upregulation of this transporter in aggressive types of breast cancer (Nimmanon et al., 2017).

Once ZIP7 is phosphorylated by CK2 and releases zinc to the cytoplasm, the subsequent zinc release causes phosphorylation of several kinases implicated with carcinogenesis, such as MAPK, PI3K-AKT, and mTOR and the inhibition of GSK-3ß. (Nimmanon et al., 2017). Therefore, it is not surprising that the use of kinase inhibitors can be beneficial for the treatment of cancer (Bhullar et al., 2018). The observation of ZIP7 phosphorylation on two residues suggests a possibility that other residues can be phosphorylated as well in order to reach maximal activation for this transporter. According to online phosphorylation site databases, several residues on ZIP7 are predicted to be phosphorylated particularly by nearby residues.

However, these residues have not been confirmed yet by residue−specific experiments and their kinases as well as their roles are still not investigated.

The revelation that ZIP7 is regulated by phosphorylation suggests that other ZIP transporters, particularly those belonging to the LIV1 subfamily, may also be regulated by phosphorylation. When using software to predict potential phosphorylation sites on ZIP6 and ZIP10, it is observed that multiple kinases are involved in ZIP6 and ZIP10 activation (Taylor, 2023). Therefore, these transporters are required to be phosphorylated before being activated (Humphrey et al., 2015). It has also been discovered that histidine residues have the ability to undergo phosphorylation (Fuhs and Hunter, 2017). It is unsurprising that proteins involved in zinc transport contain many histidine residues particularly in ZIP6 and ZIP10, as histidine is the most commonly considered as a metal-coordinating ligand (Kambe et al., 2021).Therefore, phosphorylation of these histidine residues might play a role in ZIP6 and ZIP10 activation. Nevertheless, these sites have not been confirmed through specific experiments and the exact role and responsible kinases of these sites have yet to be investigated.

1.9.2 Proteolytic cleavage of ZIP transporters

Proteolytic cleavage is a crucial post-translational modification that occurs in cells and plays a role in regulating important processes such as the cell cycle, cell death, cell proliferation, and even conditions such as cancer (Rogers and Overall, 2013). In contrast to phosphorylation, proteolysis is an irreversible process of breaking down proteins into smaller fragments. This is accomplished by a protease enzyme that cleaves the peptide bonds through hydrolysis (Rogers and Overall, 2013).

Proteolytic cleavage has been not only involved in protein degradation, but also in protein activation or inactivation, secretion and localisation (Rogers and Overall, 2013)(Humphrey et al., 2015).

Some LIV-1 family members have been reported to be proteolytically cleaved in order to be activated. For example, ZIP4 was subjected to proteolytic cleavage on its N-terminal domain during a zinc deficiency condition. Under normal conditions, ZIP4 is internalized and degraded, but it has been shown to be accumulated on the apical surface of epithelial cells under zinc deficiency conditions (Kambe and Andrews, 2009).

Furthermore, ZIP6, another member of the LIV-1 subfamily of zinc transporters, has been shown to be initially expressed in the endoplasmic reticulum as a pro-protein and then undergoes a process of proteolytic cleavage, resulting in its colocalization to the plasma membrane (Hogstrand et al., 2013). This provides as an example of how proteolytic cleavage regulates protein function and localization.

ZIP6 has a PEST cleavage site on its N-terminal region, which is a type of peptide sequence commonly found in proteins that undergo proteolytic cleavage and contribute to a shorter half-life (Hogstrand et al., 2013). Similarly, ZIP10 also has a PEST cleavage site at the N-terminus, as evidenced by the presence of various band sizes in western blot analysis. However, the significance of this cleavage for its protein function remains unclear (Nimmanon et al., 2020). Interestingly, the prion protein, which plays a role in neurodegenerative diseases, has been discovered to have originated from the LIV-1 subfamily of ZIP transporters, particularly in terms of amino acid sequences, to ZIP6 and ZIP10 (Schmitt-Ulms et al., 2009). It has been shown that it undergoes N-terminal ectodomain shedding during zinc-depleted conditions (Ehsani et al., 2012). The resemblances between this protein and members of the LIV-1 subfamily of zinc transporters suggest the critical role of N-terminal cleavage for their functional control.

This is supported by the fact that ZIP6 and ZIP10 are found in the same category of the phylogenetic tree, as seen in **Figure 1.4**. This means that both transporters can have shared function and regulation. Given that the N-terminal region contains a highly predicted site for proteolytic cleavage in regulating ZIP6 and ZIP10, it is valuable to investigate the role of this region to understand the mechanisms of these transporters.

1.9.3 Ubiquitination of ZIP transporters

Ubiquitination is a post-translational modification of proteins that plays a vital role in maintaining normal homeostasis and contributing to diseases (Kona et al., 2013). The process of ubiquitination involves the covalent attachment of ubiquitin (Ub) to lysine residues of a target protein, recognising target proteins for proteasome degradation (Mansour, 2018)(Sun et al., 2020). The formation of a Ub conjugate needs the presence of three enzymes: an E1 ubiquitin-activating enzyme, an E2 ubiquitin-conjugating enzyme, and an E3 ubiquitin ligase (Sun et al., 2020). The result of this reaction is the attachment of a single molecule of ubiquitin to a target protein, referred to as monoubiquitination.

Further attachment of multiple ubiquitin molecules makes ubiquitin chains, referred to as polyubiquitination. This polyubiquitination then triggers the degradation of the target protein by serving as a signal for recognition by the 26S proteasome (**Figure 1.10**) (Yao and Cohen, 2002)(Song and Rape, 2008). This process is extremely controlled, with the ability to have significant impacts on various cellular pathways during both cell survival and death (Yao and Cohen, 2002).

Similar to other post-translational modifications, the ubiquitination process can be reversed by the deubiquitinating enzyme (DUB) family (Song and Rape, 2008). When DUBs fail to remove ubiquitin from proteins that have already interacted with the 26S proteasome, it disrupts the functioning of the proteasome and therefore affects the homeostasis of cells (Sun et al., 2020)(Chen et al., 2022). Therefore, ubiquitination and deubiquitination have been seen to be dysregulated in various types of diseases including cancers (Sun et al., 2020).

ZIP4 was the first ZIP transporter to be established as post−translationally processed through ubiquitination (Mao et al., 2007). ZIP4 is required for the enterocytes to import zinc from the diet (Dufner-Beattie et al., 2003). It has been found that the expression level of ZIP4 is regulated in response to changes in zinc availability (Dufner-Beattie et al., 2003). This means that ZIP4 was observed to accumulate at the plasma membrane when zinc was limited, and was rapidly diminished upon zinc repletion (Dufner-Beattie et al., 2003). Years later, the regulation level of ZIP4 was discovered through ubiquitin-mediated degradation (Mao et al., 2007). ZIP4 was found to be degraded through ubiquitination when zinc concentrations were higher, which resulted in a decrease in the uptake of zinc mediated by ZIP4 (Mao et al., 2007).

Therefore, this process controls the influx of zinc into cell which in turn maintain zinc homeostasis. Similarly, ZIP14, which is responsible to import zinc and iron (Kambe et al., 2015), was also found to be ubiquitinated and degraded (Hennigar and McClung, 2016). It has been observed that ZIP14 was ubiquitinated and degraded during iron deficiency and accumulated in response to iron supplementation. This elucidates how iron is redirected from storage tissues during iron deficiency, thus enhancing the accessibility of iron for functions that require it (Hennigar and McClung, 2016).

Recently, ZIP6 has been predicted to contain many ubiquitination sites (Saravanan et al., 2022). Yet, as of now, there have not been any studies investigating the role of ubiquitin degradation in the functioning of the ZIP6 transporter. Interestingly, in laboratory culture, cells that express ZIP6 might have already undergone degradation in the dish prior to harvesting, contributing to a shorter half- life of less than 1 h and making it difficult to examine its effects (Hogstrand et al., 2013). Thus, the ZIP6-ubiquitin association sites might explain the low-level expression and instability of the recombinant ZIP6. Given that the ZIP6 transporter plays a vital role in cancer development, understanding its post−translational modifications could provide possibilities to develop a therapeutic approach to treat cancer by regulating these modifications on this protein.

Figure 1.10 The protein degradation/ubiquitination pathway

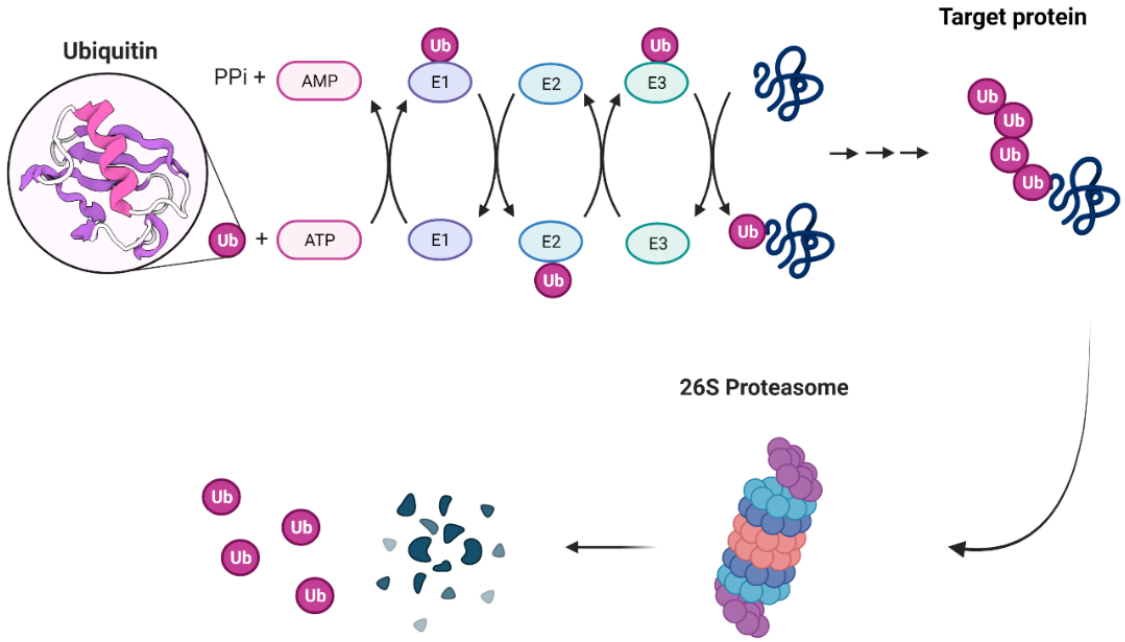

This schematic demonstrates that the process of protein ubiquitination/degradation involves enzyme complexes, specifically ubiquitin-E1, ubiquitin-E2, and ubiquitin-E3. Following this ubiquitin tagging, the tagged protein becomes a target for 26S proteasome-mediated degradation. The proteasome then degrades the targeted protein into smaller peptide segments.

1.12 Hypothesis

The hypothesis of this project are:

1) There are additional residues that are required for maximal activation of ZIP7.
2) The N-terminus of ZIP6 and ZIP10 is essential for their localisation and function.
3) Ubiquitination is an important regulation mechanism for ZIP6 as a part of its post-translational modification.

1.13 Aim and objectives

This project's general aims are to:

• Identify the additional residues responsible for the maximal activation of ZIP7.

• Assess the role of the N-terminus in the localisation and function of ZIP6 and ZIP10.

• Investigate the role of ubiquitination in the regulation of ZIP6 function.

To achieve these aims, the following objectives were pursued:

1) Exploring potential phosphorylation sites in ZIP7 using bioinformatic analysis and generating ZIP7 mutants to investigate the relevant residues.

2) Generating chimeric constructs using the ZIP7 N-terminus with the transmembrane domains of ZIP6 and/or ZIP10 to investigate the impact of this modification on the function of ZIP6 and ZIP10.

3) Determining the effect of ubiquitination on ZIP6 function by using a novel construct where all potential ubiquitin sites were mutated.

Chapter 2

Material and Methods

2.1 Cell preparation, transfection, treatment.

2.1.1 Cell culture and seeding for experiments

Human breast adenocarcinoma cells (MCF-7) were cultured in Roswell Park Memorial Institute (RPMI) medium (Gibco, UK) that was supplemented with 5% fetal bovine serum (FBS), antibiotics (10 µg/mL Streptomycin and 10 IU/mL Penicillin) and 2.5 µg/mL Amphotericin B (Gibco, UK). All cells were incubated at 37°C in a 5% C02 atmosphere and the medium was changed every three days. For experiments, cells were trypsinized at 37°C using 5 ml of Trypsin-EDTA (0.5%) (Thermo Fisher Scientific) for up to 5 minutes or until cells became suspended. Cell suspensions were collected into a universal tube and then neutralized with an equivalent volume of medium with serum. By centrifuging the cells at 168 x g for 5 minutes, the supernatant was discarded, and the pallet was resuspended with a fresh medium with serum. The number of cells present was then determined by adding 100 ul of the cell suspension into 10 ml of Isoton II using an automated cell counter (Beckman Coulter^{TM}). For either immunofluorescence or western blotting, 1-3 × 10^5 cells were required to be seeded onto 35 mm dishes. The dishes either contained 22x22 mm ultra−thin glass coverslips (0.17 mm thick) for immunofluorescence or lacked glass coverslips for western blotting.

2.1.2 Transfection

When the cells were 70−90% confluent, MCF-7 cells were transfected with plasmid DNAs of wild-type zinc transporters, mutants or chimeric constructs using Lipofectamine-3000 (Invitrogen). The plasmid DNAs consists of a carboxyl terminal V5 tag which allowed detection of V5 antibody by immunofluorescence or western blot. Separately, 4µg of plasmid DNA and 7.5µL of Lipofectamine-3000 (Invitrogen) was each diluted in 188µL of phenol-red-free RPMI medium (Gibco, UK), with no serum or antibiotics present. In under 5 minutes, the diluted DNA was mixed with the diluted Lipofectamine-3000 and allowed to incubate for 20 minutes at room temperature. After incubation, 380 µl of the mixture was added to a dish containing 1015 µl of phenol-red-free RPMI medium with serum and L−glutamine. The cells were incubated at 37°C for 16 to 24 hours before being harvested with or without treatment.

2.1.3 Treatment

For zinc treatment, the transfected cells were treated for (0, 2,5 or10 minutes) with zinc 20 µM plus sodium pyrithione 10µM in phenol−red−free RPMI medium with 200mM L-glutamine in the absence of serum.

2.2. Generation of recombinant proteins

Site-directed mutagenesis and artificially synthesized mutants were used in this project to generate recombinant proteins. Site-directed mutagenesis was used to make specific targeted changes to the DNA sequence of a gene to alter the amino acid sequence of the resulting protein. This can be used to create variants of a protein with altered function or stability. On the other hand, artificially synthesized involves chemically synthesizing the gene encoding the desired protein, rather than using a naturally occurring gene. This method can be used to create proteins that do not exist in nature or to create specific variants of a protein. However, depending on the specific aims of this project, the latter method may be more appropriate due to its -ability to make mutations that are not near each other.

2.2.1 Site−directed mutagenesis

Mutagenex Inc performed site-directed mutagenesis to generate ZIP7 mutant constructs within an ampicillin-resistant pcDNA3.1/V5-His-TOPO plasmid vector. (**Figure 2.1**). The mutation was then checked by DNA sequencing. Individual serine or threonine residues (codon AGC or ACC) were mutated to alanine (codon GCC or GCA) for a phosphoablative (null) mutant. The hydroxyl (-OH) group present in serine or threonine amino acids allows for the attachment of a phosphate group through a process called phosphorylation. When a serine or threonine is mutated to alanine, the hydroxyl group is replaced with a methyl group (-CH3) and the amino acid can no longer be phosphorylated. Mutant ZIP7 constructs which were created for this project are listed in **table 2.1**.

2.2.2 Artificially synthesized constructs

Desired DNAs are artificially synthesised by Doulix (Venice, Italy) to generate mutants and chimeric ZIP constructs. The mutation and combination constructs were confirmed by DNA sequencing. The desired DNA were then inserted in a plasmid vector consisting of a carboxyl terminal V5 tag and a CMV promoter without His tag **(Figure 2.2)**. In ZIP constructs, WT ZIP7 and other ZIP7 and ZIP6 mutants are listed in the **Table 2.2**. In chimeric ZIP6 and ZIP10 DNA constructs, the first 326 N-terminal amino acid of ZIP6 or the first 408 N-terminal amino acid of ZIP10 was replaced with the first 143 N-terminal amino acid of ZIP7, yielding a chimera that consisted of n-terminus of ZIP7 with transmembrane domains of ZIP6 (ZIP7/ZIP6) **(Figure 2.3 A)** or ZIP10 (ZIP7/ZIP10) **(Figure 2.3 B).** All the plasmids were then purified employing EndoFree Plasmid Maxi Kit (Qiagen, Germany).

Figure 2.1 Schematic structure of a plasmid vector

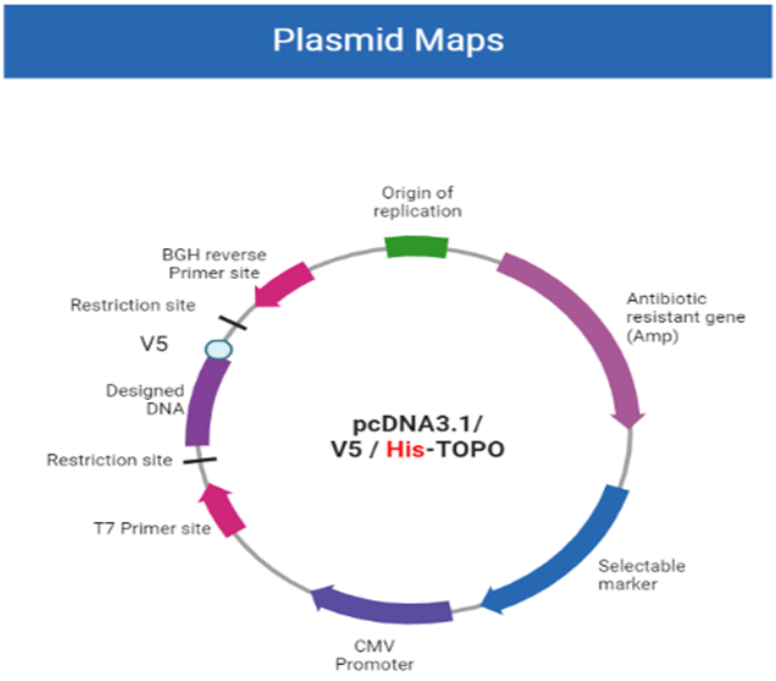

This schematic illustrates the structure of the cDNA3.1/V5−TOPO plasmid with His Tag. It consists of a carboxyl- terminal V5 tag with a BGH reverse priming site and a T7 priming site, which were employed for verification of a DNA insert. It also contains an ampicillin−resistant gene (Amp), stop codon at the end of the DNA of interest and a CMV promoter (PCMV).

Table 2.1 DNA sequence of ZIP7 mutants

Construct	Wild-Type DNA sequence	Mutant DNA sequence
ZIP7 S275A S276A (AA)	CAG**AGCTCA**GAG	CAG**GCCGCA**GAG
ZIP7 S293A (S293A)	GGG**AGC**ACC	GGG**GCC**ACC
ZIP7 T294A (T294A)	AGC**ACC**GUC	AGC**GCC**GUC

DNA sequences for ZIP7 mutants where serine or threonine residue was mutated to alanine for a phosphoablative (null) mutant.

Figure 2.2 Schematic structure of a plasmid vector without His-Tag.

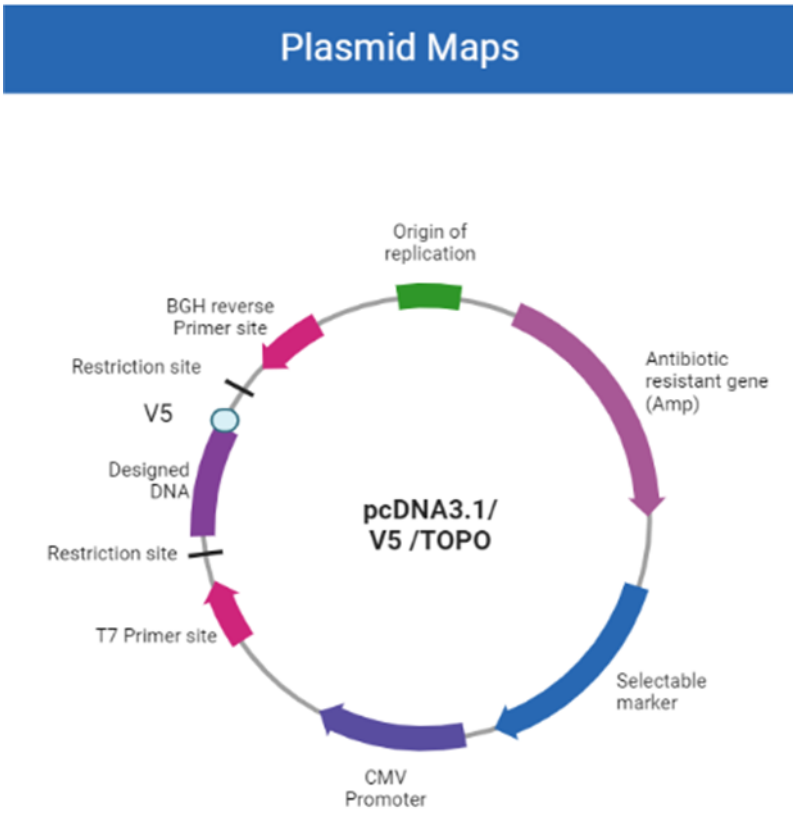

This schematic illustrates the structure of the cDNA3.1/V5−TOPO plasmid without His Tag. It consists of a carboxyl- terminal V5 tag with a BGH reverse priming site and a T7 priming site, which were employed for verification of a DNA insert. It also contains an ampicillin−resistant gene (Amp), stop codon at the end of the DNA of interest and a CMV promoter (PCMV).

Table 2.2 DNA sequence of ZIP7 mutants

Construct	Wild-Type DNA sequence	Mutant DNA sequence
ZIP7 S275A S276A (AA)	CAG**AGCTCA**GAG	CAG**GCCGCA**GAG
ZIP7 S275A S276A S293A T294A (4A)	CAG**AGCTCA**GAG/ GGG**AGCACC**GUC	CAG**GCCGCA**GAG/ GGG**GCCGCC**GUC
ZIP6 WITH ALL UBIQUITIN SITES (K467A, K468A, K472A, K456A, K457A) (ZIP6Q)	AAA AAG AAT **AAG AAG** GCA CCT GAA AAT GAT GAT GAT GTG GAG ATT **AAG AAG** CAG TTG TCC **AAG** TAT GAA	AAA AAG AAT **CAG GCG** GCA CCT GAA AAT GAT GAT GAT GTG GAG ATT **GCG GCG** CAG TTG TCC **GCG** TAT GAA

DNA sequences for ZIP7 and ZIP6 mutants where serine, threonine or lysine residue was mutated to alanine to prevent phosphorylation or ubiquitination on these sites.

Figure 2.3 schematic structure of chimeric plasmids

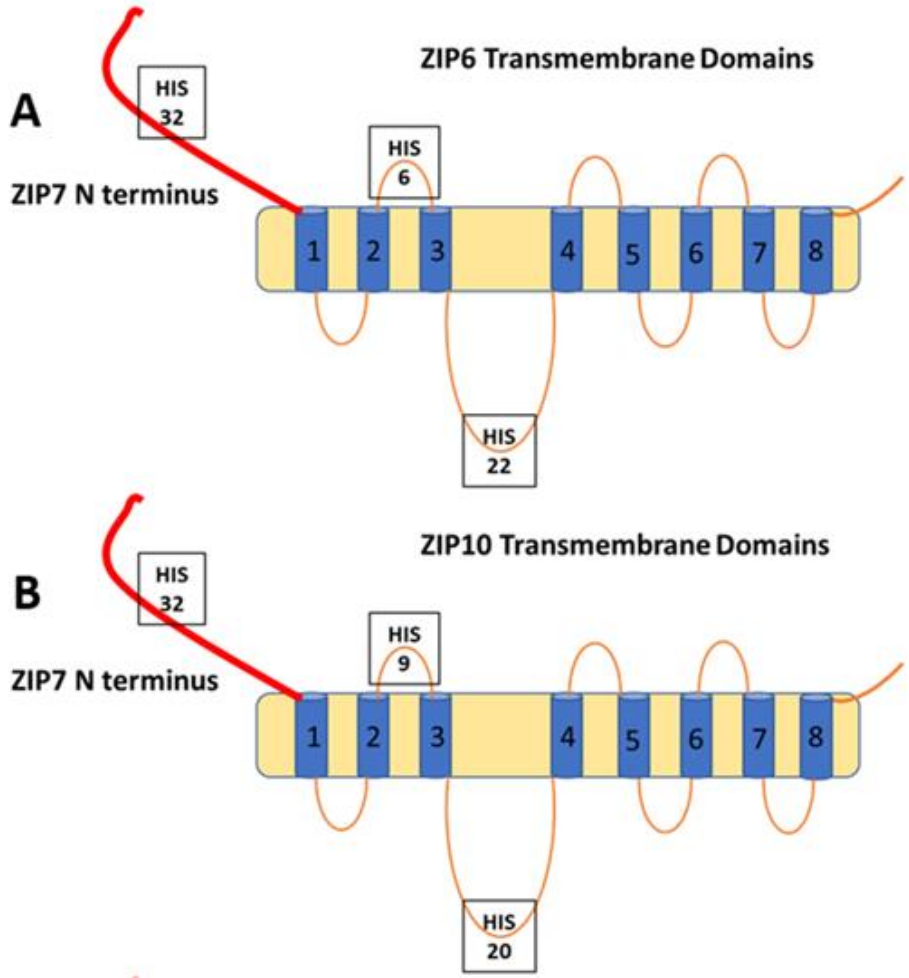

These schematic structures demonstrate chimeric plasmids of ZIP transporters. ZIP7 N-terminus on ZIP6 (A) or ZIP10 (B) were performed by Doulix (Venice, Italy).

2.3 Plasmid preparation

For the transformation process, DNA constructs were introduced by inserting designed sequences with a C-terminal V5 tag into either an ampicillin-resistant cDNA3.1/V5-His vector or a non-His-TOPO plasmid vector. These vectors were then amplified via transformation in JM-109 E. coli competent cells. Plasmid DNA was purified employing The HiSpeed Plasmid Maxi Kit (Qiagen) (**Figure 2.4**).

In brief, a single colony of the transformed competent cells was cultured in 5 ml LB broth medium supplemented with 100 µg/mL ampicillin. This mixture was then incubated at 37ºC with vigorous shaking for a period of 8 hours. 500µl from this culture was diluted in 250ml LB broth medium in the presence of 100 µg/mL ampicillin. It was then further incubated at 37ºC with intense shaking for 16 hours, followed by centrifugation at 6,500 rpm at 4 °C for 15 minutes duration. The pellet was resuspended with 10 mL buffer P1 that contained 100 µg/mL RNAse and LyseBlue. The cells were lysed with 10 mL buffer P2, neutralised with 10 mL buffer P3 and then passed through a QIAfilter Cartridge for final filtration. By using HiSpeed Maxi Tip, the DNA was purified and eluted with 15 mL buffer QF. After precipitation with isopropanol and 70% ethanol, the DNA was dissolved in 300µl of endotoxin−free Buffer TE.

The plasmid DNA was analysed by BioMate UV 3S spectrophotometer or NanoDrop™ One/One^{C} Microvolume UV-Vis Spectrophotometer (Thermo Fisher Scientific) for purity and concentration, which was determined by the ratio of the absorbance at 260 nm to the absorbance at 280 nm (OD260/OD280 ratio) and the absorbance at 260 nm (OD260), respectively **(Table 2.3).** All plasmids were then verified by immunofluorescence using anti-V5 antibody.

Figure 2.4 Schematic of plasmid purification protocol

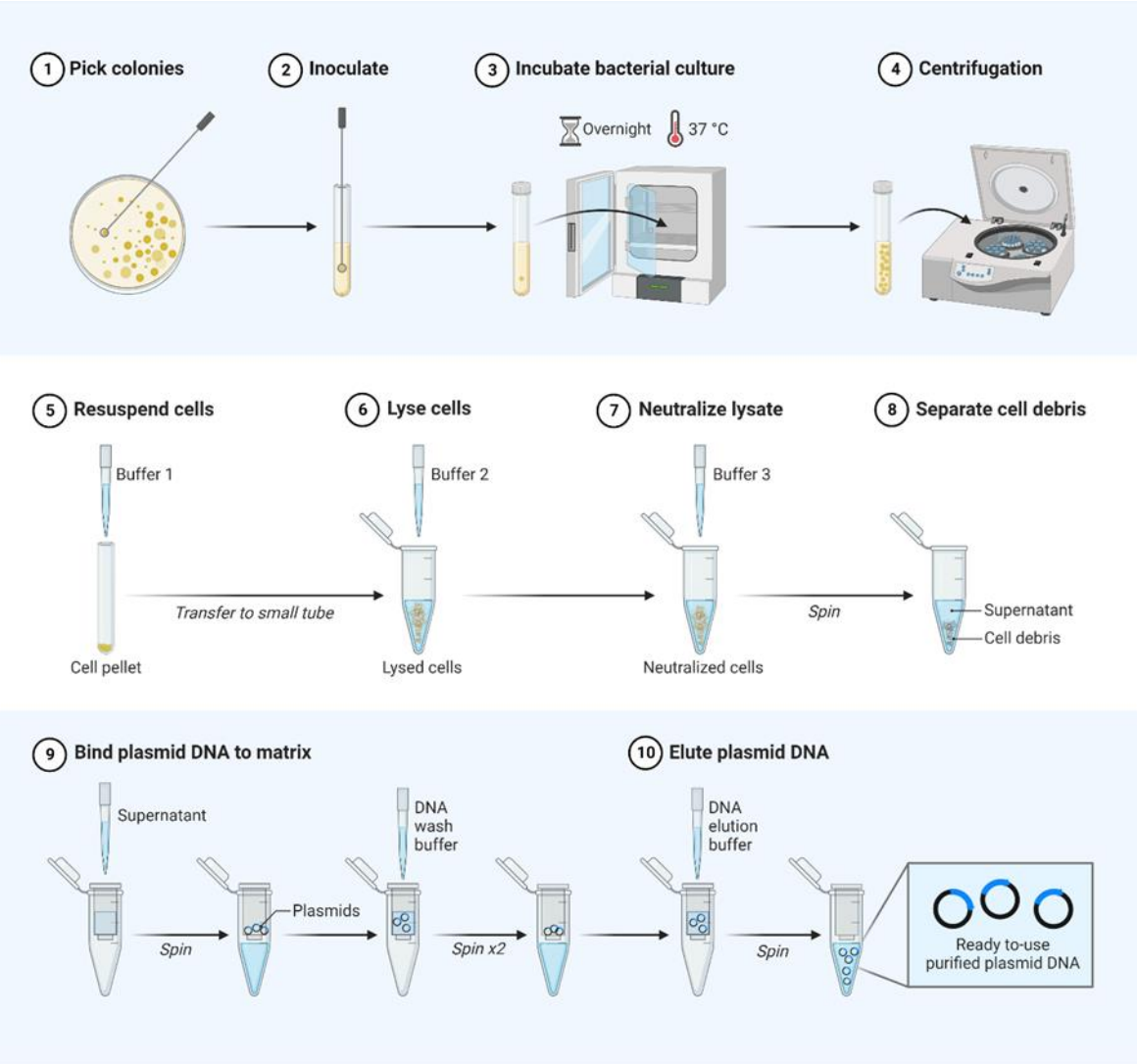

Schematic diagram of the plasmid purification method. The diagram shows the protocol steps for purification from bacterial isolation to elution plasmid DNA. This protocol was performed using The HiSpeed Plasmid Maxi Kit (Qiagen).

Table 2.3 DNA concentration and OD260/280 ratio of prepared plasmids

Plasmid	DNA concentration µg/µl	OD260/280 Ratio
ZIP7 Wild-Type	1.653	1.897
ZIP7 275A /276A	2.338	1.907
S293A	1.808	1.887
T294A	1.14	1.900
ZIP7 Wild-Type	0.8	1.85
ZIP7 Wild-Type No His	0.45	1.86
AA No His	2.3	1.80
4A No His	2.29	1.85
Chimera 7/6	1.2	1.86
Chimera 7/10	0.94	1.88
ZIP6 Wild-Type	1.48	1.89
ZIP10 Wild-Type	1.92	1.89
ZIP6 Q	2.5	1.88

The plasmid DNA was determined with a UV spectrophotometer. OD260/OD280 ratios ranged from 1.8 to 2.0, indicating the purity of the DNAs. No His means this recombinant was constructed without His-tag.

2.4 Immunofluorescence

MCF-7 cells were seeded on ultra-thin glass coverslips measuring 22x22 mm (0.17 mm thick) at 70–80% confluent. Some coverslips were subjected to time–course treatment with zinc prior to harvesting. The cells were fixed with 3.7% formaldehyde for 15 minutes and then washed ×2 by phosphate-buffered saline (PBS) for five minutes. Fixation helps to maintain the structure of cells by stabilising proteins and other biomolecules within them and immobilising antigens in the sample. The cells were made permeable by incubation in a solution of 1% bovine serum albumin (BSA) and 0.4% saponin in PBS for 15 minutes. Next, the cells were blocked by 10% normal goat serum (DAKO, UK) in the permeabilised buffer for another 15 minutes. Saponin works by disrupting the cell membrane, making primary antibodies more permeable to detect the antigens inside the cells. The cells were then incubated with primary antibodies **(Table 2.4)** for one hour in a moisture chamber, followed by washing three times. Under light protection, the cells were incubated with secondary antibodies usually a combination of Alexa Fluor-488 (green) and Alexa fluor-594 (red) (Molecular Probes, Invitrogen, USA) either with anti-rabbit or anti-mouse for 30 mins **(Table 2.5)**.

The coverslip was then mounted on a microscope slide using VECTASHIELD mounting media with DAPI (Vector Laboratories, USA), which is a fluorescent dye that stains nuclei blue and sealed with nail varnish. The slides were imaged on a Leica RPE automatic microscope, using a 63x oil immersion lens. The images were acquired and processed by using velocity software for Microsoft operating system. The pictures were processed using Image J and paint shop pro X software.

2.5 Western blot

2.5.1 sample preparation and protein assay

MCF-7 cells were cultured in 35 mm dishes until they reached approximately 80-90% of confluence, before being used in western blot analysis. Cell growth medium was aspirated, and cells washed with cold phosphate-buffered saline (PBS). PBS used to stop certain chemical reactions, such as temperature-dependent zinc signalling cascades, by lowering the temperature of the reaction. To collect adherent cells, the cells were harvested with 100µl lysis buffer (50 mM Tris, 150 mM NaCl, 25mM NaF, 5 mM EGTA, and 1% Triton X−100) and 10 % of protease inhibitor cocktail (Sigma).

Then, the cells were scraped, and the lysates were collected into an Eppendorf tube. For non-adherent cells, the medium was subjected to centrifugation at 168 x g for 8 minutes. The resulting cell pellets were then washed with ice-cold PBS and subsequently lysed in 50 µL of lysis buffer containing inhibitors. For some samples, the adherent and non-adherent cell lysates were pooled into the same tube, and it was called as a pooled sample. Lysates for either adherent or pooled samples were incubated on ice for one hour to separate the plasma membrane proteins from the membrane. Following the incubation period, the lysates were subjected to centrifugation at 12,000 rpm at 4°C for 12 minutes. The supernatant was then collected into a clean Eppendorf tube.

Table 2.4 Primary antibodies

Antibody	Supplier	Species	Dilution in IF [1]	Dilution in WB [2]	Dilution in PLA [3]
V5	Invitrogen MA5-15253	Mouse	1/1000	1/1000	1/1000
V5	ABCAM ab27671	Rabbit	1/1000	1/1000	
Total SLC39A7 (ZIP7)[4]	In house	Rabbit			1/200
pSLC39A7 (pZIP7)[5]	In house	Mouse	1/100	1/1000	
tZIP7	Protein Tech (19429-1-AP)	Rabbit	1/200	1/200	
tZIP7	ABCAM ab254566	Rabbit	1/200	1/1000	1/200
pAKT S473	CST[5] (9271)	Rabbit		1/1000	
pAKT S473	CST (4051)	Mouse		1/1000	
pSP27 S82	CST (2401)	Rabbit		1/1000	
pGSK-3α/ß S21/9	CST (9331)	Rabbit		1/1000	
pGSK-3ß S9	CST (5558)	Rabbit		1/1000	
p44/42 MAPK (Erk1/2)	CST (9102)	Rabbit		1/1000	
P70 S6 Kinase (T389)	CST (9234)	Rabbit		1/1000	
P70 S6 Kinase (T421/S424)	CST (9204)	Rabbit		1/1000	
HSP60	CST (4870)	Rabbit		1/1000	
pCDC2 Thr14	CST (2543)	Rabbit		1/1000	1/200
pCDC2 Tyr15	CST (9111)	Rabbit		1/1000	
pCDC2 Thr161	CST (9114)	Rabbit		1/1000	
pSTAT3 S727	CST (9134)	Rabbit	1/200	1/1000	1/200
pSTAT3 S727	CST (9136)	Mouse	1/200	1/1000	
p-PLK1 (T210)	CST (9062)	Rabbit		1/1000	
p-PRAS40 T246	CST (2997)	Rabbit		1/1000	
p-PYK2 Tyr402	CST (3291)	Rabbit		1/1000	
casein kinase IIα	CSBT[6] (12738)	Mouse			1/200
GSK-3α/ß	CSBT (7291)	Mouse			1/200
MAPKAPK2	CST (3042)	Rabbit			1/200
PIM-1	CST (2907)	Rabbit			1/200
p Histone H3 S10	CST (9701)	Rabbit			1/200
ZIP6	Fisher Scientific PA5-100155	Rabbit	1/200	1/1000	1/200
GAPDH−peroxidase	Sigma G9295	Mouse		1/50000	

Note: [1] **IF**, immunofluorescence, [2] **WB**, Western blot, [3] **PLA**, Proximity ligation assay

[4] **Total ZIP7**, The epitope is GRQERSTKEKQSSE (residues 264−277, the cytoplasmic loop between TM3 and TM4). [5] **pZIP7 (S275/S276).** The epitope is TKEKQpSpSEEEEK (residues 270−281, the cytoplasmic loop between TM3 and TM4). [6]**CST**, Cell Signalling Technologies; [7]**SCBT**, Santa Cruz Biotechnology.

Table 2.5 Secondary Antibodies Antibody

Antibody	Supplier	Species	Dilution in IF [1]	Dilution in WB [2]
Alexa Fluor 594	Invitrogen (A11032)	Goat anti-mouse	1/1000	
Alexa Fluor 594	Invitrogen (A11072)	Goat anti-rabbit	1/1000	
Alexa Fluor 488	Invitrogen (A10684)	Goat anti-mouse	1/1000	
Alexa Fluor 488	Invitrogen (A11034)	Goat anti-rabbit	1/1000	
HRP−linked IgG	CST (7076)	Goat anti- mouse		1/10000
HRP−linked IgG	CST 7074	Goat anti-rabbit		1/10000

Note: [1] **IF**, immunofluorescence, [2] **WB**, Western blot, **CST**, Cell Signalling Technologies.

The concentration of the protein in the lysates was assessed using the BioRad microassay method. The process involved diluting the lysate 1:400 in deionized water, adding protein assay dye reagent (BioRad) to the mixture, and measuring the absorbance at 595 nm in a 96-well plate. The protein concentration was calculated based on a standard curve of BSA (bovine serum albumin) concentrations ranging from 5 to 25 µg/ml.

100µg of the samples were prepared with 1x and 4x laemmli buffer (loading buffer) containing bromophenol blue and 0.2M Dithiothreitol (DTT) to reduce disulfide bonds in the protein structure. Protein samples were denatured by boiling for 5 minutes at 100˚C, the samples were then loaded into a SDS gel.

2.5.2 Polyacrylamide gel electrophoresis−sodium dodecyl sulphate (SDS−PAGE) and immunodetection

Proteins were separated by SDS-PAGE based on their molecular weight using resolving gels (7.5–12%), with either 10 or 15 walls, made by stacking gel, depending on the size of the protein and the number of samples analysed. **Table 2.6 and 2.7** display the composition of the resolving and stacking gels used in this project.

The schematic illustrates the key procedures involved in the Western blot technique (**Figure 2.5**). Briefly, 20µg of prepared samples and 3µl of Precision Plus Protein™ Standard (Bio-Rad) were loaded into a SDS gel, and the cassette filled with 1× running buffer. The gel was run at 120 V in 90 minutes to separate proteins in the samples.

The protein was transferred from the gel into nitrocellulose membrane (Scientific Laboratory Supplies) at 100 V for 60 minutes using transfer buffer. The transferring step was performed by placing the membrane and gel between soaked sponge and filter paper with transfer buffer as shown in figure 5 step 2. After transferring, the proteins on the membrane were visualized by staining them with 0.1% Ponceau S in 5% acetic acid, which was then washed off with Tris Buffered Saline with Tween-20 (TBST). Then, the membrane was incubated with 5% non−fat dried milk (Marvel) in TBST for 1 hour at room temperature to block non- specific proteins. After washing for 30 minutes in TBST, the membrane was incubated with 5ml primary antibodies **(Table 2.4)** overnight at 4ºC. The primary antibody solution was prepared by mixing TBST 1X, 1 mM sodium azide (NaN3), 5% Western Blocking reagent (Roche), and the primary antibody at the appropriate concentration.

The day after, the membrane was washed with 1x Tris-buffered saline containing 0.05% Tween-20 (TBST) for 20 minutes and incubated with horseradish−peroxidase (HRP)−labelled goat secondary antibody **(Table 2.5)** at room temperature. After 30 minutes washing, the membranes were probed using either Clarity TM Western ECL Substatre or SuperSignal® West Femto Maximum Sensitivity Substrate to detect the densities of the protein band. The densitometry data for each band was performed by using image J software. Microsoft Excel 365 software was used to analyse the results, with normalisation performed using V5 or GAPDH.

Table 2.6 Composition of 10% stacking gel

Reagent	Units	10% (3×1.5 mm gel)
deionised H2O 2.5	mL	6.1
TRIS-HCl buffer, pH 6.8	mL	2.5
30% acrylamide	mL	1.3
10% SDS	µL	100
10% APS 10	µL	50
TEMED	µL	10

Table 2.7 Composition of resolving gel

Reagent	Unit	7.5%	10%	12%
deionised H2O	mL	9.6	8	6
TRIS-HCl buffer, pH 8.8	mL	5	5	5
30% acrylamide	mL	5	6.8	8
10% SDS	µL	200	200	200
10% APS 10	µL	200	200	200
TEMED	µL	12	12	12

Figure 2.5 Schematic representation of western blotting technique

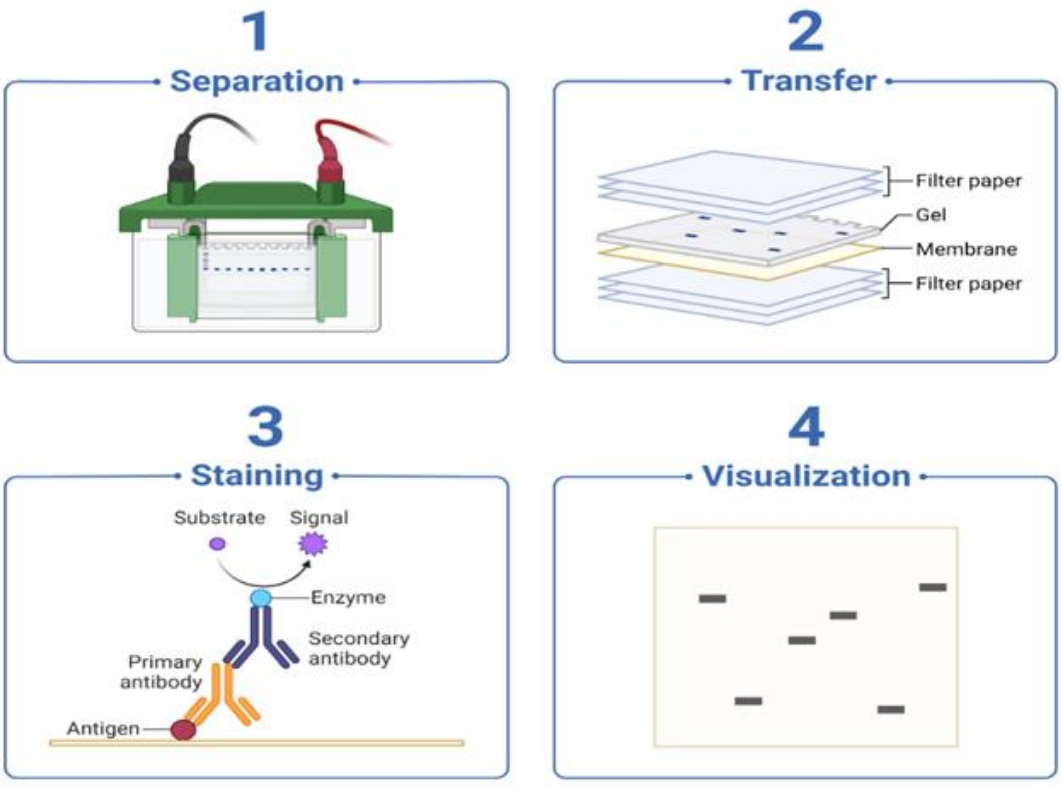

Schematic diagram shows the main steps in western blotting technique starting from separation samples to visualisation.

2.6 Determination of unknown protein molecular weight from western blot

The determination of the molecular weight of proteins within a sample was achieved by comparing the distance travelled by the protein of interest and molecular weight markers within a gel (as shown in **Figure 2.6 A**) and calculating the Rf values using a specific formula:

$$\textbf{Rf} = \frac{migration\ distance\ of\ marker}{migration\ distance\ of\ dye\ front}$$

The graph was plotted with the Rf value of each molecular weight marker against its established molecular weight (as shown in **Figure 2.6 B**). By examining the line graph, the molecular weight of the protein of interest was identified.

2.7 Proximity ligation assays (PLA)

PLA is a technique detecting the interaction between two proteins in close proximity by fluorescence (**Figure 2.7**). Our experiments were carried out using Duolink® In Situ Detection Reagents Orange. In brief, Transfected and/or treated MCF-7 cells were seeded on an 8−well chamber slid (Lab−Tek, Fisher). The slide was fixed with 3.7% formaldehyde, followed by twice washes with PBS. In pre warmed humidity chamber, the slide was permeabilised with duolink blocking solution for one hour at 37°C. The slide then was incubated with two primary antibody (**Table 2.4**) that were raised from different species for one hour at room temperature. After washing for 5 minutes, the slide was incubated with a solution of MINUS (rabbit) and PLUS (mouse) probes (Sigma−Aldrich) for one hour at 37°C, followed by an incubation with a ligation-ligase solution (Sigma−Aldrich) for 30 minutes. Under the light protection, the slide was incubated with an amplification solution containing a polymerase to enhance rolling circle amplification for 100 minutes at 37°C, followed by washing for 5 minutes. Finally, the protocol was amended by adding V5 at 1/1000 for 45 minutes at room temperature, followed by washing for 2 minutes. After, removing the gasket, 22×50mm coverslip was positioned on the slide using vectorshield, which contained DAPI. Imaging of cells was conducted on a Leica RPE automatic microscope utilizing a 63x oil immersion lens. At least five images were taken per well with 25 stacks spaced 0.3 µm apart for each captured image. The images were obtained and processed using velocity software for Microsoft operating system. The number of dots per cell was counted by using image J software. Brightness and contrast adjustments were also carried out using image J software.

Figure 2.6 Determining unknown protein by using Rf value

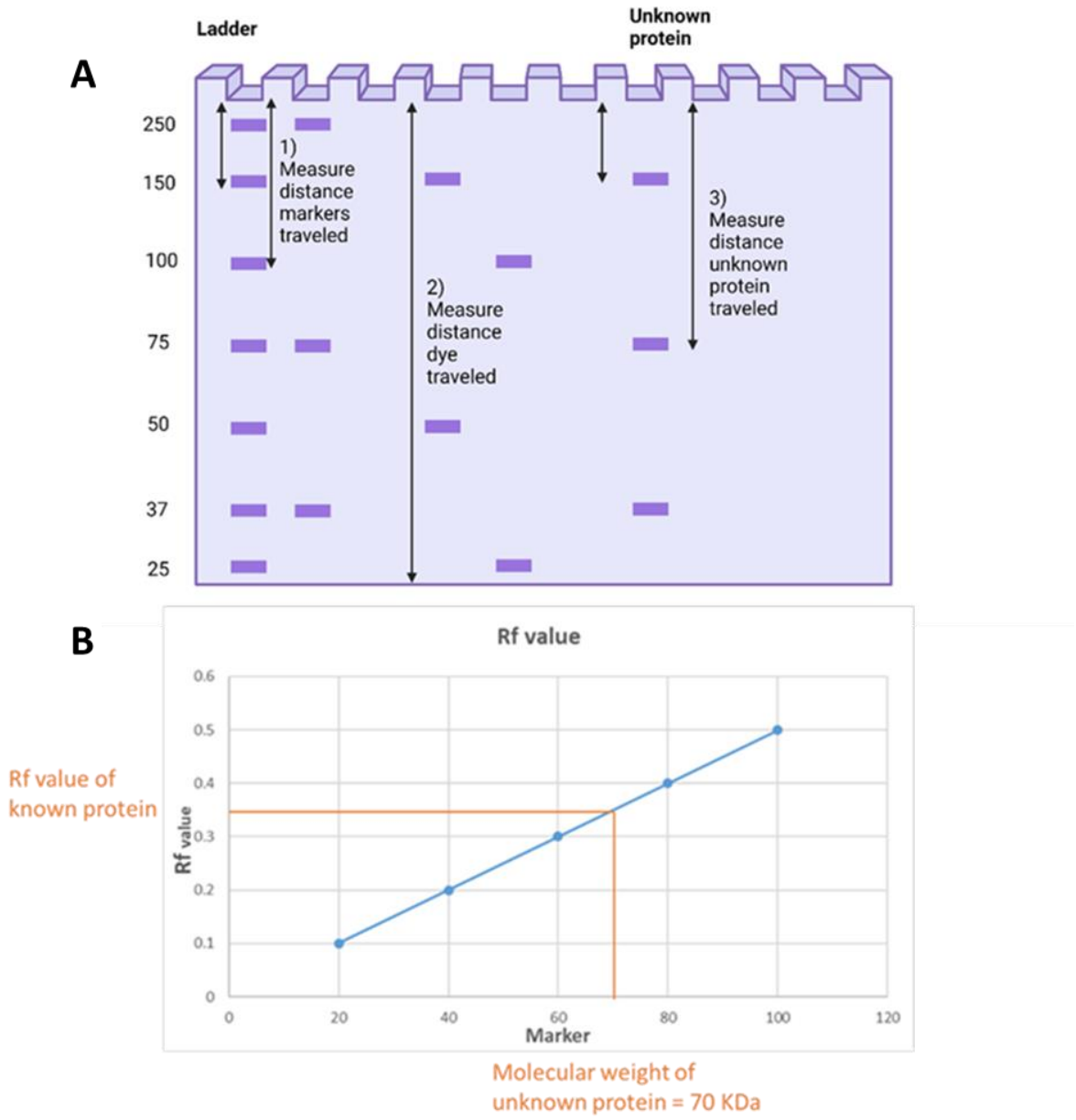

The distance each protein, both from the molecular weight markers and the protein of interest, has moved is gauged in comparison to the distance that the dye front has travelled (A). Subsequently, the Rf values of the molecular weight markers are plotted on a graph, and the graph can be used to assess the molecular weight of the protein of interest (B).

Figure 2.7 Proximity ligation assay

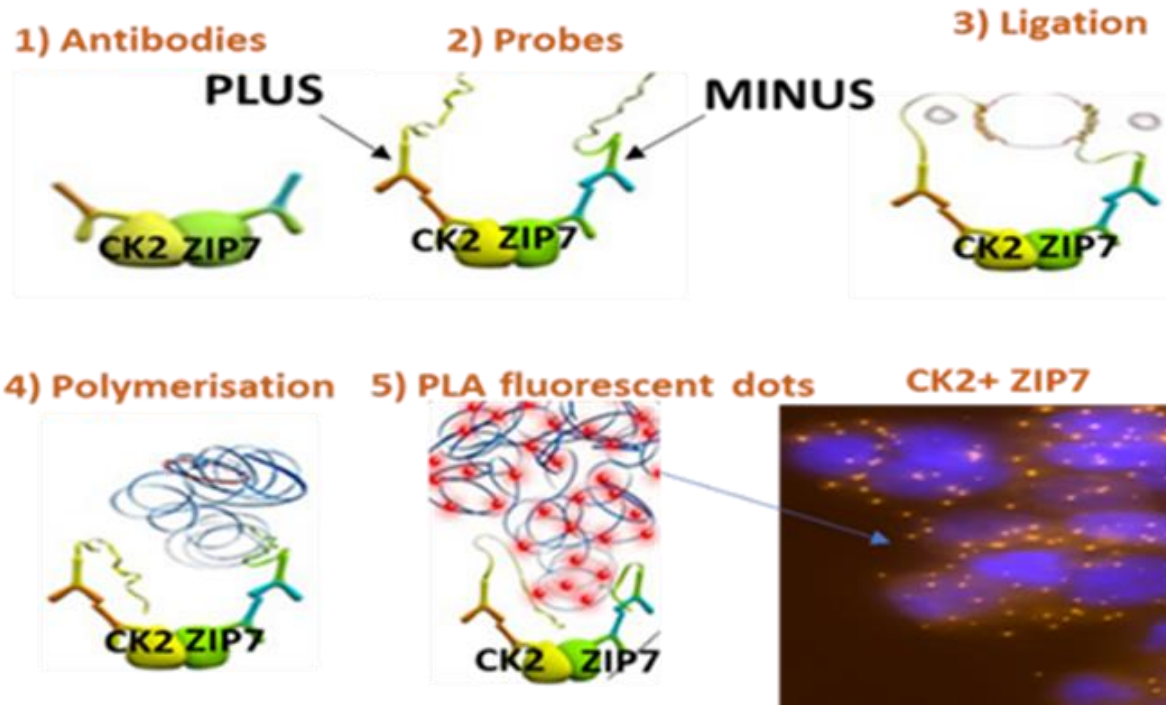

This schematic illustrates the process of PLA technique. Cells are incubated with two antibodies that are raised in different species against the two epitopes of interest. PLA probes (PLUS and MINUS) attach to the primary antibodies. This was followed by an incubation period with a ligase enzyme that carried DNA oligonucleotides and polymerase enzymes. These actions result in the amplification of the DNA ring, thus creating a rolling circle amplification reaction. Red fluorescent dots appear when two proteins are in close proximity (<40nm).

2.8 Proteome profiler antibody array

The Human Phospho-Kinase Array (ARY003B and ARY003C R&D Systems) is a membrane-based sandwich immunoassay, where 43 phosphorylated kinases can be detected simultaneously by binding to a specific target protein present in a sample **(Figure 2.8).** This experiment was carried out according to the manufacturer's instructions. Using reagents supplied with the kit, cells were lysed in 100µL Lysis Buffer 6 after transfection and treatment. Both parts of the membrane (A and B) were blocked by array buffer 1 at room temperature for one hour, followed by an incubation of the membrane with 300–400 µg of cell lysate diluted with array buffer 1 to a final volume of 2 mL at 4°C overnight. The day after, part A of the membrane was washed with 1x wash buffer and incubated with diluted Detection Antibody Cocktail A and similarly for part B for 2 hours. After washing, the membrane was incubated with Streptavidin−HRP for 30 minutes.

Finally, on a sheet protector, the membrane was applied with the Chemi-Reagent Mix and exposed to film. Signals were detected by using GeneSys image capture software with G: BOX system. Signal intensities were measured by densitometric analysis tool for Proteome Profiler Antibody Array using image J.

2.9 Statistical analysis

Statistical analysis was performed using a Paired t test or analysis of variance (ANOVA) with Dunnett's test. Significance was assumed with * = $p < 0.05$, * = $p<0.01$, and *** = $p < 0.001$. The statistical analysis was carried out utilizing GraphPad (Prism) software. The results are presented in terms of the mean and the standard error of the mean and are based on data collected from at least three biological samples.

Figure 2.8 The human phospho-kinase array

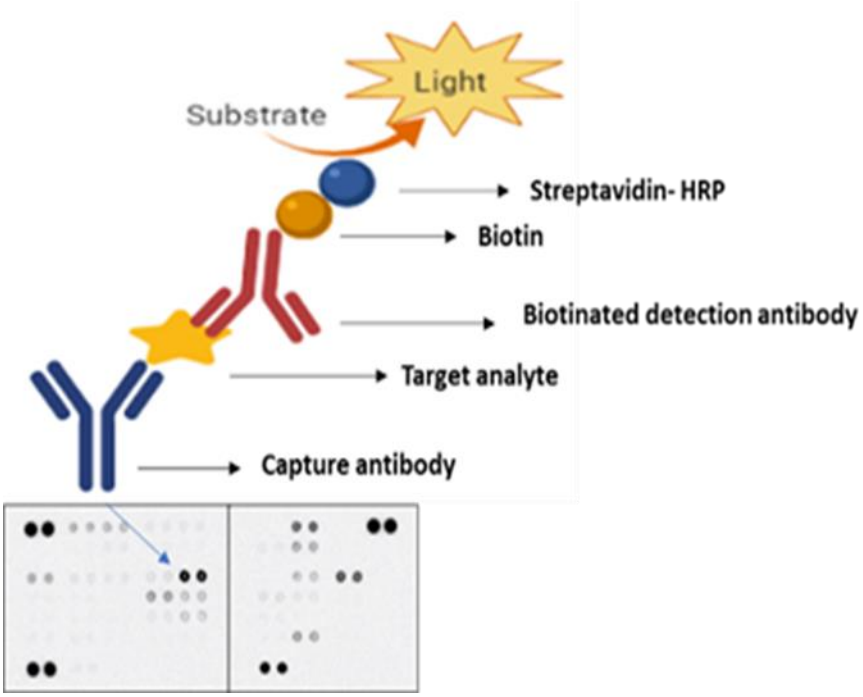

This figure demonstrates the signal detection principle for phospho-kinase arrays. Three positive control pairs are located on the left upper, left lower and right upper corners of each membrane. Capture antibodies, which are incorporated into the membrane in pairs, bind to kinases that are present in a sample. Phosphorylated kinases on specific sites are determined by the interaction between biotin and streptavidin HRP. Signals are detected by using Chemi Reagent Mix.

2.9 Materials and reagent

All material and reagent that were employed in this project are listed in **Table 2.8**

Reagent / material	Supplier	Catalogue number
Acrylamide/bis−acrylamide (30% solution 37.5:1)	Sigma−Aldrich, USA	A3699
Agarose	Bioline Ltd, London, UK	BIO−41025
Ammonium persulphate (APS)	Sigma−Aldrich, USA	A3678
Amphotericin B (Fungizone)	Invitrogen, Paisley, UK	15290
Bio−Rad protein assay dye reagent	BioRad Laboratories Ltd, Hertfordshire, UK	500−0006
Bovine serum albumin (BSA)	Sigma−Aldrich, USA	A7030
Bromophenol blue	Merck, USA	L54971322
Cell scrapers	Greiner Bio−One Ltd, Gloucestershire, UK	
Coulter Counter counting cups and lids	Sarstedt AG and Co., Nümbrecht, Germany	
Clarity, Western ECL substrate	Bio-Rad, USA	170-5061
Dimethyl sulphoxide (DMSO)	Sigma−Aldrich, USA	D8418
Di−thiothreitol (DTT)	Sigma−Aldrich, USA	10708984001
Duolink® In Situ PLA® Probe Anti-Mouse MINUS	Sigma−Aldrich, USA	DUO92004-30RXN
Duolink® In Situ PLA® Probe Anti-Rabbit PLUS	Sigma−Aldrich, USA	DUO92002-30RXN
Eppendorf tubes	Eppendorf, Hamburg, Germany	
Ethanol	Fisher Scientific, UK	10428671
Falcon tube	Fisher Scientific, UK	10585801
Foetal bovine serum (FBS)	Invitrogen, UK	26140
Formaldehyde	Fisher Scientific, UK	10041040
Glass coverslips	BDH Chemicals Ltd, UK	
Glass slides	Fisher Scientific, UK	
Glycerol	Fisher Scientific, UK	10152970
Hydrochloric Acid 5%	Fisher Scientific, UK	
Isopropanol	Fisher Scientific, UK	10723124
Isoton II azide−free balanced electrolyte solution	Beckman, UK	177402
Lab−Tek chamber slide system, 8−well glass slide	Sigma−Aldrich, USA	177402
L−glutamine	Invitrogen, UK	25030
Lipofectamine 3000 transfection reagent	Invitrogen, UK	L3000001
Lower buffer for SDS−PAGE gels (Tris 1.5 M, pH 8.8)	BioRad Laboratories Ltd, UK	161−0798
Marvel dried milk	Premium international food, UK	3023034
Magnetic stirrer	Fisher Scientific, UK	
Methanol	Fisher Scientific, UK	10499560

Mounting medium with DAPI	Sigma−Aldrich, USA	DUO82040
N,N,N',N'−tetramethylene−diamine (TEMED)	Fisher Scientific, UK	17919
Nitrocellulose Membrane	Merck, USA	GE10600002
Ponceau S	Sigma−Aldrich, USA	P3504
Penicillin/Streptomycin	Invitrogen, UK	15140
Pierce ECL Western Blotting Substrate	Thermo Scientific, USA	32209
Polyoxyethylene−sorbitan monolaurate (Tween 20)	Sigma−Aldrich, UK	93774
Precision Plus protein blue standards BioRad	BioRad Laboratories Ltd, UK	161−0393SP
Protease inhibitor cocktail (in	Sigma−Aldrich, USA	P8340
Proteome Profiler Human Phospho−Kinase Array Kit	Bio-Techne, UK	ARY003B
Proteome Profiler Human Phospho−Kinase Array Kit	Bio-Techne, UK	ARY003C
Roswell Park Memorial Institute (RPMI) medium 1640	Fisher Scientific, UK	11530586
Roswell Park Memorial Institute (RPMI) medium, phenol−red−free 1640	Fisher Scientific, UK	11564456
Sodium butyrate	Sigma−Aldrich, USA	B5887
Sodium chloride (NaCl)	Sigma−Aldrich, USA	S3014
Sodium dodecyl sulphate (SDS)	Sigma−Aldrich, USA	L3771
Sodium fluoride (NaF)	Sigma−Aldrich, USA	7681-49-4
Sodium orthovanadate (Na3VO4) Sigma−Aldrich,	Sigma−Aldrich, USA	S6508
Sterile disposable pipettes (5 mL, 10 mL and 25 mL)	Sarstedt AG and Co., Nümbrecht, Germany	
Sterile Falcon tubes (15 mL and 50 mL	Sarstedt AG and Co., Nümbrecht, Germany	
Sterile phosphate buffered saline (PBS)	Invitrogen, UK	
Sterile universal containers (30 mL)	Greiner Bio−One Ltd, UK	
SuperSignal West Dura Extended Duration Substrate SuperSignal	Thermo Scientific, USA	34075
SuperSignal West Femto Maximum Sensitivity Substrate	Thermo Scientific, USA	34094
Syringes (5 mL and 10 mL)	Thermo Scientific, USA	10178894
Tissue culture plasticware (24−well plates, filter flasks, 35 mm, 60 mm and 100 mm dishes)	Thermo Scientific, USA	10556661
Trizma (Tris) base	Sigma−Aldrich, USA	T1503
Upper buffer for SDS−PAGE gels (Tris 0.5M, pH 6.8)	BioRad Laboratories Ltd, UK	161−0799
Western blocking reagent	Roche Diagnostics, Germany	11921673001
96 Well Plate	Thermo Scientific, USA	1055-4961

Chapter 3

Computer analysis of ZIP7, ZIP6 and ZIP10 sequences

3.1 Introduction

Zinc is required for living cells to function properly, and the balance of zinc levels within cells is tightly regulated by two families of zinc transporters (Chasapis et al., 2012). ZIP transporters are responsible for cytosolic zinc concentration by influxing zinc into cells or releasing it from cellular stores (Taylor et al., 2008). It has been known that there is a relationship between many of ZIP transporters , particularly those that belong to the LIV-1 subfamily, and the development of human diseases such as cancer (Taylor et al., 2003)(Taylor et al., 2012). ZIP7 is one of these transporters that is responsible for releasing zinc from ER stores. The released zinc leads to activation of multiple downstream pathways related to the progression of cancer (Taylor et al., 2012)(Nimmanon et al., 2017). However, the regulation of how ZIP transporters function is still not fully understood. It is noteworthy that our group has reported a significant mechanism for activation of ZIP7 after phosphorylation by CK2. This mechanism involves the activation of ZIP7 through the phosphorylation of S275 and S276 residues, which are situated in the long cytoplasmic loop rich in histidine between TM3 and TM4 (Taylor et al., 2012). This emphasizes the significance of phosphorylation as a regulatory mechanism for the ZIP transporters. Knowing that ZIP7 is regulated by phosphorylation, it was speculated that there might be other residues that could be phosphorylated as well in order to reach maximal activation for this transporter.

Moreover, it has been reported that ZIP6 is activated by undergoing N-terminal cleavage while in the ER prior to relocating to the plasma membrane. This cleavage occurs at a PEST site that characteristic of proteins with a short half-life (Hogstrand et al., 2013). Whether ZIP6 is required to undergo any post-translational modifications before and after N-terminal cleavage still needs to be studied. The fact that ZIP6 and ZIP10 were found to be a heteromer (Taylor et al., 2016) may indicate that they both need to be controlled in a similar manner , which needs further investigation.

Therefore, the aims of this chapter are to analyse sequences of ZIP transporters and to discover any additional potential phosphorylation sites and candidate kinases mainly in ZIP7, ZIP6, and ZIP10. This chapter also investigates the usefulness of ZIP expressions as prognostic indicators in clinical samples of breast cancer and how their expression correlates with patient survival.

In order to accomplish this, a computational examination of the amino acid sequences of all ZIP transporters was conducted using various online databases.

3.2 Methods

Table 3.1 displays the online database and platforms that were used. To explore the sequences of ZIP transporters, all amino acid sequences of human ZIP transporters (ZIP1 to ZIP14) were obtained in a text based FASTA format from the UniProt page on the National Center for Biotechnology Information (NCBI) gene database. After obtaining the amino acid sequences of ZIP transporters, a phylogenetic tree was created using the Phylogeny.fr web service. Next, the LIV-1 subfamilies were aligned in the FASTA format using the CLUSTAL O program for multiple sequence alignment, and then shaded using the online program Boxshade (Swiss Institute of Bioinformatics). The potential transmembrane (TM) domains of the LIV-1 subfamily were identified by employing several online platforms such as CCTOP, TM Pred and ELM.

To discover the potential phosphorylation sites in ZIP transporters, the subsequent websites were employed: PhosphoNET (Kinexus Bioinformatics Corporation), NetPhorest 3.1. and PHOSIDA (Max Planck Institute of Biochemistry). The number of mass spectrometry studies on these potential phosphorylation sites was obtained from PhosphoSitePlus (PSP). The amino acid sequences for the identified phosphorylation sites and their positions were confirmed by comparing them with the ones obtained from the UniProtKB/Swiss-Prot database (The European Bioinformatics Institute). Moreover, Potential proteolytically−cleaved PEST motifs were detected employing the Emboss Pestfind platform. Additionally, the AlphaFold database, which utilises deep learning algorithms for protein folding predictions, was employed to obtain a predictive structure of ZIP transporters.

A publicly available online tool for gene expression analysis was employed to explore the levels of ZIP transporters in tumour breast tissue samples compared to corresponding normal breast tissues (GEPIA2) (Tang et al., 2019). The data ZIP gene expression obtained from The Cancer Genome Atlas (TCGA) and Genotype-Tissue Expression (GTEx) databases. Another publicly available online database called KmPlot was used to evaluate the correlation between ZIP expression data and survival in patients with breast cancer (Győrffy, 2021).

Data were graphically represented using Affymetrix microarray expression data of messenger RNA (mRNA) for ZIP7 (202667_s_at), ZIP6 (202088_at), and ZIP10 (225295_at) in tumour samples derived from patients with breast cancer. The patient groups were categorized based on "auto-selected" cutoffs and then analysed for both overall survival (OS) and relapse-free survival (RFS). The patient groups were further restricted to those who were treated with either systemic endocrine therapy or only tamoxifen for further analysis.

3.3 Results

3.3.1 Analysis of the sequences of amino acids in ZIP transporters

To illustrate their molecular similarities and evolutionary connections, a phylogenetic tree diagram was initially constructed using the peptide sequences of human ZIP transporters (**Figure 3.1**). The amino acid sequences of the human ZIP transporters were obtained from the NCBI database in the text- based FASTA format. ZIP transporters are categorised according to the phylogenetic tree into four subfamilies, including gufA (ZIP11), subfamily I (ZIP9), subfamily II (ZIP1-3), and the LIV−1 subfamily (4-8, 10, and 12-14). In the phylogenetic tree, if two members are located in the same branch of a tree, it indicates that they have a shared ancestor and are more closely related to each other. ZIP7 and ZIP13 are in the same category of a family tree, indicating that they are closely related to one another. This is further supported by the unique positioning of these two zinc transporters; they are situated on the membrane of intracellular storage compartments, not on the plasma membrane (Kambe et al., 2021). Additionally, ZIP6 and ZIP10 are found in the same branch, indicating that they are also closely related. This is strengthened by the fact that ZIP6 and ZIP10 form a heteromer to become functional (Taylor et al., 2016). Although ZIP5 is not directly linked to ZIP6 and ZIP10, it is believed to have a closer connection to them than to other members of the family because it is on the same branch of the phylogenetic tree. Finally, ZIP8 and ZIP14 are categorized together because their ability to transport other metals such as cadmium, manganese, as well as iron (Lichten and Cousins, 2009)(Hennigar and McClung, 2016).

Table 3.1 Online databases and platforms used for the bioinformatic analysis.

Data	Platforms	Reference
Amino acid sequences	NCBI https://www.ncbi.nlm.nih.gov/gene	-
Phylogenetic tree generation	https://www.phylogeny.fr/	(Dereeper et al., 2008)
Sequence alignment	CLUSTAL Omega https://www.ebi.ac.uk/Tools/msa/clustalo/	(Sievers and Higgins, 2018)
Alignment shedding	BoxShade	(Artimo et al., 2012)
TM prediction	CCTO https://cctop.ttk.hu/ TMPred https://services.healthtech.dtu.dk/ ELM http://elm.eu.org/	(Dinkel et al., 2011)
PEST motif analysis	EMBOSS:Pestfind https://emboss.bioinformatics.nl/cgi-bin/emboss/epestfind	-
Phosphorylation sites	PhosphoNET http://www.phosphonet.ca/ NetPhorest3.1. https://services.healthtech.dtu.dk/service.php?NetPhos-3.1 PHOSIDA http://141.61.102.18/phosida/index.aspx PhosphoSitePlus https://www.phosphosite.org/homeAction.action	(Gnad et al., 2007) (Hornbeck et al., 2015)
Predicted ZIP structure	Alphafold https://alphafold.ebi.ac.uk/	(Ruff and Pappu, 2021)
Ubiquitination Sites prediction	PLMD 3.0 http://plmd.biocuckoo.org/ PhosphoSitePlus https://www.phosphosite.org/homeAction.action	(Xu et al., 2017)(Hornbeck et al., 2015)
Gene expression in cancers samples	GEPIA2 http://gepia2.cancer-pku.cn/#index	(Tang et al., 2019)
Correlation between the expression genes mRNA and survival in cancer patients	KmPlot www.kmplot.com	(Győrffy, 2021)

Figure 3.1 Phylogenetic tree of the human ZIP family of zinc transporters

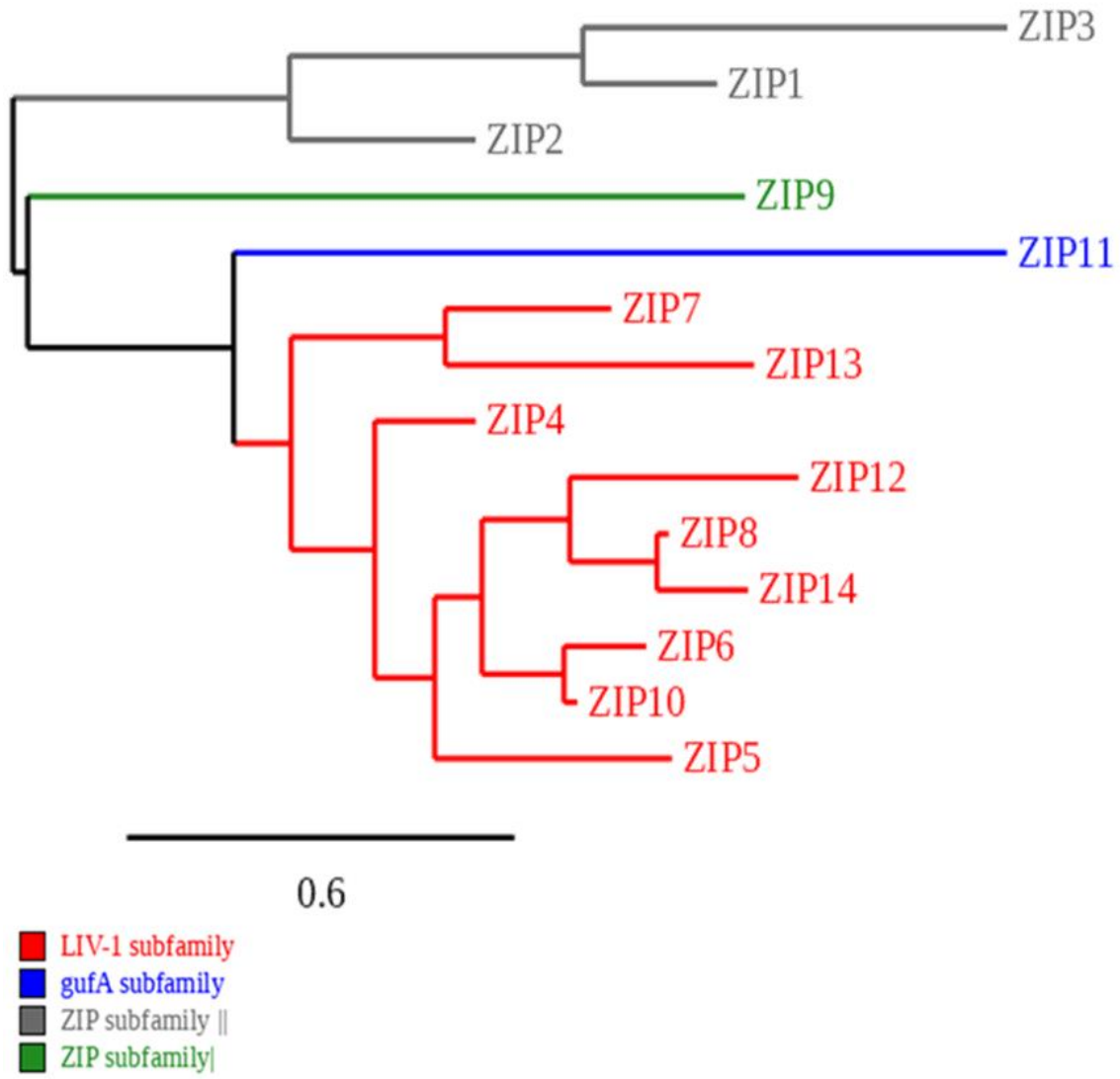

This diagram demonstrates the categorisation of ZIP transporters according to Phylogenetic tree (Larkin et al., 2007). The horizontal axis of the phylogram is measured by the genetic alterations, and the degree of these changes is demonstrated by the scale shown at the bottom bar. The sequences of ZIP proteins were retrieved in FASTA format by using the NCBI database and then the tree was obtained by using the Phylogeny.fr web service (Dereeper et al., 2008).

3.3.2 Computer analysis of LIV-1 subfamily sequences

The LIV-1 subfamily is the largest subgroup in zinc transporters as seen in the phylogenetic tree (**Figure 3.1**). Therefore, the CLUSTAL O program was employed to align the peptide sequences of the human LIV-1 subfamily, and then the resulting alignment was shaded using the Boxshade online program. In the shading, black residues highlight identical amino acids, while grey residues represent those from similar families (**Figure 3.2**). Based on previous computer sequence analysis, all TM regions were identified. Analysing the protein sequences of the zinc transporters has generated valuable insights into the LIV-1 subfamily and its potential role within cells. The LIV-1 subfamily consists of nine members (ZIP4, ZIP5, ZIP6, ZIP7, ZIP8, ZIP10, ZIP12, ZIP13, and ZIP14) and all they are predicted to have eight transmembrane domains connected with N and C−terminus and a long intracytoplasmic loop between TM3 and TM4. In general, the transmembrane domains showed the greatest similarity, which suggests that these proteins are involved in transporting zinc. In contrast, the N-terminus and the loops between TMs highly exhibited diversity, highlighting the potential for different regulation for each transporter. The long cytoplasmic loop is classified as a histidine-rich region, which means it contains a series of consecutive HX repeats (where H represents for histidine and X stands any amino acid). However, the LIV-1 family of zinc transporters has some unique characteristics that are not found in the other members of the ZIP family, which will be discussed below in more detail.

3.3.3 Identification of distinctive features of the LIV-1 subfamily

Compared to all other ZIP transporters, the LIV-1 subfamily exhibits certain distinct features. These consist of an extended histidine-rich N-terminus, a CPALLY motif, a HEXPHEXPHGD region inside TM5 as well as the potential for a PEST cleavage site in ZIP6 and ZIP10.

Figure3.2 Alignment of human LIV-1 subfamily sequences

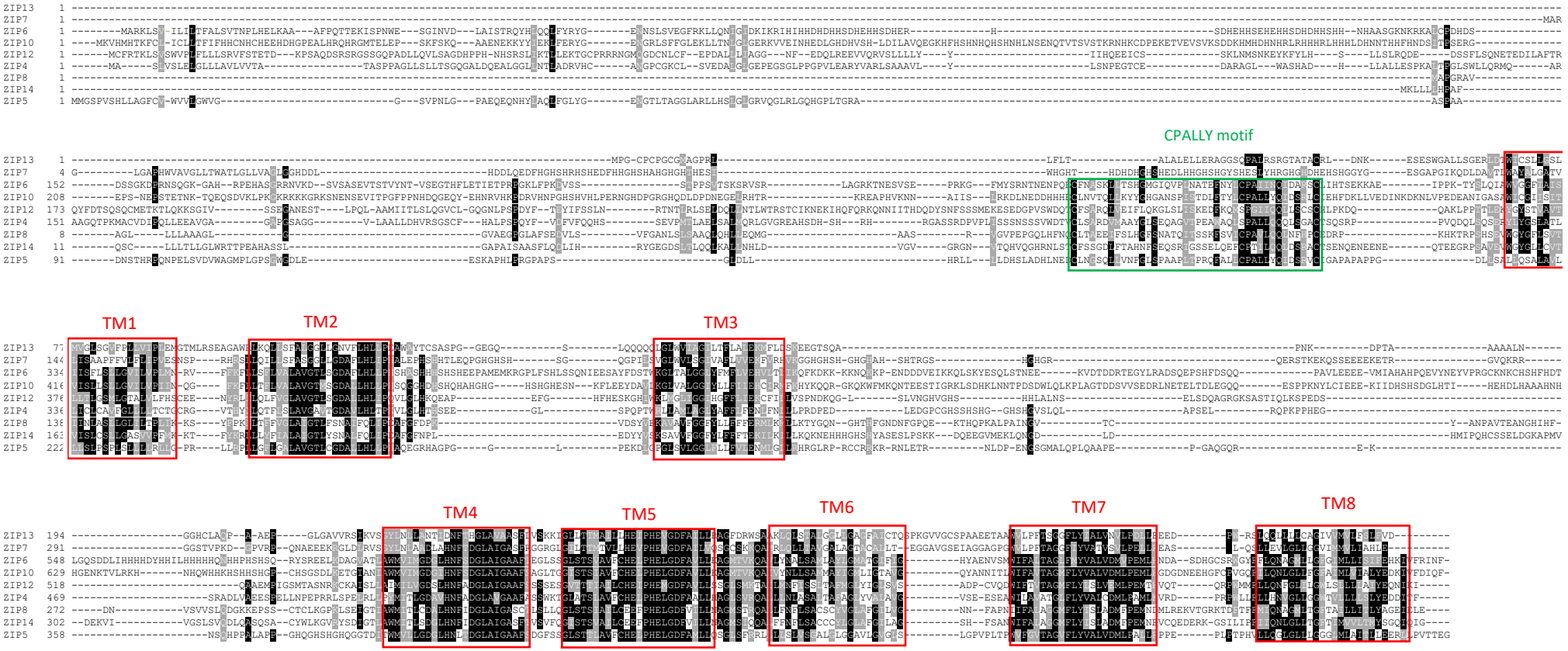

Amino acid sequences of all nine human members of LIV-1 subfamily were aligned employing CLUSTAL O (Sievers and Higgins, 2018) and then shaded using the online program BoxShade (Artimo et al., 2012)(Sievers and Higgins, 2018). In the shading, black residues highlight identical amino acids, while grey residues represent those from similar families. The CPALLY motif, which consists of three cysteine residues that are commonly found in the N-terminus of the LIV-1 subfamily, was highlighted with a green box. However, ZIP7 and ZIP13 did not have this motif. Additionally, the predicted transmembrane regions were also highlighted with red boxes.

3.3.3.1 An extended N−terminus containing histidine−rich regions and a CPALLY motif

The LIV-1 subfamily has a lengthy N-terminus ranging from 68 amino acids in ZIP13 to 408 amino acids in ZIP10 (**Figure 3.3**). This indicates that a lengthy N-terminus is a distinct feature of the LIV-1 subfamily, suggesting a more intricate post-translational modifications for these members as the signal sequences are located in the N-terminus region and the post-translational modifications in the N-terminus has been demonstrated to play a role in regulating the function of the protein (Chen and Kashina, 2021). The presence of histidine-rich regions is not only in the N-terminus, but also found in the extracytoplasmic loop between TM2 and TM3 as well as in the long cytoplasmic loop between TM3 and TM4. The histidine-rich regions have been identified as typical features of the LIV-1 subfamily (**Figure 3.3**) (Taylor et al., 2003). The LIV-1 subfamily possesses histidine residues ranging from a minimum of 10 residues in ZIP8 to 76 residues in ZIP10, which is more than 3 times higher compared with other ZIP transporters. This suggests a considerably higher zinc−binding capacity of the LIV−1 subfamily than other subfamilies, as histidine is known to be a zinc-binding amino acid (Guerinot, 2000).

The presence of a CPALLY motif (C=cysteine, P=proline, A=alanine, L=leucine, Y=tyrosine) is another distinct feature of the LIV-1 subfamily, which are positioned in the N-terminus near TM1. This motif contains three cysteine residues and one proline residue, all of which are highly conserved and identical across the subfamily. It is noteworthy that within the LIV-1 subfamily, only transporters that localize to the plasma membrane contain this CPALLY motif where it is absent in ZIP7 and ZIP13. It has been suggested that the CPALLY motif can sustain structural stability for members of the LIV-1 subfamily. This is due to the cysteine residues within the CPALLY motif have thiol groups that are essential for creating disulfide bonds, which help to stabilize structure of proteins (Taylor et al., 2003). Additionally, another conserved cysteine residue in TM5 which was placed immediately close to the HEXPHEXGD motif. This cysteine residue was found in all members of the LIV-1 subfamily that located in the plasma membrane (**Figure 3.4**).

3.3.3.2 A HEXPHEXGD consensus motif in TM5

In TM5, the motif HEXPHEXGD (H=histidine, E=glutamate, P=proline, G=glutamine, D=aspartate, X=any amino acid) exhibited high level of similarity suggesting it plays a significant role in the protein function of LIV-1 subfamily. This strongly preserved site is thought to be a zinc binding site, as it resembles the catalytic zinc-binding region found in the zincin of metalloproteinases (Hooper, 1994). Both X residues (any amino acid) showed a considerable level of similarity and likeness among the LIV-1 subfamily. This indicates that the HEXPHEXGD motif is widely accepted as standard motif for the LIV-1 subfamily (**Figure 3.5**).

3.3.3.3 A PEST site in the N−terminus of ZIP6 and ZIP10

The PEST motif has been identified as a possible site for proteolytic cleavage (Meyer et al., 2011). Employing the Emboss Pestfind platform, the LIV-1 transporters were analysed for the presence of the PEST motif. ZIP6 and ZIP10 were seen to have strong PEST motifs with PEST scores higher than the threshold score of +5. ZIP6 contained a strong PEST motif positioned in its N-terminus, prior to the CPALLY motif, which had a PEST score of +5.07. While ZIP10 possessed two PEST motifs: the first one in the N-terminus preceding the CPALLY motif, and the other in the cytoplasmic loop between TM3 and TM4. These PEST motifs had PEST scores of +16.60 and +7.97, respectively (**Figure 3.6**). It is noteworthy that there are many PEST motifs particularly in ZIP10, but they did not reach the threshold score. Therefore, they were reported as poor PEST motifs. PEST motifs are usually linked to a shortened half−life of a protein as a result of proteolytic degradation (Meyer et al., 2011). Interestingly, these motifs in ZIP6 have been reported to trigger the activation of this transporter through N−terminal cleavage (Hogstrand et al., 2013), suggesting the vital role for the N-terminus region in ZIP6 and ZIP10 function as well.

Figure 3.3 Structure of the LIV−1 subfamily of ZIP transporters

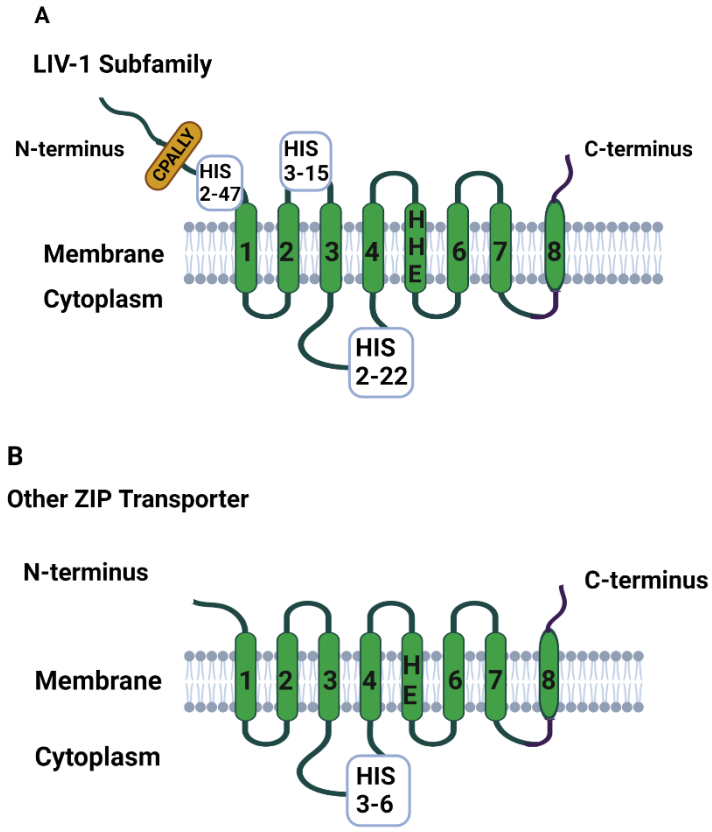

These diagrams show a schematic structure of LIV-1 subfamily (**A**), as compared to other ZIP transporters (**B**). Unique characteristics of this subfamily consist of a longer N-terminal and added regions rich in histidine, located in the N-terminal and the extra-cytoplasmic loop between TM2 and TM3 and between TM3 and TM4. Numbers of histidine detected in particular regions are shown in boxes.

Figure 3.4 The CPALLY motif in the LIV−1 subfamily of ZIP transporters

```
ZIP12   341 CFSARQLVEIFLQKGLSLISKEDFKQMSPGIIQQLLSCSC
ZIP4    270 CLSARDVMAAYGLSEQAGVTPEAWAQLSPALLQQQLSGAC
ZIP8     74 CLTAEEIFSLHGFSNATQITSSKFSVICPAVLQQLNFHPC
ZIP14    91 CFSSGDLFTAHNFSEQSRIGSSELQEFCPTILQQLDSRAC
ZIP5    158 CLNGSQLLVNFGLSPAAPLTPRQFALLCPALLYQIDSRVC
ZIP10   337 CLNVTQLLKYYGHGANSPISTDLFTYLCPALLYQIDSRLC
ZIP6    246 CFNASKLLTSHGMGIQVPLNATEFNYLCPAIINQIDARSC
```

Using the CLUSTAL O platform (Sievers and Higgins, 2018) for multiple sequence alignment, the CPALLY motif seen in ZIP12,ZIP4,ZIP8.ZIP14,ZIP5 ZIP10 and ZIP6 was aligned. The Boxshade (Artimo et al., 2012) was used to shade residues that showed at least 70% identity (black) or similar amino acid families (grey).

Figure 3.5 HEXPHEXGD motif in TM5 in the LIV-1 subfamily.

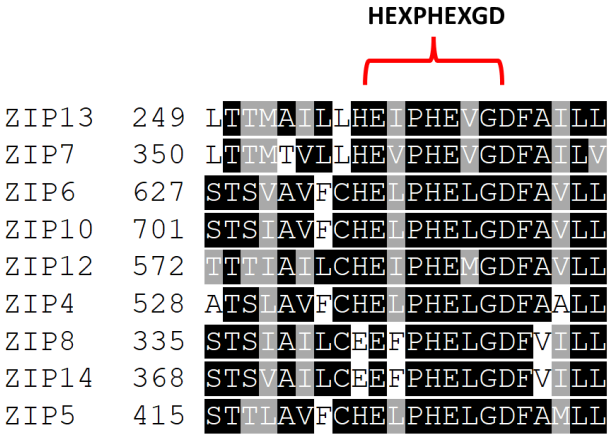

Using the CLUSTAL O platform for multiple sequence alignment, the HEXPHEXGD motif found in the LIV-1 subfamily was aligned. The Boxshade (Artimo et al., 2012) was used to shade residues that showed at least 70% identity (black) or similar amino acid families (grey).

Figure 3.6 Potential proteolytic cleavage sites in ZIP6 and ZIP10

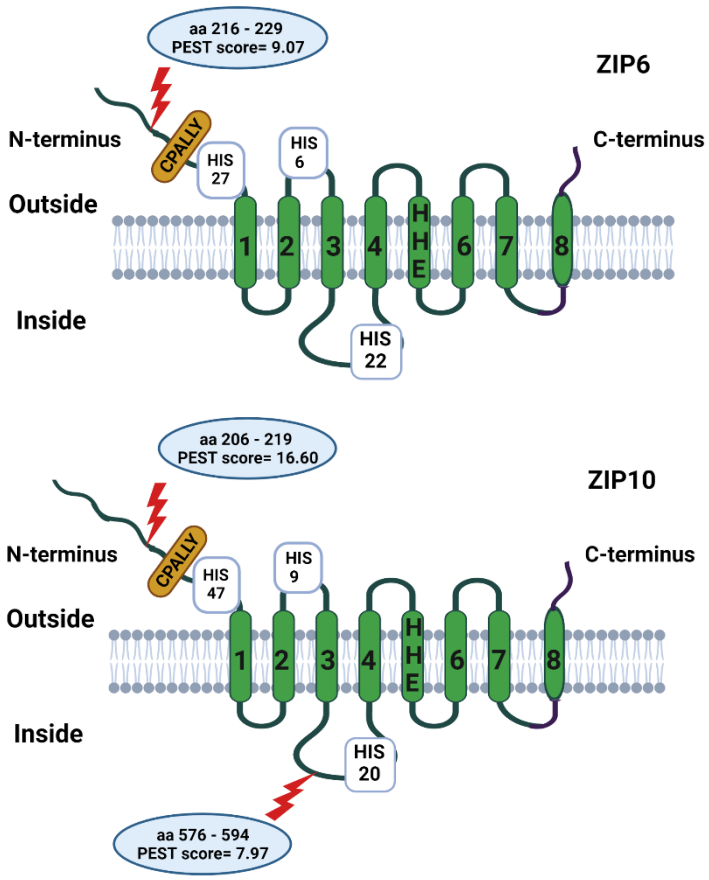

Thease schematics show the predicted PEST sites in ZIP6 and ZIP10. The PEST motifs were Iindicated using Emboss Pestfind platform with the human sequence of ZIP6 and ZIP10 in FASTA format.

3.3.4 Analysis of LIV-1 subfamily by using artificial intelligence

Artificial intelligence has enabled the creation of AlphaFold, a tool that has made a huge improvement in predicting the structure of large and complicated proteins, including zinc transporters proteins such as the LIV-1 subfamily (Ruff and Pappu, 2021). This allows for a substantial comparison of the predicted structure of the LIV-1 subfamily. As this project mainly focused on three zinc transporters ZIP7, ZIP6 and ZIP10, therefore, all of them were predicted through alphaFold (Ruff and Pappu, 2021). As shown in **Figure 3.7**, eight transmembrane domains for all the three ZIPs were apparently seen, which matches the current understanding of ZIP transporters. Additionally, the clearly defined CPALLY motif in the N-terminus of both ZIP6 and ZIP10 was also predicted. Interestingly, ZIP7, which is member of the LIV-1 family but not located on the plasma membrane, do not have this motif. This supports the idea that the motif could be involved in interacting with the pore region and controlling movement through the plasma membrane. Interestingly, both ZIP6 and ZIP10 possess an apparent extension of their TM2 that extends from both sides of the TM region. This unique helical extension is not found in other transporters of the LIV-1 subfamily, implying that it might be associated with the distinct functions of ZIP6 and ZIP10.

3.3.5 ZIP7, ZIP6 and ZIP10 phosphorylation site identification with kinase prediction

The discovery of the activation of ZIP7 through phosphorylation on residues S275 and S276 by CK2 leads to the hypothesis that phosphorylation is important in controlling ZIP transporters post-translationally. Various online databases were used to thoroughly explore the phosphorylation sites in three members of the LIV-1 subfamily, ZIP7, ZIP6 and ZIP10. To narrow the vast number of phosphorylation sites and exclude fewer probable ones, only sites verified through mass spectrometry experiments were listed (**Table 3.2**). These identified sites were compiled and presented with their predicted kinases. Identification of phosphorylation sites was also restricted to residues situated in the cytoplasmic loop between TM3 and TM4, as this region is believed to be functionally significant in the regulation of the LIV-1 subfamily (Taylor et al., 2003). Additionally, the two experimentally confirmed phosphorylation sites in ZIP7, S275 and S276, are situated within this same cytoplasmic loop (Taylor et al., 2012).

For ZIP7 phosphorylation site prediction, S293 and T294 along with the two confirmed residues S275 and S 276 are the only sites shown to be predicted by the phosphorylation prediction databases. These adjacent residues could be required for maximal activation of ZIP7. Interestingly, S293 and T294 are detected to be phosphorylated by MAPKAPK3-2 and PIM1-3 respectively, and these two kinases are known to play a vital role in tumour progression and proliferation which suggests a role for ZIP7 in driving cancer growth (Soni et al., 2019b)(Luszczak et al., 2020).

Through computational analysis, multiple potential sites of phosphorylation were identified located in the cytosolic loop of ZIP6 between TM3 and TM4 as seen in the **table 3.2.** These sites were predicted to be phosphorylated by kinases like GSK-3β, PLK1, CK1, as well as CK2 which most of these kinases are linked with cell cycle regulation. In ZIP6, residues S471, S475, S478, T479, T486, T490, S498, S502, Y528 and Y531 were also identified. S478 has been observed 26 times in mass spectrometry studies, suggesting the phosphorylation in this site is likely to be real. In addition, the residue tyrosine 528 (Y528) has the greatest number of references citing its phosphorylation (126 records), suggesting that this residue plays a significant role in the regulation of ZIP6 through post - translational modification.

Interestingly, most of these selected sites are predicted to be phosphorylated by CK2, the same kinase that has been shown to activate ZIP7 (Taylor et al., 2012). GSK-3ß and cdc2 are also shown as predicted kinases to phosphorylate ZIP6 at serine and threonine residues. Moreover, Src group of kinases is predicted to phosphorylate both tyrosine residues Y528 and Y531. All these kinases are linked with the regulation of cell growth, survival and migration (Sun et al., 2008).

In ZIP10, T536, S539, T540, S546, T553, S570, S573, T583, S591 and Y596 were identified to be phosphorylated. The phosphorylation of serine 591 (S591) is the residue with the highest number of citations (18 records), which suggests that this modification plays a crucial role in regulating ZIP10. Interestingly, ZIP10 was predicted to be phosphorylated by the same kinases that phosphorylated ZIP6 including cdc2 and GSK-3ß. Moreover, PLK1 was predicted to phosphorylate ZIP10, which was an interesting result, as PLK is activated for mitosis (Silva and Cassimeris, 2013), suggesting the role of ZIP10 modification during mitosis.

3.3.6 Further bioinformatic analysis for ZIP6

The mechanisms responsible for the localization and functioning of zinc transporters including ZIP6 are frequently shown to be due to post-translational modifications (Taylor et al., 2012)(Hogstrand et al., 2013) (Taylor et al., 2016). Other than the phosphorylation sites, multiple ubiquitination sites have been found in ZIP6 on the cytoplasmic loop between TM3 and TM4. By employing online databases like PhosphoSitePlus and PLMD 3.0 (Hornbeck et al., 2015), ZIP6 was shown to have several predicted ubiquitination sites on Lysine residues including K456, K457, K467, K468, K472 and K483. These residues were verified through mass spectrometry experiments (Hornbeck et al., 2015)(Xu et al., 2017). Numerous lysine pairs on the ZIP6 sequence may serve as proteolytic signals (Taylor et al., 2003). Furthermore, The low expression and instability of ZIP6 was supposed to be attributed to ubiquitin degradation sites (Hogstrand et al., 2013). Therefore, inhibitor of ubiquitination pathways, could potentially increase the expression of ZIP6. However, this has not been experimentally verified.

Figure 3.7 AlphaFold predicted structure of three LIV-1 family members.

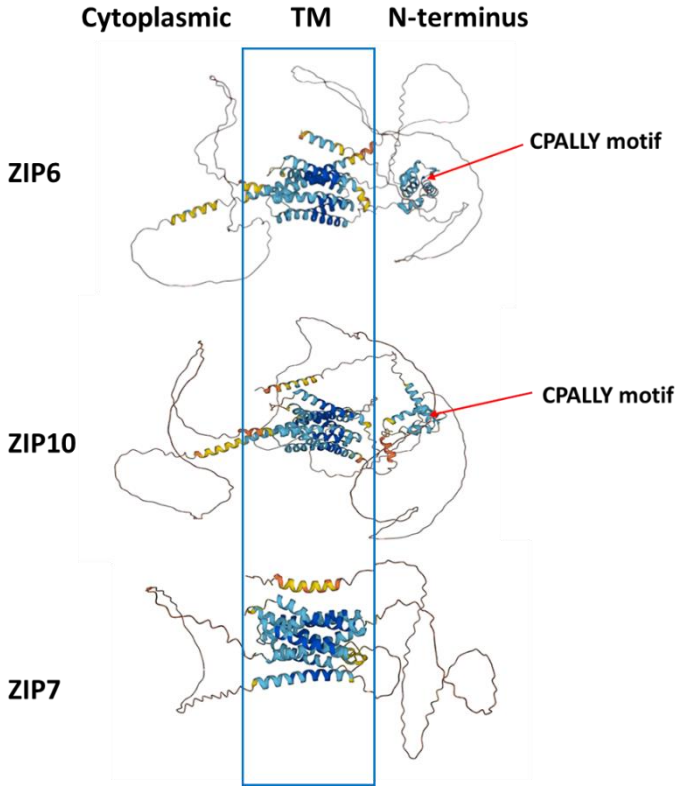

Three LIV-1 family members were predicted through AlphaFold (Ruff and Pappu, 2021). Eight transmembrane domains were predicted as indicated by the blue box. The presence of a distinct CPALLY motif in the N-terminus of both ZIP6 and ZIP10 is also visible as indicated by the red arrows. Moreover, both ZIP6 and ZIP10 possess an apparent extension of their TM2 that extends from both sides of the TM region

Table 3.2 ZIP Phosphorylation sites and predicted kinases

				Predicted Kinases Database		
ZIP	**site**	**Sequence**	**Number of MS studies**	**Kinexus**	**NetPhos-3.1**	**PHOSIDA**
ZIP7	S275	KEKQSSEEE	26	CK2, CK1 and PLK3	CK2, cdc2 and CAMK2	CK2
	S276	EKQSSEEEE	26	CK2, CK1 and ATR	CK2,1 and cdc2	CK2
	S293	RRGGSTVPK	3	MAPKAPK2/3and CHK2	PKA, PKG and CAMK2	CAMK2
	T294	RGGSTVPKD	2	PIM1,2 and 3	PKC, GSK3 and CAMK2	-
ZIP6	S471	KKQLSKYES	3	-	PKA, CK2 and PKC	CK2
	S475	SKYESQLST	4	-	CAMK2, GSK3 and ATM	CK1
	S478	ESQLSTNEE	26	-	CK2, cdc2 and CAMK2	CK1
	T479	SQLSTNEEK	5	-	CK2 PKC and GSK3	CK2
	T486	EKVDTDDRT	2	-	CK2, cdc2 and GSK3	-
	T490	TDDRTEGYL	1	-	GSK3, CK2 and CAMK2	-
	S498	LRADSQEPS	1	-	DNAPK, ATM and CAMK2	GSK3
	S502	SQEPSHFDS	1	-	GSK3, CK2 and CAMK2	CK1
	Y528	PQEVYNEYV	126	-	EGFR and SRC	EGFR
	Y531	VYNEYVPRG	65	-	EGFR and SRC	EGFR
ZIP10	T536	MKQNTEEST	5	ATR, DNAPK and MEK1	CAMK2, GSK3 and CK1	-
	S539	NTEESTIGR	7	PIM1, BARK1 and PLK3	GSK3, cdc2 and CAMK2	-
	T540	TEESTIGRK	3	LRRK2, PLK3and HIPK2	GSK3, CAMK2 and CK1	PLK1
	S546	GRKLSDHKL	6	PIM3,1 and 2	PKA, RSK and PKG	PKA
	T553	KLNNTPDSD	6	JNK1,3 and 2	p38MAPK, GSK3 and CK2	NEK6
	S570	GTDDSVVSE	2	PIM2,1 and NEK10	Cdc2, CAMK2 and GSK3	PLK1
	S573	DSVVSEDRL	2	CK2, PIM2 and 1	CK2,1 and CAMK2	CK1
	T583	ETELTDLEG	1	CK2,1 and BARK1	CK2 and cdc2	CK2
	S591	GQQESPPKN	18	CDK2,1 and JNK1	Cdk5, GSK3 and CAMK2	CDK2
	Y596	PPKNYLCIE	10	SYK and FGR	EGFR and SRK	ALK

The red-colored residues represent the specific residues that undergo phosphorylation. Total number of MS studies is shown where this site of modification was identified using proteomic discovery mass spectrometry, sourced from PhosphoSite Plus (Hornbeck et al., 2015). Predicted phosphorylation residues on the loop between TM3 and TM4 of ZIP7, ZIP6 and ZIP10 was obtained by using of Kinexus, NetPhos-3.1 and PHOSIDA.

3.3.7 Examination of ZIP transporters in clinical samples using publicly available online databases

To investigate prognostic significance and the potential therapeutic of ZIP transporters in breast invasive carcinoma (BRCA), GEPIA 2 server (Tang et al., 2019) was employed to compare the mRNA expression level of ZIP transporters in breast tumour samples with normal healthy samples. All findings demonstrate gene expression data obtained from The Cancer Genome Atlas (TCGA) and the Genotype-Tissue Expression (GTEx) databases. The data were filtered to represent only differential gene expression connections. Initially, all 9 human members of the LIV-subfamily of ZIP transporters were analysed. Within the LIV-1 subfamily, only ZIP4, ZIP6, and ZIP7 exhibited significant differences between normal and tumour tissues, all of which displayed a substantial increase in tumour tissues ($P < 0.01$) (**figure 3.8**). These finding indicates that all these transporters are potential biomarkers for aggressive breast cancer. In contrast, ZIP10 exhibited a tendency to increase in tumour samples but it was not significant. The fact that the level of ZIP6 was significantly increased in many different tumour tissues whereas the level of ZIP10 was only slightly increased suggest that ZIP6 may be more dominant than ZIP10 in this process.

3.3.8 Investigation the effect of ZIP expression on the outcome of patient survival in breast cancer

Having established that ZIP7 and ZIP6 are significantly increased in tumour samples, the next aim was to investigate how this change impacts the prognosis and progression of the disease. To achieve this, the Kaplan-Meier Plotter tools was used to generate a correlation between ZIP6 and ZIP7 expression and the survival of breast cancer patients with various molecular subtype. The Kaplan-Meier Plotter is a publicly available online database that analyses the impact of more than 50.000 genes on the clinical outcome of patients with 21 distinct types of cancer, such as breast cancer, with a sample size of 7,830 (Győrffy, 2021). Gene expression data and the survival information are obtained from The Cancer Genome Atlas (TCGA), Gene Expression Omnibus (GEO) and European Genome- phenome Atlas (EGA). Data on ZIP7 (202667_s_at), ZIP6 (202088_at) and ZIP 10 (225295_at) expression in breast cancer tumour samples were obtained using Affymetrix microarray technology to analyse messenger RNA (mRNA).

JetSet optimized probes were used for ZIP7, ZIP6 and ZIP10. The cut-off value of gene expression was determined using the auto-select best cut-off method, which divided the patient samples into two groups for generating corresponding plots. An assessment was performed to determine the correlation between the ZIP7, ZIP6 and ZIP10 with overall survival (OS) relapse-free survival (RFS). Additional analysis was conducted by limiting the patient groups to those who received systemic endocrine therapy and those who were treated with tamoxifen only. Both evaluations included patients who were treated with chemotherapy. The Kaplan-Meier plotter website was used to calculate log-rank P-values. A P-value < 0.05 was considered to indicate a statistically significant difference between high and low ZIP7 or ZIP6 expression.

In general, an elevated level of ZIP7 in patients was strongly associated with a worse prognosis. Patients with high levels of ZIP7 tend to have lower rates of OS (66.12 months) and RFS (171.43 months), compared to 105.44 and 216.66 months, respectively (**Figure 3.9 A**). It is noticeable that the OS of patients who received systemic endocrine therapy was not influenced by their ZIP7 levels. However, the RFS of these patients was notably lower (**Figure 3.9 B**). When the subgroup analysis was restricted to patients who received only tamoxifen treatment, a marked decrease in RFS was observed, while the OS remained unaffected (**Figure 3.9 C**). These findings suggest that high expression of ZIP7 indicate a lack of response to tamoxifen treatment and could potentially be a mechanism for the development of resistance.

In contrast, investigation of ZIP6 exhibited a significant positive association between expression and prognosis, with patients who had high levels of ZIP6 showing increased OS (125.92 months) and RFS (65 months), compared to 63.52 and 28.96 months, respectively (**Figure 3.10 A**). Moreover, the OS patients who received systemic endocrine therapy were not influenced by their ZIP6 levels. However, high expression of ZIP6 had significantly improved RSF in these patients (**Figure 3.10 B**). Additional investigation based on treatment indicated that in patients who only received tamoxifen, ZIP6 expression did not have a significant effect on both OS and RFS (**Figure 3.10 C**). These findings indicate that ZIP6 was linked to a better prognosis in breast cancer patients who received systemic endocrine therapy. Therefore, it could potentially be a biomarker of good prognosis in breast cancer.

In ZIP10, high expression was negatively correlated with RFS (36.96 months), compared to 42 months in the low expression group (**Figure 3.11 A**).

No change was noticed in RFS within patients who received systemic endocrine therapy or tamoxifen alone groups (**Figure 3.11 B and C**). However, no data was available related to OS in these two groups.

Figure 3.8 Differences in expression level of LIV-1 subfamily members in matched cancerous and normal breast tissues

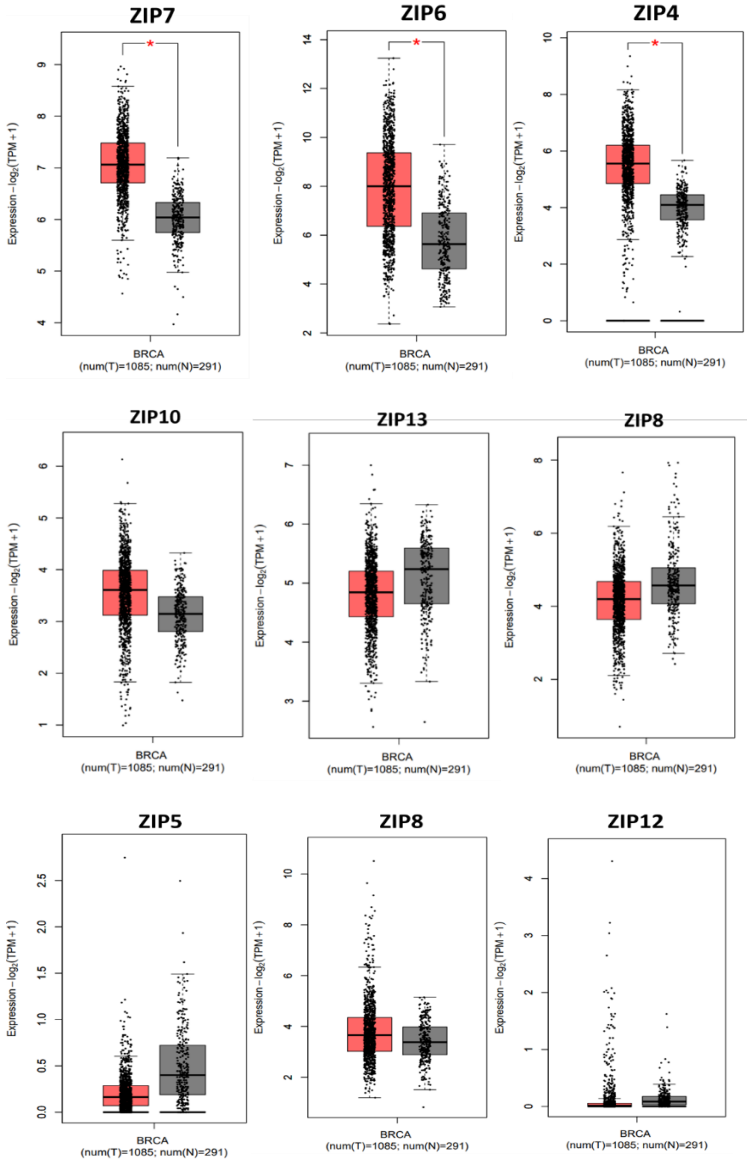

The GEPIA 2 (Tang et al., 2019) generated boxplots exhbiting the variations in the LIV-1 members expression between normal and cancerous breast tissues (Tang et al., 2019). Grey and red boxes represent normal and cancerous tissues, respectively. All data were based on matched gene expression data obtained from TGCA and GTEx databases. the X-axes indicate the number of normal (N) and tumour (T) samples analyzed.

Figure 3.9 ZIP7 related to overall survival and relapse-free survival after chemotherapy

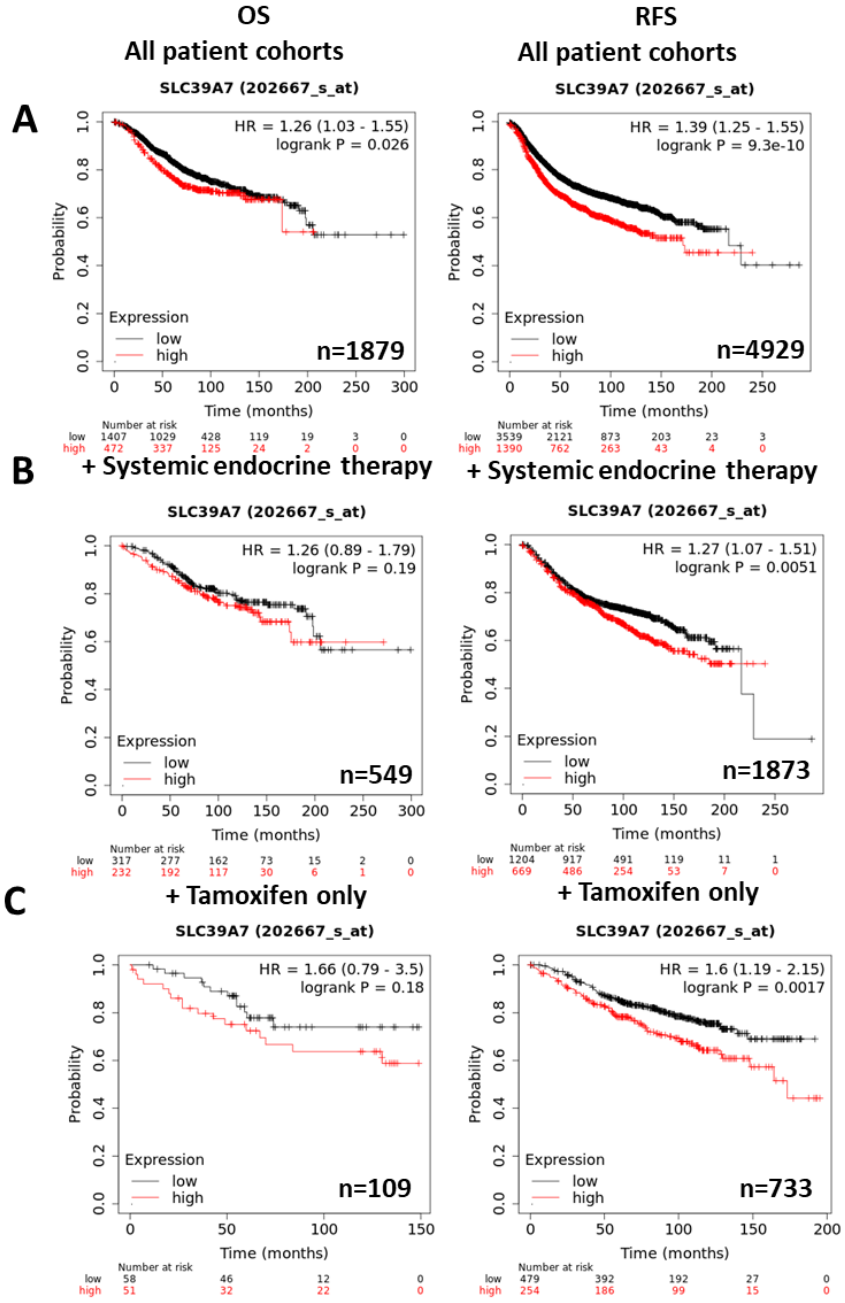

The relationship between ZIP7 mRNA expression and OS and RFS in breast cancer patients was generated using Kaplan-Meier plots (Győrffy, 2021). The KMPlot tool was used to generate these plots, with the expression groups distinguished by "auto-selected" thresholds. The probe sets were optimised using the "JetSet" function. The scope of patient groups was gradually refined from an unrestricted analysis (A), to those who underwent systemic endocrine therapy (B), and finally to those specifically treated with tamoxifen (C). The diagrams illustrate hazard ratios (HRs) and significance values (P), along with the number of patients incorporated in each analysis (n).

Figure 3.10 ZIP6 related to overall survival and relapse-free survival after chemotherapy

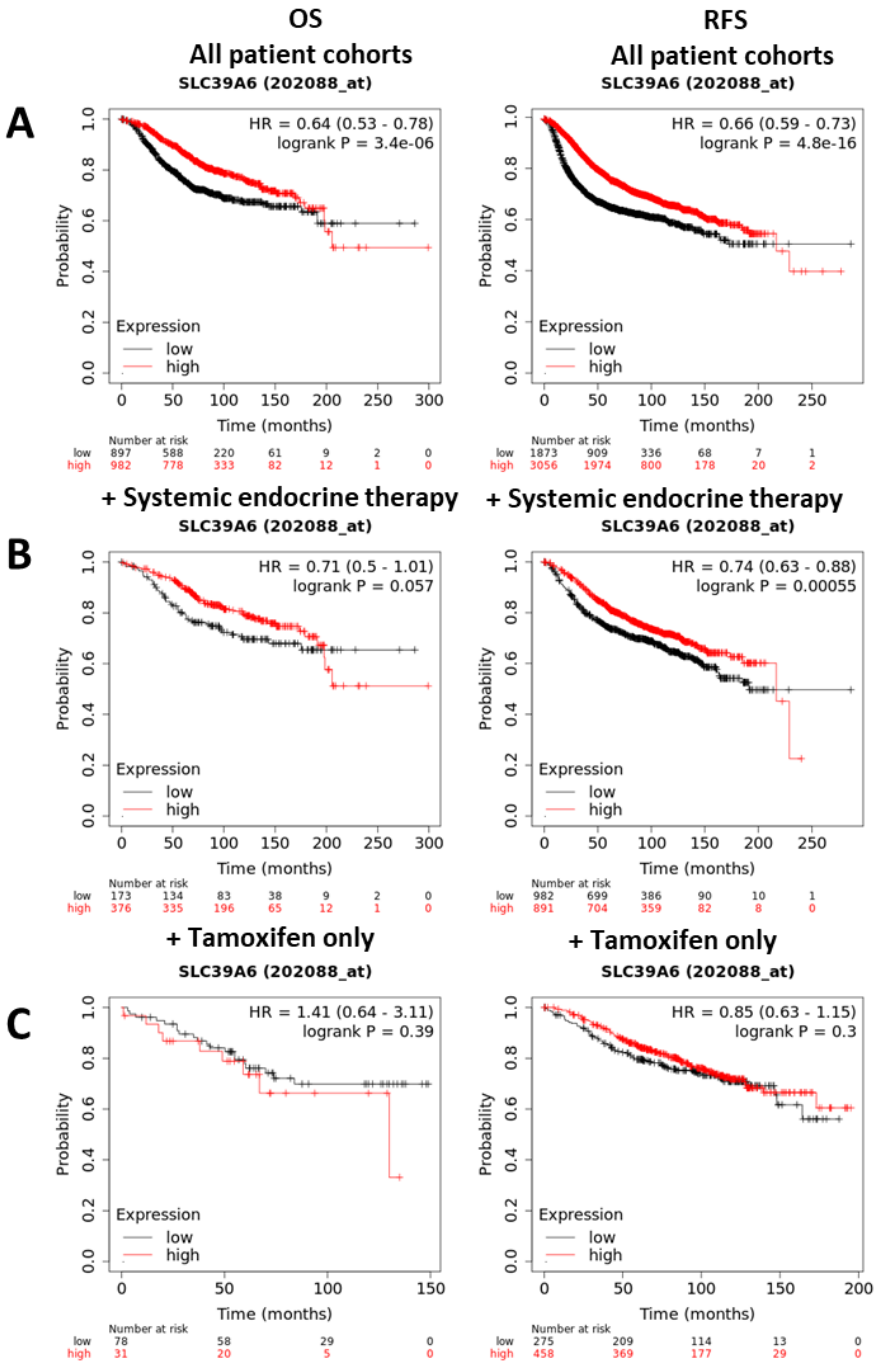

The relationship between ZIP6 mRNA expression and OS and RFS in breast cancer patients was generated using Kaplan-Meier plots (Győrffy, 2021). The KMPlot tool was used to generate these plots, with the expression groups distinguished by "auto-selected" thresholds. The probe sets were optimised using the "JetSet" function. The scope of patient groups was gradually refined from an unrestricted analysis (A), to those who underwent systemic endocrine therapy (B), and finally to those specifically treated with tamoxifen (C). The diagrams illustrate hazard ratios (HRs) and significance values (P), along with the number of patients incorporated in each analysis (n).

Figure 3.11 ZIP10 related to overall survival and relapse-free survival after chemotherapy

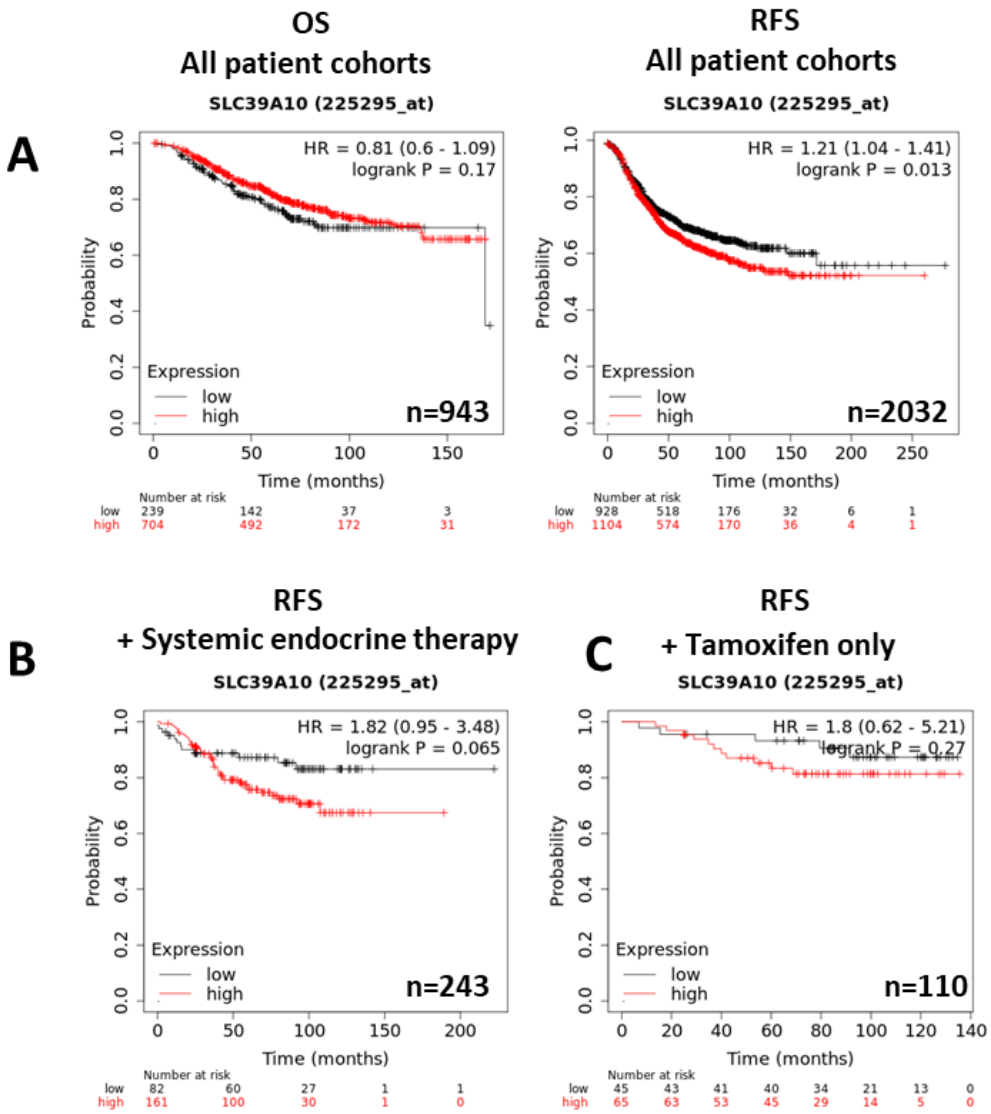

The relationship between ZIP10 mRNA expression and OS and RFS in breast cancer patients was generated using Kaplan-Meier plots (Győrffy, 2021). The KMPlot tool was used to generate these plots, with the expression groups distinguished by "auto-selected" thresholds. The probe sets were optimised using the "JetSet" function. The scope of patient groups was gradually refined from an unrestricted analysis (A), to those who underwent systemic endocrine therapy (B), and finally to those specifically treated with tamoxifen (C). The diagrams illustrate hazard ratios (HRs) and significance values (P), along with the number of patients incorporated in each analysis (n).

3.4 Chapter Summary

The analysis of ZIP transporters employing computational sequencing showed all ZIP transporters contain eight transmembrane domains and provided that the LIV-1 subfamily possesses distinct features when compared to all other ZIP transporters (**Figure 3.2**). Compared to other subfamilies, the members of the LIV-1 subfamily appear to have a longer N-terminus (**Figure 3.3**), indicating that these ZIP transporters may have a more complicated post-translational regulation. Moreover, apart from ZIP7 and ZIP13, the CPALLY motif was found in the N-terminus of members of the LIV-1 subfamily (**Figure 3.4 and Figure 3.7**). This sequence, which is located preceding TM1, includes three consensus cysteine residues. Furthermore, a unique conserved motif, HEXPHEXPHGD motif, was observed in TM5, indicating its importance to the protein function of LIV-1 subfamily (**Figure 3.5**). The N-terminus of ZIP6 and ZIP10 consists of a PEST motif, which is distinctive and supports previous studies that have showed proteolytic cleavage as an important mechanism for these two ZIP transporters (**Figure 3.6**).

Furthermore, the investigation of phosphorylation sites identified several locations in the cytoplasmic loop between TM3 and TM4 of ZIP7, ZIP6 and ZIP10, which had been validated through mass spectrometry (**Table 3.2**). In ZIP7, investigation into additional phosphorylation sites revealed the potential phosphorylation of S293 and T294, which are predicted to be significant sites of phosphorylation and will be subject to experimental examination in the next chapter. ZIP6 also revealed multiple phosphorylation and ubiquitination sites in various online databases, indicating that these residues might be essential for the localisation and regulation of ZIP6. Chapter 5 will conduct further investigation of these ubiquitin potential sites on ZIP6.

By using human tumour databases, the prognostic value of ZIP transporters in breast invasive carcinoma was assessed. ZIP7, ZIP6 and ZIP4 showed a significant increase in cancer tissue, while ZIP10 indicated a tendency to increase but not significant (**Figure 3.8**). This suggests the role of these transporters in driving cell growth and/or cell division. The impact of ZIP expression on disease progression was also investigated using Kaplan-Meier plots tool. An elevated level of ZIP7 was correlated with a decrease OS and RFS, indicating that ZIP7 could play a role in driving breast cancer progression (**Figure 3.9**).

In contrast, ZIP6 was positively correlated with improved OS and RFS (**Figure 3.10**). Therefore, it could potentially be a biomarker of good prognosis in breast cancer.

Chapter 4

Identification of novel phosphorylation sites on ZIP7 transporter and characterization of the responsible kinases

4.1 Introduction

Zinc, which is a vital micronutrient for the body, has been associated with several diseases, such as breast cancer. ZIP7, which is a zinc transporter located on the ER, plays a vital role in the progression of tamoxifen resistance in breast cancer, which contributes to aggressive behaviour in tamoxifen-resistant cells (Taylor et al., 2008). This is supported by the data showing that elevated expression of ZIP7 is associated with unfavourable clinical outcomes of breast cancer. In the previous chapter, the bioinformatics data identified four potential phosphorylation sites in ZIP7. Out of all the identified sites, only the two specific residues located in ZIP7, namely S275 and S276, have been experimentally verified to be phosphorylated by CK2 (Taylor et al., 2012). The CK2 activation of ZIP7 promotes zinc release from cellular stores into the cytoplasm. The released zinc then inhibits protein tyrosine phosphatases and activates cellular serine kinases such as MAPK, mTOR and PI3K-AKT, which together enhance tumour cell growth and motility (Nimmanon et al., 2017). In a previous section, the exploration of databases had revealed the existence of additional sites where phosphorylation occurs on ZIP7. These sites, namely S293 and T294, are located in the same cytoplasmic loop as S275 and S276. However, it is still not experimentally confirmed whether S293 and T294 residues are required for maximal activation of ZIP7 transporter. Therefore, this chapter aims to confirm the potential residues on ZIP7 that are involved with phosphorylation and investigate the role of responsible kinases in ZIP7 activation.

This chapter will firstly examine the role of potential residues in ZIP7 by using immunofluorescence and western blot techniques. These experiments were designed to see the effect of S293 and T294 residues on ZIP7 activation by employing ZIP7 mutations, where the active site residue had been changed with an alanine in order to prevent phosphorylation. Secondly, the chapter will confirm the kinases that physically interact with ZIP7 by using proximity ligation assay. Finally, the downstream effect of these kinases on ZIP7 activation will be investigated. These experiments were designed to identify the signalling pathways involved in ZIP7 activation by using phosphokinase arrays.

Overall, this chapter will provide further information concerning the phosphorylation of ZIP7 and how this contributes to the understanding of the molecular mechanisms of ZIP7 activation.

4.2 Methods

All ZIP7 mutant constructs have been placed into a plasmid vector that is resistant to ampicillin, with or without His tag. The constructs without a His tag are referred to as No His. The constructs were then amplified by transforming them into the JM109 E. coli. The EndoFree Plasmid Maxi Kit (Qiagen) was used to purify the plasmids of ZIP7 mutant constructs. The purity and concentration of the plasmid DNA was determined using a UV spectrophotometer, which revealed that the OD260/OD280 ratios were in the desired range of 1.8-2.0. This indicates the purity of the DNA. The DNA concentration ranged from 0.45 to 2.33 µg/µL. (**Table 4.1**). For information on the techniques used for transfection (Section2.1.2) and zinc treatment (Section 2.1.3), generation of recombinant proteins (2.2), plasmid preparation (Section 2.3), immunofluorescence (Section 2.4), and western blotting (Section 2.5), proximity ligation assays (Section 2.7), Phospho-Kinase Array (Section 2.8) please refer to Chapter 2.

Table 4.1 DNA concentration and OD260/280 ratio of prepared plasmids

Plasmid	DNA concentration µg/µl	OD260/280 Ratio
ZIP7 Wild-Type	1.653	1.897
ZIP7 275A /276A	2.338	1.907
S293A	1.808	1.887
T294A	1.14	1.900
ZIP7 Wild-Type	0.8	1.85
ZIP7 Wild-Type No His	0.45	1.86
AA No His	2.3	1.80
4A No His	2.29	1.85

The plasmid DNA was determined with a UV spectrophotometer. OD260/OD280 ratios ranged from 1.8 to 2.0, indicating the purity of the DNAs. No His means the plasmid vector was made without His tag.

4.3 Results

4.3.1 Using pZIP7 antibody to recognise the activated ZIP7 and investigate its downstream targets.

The first set of questions aimed to examine the role of potential residues in ZIP7 and investigate the downstream effects of ZIP7 activation. In order to investigate these, MCF-7 cells were initially transfected with wild type ZIP7 (WT) and S275A/S276A (AA) to test their transfection efficiency and localisation pattern.

4.3.1.1 Verification of ZIP7 WT and AA mutant

Immunofluorescence was performed using a V5 antibody which binds to the C−terminal V5 tag of the recombinant proteins. **Figure 4.1 A** showed a robust transfection of WT and AA in MCF-7 cells confirming by V5 (red) and illustrated the location of the recombinant protein on the endoplasmic membrane. When the transfected cells were viewed more closely, it was evident that the recombinant proteins were expressed strongly and exhibited an ER localization pattern, as is typical of ZIP7. This finding was in agreement with a previous study that showed the co-localization of ZIP7 with the ER marker (Calreticulin) in CHO cells (Taylor et al., 2004). To determine the transfection rate, the number of cells expressing the V5 tag was quantified in three randomly selected visual fields. The percentage of transfection efficiency ranged from 40% to 47%, confirming a comparable rate (**Figure 4.1 B**).

4.3.1.2 The ability of pZIP7 antibody to recognise activated ZIP7

The pZIP7 antibody used was made in house as a monoclonal antibody that binds to ZIP7 when it is phosphorylated on S275 and S276 (Ziliotto et al., 2019). The peptide epitope for this antibody is TKEKQ pS pS EEEEK (positions 270−281) on a long cytoplasmic loop between TM3 and TM4 of ZIP7 (**Figure 4.2**). To examine the specificity of this antibody in recognising the activated ZIP7, immunofluorescence was performed in MCF-7 cells transfected with ZIP7 WT and ZIP7 AA where serine residues S275 and S276 were mutated to alanine in an effort to produce a phosphoablative (null) mutant. The recombinant proteins were identified through the use of a V5 antibody. In MCF-7 cells transfected with WT ZIP7, 20% of these cells were positive for the pZIP7 antibody in basal conditions. When cells were treated with zinc and sodium pyrithione for 10 minutes, a significant increase was observed in the number of transfected cells that tested positive for pZIP7, around 40%. This indicates the ability of the pZIP7 antibody to recognise the active form of ZIP7 (**Figure 4.3 A**).

In contrast, no pZIP7 antibody recognition was observed in the AA mutant, either in basal condition or after stimulating by zinc. This result further confirms that the S275 and S276 residues in ZIP7 are instrumental in the activation of ZIP7 (**Figure 4.3 B**). This finding also provides additional evidence supporting the previous results, which demonstrated that the elimination of two serine residues (S275/S276) inhibited the phosphorylation of ZIP7 by CK2.

4.3.1.3 Confirmation that AKT activation is downstream of ZIP7 activation

When CK2 phosphorylates ZIP7, it triggers the release of zinc from cellular stores. This release then inhibits tyrosine phosphatases, which are important in the growth and spread of cancer, and the activation of tyrosine kinases (Taylor et al., 2012). To confirm a ZIP7-mediated zinc release and downstream effector of this release, western blot was performed with cells transfected with WT and AA mutant in the presence and absence of zinc as an external stimulation. The western blot showed a significant increase in ZIP7 activity after zinc treatment in WT samples. In contrast, no increase was observed in AA sample after zinc treatment (**Figure 4.4 A**). Furthermore, the activated ZIP7 was significantly higher in WT compared with AA after zinc treatment (**Figure 4.4 B**), confirming the responsibility of S275 and S276 residues for the activation of ZIP7 and the ability of pZIP7 to recognise these residues when they are phosphorylated.

AKT has previously been demonstrated to be activated as an early indicator of the downstream pathway triggered by zinc release mediated by ZIP7 (Nimmanon et al., 2017). To validate previous observations that the introduction of zinc leads to an increase in ZIP7-mediated zinc release, western blotting was performed in cells transfected with WT and AA mutant. Zinc treatment significantly increased $pAKT^{S473}$ activity in WT and AA samples (**Figure 4.4 A**). Interestingly, AA mutant significantly attenuated effect of zinc compared to WT ZIP7, as judged by $pAKT^{S473}$ activation (**Figure 4.4 C**). This activation of AKT is consistent with the early phosphorylation of ZIP7 on residues S275 and S276 by CK2, which was observed two minutes after the administration of zinc (Taylor et al., 2012). These results suggest that less activation of ZIP7 leads to a reduced activation of AKT, confirming the AKT activation as a reliable marker of zinc release facilitated by ZIP7 activation. However, the AA mutant did not completely inhibit the activation of ZIP7, this could indicate that other residues might be involved in ZIP7 activation along with S275 and S276.

Figure 4.1 Verification of ZIP7 WT and AA mutant

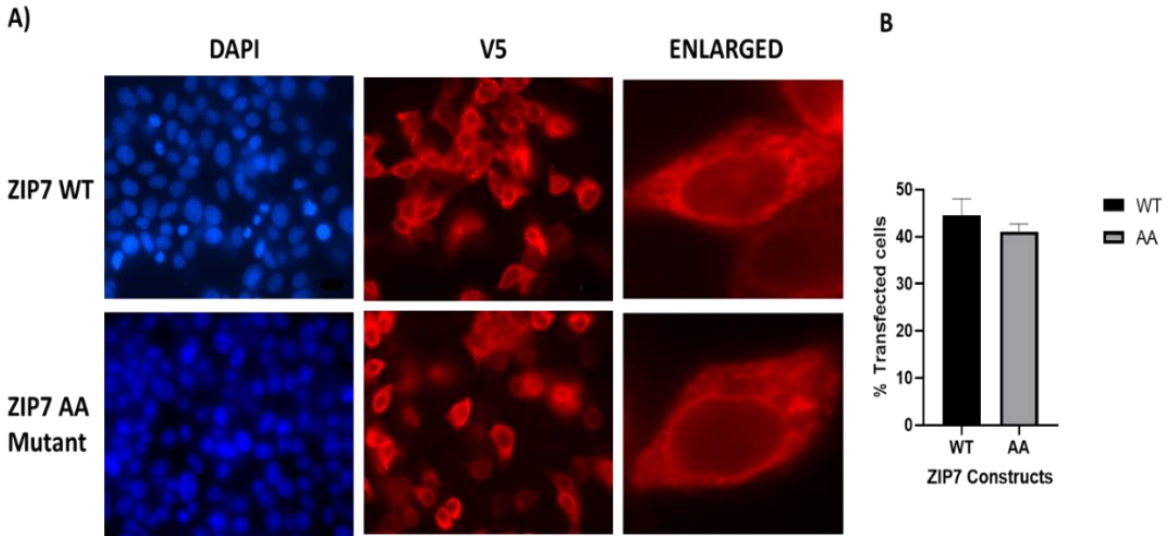

MCF-7 cells were transfected with wild-type (WT) or S275A/S276A (AA) ZIP7 mutant. The cells were stained for V5 (red) and DAPI (blue) and imaged using a 63x magnification lens on Leica RPE automatic microscope (**A**). Demonstration a robust transfection of both mutants confirmed by calculating the percentage of V5 positive cells among the total number of cells that expressed DAPI staining in three random representative fields (**B**). Scale bar, 10 µm

Figure 4.2 The peptide epitope of the pZIP7 antibody

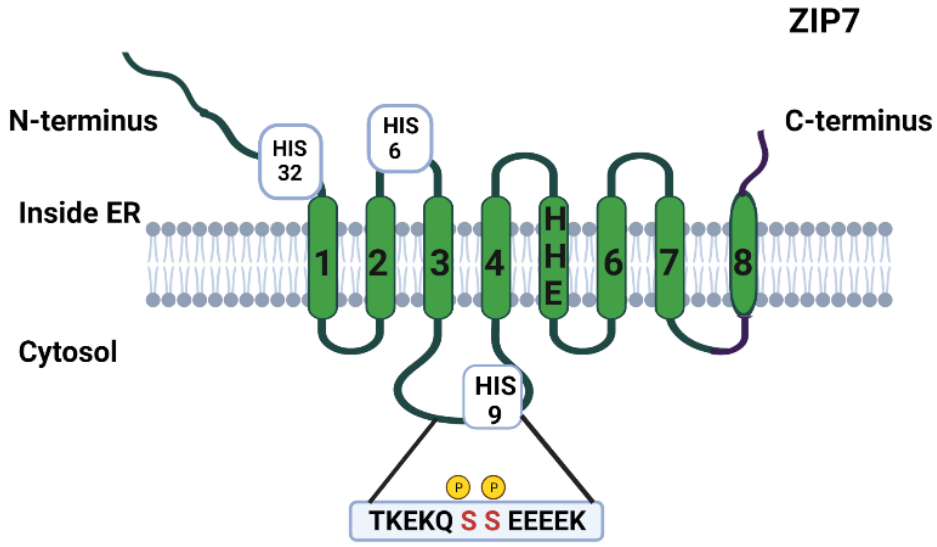

The pZIP7 antibody has been developed by our group that binds to two phosphorylated serine residues on 275 and 276 (Ziliotto et al., 2019). The peptide epitope for this antibody is TKEKQ pS pS EEEEK (positions 270−281).

Figure 4.3 A ZIP7 antibody recognises phosphorylated ZIP7 after zinc treatment

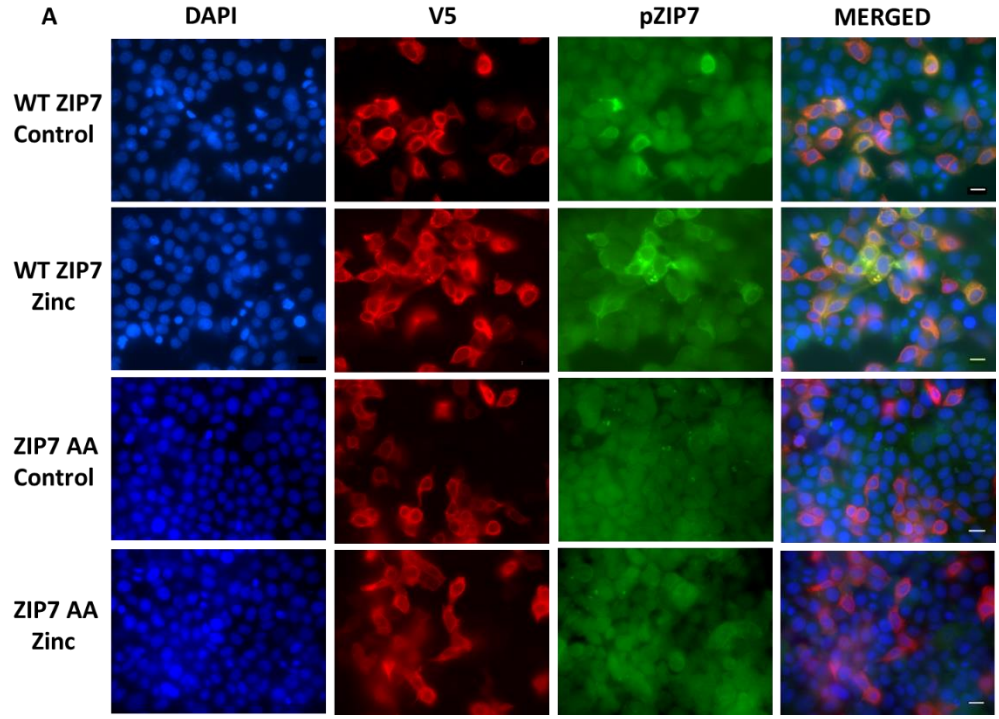

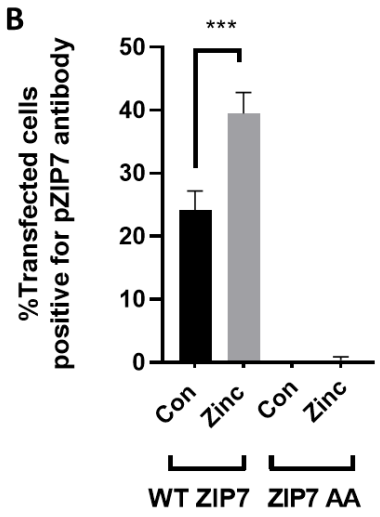

MCF-7 cells were transfected with wild-type (WT) or S275A/S276A (AA) ZIP7 mutant and then treated without zinc and with zinc 20µM plus sodium pyrithione 10µM for 10 minutes. Cells were stained for DAPI (blue) , V5 (red) and pZIP7 (green) and imaged using a 63x magnification lens on Leica RPE automatic microscope (**A**).The difference between the expression of pZIP7 antibody in WT cells with and without zinc was significant as shown in a graph as mean of 3 random representative fields ± standard error (**B**)*** $p < 0.0001$. scale bar 10, um

Figure 4.4 The ability of pZIP7 antibody to detect phosphorylated ZIP7 and its downstream target

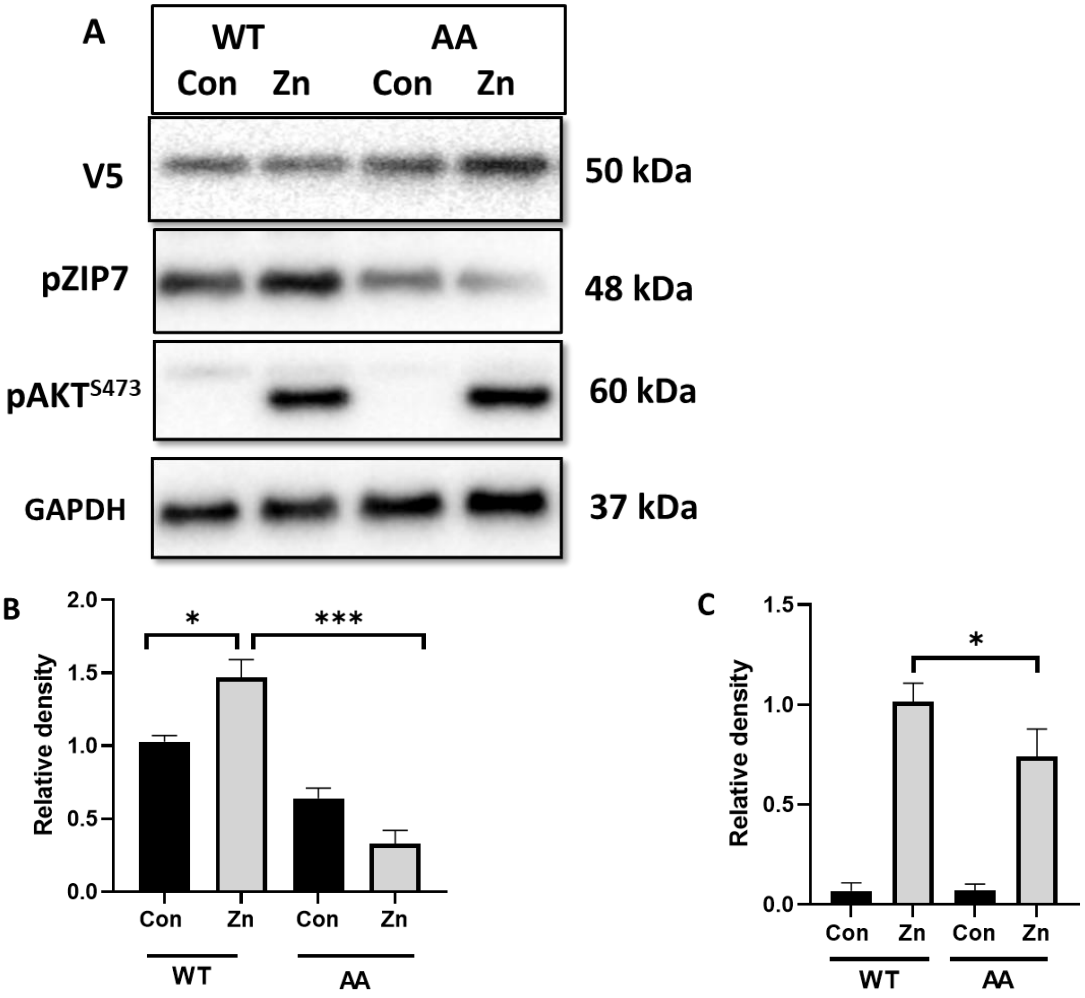

MCF-7 cells were transfected with wild-type ZIP7 (WT) or S275A/276A AA and then treated without zinc (Con) and with zinc 20µM plus sodium pyrithione 10µM for 10 minutes (Zn). A representative band probing for pZIP7, pAKT^{S473}, V5 and GAPDH is shown in (**A**). Densitometric data normalised to V5 are demonstrated for pZIP7 (**B**) and pAKT^{S473} (**C**) in a bar graph as mean ± standard error (n = 3).

4.3.2 Involvement of potential phosphorylation sites in ZIP7 activation

It has been shown that the ZIP7 is phosphorylated by CK2 on S275 and S276 residues in order to release zinc from cellular stores (Taylor et al., 2012). However, the previous results showed that blocking these two residues was not able to completely inhibit the activation of ZIP7. Therefore, the protein sequence of ZIP7 was examined for any additional potential phosphorylation sites that could be involved in activating ZIP7. Three websites were employed including Kinexus, PHOSIDA and NetPhos-3.1 to explore predicted phosphorylation sites on ZIP7. As shown in chapter 3 (**Table 3.2**), two residues S293 and T294 on ZIP7 were predicted to be phosphorylated by MAPKAPK3-2 and PIM1-3 respectively. Interestingly, these two kinases play a vital role in cell progression and proliferation (Soni et al., 2019a) (Yang et al., 2018). This could indicate that the role of MAPKAPK2-3 and PIM1-3 in cell proliferation might be facilitated through phosphorylation of ZIP7 on S293 and T294 residues.

4.3.2.1 S293A and T294A ZIP7 mutants are robustly transfected

To investigate the effect of these sites on ZIP7 activation, the DNA sequences of S293A and T294A were prepared where serine (S293) and threonine (T294) were individually mutated to alanine to prevent phosphorylation at these residues. To verify that the transfection efficiency was comparable to the wild type ZIP7, immunofluorescence was performed. This involved staining MCF-7 cells that had been transfected with the WT ZIP7 and the mutant ZIP7 constructs with a V5 antibody. The results demonstrated that the WT ZIP7 and mutants were robustly transfected (red) and showed their location on the ER (**Figure 4.5 A**). As expected, enlarged images of the cells transfected with these mutants observed that V5 were localized in the same area, exhibiting an ER-like pattern of staining as is typical of WT ZIP7. The proportion of cells positive for the V5 tag was counted in four randomly selected visual fields in order to determine the transfection rate. Therefore, the transfection rates of cells transfected with ZIP7 S293A and ZIP7 T294A were 42% and 39%, respectively. Meanwhile, cells transfected with WT ZIP7 had a transfection rate of 41 % (**Figure 4.5 B**). This transfection rate of the WT ZIP7 and the S293A and T294A mutant constructs showed no significant difference based on statistical analysis, meaning they were comparable.

Figure 4.5 A robust transfection of S293A and T294A mutants

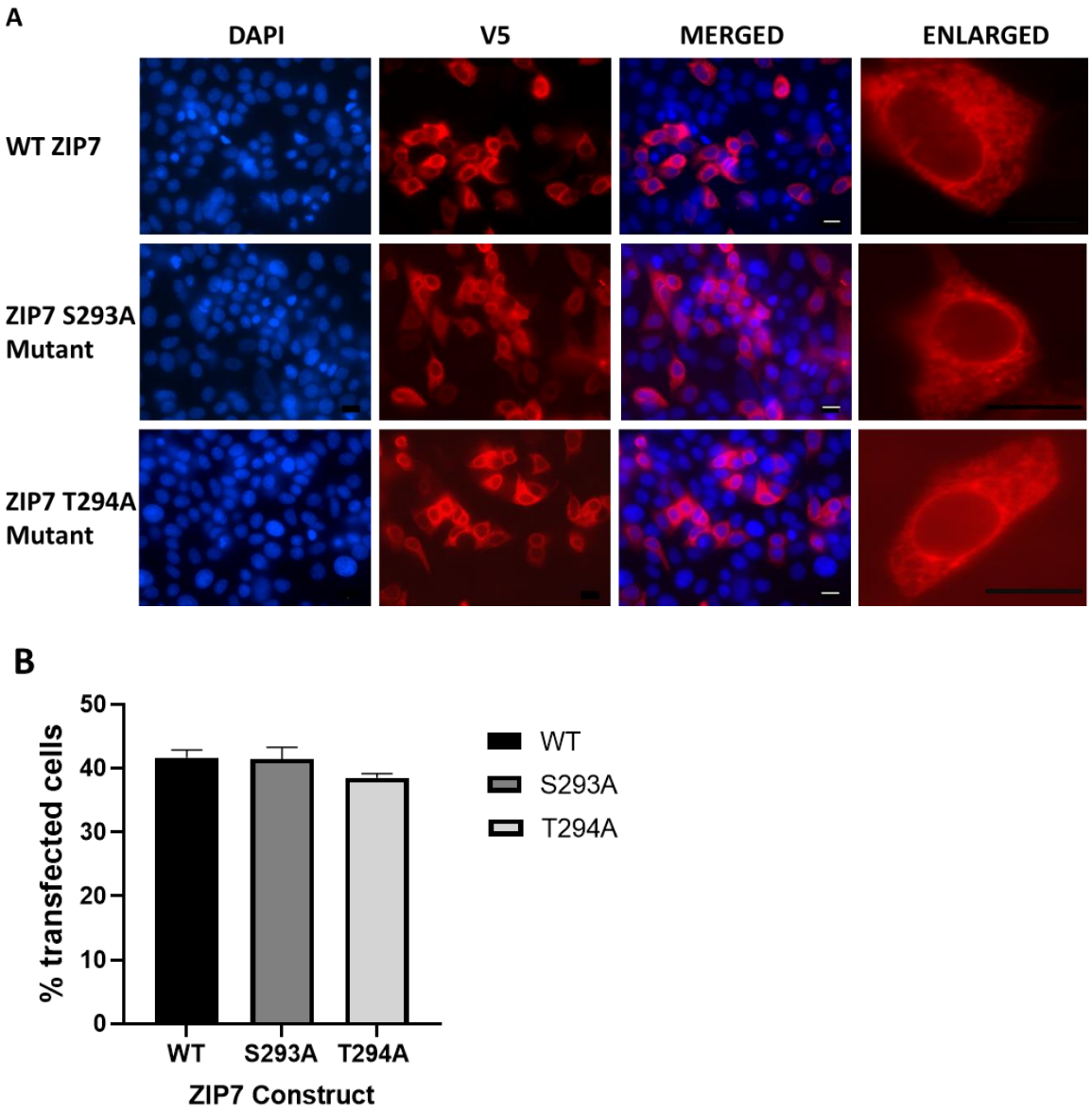

MCF-7 cells were transfected with WT ZIP7, ZIP7 S293A mutant and ZIP7 T294A mutant. The cells were stained for V5 (red) and DAPI (blue) and imaged using a 63x magnification lens on Leica RPE automatic microscope (**A**). Demonstration a robust transfection of WT and both mutants confirmed by calculating the percentage of V5 positive cells among the total number of cells that expressed DAPI staining in four random representative fields (**B**). scale bar, 10 µm

4.3.2.2 The role of S293 and T294 residues in activating ZIP7

To examine the impact of S293A and T294A mutations on the activation of ZIP7 and the ability of pZIP7 antibody to bind the activated form of ZIP7, immunofluorescence was performed in cells transfected with WT ZIP7, S293A or T294A, both with and without zinc treatment. The cells were stained with a V5 antibody. The cells transfected with WT ZIP7 showed a typical pattern of ZIP7 activation (**Figure 4.6 A**). Following zinc treatment, the percentage of cells with activated ZIP7 (pZIP7) increased significantly from 24% to 41% (**Figure 4.6 B**). For the S293A mutant, it appeared that the pZIP7 antibody was capable of recognising the activated ZIP7 in a basal condition. However, this activation of ZIP7 significantly decreased from 38 % to 23 % after zinc treatment. This indicates that the S293 residue might have a stimulatory role on ZIP7 activation by zinc (**Figure 4.6 A and B**). In contrast, no significant differences were found between control and zinc treatment in the cells transfected with T294A, as the pZIP7 level remained around 30% to 28 %. This suggests that S293 residue may play a more dominant role in ZIP7 activation (**Figure 4.6 A and B**). Nevertheless, both mutants decreased the pZIP7 level after zinc treatment compared to WT ZIP7, highlighting their potential roles in ZIP7 activation.

AKT is an indicator of downstream pathway of zinc release mediated by ZIP7. To investigate the role of S293 and T294 residues in ZIP7 activation, western blot was performed in the cells transfected with WT ZIP7, ZIP7 AA, ZIP7 S293A mutant and ZIP7 T294A mutant. The result showed that zinc treatment significantly increases $pAKT^{S473}$ activity in all samples compared to the time zero (**Figure 4.7 A**). AA and T294A mutants significantly attenuated effect of zinc compared to WT ZIP7, suggesting the role of T294 in ZIP7 activation along with S275 and S276 residues. Additionally, there was a decrease in AKT activation in the S293A mutant compared to WT ZIP7, but the difference was not statistically significant. These results showed that the ZIP7 AA and T294A statistically decreased the effect of ZIP7 activation as judged by the level of $pAKT^{S473}$ after 10 minutes of zinc treatment while the S293A mutant showed a decrease level but not statistically significant compared to the time zero (**Figure 4.7 B**), suggesting that these S293 and T294 residues may be required for ZIP7 activation.

Figure 4.6 The ability of pZIP7 antibody to detect phosphorylated ZIP7 in S293A and T294A mutants

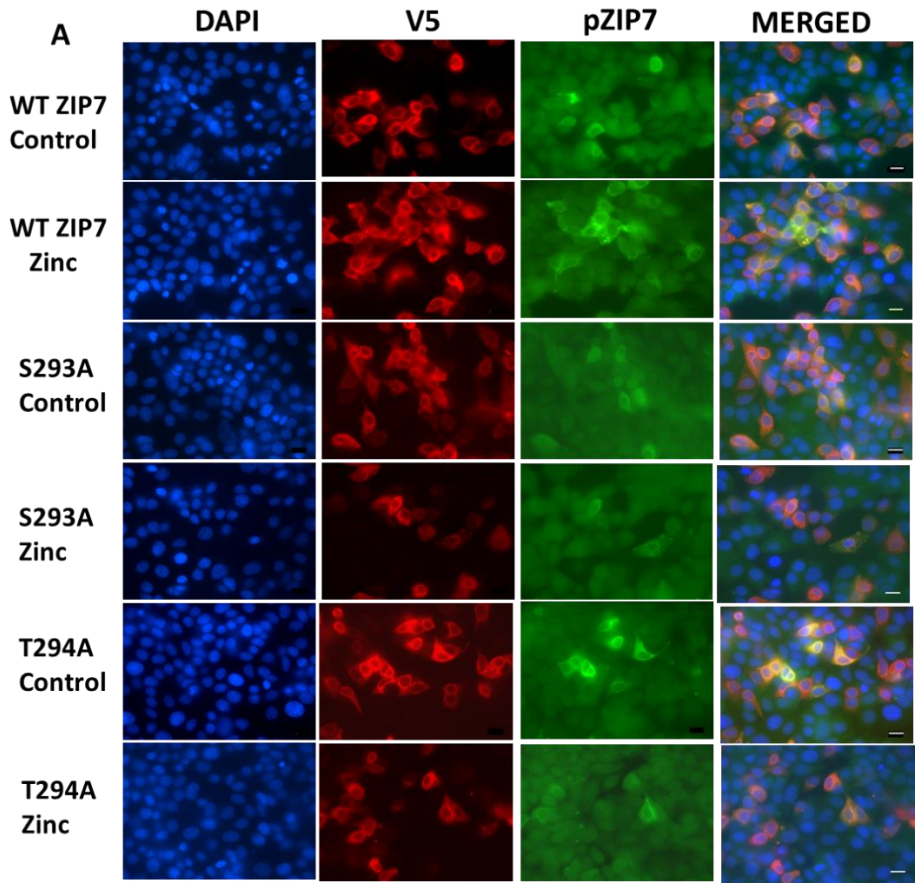

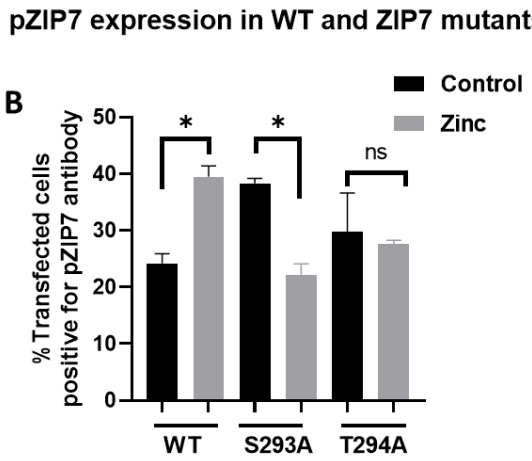

MCF-7 cells were transfected with WT ZIP7, S293A and T294A ZIP7 mutant and then treated without zinc and with zinc plus sodium pyrithione. Cells were stained for DAPI (blue), V5 (red) and pZIP7 (green) and imaged using a 63x magnification lens on Leica RPE automatic microscope (**A**). The difference between the expression of pZIP7 antibody in WT ZIP7 and S293A cells with and without zinc was significant as shown in a graph as mean of 3 random representative fields of the same coverslip ± standard error (**B**)*$p < 0.05$. scale bar 10, um

Figure 4.7 Involvement of multiple residues in ZIP7 activation

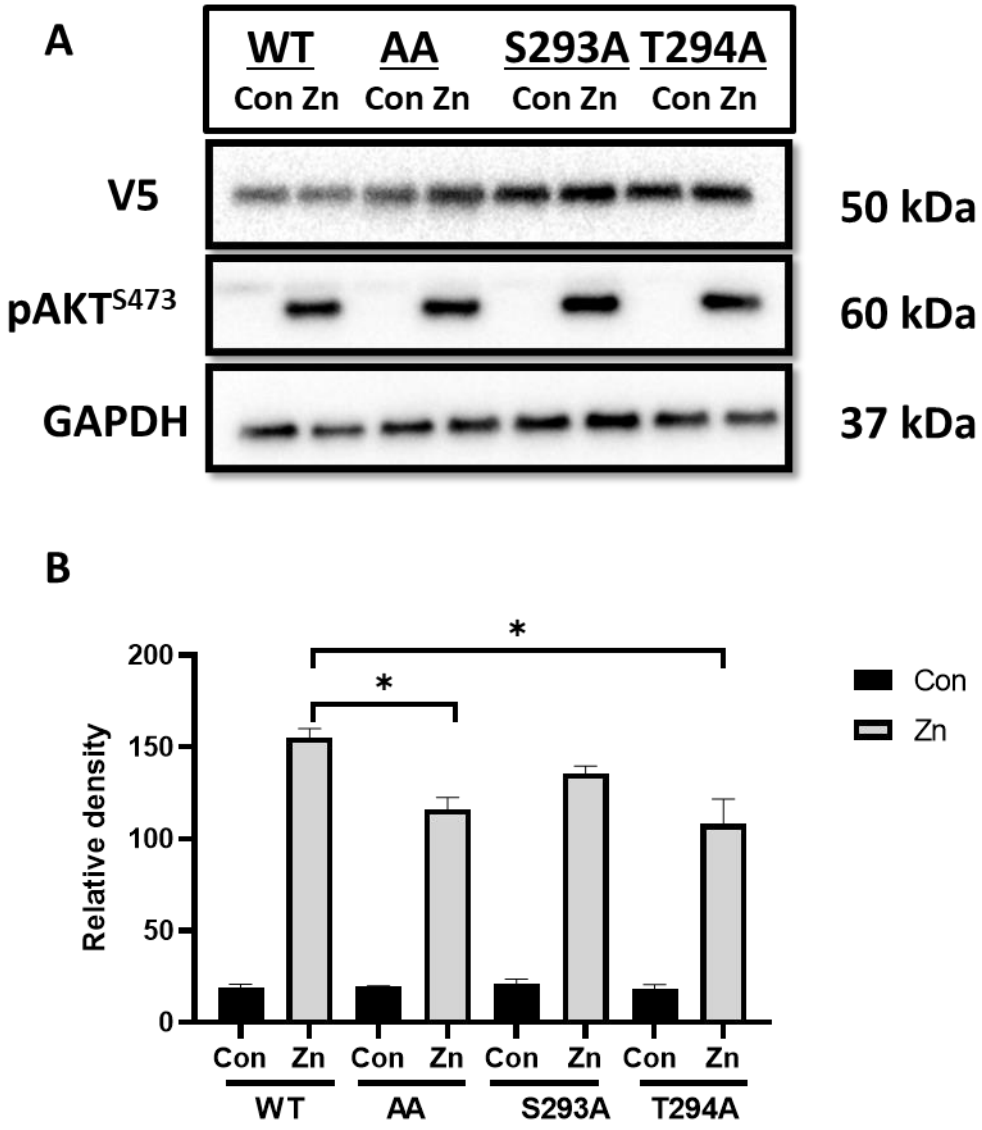

MCF-7 cells were transfected with WT ZIP7, S275A/276A AA, ZIP7 S293A and ZIP7 T294A and then treated without zinc (Con) and with zinc 20µM plus sodium pyrithione 10µM for 10 minutes (Zn). A representative band probing for pAKT^{S473}, V5 and GAPDH is illustrated in (**A**). The bar graph shows the densitometric data, which has been normalized to V5, for pAKT^{S473} (**B**). The data is represented as the mean ± standard error (n = 3).

4.3.3 MAPKAPK2 kinase binding to ZIP7 in WT cells

ZIP7 has been reported to bind to CK2 in order to release zinc from cellular stores through phosphorylation on S275 and S276 residues. The phosphorylation sites database, which used proteomic discovery mode mass spectrometry, has predicted that MAPKAP2 is also bound to ZIP7 on S293 residues. However, as there are no residue-specific experiments that confirm this prediction, it is recommended to examine any association between ZIP7 and MAPKAPK2, particularly regarding ZIP7-mediated zinc release. Therefore, proximity ligation assay, in which a florescent dot emerges wherever two molecules are in close proximity (< 40 nm), was performed using ZIP7 with CK2 and MAPKAPK2 antibodies. In a time-course zinc treatment (0,2,5,20), the results showed the interaction between ZIP7 and CK2, as evidenced by the number of dots at 2 minutes (9.2 dots per transfected cell) after zinc treatment in MCF-7 cells, compared to 0 and 20 minutes, with 0 and 3 dots per transfected cell, respectively (**Figure 4.8 A)**. Quantification of these interactions showed a substantial increase in the association between ZIP7 and CK2a at 2 minutes, with their connection nearly returning to levels observed prior to stimulation after 20 minutes. The negative control using CK2 only revealed a considerably lower number of PLA dots (**Figure 4.8 B**). Moreover, representative images showed a significant interaction between ZIP7 and MAPKAPK2 in MCF-7 cells. The PLA signals were detected as distinct fluorescent dots, indicating that the ZIP7 and MAPKKAPK2 were in close proximity and likely forming a protein complex (**Figure 4.9 A**). The number of dots per transfected cell was quantified, and the results demonstrated a significant increase of dots at 2 minutes (8.7 dots) compared to the 0 and 20 minutes, with 1 and 3 dots per transfected cell, respectively. This finding confirmed the specific interaction between ZIP7 and MAPKAPK2. The negative controls using MAPKAPK2 only and ZIP7 and MAPKAPK2 without probe revealed a considerably lower number of PLA dots (**Figure 4.9 B**). The negative control confirmed that the dots observed in the sample, due to the use of antibodies, were the result of the interaction between the two proteins. Taken together, this finding confirms the role of MAPKAPK2 kinase in phosphorylation of ZIP7, similar to CK2, and subsequently its effect on ZIP7 activation.

Figure 4.8 The binding of ZIP7 with CK2 by using proximity ligation assay

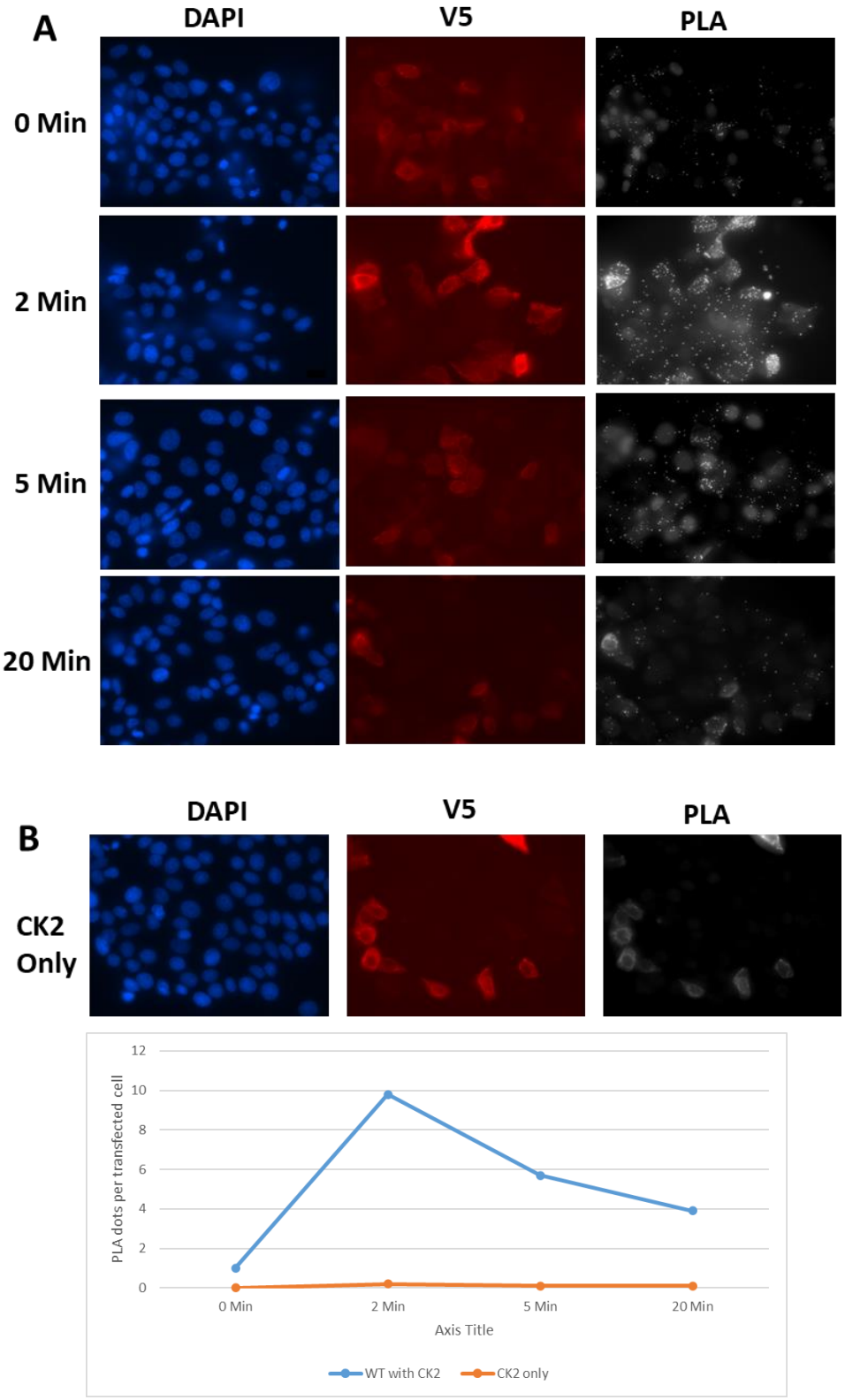

On 8−well chamber slides, cells were transfected with WT and treated by zinc for a time course treatment (0,2 ,5 and 20 minutes). A PLA anti-total ZIP7 with anti-CK2 antibodies was performed (**A**). CK2 only was used as negative control (**B**). The collected results are expressed as dots per transfected cell, and were obtained from 18-22 stacks, taken 0.3µm apart, from four randomly chosen representative fields on the same slide. Scale bar 10 µm.

Figure 4.9 The binding of ZIP7 with MAPKAPK2 by using proximity ligation assay

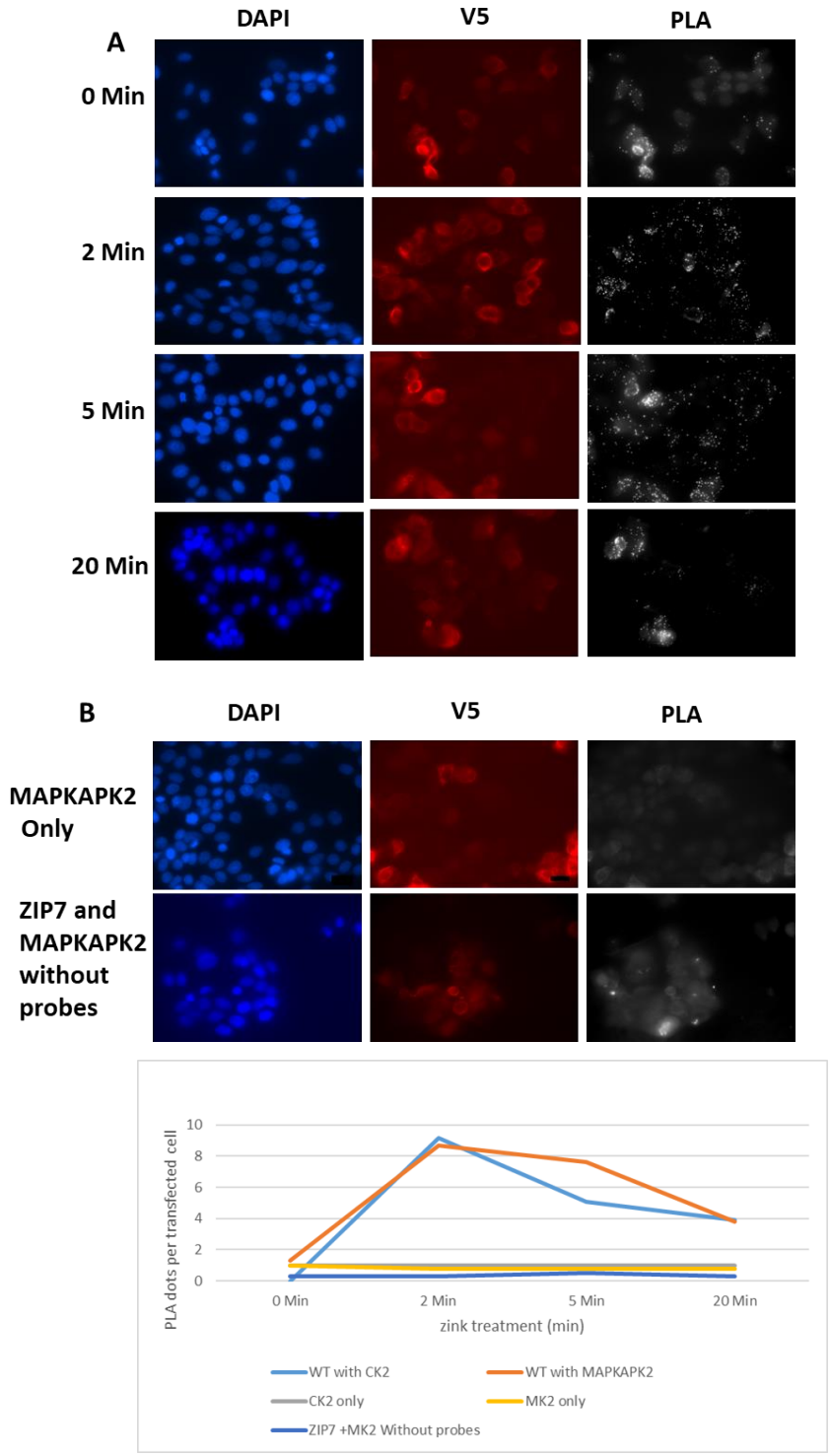

On 8−well chamber slides, cells were transfected with WT and treated by zinc for a time course treatment (0,2 ,5 and 20 minutes). A PLA using anti-total ZIP7 with anti-MAPKAPK2 antibodies was performed (**A**). MAPKAPK2 only and ZIP7 and MAPKAPK2 without probe were used as negative control (**B**). The collected results are expressed as dots per transfected cell, and were obtained from 18-22 stacks, taken 0.3µm apart, from four randomly chosen representative fields on the same slide. Scale bar 10 µm.

4.3.4 Investigating downstream targets of ZIP7-mediated zinc release in WT compared with ZIP7 mutants

It has been shown that ZIP7-mediated zinc release after binding of CK2 on S275 and S276 leads to activate phosphorylation of tyrosine kinases (Taylor et al., 2012). Furthermore, the previous results showed that MAPKAPK2 could also phosphorylate ZIP7, possibly on S293 residue, subsequently activating multiple tyrosine kinases. It was exciting to see if there is any potential role of 293 and 294 residues in activating tyrosine kinases. To explore the downstream targets of ZIP7 activation, MCF-7 cells were transfected with WT ZIP7 and ZIP7 mutants. Additionally, the cells were treated with exogenous zinc in order to stimulate ZIP7−mediated zinc release from cellular stores. Phosphokinase arrays and western blot were employed to explore and confirm the targets of ZIP7 activation.

Phosphokinase array is a high-throughput method that identifies the activation of 43 different cellular kinases simultaneously, along with their specific phosphorylated sites. MCF-7 cells were transfected with WT and other ZIP7 mutants including AA, S293A and T294A with and without zinc. The zinc treatment was performed for 10 minute to provide sufficient time for zinc to be released from cellular stores for kinase phosphorylation to occur. The data are displayed in three figures including images of the signals in the arrays (**Figure 4.10**), a bar graph illustrating the densitometric measurements for each pair of duplicate spots corresponding to all the identified kinases (**Figure 4.11**), and bar graphs showing densitometric values for the highly activated kinases (**Figure 4.12**).

The arrays data revealed that cells transfected with WT and other ZIP7 mutants had an increase in intensity to many spots, especially after 10 minutes of zinc treatment (**Figure 4.10**). The images display noticeable spots of phosphorylated kinases including pAKT^{S473}, pGSK-3α/ß$^{S21/S9}$, pERK1/2$^{T202/Y204\ \ T185/Y187}$, pCREB^{S133}, and pHSP27$^{S78,\ S82}$ which are indicated by arrows. Interestingly, some of these kinases have been shown to be directly downstream effects of the zinc release mediated by ZIP7 (Nimmanon et al., 2017). Notably, significant phosphorylation of ZIP7 is shown at 2 minutes of zinc treatment (Taylor et al., 2012). However, it is worth noting that three pairs of dark reference points can be found at the top-right, top-left, and bottom-left corners, which are used for alignment.

To evaluate the levels of each kinase, a bar graph was created, presenting the densitometric values of the corresponding duplicate dot pairs for all detected kinases at 0 and 10 minutes of zinc treatment. Kinases with a change in density more than 15000 units were considered as highly activated kinases. To minimize false positive results arising from variations in background intensity, differences of below than 2,000 units were deemed negative.

Generally, the arrays data revealed that cells transfected with WT and other ZIP7 mutants with had induced phosphorylation (>15,000 density units) of pERK1/2$^{T202/Y204, T185/Y187}$, pGSK-3α/ß$^{S21/S9}$, pAKT^{S473}, pCREB^{S133}, and pHSP27$^{S78, S82}$. Additionally, a mild increase in phosphorylation (5,000−15.000 density units) was seen for pPRAS40^{T246} (**Figure 4.11**). To analyse these further, the densitometric values of the highly activated kinases were represented in separate bar graphs. As seen in the **Figure 4.12**, a marked increase in the phosphorylation of pERK1/2$^{T202/Y204, T185/Y187}$, pGSK-3α/ß$^{S21/S9}$, pAKT^{S473}, pCREB^{S133}, and pHSP27$^{S78, S82}$ was observed in WT ZIP7 and ZIP7 mutants in zinc treatment compared to the control. This finding confirmed that all these kinases are directly downstream effects of the zinc release mediated by ZIP7.

As a result of zinc treatment, the phosphorylation of pAKT^{S473}, pERK1/2$^{T202/Y204, T185/Y187}$ and pCREB^{S133} increased in the cell expressing WT ZIP7 and S293A mutant while it decreased in the AA and T294A mutant after zinc treatment. This indicates the T294 residue is essential for ZIP7 activation as the same as S275 and S276. The phosphorylation of pHSP27$^{S78, S82}$ was highly increased only in the WT ZIP7 compared with ZIP7 mutants, suggesting that the phosphorylation of this kinase is ZIP7−dependent. Phosphorylation of pGSK-3α/ß$^{S21/S9}$ was markedly increased in all the samples even in the control, this could be as a result of transfection with WT ZIP7 or ZIP7 mutants.

Figure 4.10 The effect of ZIP7 on phospho-kinase activation

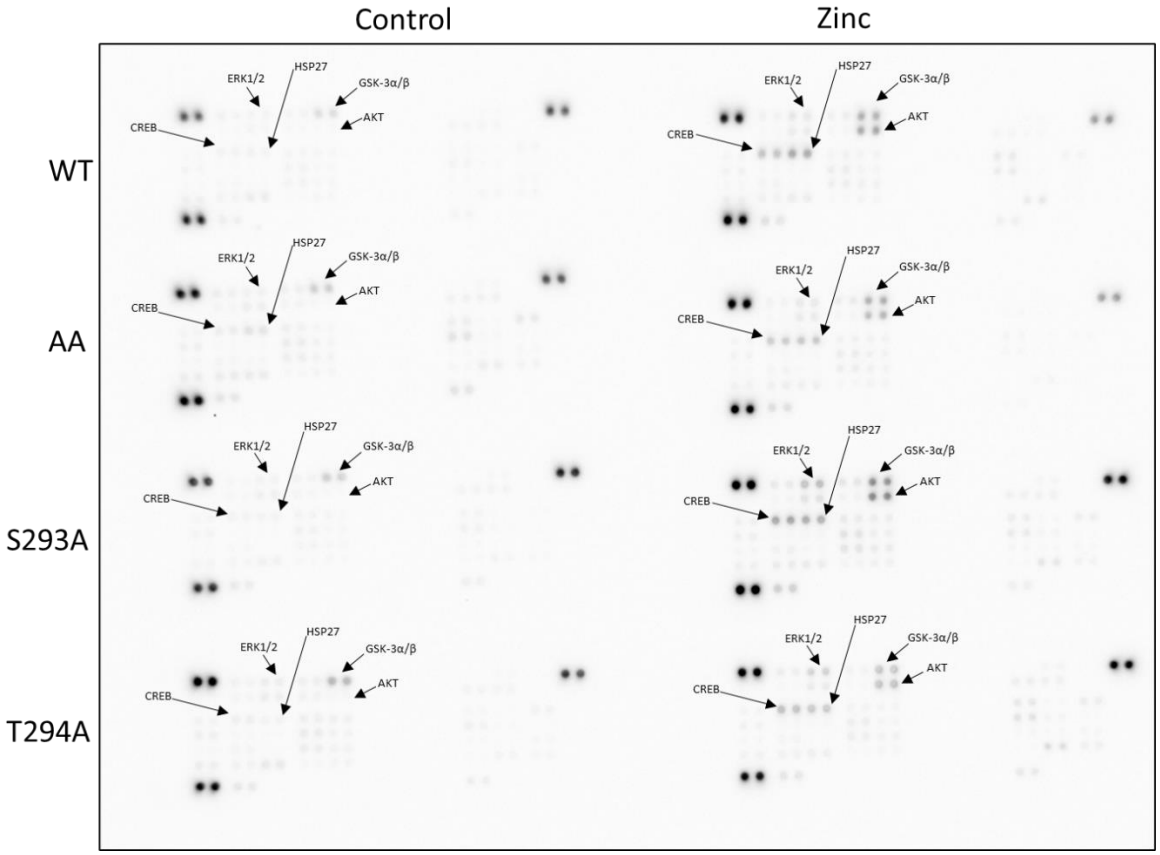

MCF−7 cells were transfected with WT ZIP7 and other ZIP7 mutants including AA, S293A and T294A. After transfection, the cells were either untreated or treated with zinc plus sodium pyrithione for 10 minutes. The human phospho-kinase antibody arrays (ARY003B) (R&D Systems) were employed to examine 43 phosphorylated kinases. Signals for each kinase appear as a pair of duplicate spots, with three pairs of dark reference at the top-right, top-left, and bottom-left corners, which are used for alignment. The kinases that demonstrate changes in phosphorylation (>15,000 density units) in the WT cells when compared to theS293A and T294A mutants in the presence and absence of zinc are indicated with arrows.

Figure 4.11 Densitometric analysis of phospho−kinase arrays in transfected MCF−7 stimulated with and without zinc treatment.

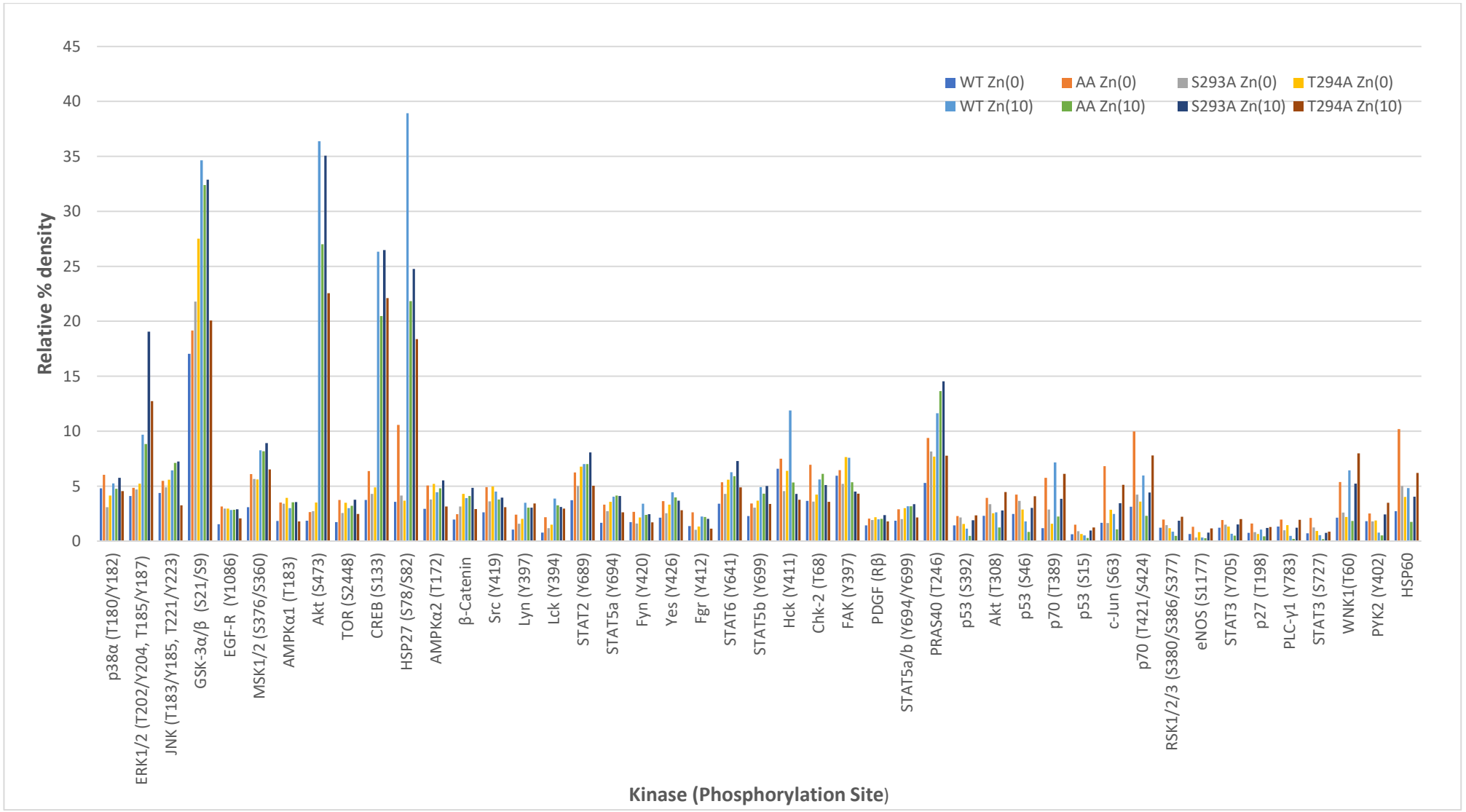

MCF−7 cells were transfected with WT ZIP7 or mutant ZIP7 including S275A/S276A (AA), S293A and T294A and were either untreated (0) or treated with zinc plus sodium pyrithione for 10 minutes before harvesting (10). The phosphorylation of selected kinases at the residues specified beneath the kinase names was identified using the human phospho-kinase antibody arrays (ARY003B) (R&D Systems). Normalised data are shown as the average of duplicate dots for each kinase (n=2).

Figure 4.12 The effect of ZIP7 mutations on kinase activation

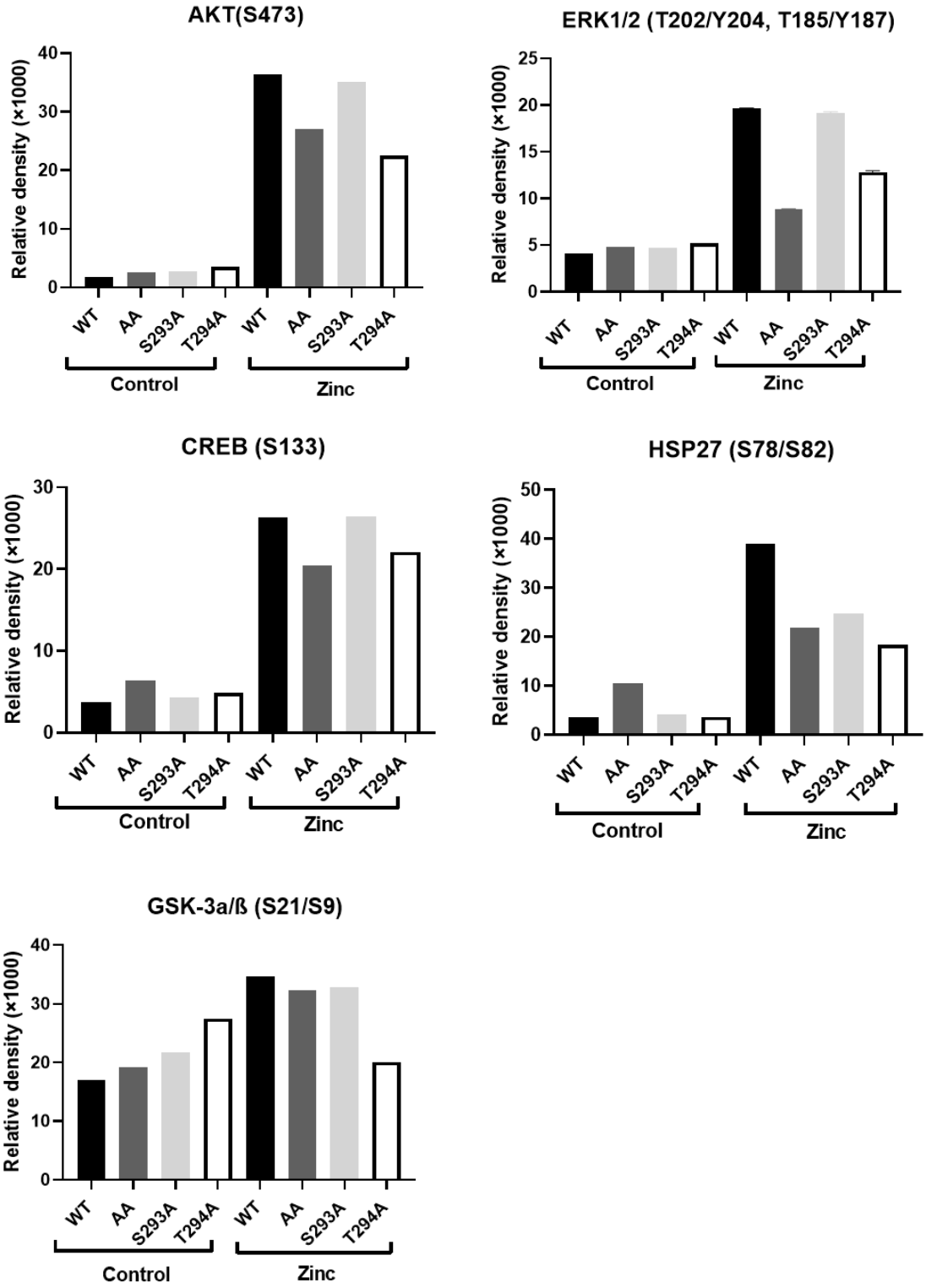

MCF−7 cells were transfected with WT ZIP7 and other ZIP7 mutants including AA, S293A and T294A. After transfection, the cells were treated without zinc (Control) and with zinc 20µM plus sodium pyrithione 10µM for 10 minutes (Zinc). The human phospho-kinase antibody arrays (ARY003B) (R&D Systems) were used to examine 43 phosphorylated kinases. The average densities of each kinase that change more than 15,000 units in WT compared with other ZIP7 mutants in the presence of zinc are demonstrated (n=2)

4.3.5 Western blotting confirms kinases activation in WT compared with other ZIP7 mutants

The phospho-kinase arrays have been employed to point the direction of what downstream kinases are involved in ZIP7 mediated zinc release and the effect of mutated residues on these kinases. Cells transfected with WT ZIP7 showed high phosphorylation levels in most kinases after zinc treatment compared to ZIP7 mutants. However, the S293A mutant showed elevated phosphorylation levels in some kinases, which were similar to those observed in the WT ZIP7. To confirm the phosphorylation of highly activated kinases due to ZIP7 overexpression and the effect of ZIP7 mutants on ZIP7 activation, western blotting was performed in cells transfected with WT ZIP7 and ZIP7 mutants treated with zinc for 10 minutes. This experiment allowed for observation of the effect of S293 and T294 residues on ZIP7 activation compared to S275 and S276. The kinases confirmed by western blot were pAKT^{S473}, pGSK-3α/ß$^{S21/S9}$, pCREB^{S133}, pHSP27$^{S78,\ S82}$ and pERK1/2$^{T202/Y204,\ T185/Y187}$.

Zinc treatment induced ZIP7-mediated zinc release as judged by the phosphorylation of pAKT^{S473}. Consequently, all samples showed a significant increase in pAKT^{S473} activation compared to control. Interestingly, the results showed that the ZIP7 AA and T294A mutants significantly decreased the effect of ZIP7 activation as judged by the level of pAKT^{S473} after 10 minutes of zinc treatment while the S293A mutant showed a decreased level but this was not statistically significant compared to WT ZIP7 (**Figure 4.13 A**), suggesting that these S293 and T294 residues are required for ZIP7 maximal activation.

Next, the phosphorylation of pGSK-3α/ß$^{S21/S9}$ was analysed. GSK-3 was shown to be inhibited in order to undergo phosphorylation, which could occur either directly due to released zinc or indirectly through AKT activation (Lee et al., 2009) (Nimmanon et al., 2017). Cells transfected with WT ZIP7 showed a significant increase in phosphorylation levels of GSK-3α/ß following zinc treatment, confirming that GSK-3α/ß is inhibited in response to ZIP7-mediated zinc release (**Figure 4.13 B**). In contrast, AA mutant showed a significant reduction in pGSK-3α/ß$^{S21/S9}$ phosphorylation levels compared with WT ZIP7, suggesting the role of S275 and S276 in preventing ZIP7 activation.

Moreover, S293A and T294A mutants significantly attenuated the effect of ZIP7 activation as they showed a reduction in phosphorylation levels of pGSK-3α/ß$^{S21/S9}$ compared with WT ZIP7, confirming the involvement of these two residues in ZIP7 activation.

Phosphorylation of pCREB^{S133} and pHSP27$^{S78,\ S82}$ was also analysed. The results showed the phosphorylation levels of these kinases were significantly upregulated in WT ZIP7 following zinc treatment compared to control (**Figure 4.13 C**) (**Figure 4.14 A**). This suggested that these kinases are also activated in response to ZIP7-mediated release. The phosphorylation levels of pCREB^{S133} and pHSP27$^{S78,\ S82}$ significantly reduced in AA mutant compared to WT ZIP7, indicating that the phosphorylation of CREB and HSP27 occurs in response to zinc release mediated by ZIP7 transporter. Interestingly, S293A and T294A mutants significantly reduced the effect of ZIP7 activation, as they decreased the phosphorylation levels of CREB and HSP27 compared with WT ZIP7, confirming the involvement of these two residues in ZIP7 activation.

Finally, ERK1/2 phosphorylation has been identified as an early response to ZIP7 activation, similar to AKT (Nimmanon et al., 2017). The western blotting result confirmed this finding, revealing that the phosphorylation of pERK1/2$^{T202/Y204,\ T185/Y187}$ was significantly elevated in WT ZIP7 following zinc treatment compared to control (**Figure 4.14 B**). However, the phosphorylation level of pERK1/2$^{T202/Y204,\ T185/Y187}$ in the AA, S293A and T294A remained high following zinc treatment. It is worth noting that the optimal time for CK2 binding to ZIP7 is 2 minutes (Taylor et al., 2012). Given that ERK1/2 has been reported as an early response to ZIP7 activation, the 10 minutes zinc treatment duration was sufficient for endogenous ZIP7 to be activated. This could be elucidated by investigating ERK1/2 phosphorylation at 5 minutes following zinc treatment.

Figure 4.13 Confirmation of the role of S293 and T294 in ZIP7-mediated stimulation of kinase phosphorylation

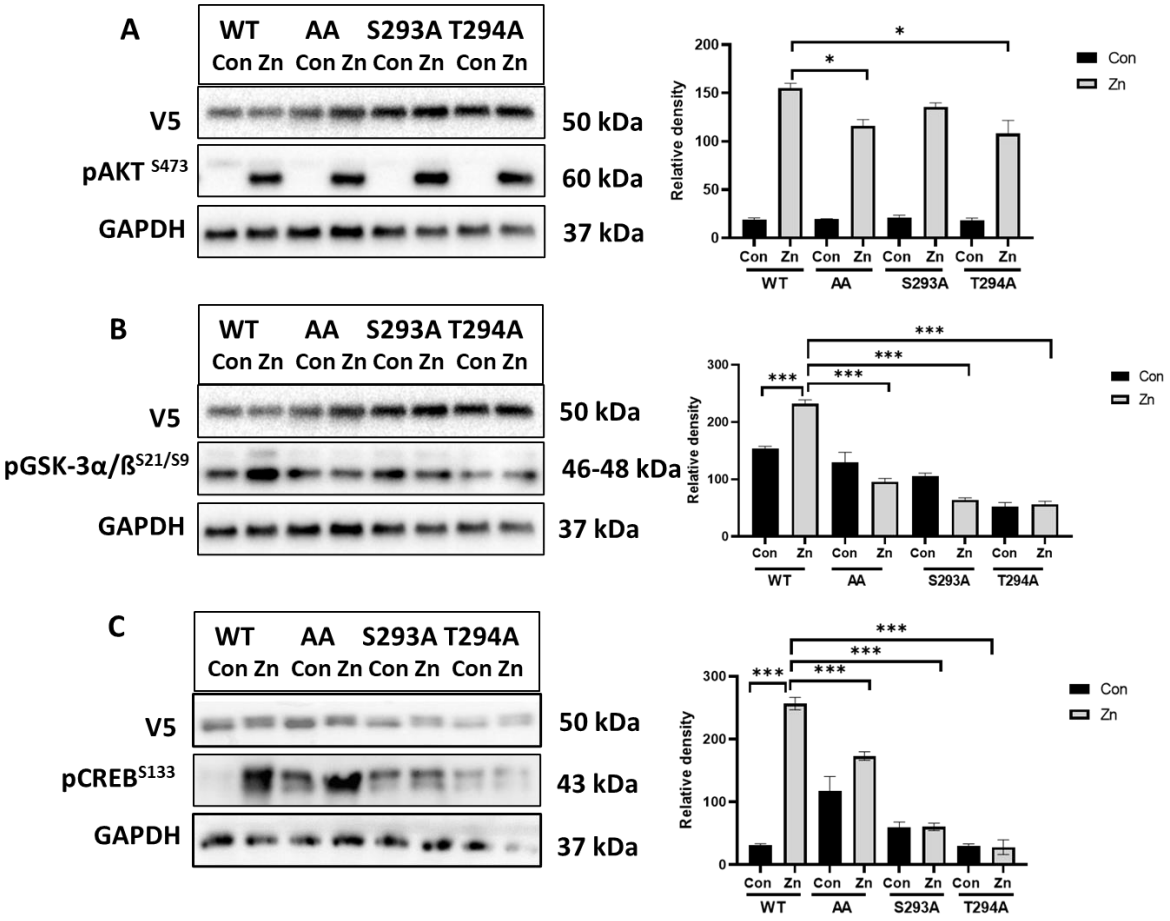

MCF-7 cells were transfected with WT and other ZIP7 mutants including S275A/S276A (AA), S293A and T294A, then untreated (Con) or treated with 20µM zinc and sodium pyrithione 10µM for 10 minutes (Zn). The blot was probed for pAKT^{S473} (**A**), pGSK-3α/ß^{S21,9} (**B**) and pCREB^{S133} (**C**). GAPDH was utilised as a loading control. The bar graph shows the densitometric data, which has been normalized to V5 and presented as mean ± standard error (n=3). ∗∗∗= p<0.001

Figure 4.14 Confirmation of the role of S293 and T294 in ZIP7-mediated stimulation of kinase phosphorylation

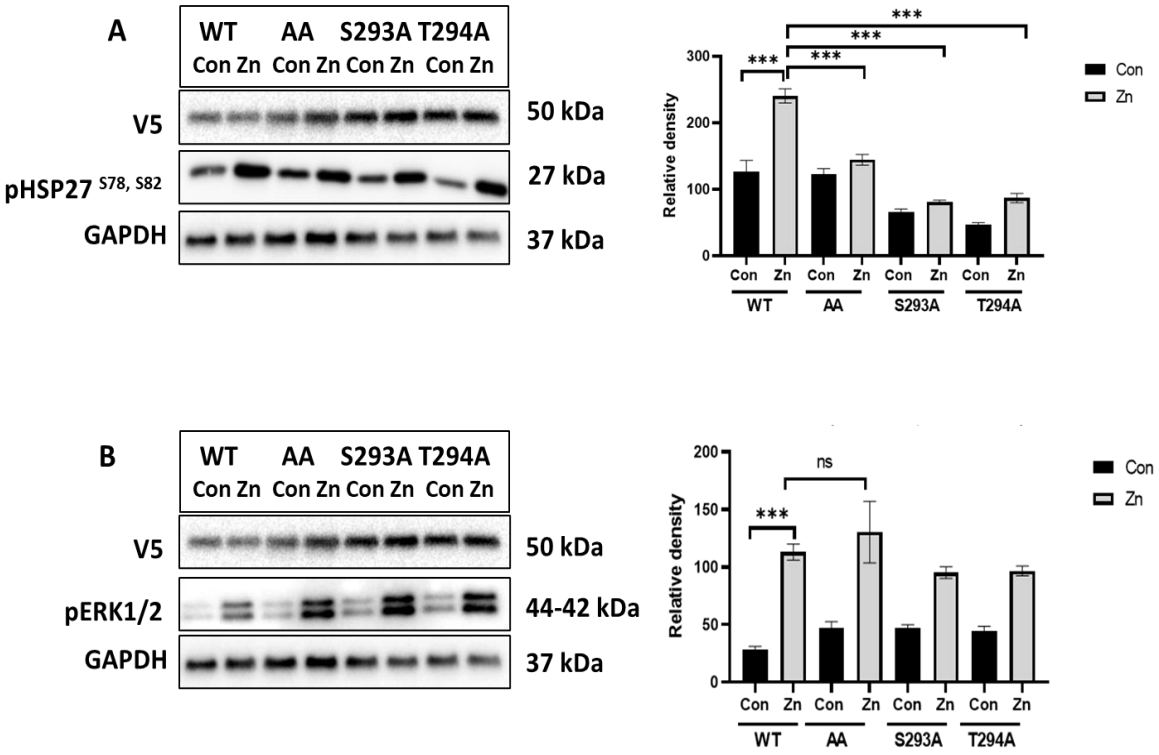

MCF-7 cells were transfected with WT and other ZIP7 mutants including S275A/S276A (AA), S293A and T294A, then untreated (Con) or treated with 20µM zinc and sodium pyrithione 10µM for 10 minutes (Zn). The blot was probed for pHSP27^{S78,82} (**A**) and pERK1/2$^{T202/Y204,\ T185/Y187}$ (**B**). GAPDH was utilised as a loading control. The bar graph shows the densitometric data, which has been normalized to V5 and presented as mean ± standard error (n=3). ***= p<0.001

4.3.6 Exploring the functional impact of S293 and T294 residues on ZIP7 maximal activation

ZIP7 is known to be activated by protein kinase II (CK2) through phosphorylation of serine residues S275 and S276, which leads to ZIP7 activation and then release of zinc from cellular stores into the cytoplasm (Taylor et al., 2012). The released zinc then inhibits protein tyrosine phosphatases and activates cellular kinases associated with tumour cell growth and motility (Nimmanon et al., 2017). Recently, S293 and T294 have shown potential roles in ZIP7 activation, suggesting that they could be required for the maximal activation of ZIP7. Therefore, all four residues in ZIP7 (S275, S276, S293 and T294), collectively referred to as the 4A mutant in this chapter, were simultaneously mutated to alanine in the same construct to further investigate their role in ZIP7 activation and subsequent impact on downstream targets of ZIP7-mediated zinc release. It is worth noting that the 4A mutant was designed in a construct without a His tag. Thus, an initial investigation was conducted to test the transfection efficiency and assess the impact of the His-tag on the construct, in comparison with WT ZIP7, before proceeding with performing the main experiments.

4.3.6.1 Effect of His tag on the activation of recombinant ZIP7

Many recombinant proteins have been modified to add polyhistidine fragments (His-Tag) onto their DNA sequence for stability and purification purposes (Booth et al., 2018). However, this additional sequence of a polyhistidine tag may interfere with zinc activity as histidine has a high affinity for zinc and plays a role in zinc transport activity (Zhang et al., 2019). Therefore, two recombinant proteins of wild-type ZIP7 (WT) were designed with and without a His-tag to investigate the effect of this tag on the activation of ZIP7. WT ZIP7 constructs with and without His-tag were initially tested for the transfection efficiency and localisation pattern. Immunofluorescence was performed using V5 antibody which binds to the C−terminal V5 tag of the recombinant proteins. The results showed a robust transfection of both constructs in MCF-7 cells as confirmed by V5 (red) and illustrated the location of the recombinant protein on the endoplasmic membrane (**Figure 4.15 A**). Enlarged images of the transfected cells exhibited an ER-like localization pattern of the recombinant proteins, indicating that the removal of the His-tag does not affect the localisation of ZIP7 at the ER. This finding was in agreement with a previous study that showed the co-localization of ZIP7 with the ER marker (Calreticulin) in CHO cells (Taylor et al., 2004).

To determine the transfection rate, the number of cells expressing the V5 tag was quantified in three randomly selected visual fields. The percentage of transfection efficacy ranged from 40% to 47% (**Figure 4.15 B**), meaning they are comparable.

Next, the effect of the His-tag on the ZIP7 activation was evaluated. Using immunofluorescence, the results showed that the recombinant proteins lacking a His-tag efficiently generated more cells that were positive for the pZIP7 antibody (**Figure 4.16 A**). This antibody was used to determine the activation of ZIP7-mediated zinc release when S275 and S276 of ZIP7 became phosphorylated (Ziliotto et al., 2019). From the graph, the effect of the His-tag on the ZIP7 activation can be observed, as the number of pZIP7 positive cells did not distinctly increase following zinc treatment when the construct contained a His tag (**Figure 4.16 B**), suggesting the potential binding of the histidine to zinc and reducing the zinc transport effect.

Western blotting was also performed, in order to further assess the effect of the His-tag on the activation of pZIP7. In this experiment, the AA mutant, in which the S275 and S276 residues were changed to alanine, was also used both with and without the His-tag. This allowed for a more thorough investigation of the potential impact of the His-tag on ZIP7 activation. MCF-7 cells were transfected with WT and AA mutant of these recombinant proteins in the presence and absence of zinc as an external stimulation.

In the recombinant construct with His-Tag, results demonstrated a remarkable increase in the activation of pZIP7 in WT ZIP7 compared with AA mutant following zinc treatment, confirming the ability of AA mutant to reduce the effect of ZIP7 activation (**Figure 4.17 A**). In the construct lacking the His-Tag, the AA mutant demonstrated a more marked reduction in ZIP7 activation compared to WT ZIP7 upon zinc treatment (**Figure 4.17 A**). This observation confirms that the absence of the His-Tag provides a more distinct differentiation between the WT and AA mutant following zinc treatment (**Figure 4.17 B**). Collectively, these findings indicate the possibility of the His-Tag binding to zinc in the endoplasmic reticulum and delaying it releases to the cytoplasm. Thus, the constructs without a His-Tag were used for all the following experiments.

Figure 4.15 Verification of ZIP7 WT with and without His-tag

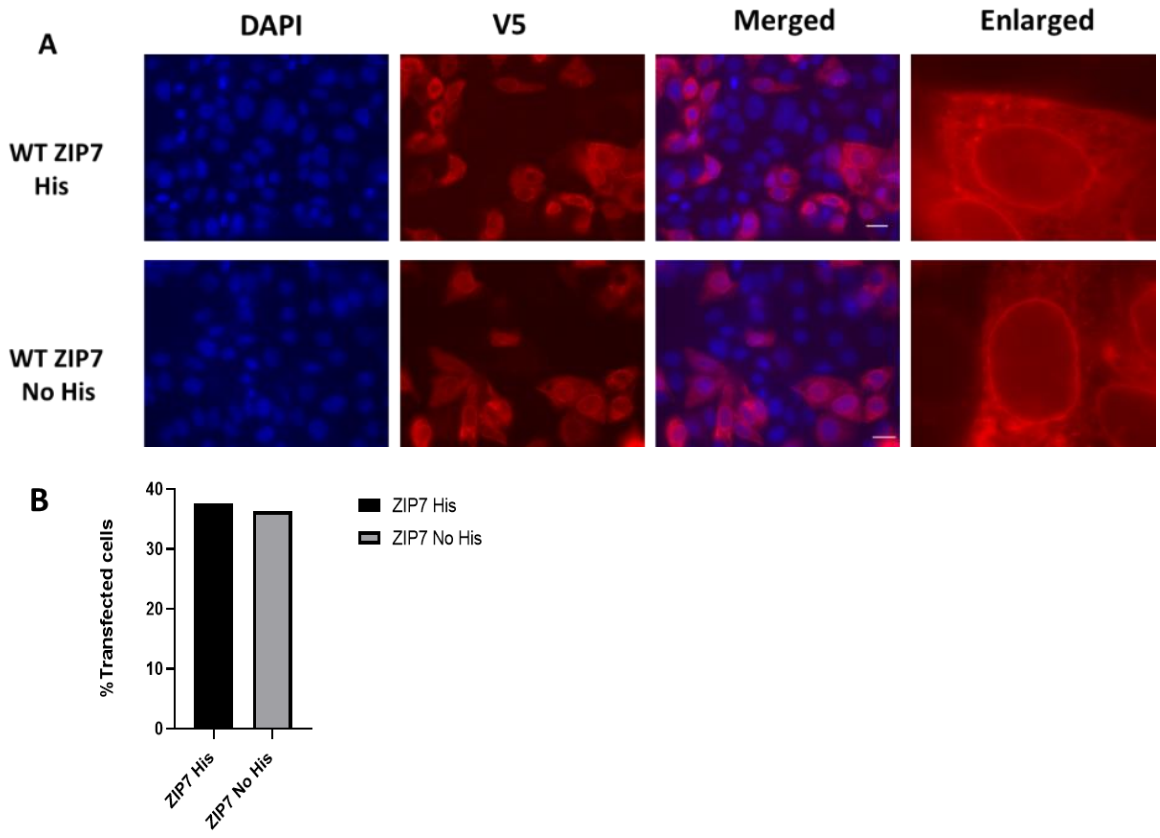

MCF-7 cells were transfected with a wild-type (WT) ZIP7 plasmid that encodes with and without His-Tag. The cells were stained for DAPI (blue) and V5 Alexa Fluor 594 (red) and then imaged using a 63x magnification lens on a Leica RPE automatic microscope (**A**). The demonstration of positive pZIP7 cells in both samples was confirmed by counting the percentage of V5-positive cells that were also positive for pZIP7 in eight random representative fields per coverslip (**B**). (n=3) Scale bar, 10 μm

Figure 4.16 Effect of His tag on the activation of recombinant ZIP7

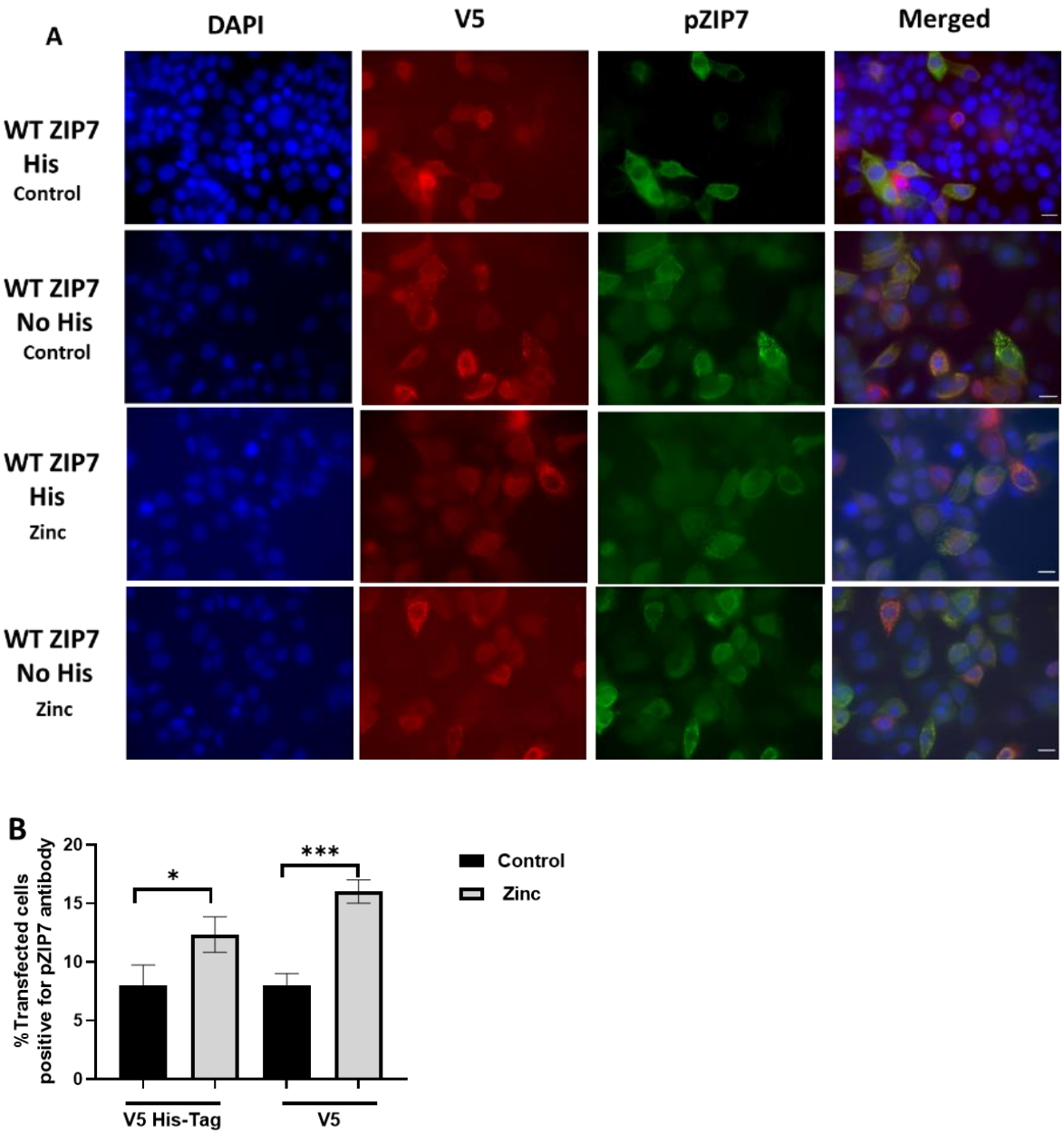

MCF-7 cells were transfected with wild-type (WT) ZIP7 construct that encodes with and without His-Tag. The cells were stained for DAPI (blue), V5 Alexa Fluor 594 (red) and pZIP7 Alexa Fluor 488 (green) and imaged using a 63x magnification lens on Leica RPE automatic microscope (**A**). Demonstration of positive pZIP7 cells of both samples was confirmed by counting the percentage of V5 positive cells that were also positive for pZIP7 in eight random representative fields per coverslip (**B**). (n=3) Scale bar, 10 μm

Figure 4.17 Using western blot to assess the effect of His tag on the activation of recombinant ZIP7

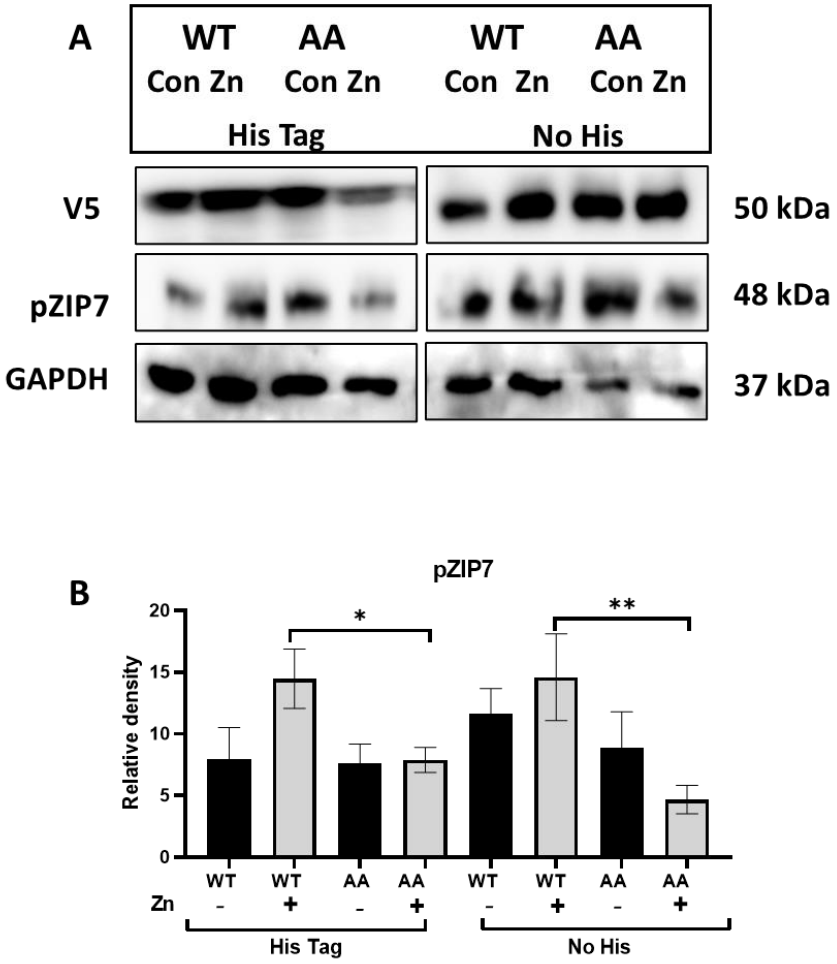

MCF7 cells were transfected with WT ZIP7 and AA mutants with and without His tag for 24 hours (**A**). Immunoblotting using pZIP7 (**B**) was performed with and without zinc treatment. GAPDH was utilised as a loading control. The bar graph shows the densitometric data, which has been normalized to V5 and presented as mean ± standard error (n=3).

4.3.7 The effect of S293 and T294 residues on downstream targets of ZIP7-mediated zinc release

ZIP7 activation is facilitated by CK2 through the phosphorylation of serine residues S275 and S276, subsequently cause the release of zinc from intracellular stores into the cytoplasm. (Taylor et al., 2012). The released zinc then inhibits protein tyrosine phosphatases and activates cellular serine kinases such as MAPK, mTOR and PI3K-AKT, which together enhance tumour cell growth and motility (Nimmanon et al., 2017). Recently, S293 and T294 have shown potential roles in ZIP7 activation, suggesting that they could be required for the maximal activation of ZIP7.

Therefore, all four residues in ZIP7 (S275, S276, S293 and T294) were mutated to alanine in the same construct in order to investigate their role in ZIP7 activation and subsequent impact on downstream targets of the zinc release mediated by ZIP7.

Immunofluorescence was performed to examine the specificity of pZIP7 antibody in determining the activated ZIP7. MCF-7 cells were transfected with wild-type ZIP7 (WT), S275A/S276A (AA) and S275A/S276A/S293A/T294A (4A) where serine and threonine residues were mutated to alanine for a phosphoablative (null) mutant. As shown in **Figure 4.18 A**, 20% of cells transfected with WT (V5−positive cells) were positive for pZIP7 antibody.

Moreover, the number of WT transfected cells that were positive for pZIP7 significantly increased after 10-minute of external zinc stimulation. In contrast, no positive cells for this antibody were observed in the cells transfected with the ZIP7 AA or 4A mutants (**Figure 4.18 B**). The observation of some non-transfected cells exhibiting pZIP7 staining confirms the negative pZIP7 staining for the phosphoablative mutants. These findings confirm the specificity of the pZIP7 antibody in recognising only the active form of ZIP7, where residues S275 and S276 are phosphorylated. It should be noted that the peptide epitope for this antibody is TKEKQ pS pS EEEEK (positions 270−281) on a long cytoplasmic loop between TM3 and TM4 of ZIP7. Therefore, it is expected to not recognise the phosphorylation state in S293 and T294 residues. For that reason, the western blot is needed to investigate the downstream targets of ZIP7 activation using the 4A construct in comparison with WT ZIP7 and the AA mutant.

AKT is an indicator of downstream pathway of ZIP7 activation (Taylor et al., 2012). To investigate the involvement of S293 and T294 residues in ZIP7 activation, western blot was performed in the cells transfected with WT ZIP7, ZIP7 AA, ZIP7 4A mutants. The result showed that zinc treatment significantly increased $pAKT^{S473}$ activity in all samples compared to the time zero (**Figure 4.19 A**). AA mutant significantly attenuated effect of zinc compared to WT ZIP7. Interestingly, this effect was further amplified by 4A mutant, being significantly decreased versus the WT and AA (**Figure 4.19 B**). suggesting an additive action of ZIP7-phosphoryltion sites. Collectively, these findings imply the involvement of S293 and T294 residues along with S275 and S276 in the activation of ZIP7.

Figure 4.18 The effect of zinc treatment on WT ZIP7 and Its mutants

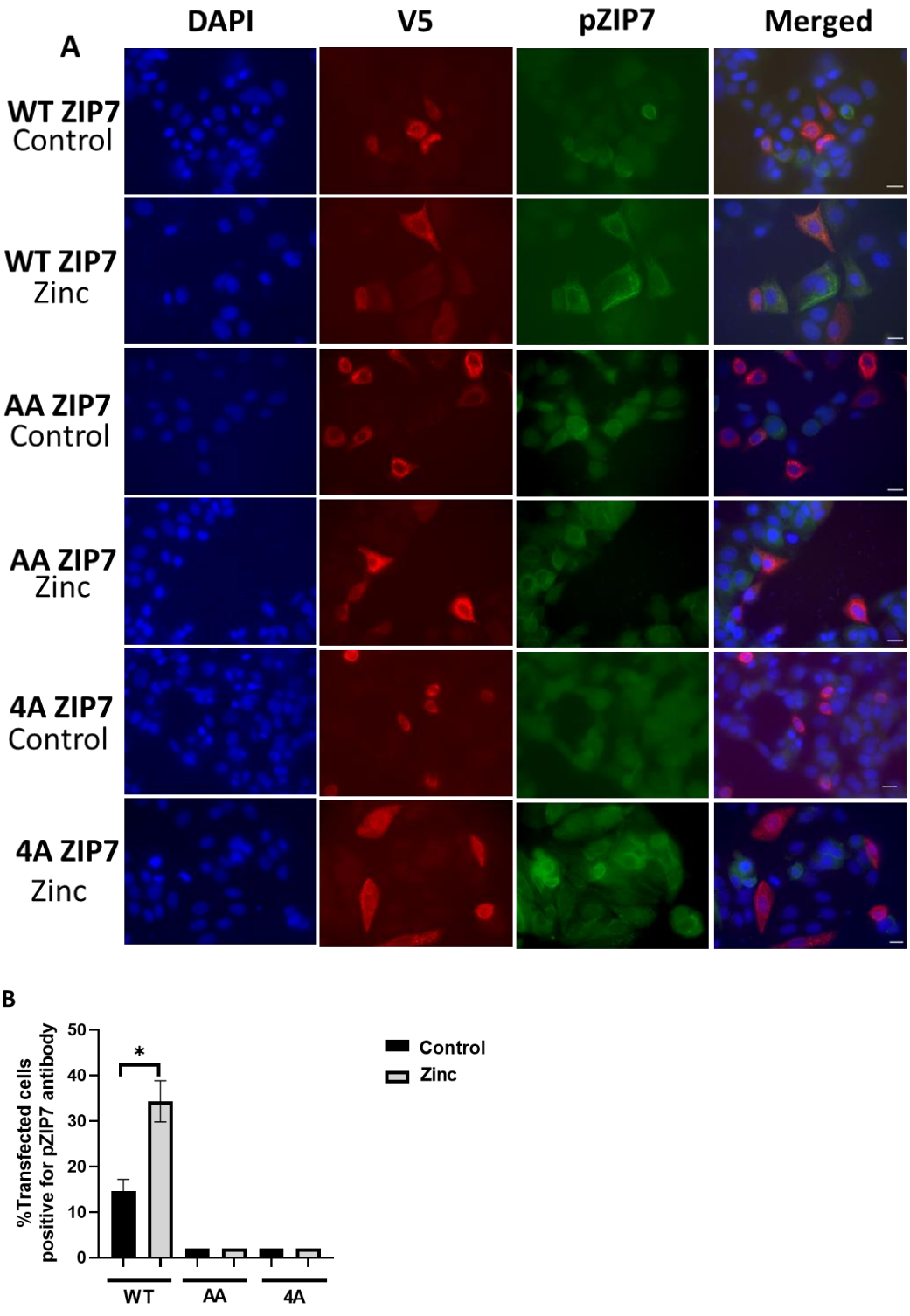

MCF-7 cells were transfected with wild-type (WT),S275A/S276A (AA) and 4A ZIP7 mutant and then treated without zinc (Control) and with zinc 20µM plus sodium pyrithione 10µM for 10 minutes (Zinc). **A**. Cells were stained for DAPI (blue) , V5 (red) and pZIP7 (green) and imaged using a 63x magnification lens on Leica RPE automatic microscope. **B**. Demonstration of positive pZIP7 cells of samples was confirmed by counting the percentage of V5 positive cells that were also positive for pZIP7 in five random representative fields per coverslips. Scale bar, 10 µm (n=3)

Figure 4.19 The effect of ZIP7 4A mutant on downstream target of ZIP7-mediated zinc release

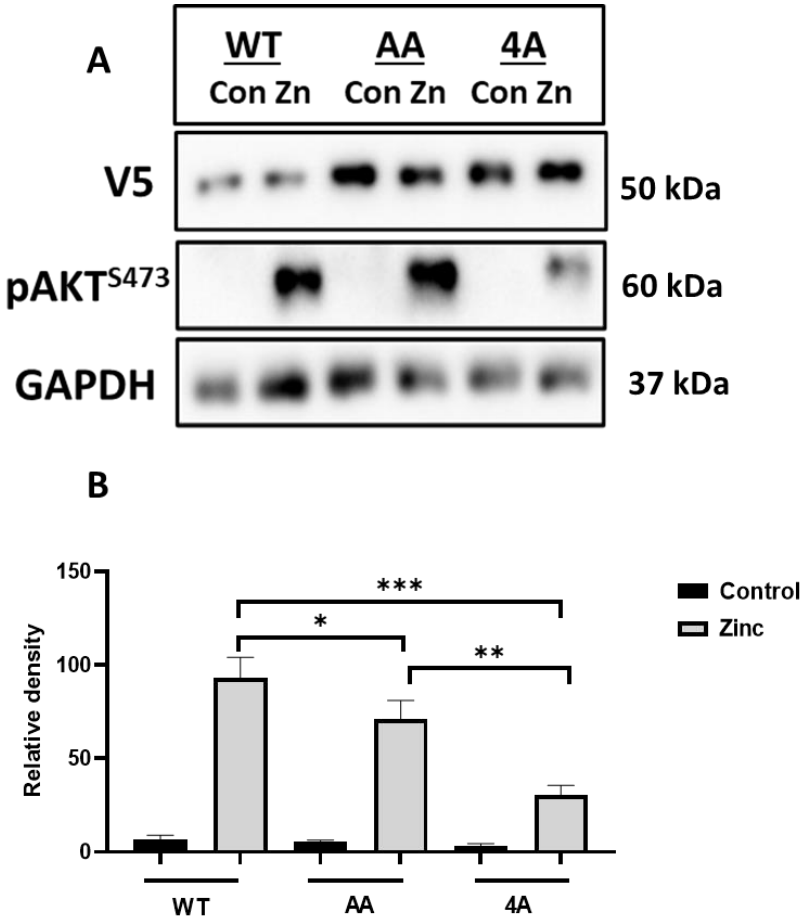

MCF7 cells were transfected with WT ZIP7, AA and 4A mutants, then untreated (Con) or treated with 20µM zinc and sodium pyrithione 10µM for 10 minutes (Zn). **A**.The blot was probed for pAKT^{S473}. GAPDH was utilised as a loading control. **B**. The bar graph shows the densitometric data, which has been normalized to V5 and illustrated as mean ± standard error (n=3).

4.3.8 The association of ZIP7 with predicted kinases MAPKAPK2 and PIM1

ZIP7 has been reported to bind to CK2 in order to release zinc from cellular stores through phosphorylation on S275 and S276 residues (Taylor et al., 2012). Phosphorylation site database, which used proteomic discovery mode mass spectrometry, has predicted that the MAPKAP2 and PIM1 may also bind to ZIP7 on S293 and T294 residues, respectively. However, since no residue−specific experiments were employed to confirm this prediction, it was encouraged to decipher any association between ZIP7 and these predicted kinases particularly regarding to ZIP7-mediated zinc release.

Therefore, a proximity ligation assay, in which florescent dots appear wherever two molecules are in close proximity (< 40 nm), was performed using ZIP7 with CK2, MAPKAPK2 and PIM1 antibodies. These experiments were performed on MCF-7 cells transfected with WT ZIP7 and ZIP7 4A mutant. Exogenous zinc was then applied at various time points (0, 2, 5 and 20 minutes) to stimulate ZIP7 activation. The generated dots were then quantified per transfected cell.

Initially, the association between ZIP7 and CK2 was established as a positive control to provide a reliable basis for subsequent experiments. The results demonstrated an interaction between ZIP7 and CK2 in WT, as evidenced by the number of dots at 2 minutes (13 dots per transfected cell) after zinc treatment in MCF-7 cells, compared to 0 and 20 minutes, which had 3 and 2 dots per transfected cell, respectively (**Figure 4.20**). This finding confirmed the association of ZIP7 with CK2 as has been previously reported (Taylor et al., 2012). Interestingly, the 4A ZIP7 mutation effectively prevented the increase in ZIP7-CK2 association, as evidenced by the reduced number of dots (6) observed at 2 minutes following zinc treatment (**Figure 4.21**). This indicates the important role of all four residues in ZIP7 activation. Quantification of these interactions showed a substantial increase in association of ZIP7 and CK2 at 2 min in WT ZIP7 compared with 4A mutant, with their connection nearly returning to levels observed prior to stimulation after 20 minutes.

Next, the association of ZIP7 with its predicted kinase, MAPKAPK2, was further investigated. The representative images showed a significant interaction between ZIP7 and MAPKAPK2 in WT ZIP7-transfected cells. The PLA signals were detected as distinct fluorescent dots, indicating that ZIP7 and MAPKKAPK2 were in close proximity and likely forming a protein complex (**Figure 4.22**).

The number of dots per transfected cell was quantified, and the results demonstrated a marked increase of dots at 2 minutes (19 dots) compared to the 0 and 20 minutes, with 1 and 4 dots per transfected cell, respectively. This finding confirmed the specific interaction between ZIP7 and MAPKAPK2. In contrast, the 4A mutant strongly weakened the interaction between ZIP7 and MAPKAPK2 kinases **(Figure 4.23)**, suggesting a potential disruption of their functional association. This indication is supported by the results, which revealed that an average of 5 dots was observed per cell transfected with 4A mutant after 2 minutes following zinc treatment.

The number of dots returned to pre-stimulation levels after 20 minutes, with zero dots observed per transfected cell. The analysis revealed a significant increase in the binding of ZIP7 and MAPKAPK2 at 2 min in WT ZIP7 compared with 4A mutant, confirming the binding of MAPKAPK2 to ZIP7 at the predicted S293 residue**.**

Finally, the binding between ZIP7 and PIM1 was also investigated using PLA. The results demonstrated an association between these two molecules. The presence of distinct fluorescent dots following zinc stimulation demonstrated that ZIP7 and PIM1 were in close proximity, suggesting the likely formation of a protein- protein binding between them. This binding is confirmed by the number of dots at 2 minutes (12 dots per transfected cell) after zinc treatment in WT ZIP7, compared to 0 and 20 minutes, which had 2 and 4 dots per transfected cell, respectively (**Figure 4.24**). This suggests that PIM1 plays a role in the modification of ZIP7. Interestingly, the 4A mutant successfully attenuated this binding between ZIP7 and PIM1, highlighting the potential role of the mutated residues in modulating ZIP7 modification. The images showed a decrease in the number of dots observed in cells transfected with 4A mutant, with only four dots visible at 2 minutes following zinc treatment (**Figure 4.25**). The number of dots then returned to the pre-stimulation level after 20 minutes at zero to one per transfected cells. Statistical analysis of these interactions showed a significant increase in the association between ZIP7 and PIM1 at 2 minutes in WT ZIP7 compared to the 4A mutant, confirming the binding of PIM1 to ZIP7 at the predicted T294 residue.

Negative control experiments were conducted individually using each antibody, resulting in only a few observed dots across the images (**Figure 4.26**), validating the lack of background staining from the antibodies. When the antibody was utilised separately, the average count of dots per cell was calculated to be less than one.

In conclusion, the number of dots observed in the interaction between MAPKAPK2, PIM1, and ZIP7 at 2 minutes was comparable to those observed with CK2, confirming the binding of these kinases to ZIP7. Additionally, the ability of the 4A mutant to diminish these binding highlights the role of S293 and T294 residues in ZIP7 modification and, subsequently, in ZIP7-mediated zinc release.

Figure 4.20 The binding of ZIP7 with CK2 by using proximity ligation assay

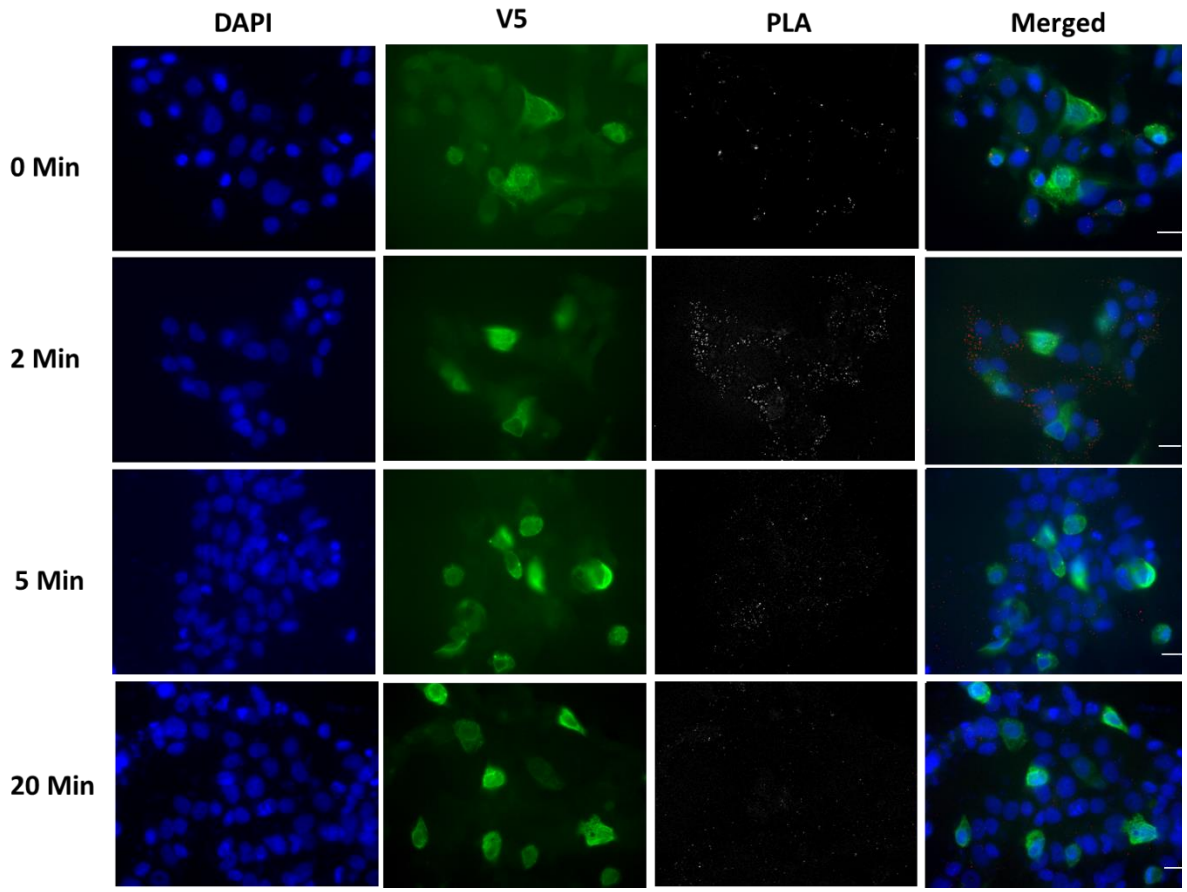

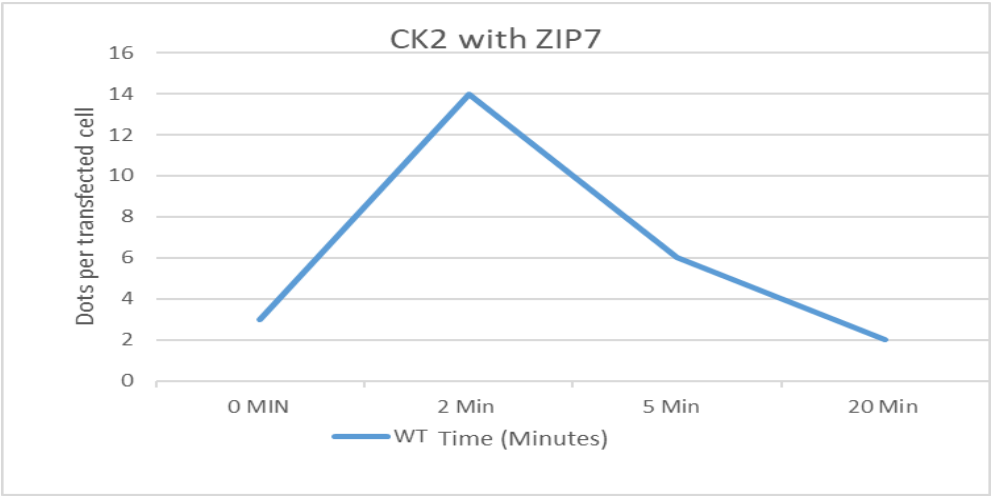

On 8−well chamber slides, cells were transfected with WT ZIP7 mutant and then treated by zinc for a time course treatment (0,2 ,5 and 20 minutes). A PLA using anti-total ZIP7 and anti-CK2 antibodies was performed. The PLA dots were converted into black and white images to enhance visual quality. The collected results are expressed as dots per transfected cell, and were obtained from 18-22 stacks, taken 0.3µm apart, from four randomly chosen representative fields on the same slide. Scale bar, 10 µm

Figure 4.21 4A mutant prevents the binding of ZIP7 with CK2

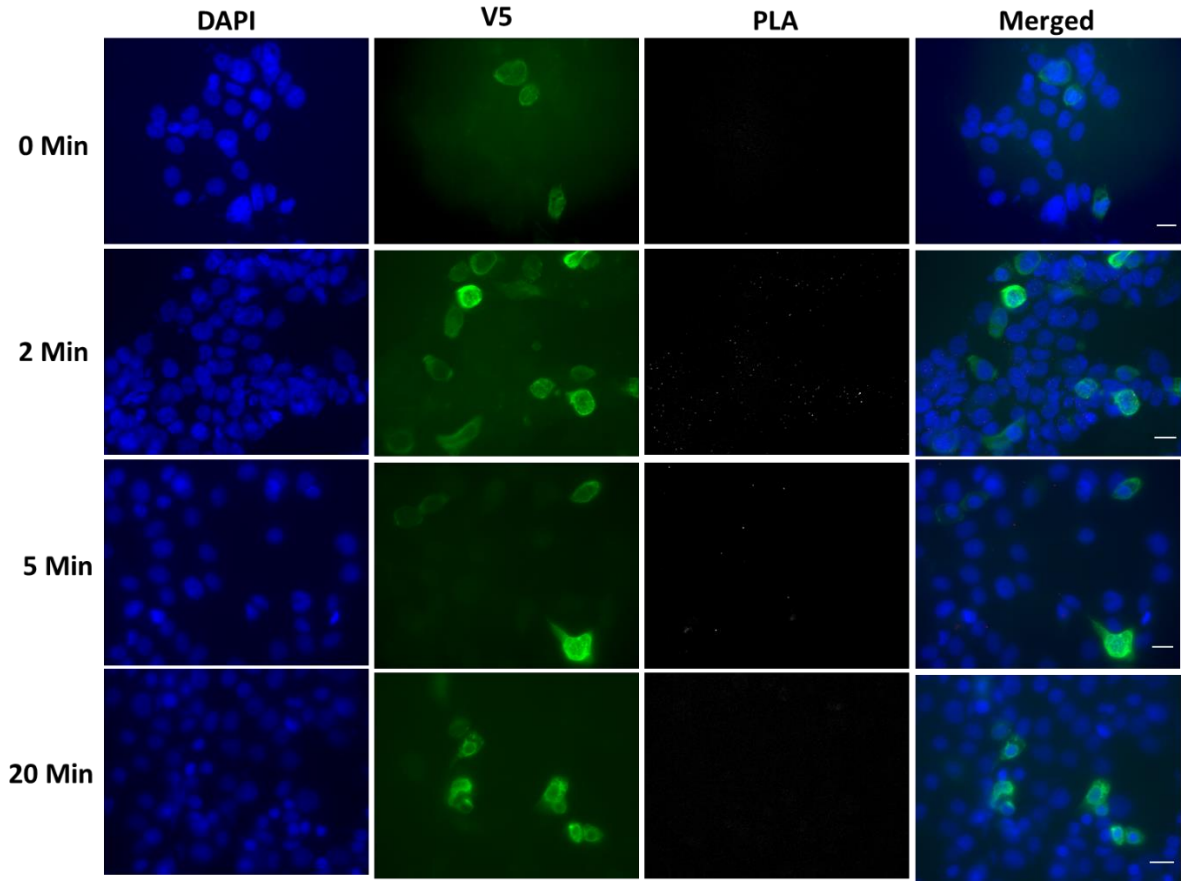

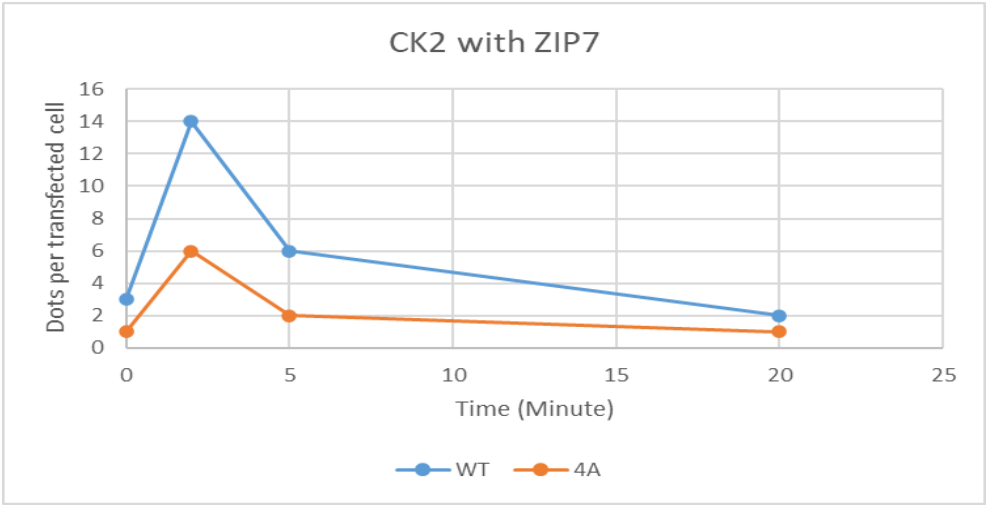

On 8−well chamber slides, cells were transfected with ZIP7 4A mutant and then treated by zinc for a time course treatment (0,2 ,5 and 20 minutes). A PLA using anti-total ZIP7 and anti-CK2 antibodies was performed. The PLA dots were converted into black and white images to enhance visual quality. The collected results are expressed as dots per transfected cell, and were obtained from 18-22 stacks, taken 0.3µm apart, from four randomly chosen representative fields on the same slide. Scale bar, 10 µm

Figure 4.22 The binding of ZIP7 with MAPKAPK2 by using proximity ligation assay

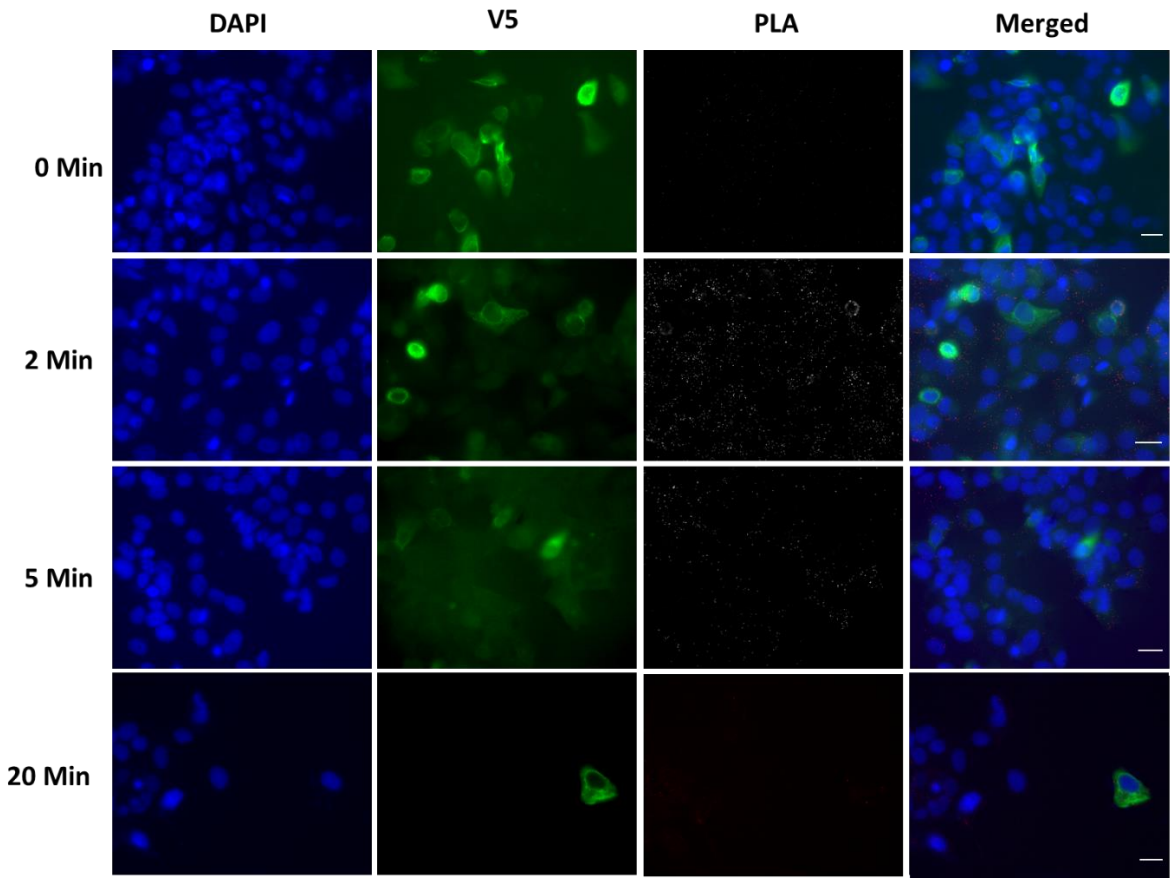

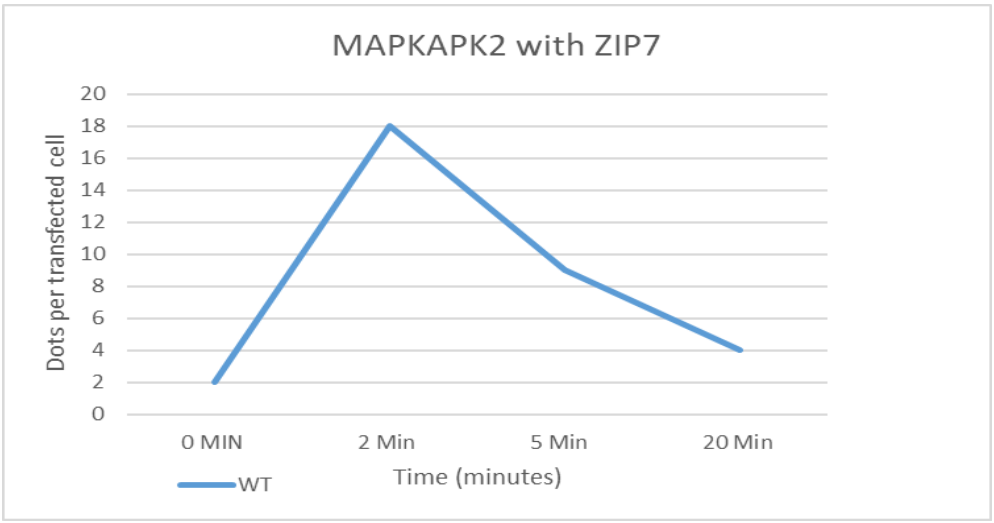

On 8−well chamber slides, cells were transfected with WT ZIP7 then treated by zinc for a time course treatment (0,2 ,5 and 20 minutes). A PLA using Anti- total ZIP7 and Anti-MAPKAPK2 antibodies was performed. The PLA dots were converted into black and white images to enhance visual quality. The collected results are expressed as dots per transfected cell, and were obtained from 18-22 stacks, taken 0.3µm apart, from four randomly chosen representative fields on the same slide. Scale bar, 10 µm

Figure 4.23 4A mutant prevents the binding of ZIP7 with MAPKAPK2

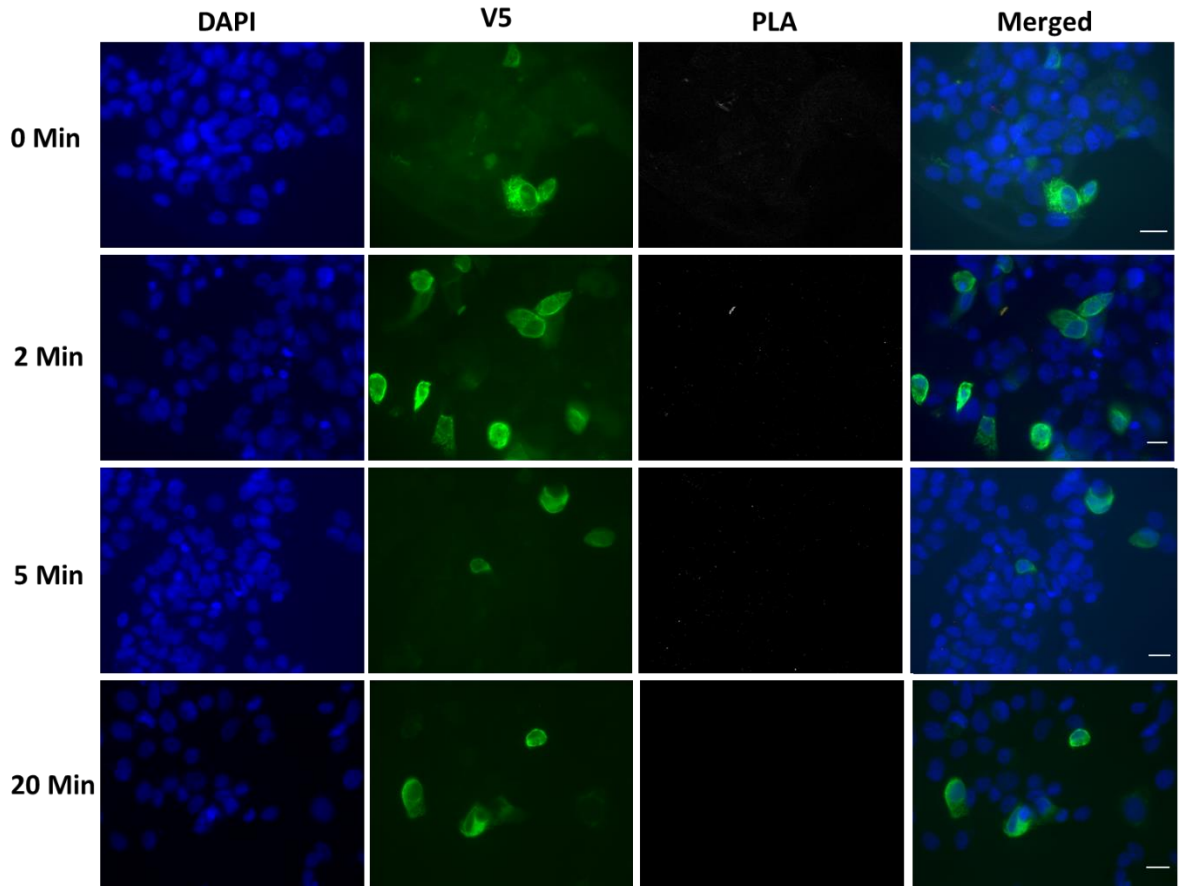

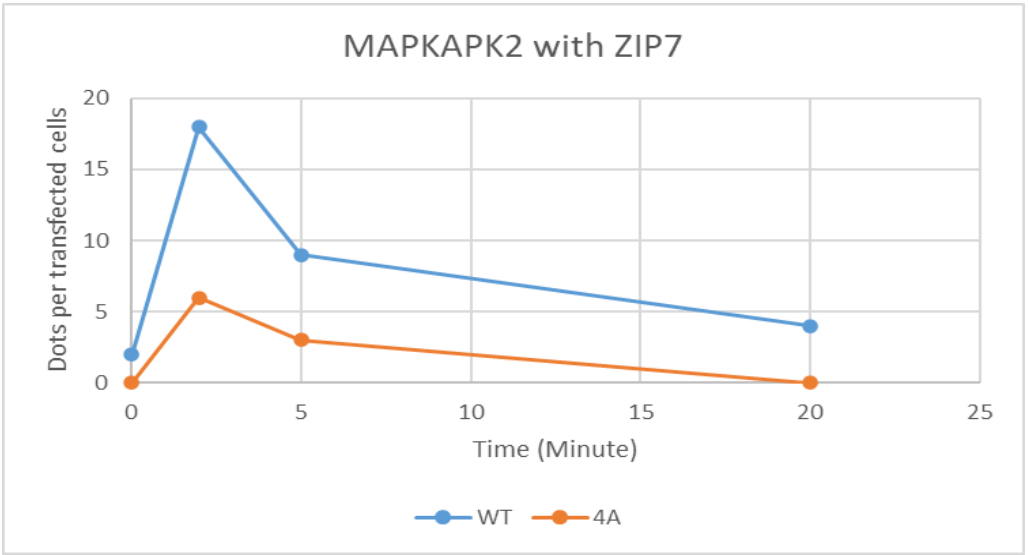

On 8−well chamber slides, cells were transfected with 4A ZIP7 mutant then treated by zinc for a time course treatment (0,2 ,5 and 20 minutes). A PLA using Anti- total ZIP7 and Anti-MAPKAPK2 antibodies was performed. The PLA dots were converted into black and white images to enhance visual quality. The collected results are expressed as dots per transfected cell, and were obtained from 18-22 stacks, taken 0.3µm apart, from four randomly chosen representative fields on the same slide. Scale bar, 10 µm

Figure 4.24 The binding of ZIP7 with PIM1 by using proximity ligation assay

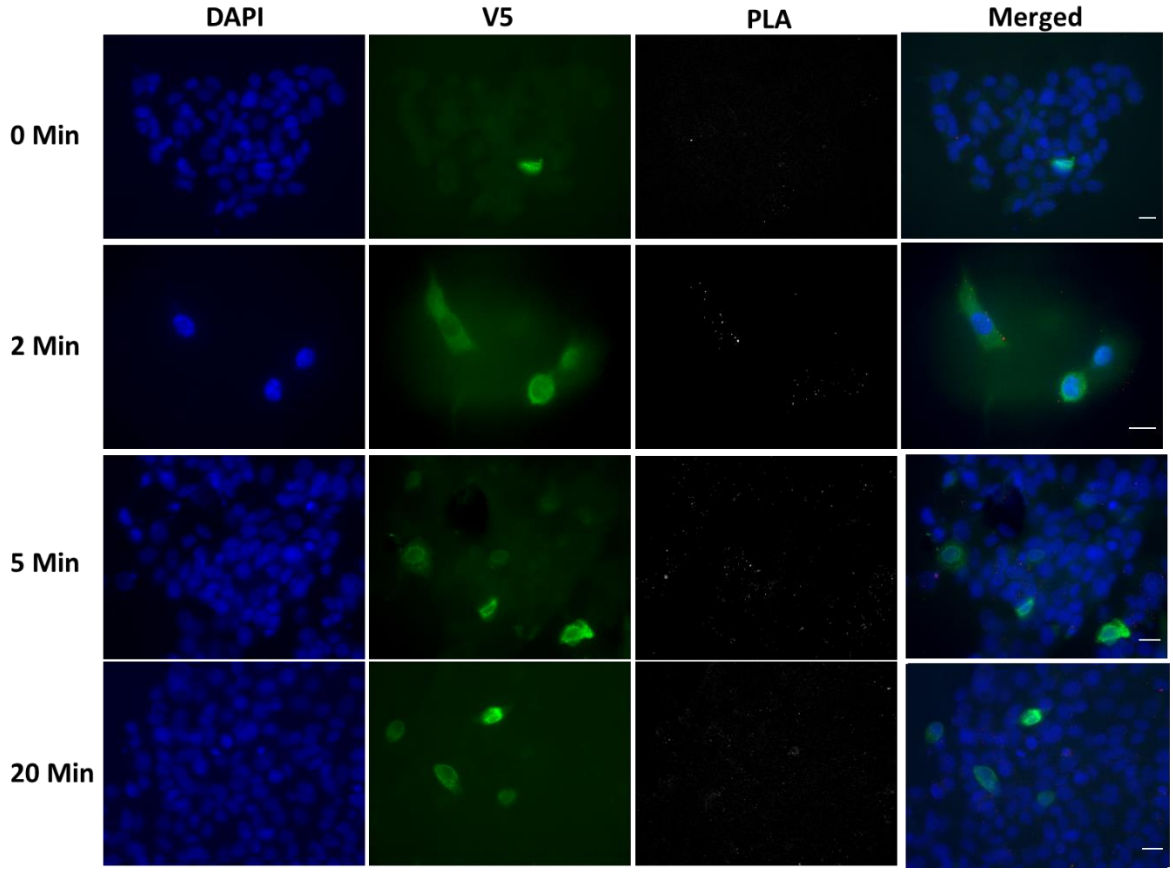

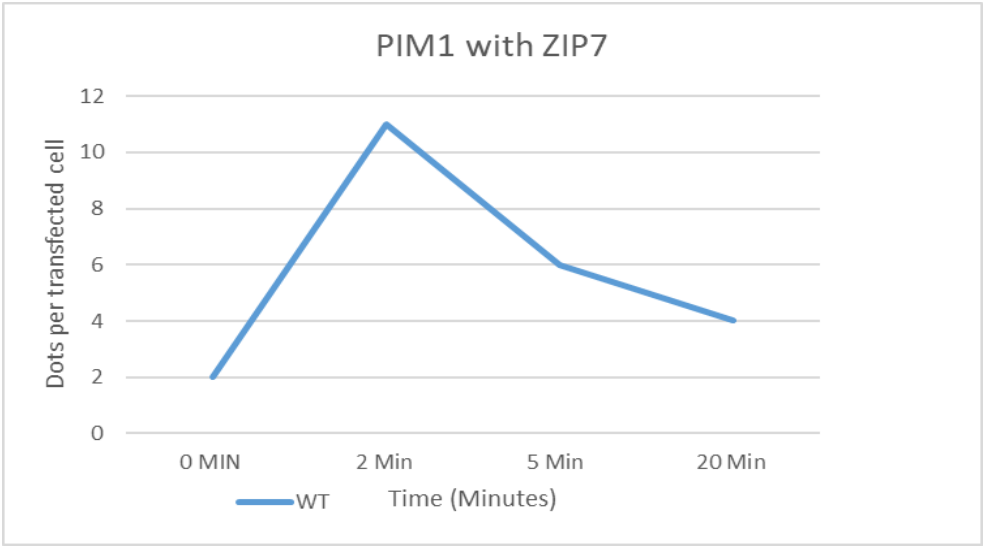

On 8−well chamber slides, cells were transfected with WT ZIP7 and then treated by zinc for a time course treatment (0,2 ,5 and 20 minutes). A PLA using Anti-ZIP7 and anti-PIM1 antibodies was performed. The PLA dots were converted into black and white images to enhance visual quality. The collected results are expressed as dots per transfected cell, and were obtained from 18-22 stacks, taken 0.3µm apart, from four randomly chosen representative fields on the same slide. Scale bar, 10 µm

Figure 4.25 4A mutant prevents the binding of ZIP7 with PIM1

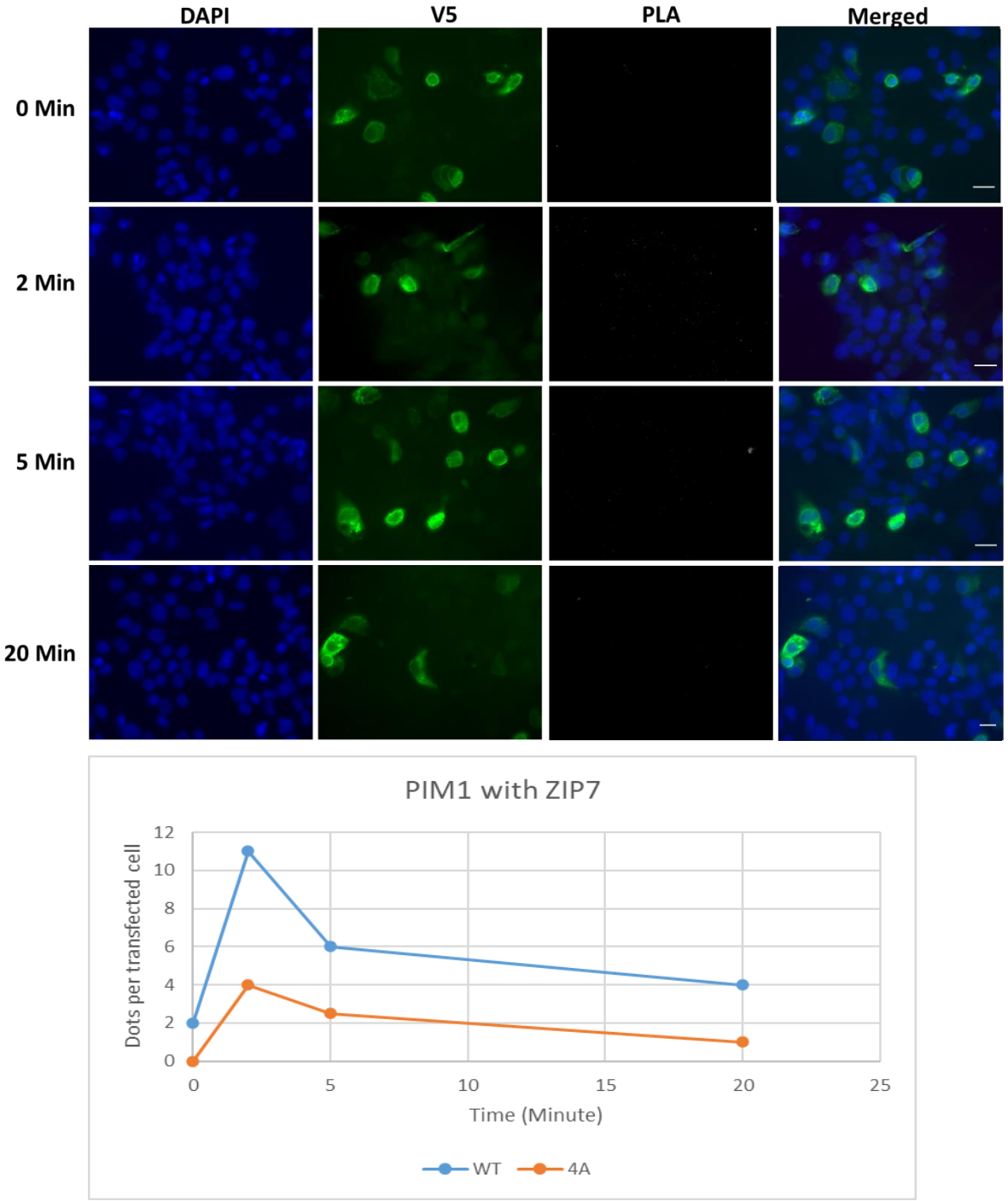

On 8−well chamber slides, cells were transfected with 4A ZIP7 mutant and then treated by zinc for a time course treatment (0,2 ,5 and 20 minutes). A PLA using Anti-ZIP7 and anti-PIM1 antibodies was performed. The PLA dots were converted into black and white images to enhance visual quality. The collected results are expressed as dots per transfected cell, and were obtained from 18-22 stacks, taken 0.3µm apart, from four randomly chosen representative fields on the same slide. Scale bar, 10 µm

Figure 4.26 Negative control for PLA experiments

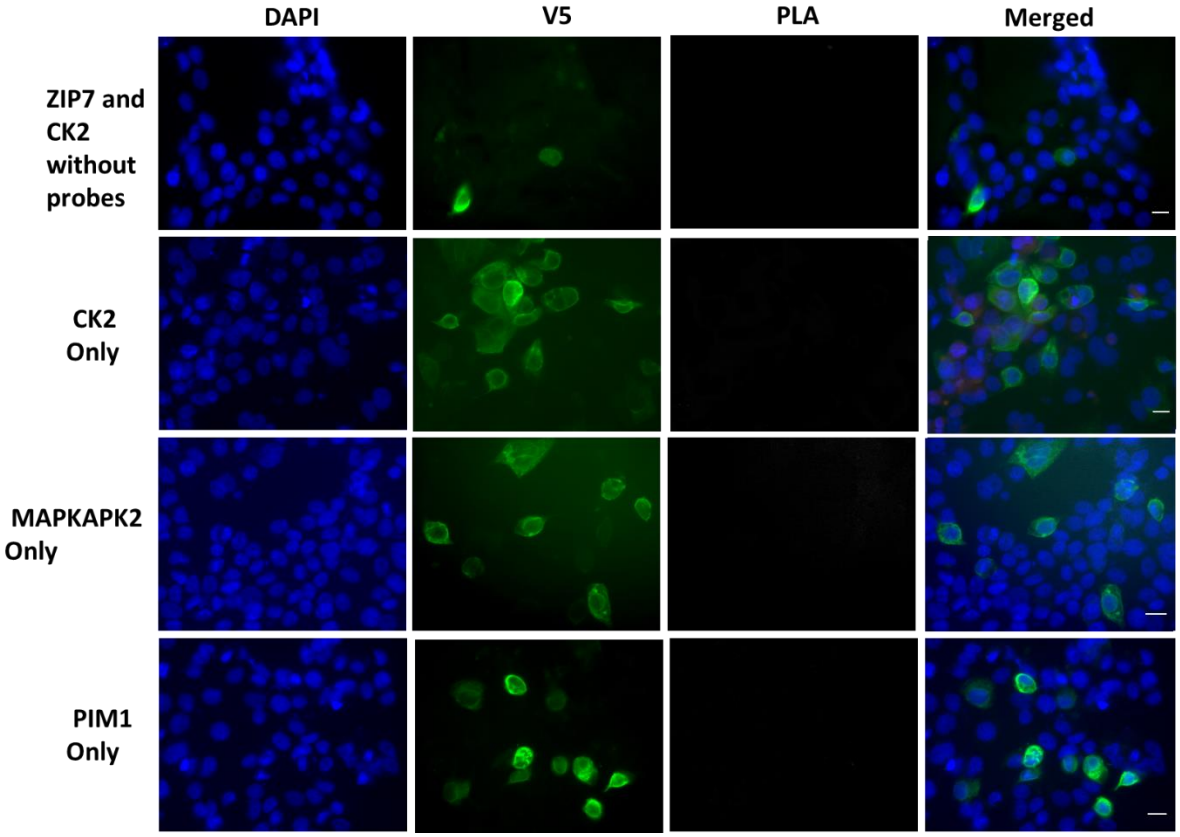

On 8−well chamber slides, cells were transfected with WT (A) treated by zinc for 2 minutes. A proximity ligation assay using CK2 and ZIP7 without probes, CK2 only, MAPKAPK2 only and PIM1 only antibodies was performed. When the antibody was used individually, the average number of dots per cell was calculated to be less than one. The PLA dots were converted into black and white images to enhance visual quality. The collected results are expressed as dots per transfected cell, and were obtained from 18-22 stacks, taken 0.3µm apart, from four randomly chosen representative fields on the same slide. Scale bar, 10 µm

4.3.9 Exploring the downstream targets affected by ZIP7-mediated zinc release in WT compared with 4A ZIP7 mutant

After examining the upstream regulator of ZIP7, it was important to determine the downstream targets influenced by ZIP7 activation. In order to perform that, Phosphokinase array was used. The Phosphokinase array is a high-throughput method that identifies the activation of 37 different cellular kinases simultaneously, along with their specific phosphorylated sites. MCF-7 cells were transfected with WT and 4A ZIP7 mutant with and without zinc. The zinc treatment was performed for 10 minute to provide sufficient time for zinc to be released from cellular stores for kinase phosphorylation to occur.

The arrays data demonstrated that cells transfected with WT and 4A mutant had an increase in intensity to some spots, especially following zinc treatment (**Figure 4.27**). The images display noticeable spots of phosphorylated kinases including pGSK-3α/ß$^{S21/S9}$, pHSP27$^{S78,\ S82}$, pSTAT5 AB$^{Y694/Y699}$ and HSP60 which are indicated by arrows. However, it is worth noting that three pairs of dark reference points can be found at the top-right, top-left, and bottom-left corners, which are used for alignment. The change in density of each phosphorylated kinases dot was then measured and represented using heat maps and bar graphs.

To evaluate the levels of each kinase, a bar graph was created, presenting the densitometric values of the corresponding duplicate dot pairs for all detected kinases at 0 and 10 minutes of zinc treatment. Kinases with changes in density more than 1500 units were considered as highly activated kinases. To minimize false positive results arising from variations in background intensity, differences below 200 units were deemed negative.

Generally, the arrays data revealed that cells transfected with WT and 4A mutant had induced phosphorylation (>1500 density units) of pGSK-3α/ß $^{S21/S9}$, pHSP27$^{S78,\ S82}$, pSTAT5 AB$^{Y694/Y699}$ and HSP60. Additionally, a mild increase in phosphorylation (500−1000 density units) was seen for pERK1/2 $^{T202/Y204,\ T185/Y187}$ (**Figure 4.28**). To analyses these further, the densitometric values of the highly activated kinases were represented in separate bar graphs.

As seen in the **Figure 4.29**, a noticeable increase in the phosphorylation of pERK1/2$^{T202/Y204,\ T185/Y187}$, pGSK-3α/ß$^{S21/S9}$ and pHSP27$^{S78,\ S82}$ was observed in WT ZIP7 and 4A mutant in zinc treatment compared to the control. This finding confirmed that these kinases are directly downstream of the zinc release mediated by ZIP7. As a result of zinc treatment, the phosphorylation of these three kinases increased in the cell expressing WT ZIP7 while it decreased in the 4A mutant. This indicates the effectiveness of mutating all four residues in attenuating ZIP7 activation. The phosphorylation of pSTAT5 AB$^{Y694/699}$ showed a slight increase in all samples, this could be attributed to transfection. However, western blotting is required to determine the expression level of this kinase. Finally, the activation of HSP60 was highly increased only in the WT ZIP7 either with or without zinc treatment compared with 4A mutant, suggesting that the activation of this protein was ZIP7−dependent.

Figure 4.27 Phospho-kinase arrays in transfected MCF-7 with WT and 4A ZIP7 stimulated with zinc

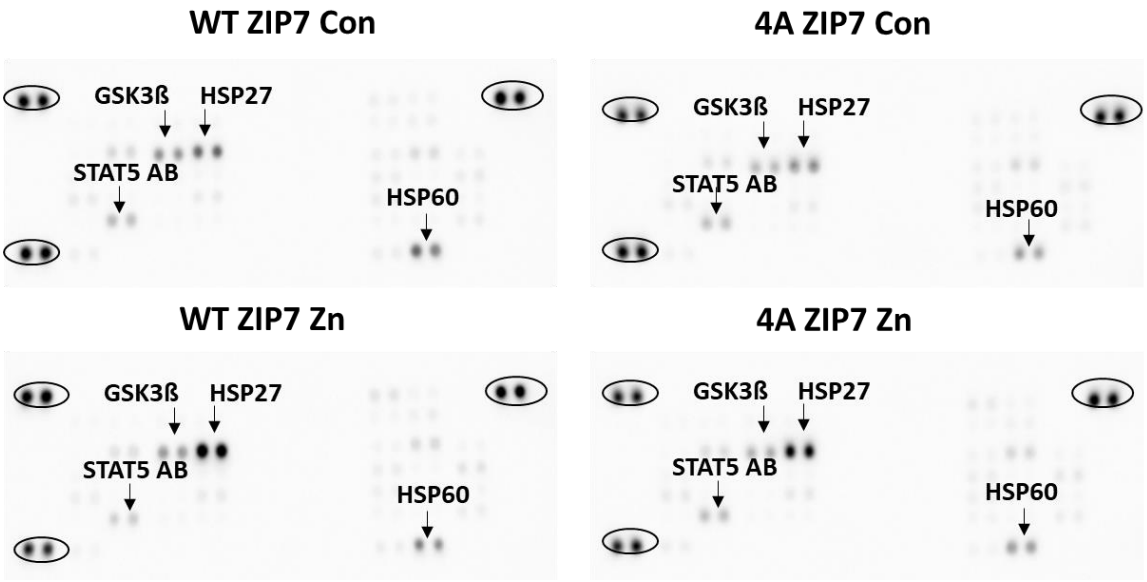

MCF−7 cells were transfected with WT ZIP7 and 4A mutant. After transfection, the cells were treated without zinc and with zinc 20µM plus sodium pyrithione 10µM for 10 minutes. The human phospho-kinase antibody arrays (ARY003C; R&D Systems) were used to examine 37 phosphorylated kinases and 2 total proteins. Signals for each kinase appear as a pair of duplicate spots, with three pairs of dark reference at the top-right, top-left, and bottom-left corners, which are used for alignment. The kinases that show changes in phosphorylation (>1500 density units) in the WT cells when compared to 4A mutant in the presence and absence of zinc are indicated with arrows.

Figure 4.28 Densitometric analysis of phospho−kinase arrays in transfected MCF−7 with WT ZIP7 and 4A mutant stimulated with zinc treatment.

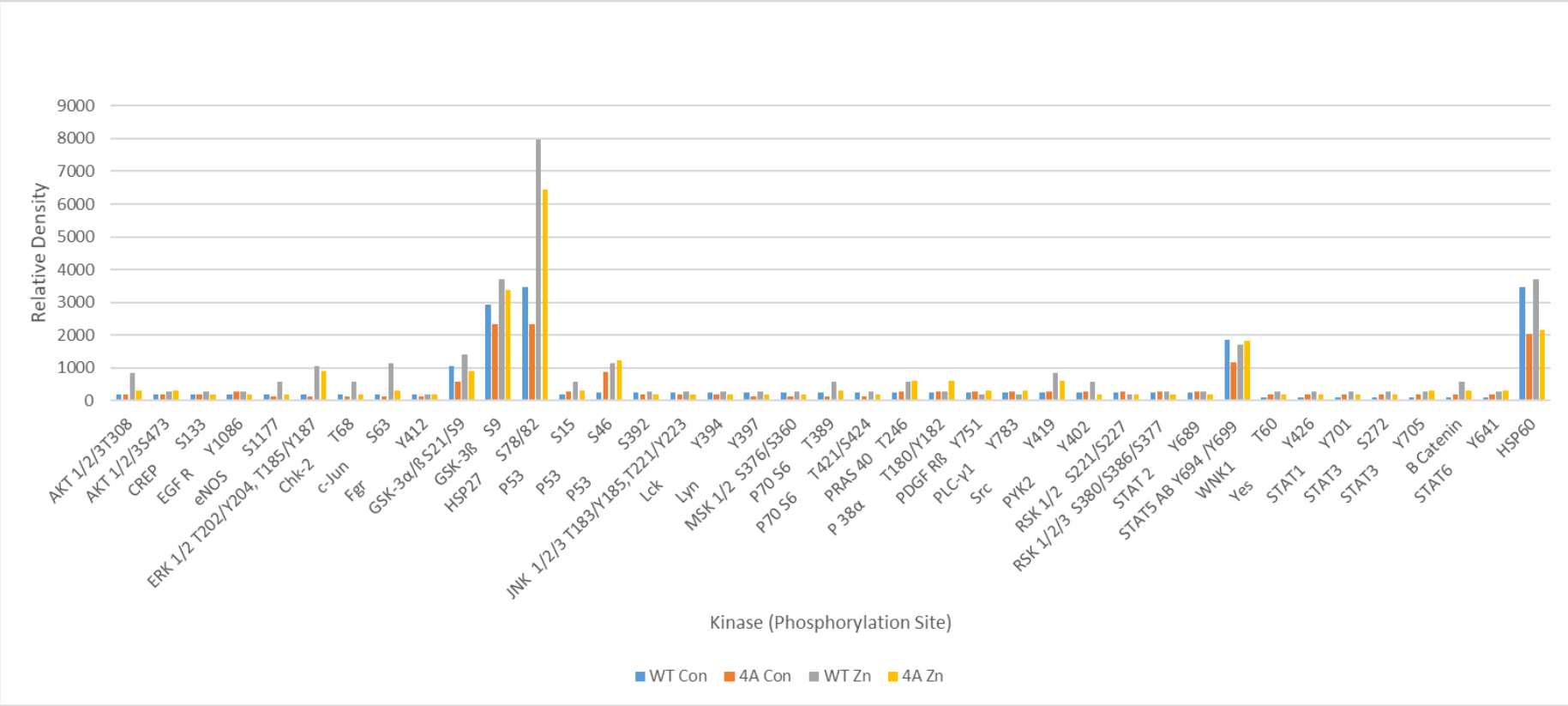

MCF−7 cells were transfected with WT ZIP7 and 4A mutant. After transfection, the cells were treated without zinc and with zinc 20µM plus sodium pyrithione 10µM for 10 minutes. The phosphorylation of selected kinases at the residues specified beneath the kinase names was identified using the human phospho-kinase antibody arrays (ARY003C) (R&D Systems). Normalised data are shown as the average of duplicate dots for each kinase (n=2).

Figure 4.29 Most activated kinases in WT compared with 4A ZIP7 mutant

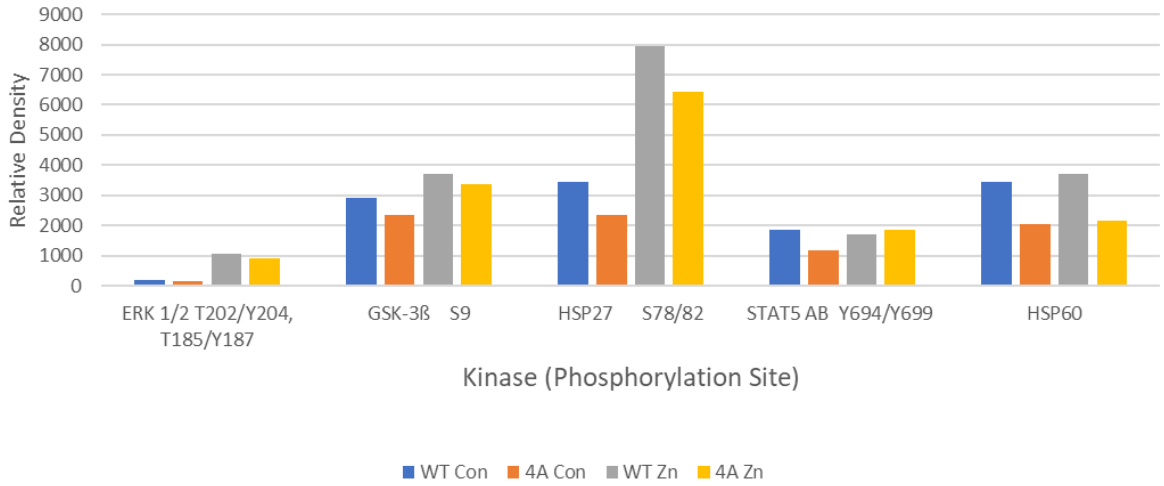

MCF−7 cells were transfected with WT ZIP7 and 4A mutant. After transfection, the cells were treated without zinc and with zinc 20µM plus sodium pyrithione 10µM for 10 minutes. The human phospho-kinase antibody arrays (ARY003C; R&D Systems) were used to examine 37 phosphorylated kinases and 2 total proteins. The average densities of each kinase that change more than 1500 units in WT compared with 4A ZIP7 mutant in the presence of zinc are indicated (n=2)

4.3.10 Western blotting confirmed kinases activation in WT compared with 4A ZIP7 mutant

In the prior section, phospho-kinase arrays were employed to systematically explore the impact of introducing mutations at all critical ZIP7 residues (S275, S276, S293 and T294) on the downstream targets of the zinc release pathways mediated by ZIP7. The 4A ZIP7 mutant showed a noticeable decrease in the phosphorylation of specific kinases in comparison to WT when stimulated by zinc. This observation indicates the functional consequences of mutated residues on the downstream signalling pathways mediated by ZIP7 in response to zinc release. To validate these findings, western blot was performed in cells transfected with WT, AA and 4A mutant, followed by a 10-minute zinc treatment. The reason to include the AA mutant in this experiment to investigate the impact of the additional residues (S293 and T294), comparison to S275 and S276 alone. This allowed to elucidate specific contributions of these residues to maximal ZIP7 activation and their roles in modulating the downstream signalling pathways. The kinases selected to be confirmed by western blot were pGSK-3ß^{S9}, pHSP27$^{S78,\ S82\ and}$ pERK1/2$^{T202/Y204,\ T185/Y187}$.

GSK-3ß (S9) has been reported to be one of the downstream effectors of ZIP7-mediated zinc release from the ER (Taylor et al., 2012). Consistently, the phosphorylation of pGSK-3ß^{S9} was significantly increased in WT ZIP7 following zinc treatment (**Figure 4.30 A**), confirming its involvement in the signalling events triggered by ZIP7 activation. AA mutant significantly reduced effect of zinc compared to WT ZIP7. Interestingly, this effect was further amplified by 4A mutant, being significantly decreased versus the WT and AA, suggesting an additive action of ZIP7-phosphorylation sites.

Next, pHSP27$^{S78,\ S82}$ was also analysed by western blot. The result illustrated that cells transfected with WT showed a significant increase in phosphorylation following zinc treatment compared to the control, confirming the data from the phosphokinase arrays (**Figure 4.30 B**). This, in turn, suggests the pHSP27^{S78,82} is a confirmed downstream target of ZIP7 in response to zinc release. In contrast, AA mutant diminished the effect of zinc release, as the phosphorylation level was significantly decreased compared with WT after stimulation with zinc. Notably, the 4A mutant effectively attenuated the effect of zinc release on HSP27 activation to a greater extent than the AA mutant. This confirmes the requirement of additional residues for achieving maximal ZIP7 activation.

Finally, the phosphorylation of pERK1/2$^{T202/Y204,\ T185/Y187}$ in cells transfected with WT ZIP7 also showed a significant increase following zinc treatment compared to the control (**Figure 4.30 C**). Interestingly, the AA mutant seemed to have no noticeable effect on the phosphorylation level of pERK1/2$^{T202/Y204,\ T185/Y187}$, as the levels in response to zinc were similar to those observed with WT. Conversely, the 4A mutant effectively diminished the phosphorylation level of pERK1/2$^{T202/Y204,\ T185/Y187}$ compared with WT, indicating that the S293 and/or T294 residues are essential activating ERK1/2 by ZIP7-mediated zinc release.

Figure 4.30 Western blotting confirmed kinases activation in WT compared with 4A ZIP7 mutant

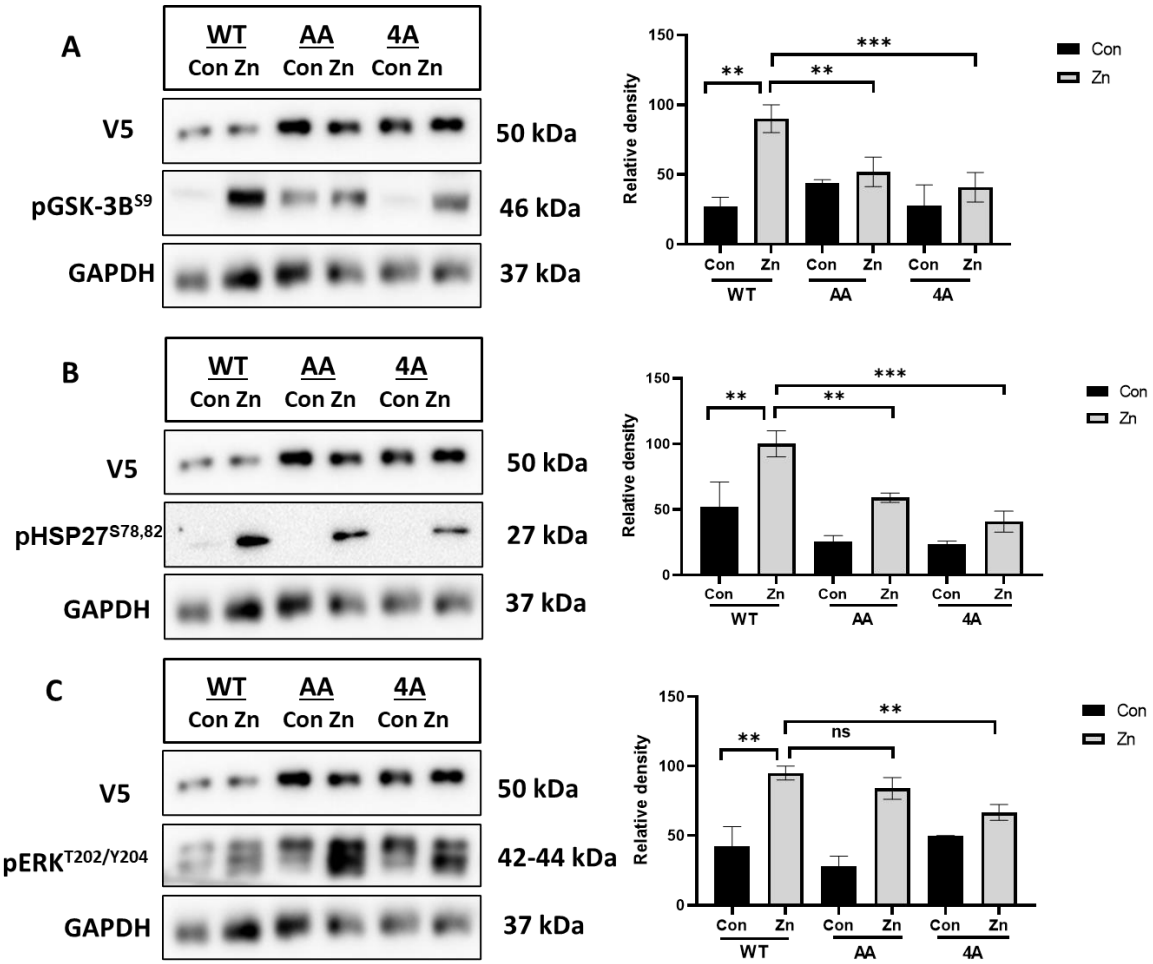

MCF7 cells were transfected with WT ZIP7, AA and 4A mutant, then treated without zinc and with zinc 20µM (Zn) plus sodium pyrithione 10µm for 10 minutes. The blot was probed for pGSK-3ß^{S9} (**A**), pHSP27^{S78,82} (**B**) and pERK1/2 $^{T202/Y204, T185/Y187}$ (**C**). GAPDH was utilised as a loading control All data were analysed and normalised to V5 using ImageJ. (n=3)

4.4 Chapter summary

This chapter provided additional validation that the pZIP7 antibody specifically binds to the active form of ZIP7 when phosphorylated at residues S275 and S276. Using an immunofluorescence technique, the pZIP7 showed its capacity to identify the active form of ZIP7 in WT samples, while failing to bind to the S275 and S276 residues when mutated to alanine in the AA mutant. Employing the same technique, a notable rise in the proportion of cells transfected with WT ZIP7 that showed positive for pZIP7 was observed after zinc treatment, implying the ability of zinc to stimulate ZIP-mediated zinc release (**Figure 4.3**). The ZIP7-mediated zinc release was also detected in WT following zinc treatment as judged by AKT activation, whereas the AA mutant significantly reduced the effect on AKT (**Figure 4.4**). Moreover, analysis of the database suggested the potential for ZIP7 to also be phosphorylated on S293 and T294. Using immunofluorescence and western blot techniques, the involvement of S293 and T294 in ZIP7 activation was demonstrated by using the pZIP7 and investigating the AKT activation in S293A and T294A mutants compared with WT ZIP7 **(Figure 4.6 and 4.7**). Additionally, proximity ligation assay confirmed the binding of CK2 with ZIP7 at 2 minutes after zinc treatment, in agreement with a previous report (Taylor et al., 2012) and also exhibited the binding of predicted kinases (MAPKAP2) with ZIP7 in a manner similar to that of CK2 (**Figure 4.8 and 9**). Next, the downstream targets of individual residues of ZIP7 were explored by using phosphokinase arrays, and the results generated several kinases such as pAKT^{S473}, pGSK-3α/ß$^{S21/S9}$, pCREB^{S133}, pHSP27^{S78,S82} and pERK1/2$^{T202/Y204,\ T185/Y187}$ which were activated (**Figure 4.10,11, and 12**). The activation of these kinases was then confirmed by using western blot which showed how zinc release mediated by ZIP7 influences the activation of downstream signalling pathways and the requirement for S293 and T294 residues for this activation (**Figure 4.13 and 14**).

To further investigate the impact of S293 and T294 residues on ZIP7 activation, a novel construct of ZIP7 (4A), where all these four residues had been mutated to alanine, was used. As the 4A mutant was constructed in a plasmid vector without any His-Tag, the effect of His-Tag was initially investigated.

Using immunofluorescence and western blot techniques, the results showed that the construct lacking the His-Tag produced a more distinct differentiation between the WT and AA mutant following zinc treatment (**Figure 4.16 and 4.17**).

In comparison with WT and AA, the effect of ZIP7 activation was further reduced by 4A mutant as indicated by pZIP7 and AKT activation, (**Figure 4.18 and 4.19**), suggesting an additive action of ZIP7-phosphorylation sites. Moreover, MAPKAPK2 and PIM1 are predicted to bind to ZIP7 on residues S293 and T294, respectively. The association of these kinases with ZIP7 was confirmed by using proximity ligation assay, showing a significant interaction after 2 minutes in a manner similar to that of CK2 (**Figure 4.20,21,22,23,24 and 25**) (Taylor et al., 2012).

Finally, the downstream targets of S293 and T294 residues of ZIP7 were explored by using phosphokinase arrays and confirmed by western blot (**Figure 4.27,28,29 and 30**). Phosphorylation of pGSK-3ß^{S9}, pHSP27^{S78,82}, and pERK1/2$^{T202/Y204,\ T185/Y187}$ was demonstrated to be downstream effectors of the zinc release mediated by ZIP7, with WT exhibiting increased activation following zinc treatment. In contrast, the AA mutant decreased the effects on these kinases, while the 4A mutant further diminished the impact, indicating the importance of additional residues, S293 and T294, in achieving maximal ZIP7 activation and modulating downstream signalling pathways.

Chapter 5

Exploration of ZIP6 and ZIP10 Zinc Transporters using Novel Constructs with N-Termini and Ubiquitin Modifications

5.1 Introduction

ZIP6 and ZIP10 are two close homologues within the LIV-1 subfamily, sharing a sequence similarity of 43.5% and belong to the same branch of the ZIP family phylogenetic tree (**Figure 3.1**). Both zinc transporter ZIP6 and ZIP10 have been independently implicated in various types of cancer including breast cancer (Takatani-Nakase, 2018)(Saravanan et al., 2022). ZIP6 was found to be more commonly associated with estrogen receptor-positive breast cancers spreading to lymph nodes (Grattan and Freake, 2012). The expression level of ZIP6 has been shown to be significantly elevated in tumours compared with normal breast tissue using clinical cancer databases. Therefore, ZIP6 was proposed as a dependable tumour marker for identifying estrogen receptor positive breast cancers (Tang et al., 2019)(Jones et al., 2022). Similarly, ZIP10 has also been linked to aggressive breast cancer and its spread to the lymph nodes. This is supported by the fact that the ZIP10 mRNA expression was notably elevated in breast cancer patients with lymph node metastasis compared to those without such metastasis (Kagara et al., 2007b).

ZIP6 and ZIP10 have been separately identified as capable of initiating cell rounding and detachment, which consequently triggers the EMT process (Taylor et al., 2016). This mechanism appears to be employed by cells to detach from tumours and subsequently metastasise. Recently, our group has discovered the essential role of ZIP6 and ZIP10 to form a heteromer, which facilitates zinc influx, subsequently triggering mitosis (Nimmanon et al., 2020). To initiate mitosis, the ZIP6/ZIP10 heteromer must first be translocated to the plasma membrane by cleavage of the N-terminus of ZIP6 (Nimmanon et al., 2020).

ZIP6 and ZIP10 have been shown to undergo proteolytic cleavage, which is an integral aspect of their functional activity (Hogstrand et al., 2013)(Ehsani et al., 2012). Both transporters possess a strongly predicted PEST site located in the middle region of their N-terminus (Chapter 3.3.3.3). Bands obtained by western blotting for ZIP6 are consistent with ZIP6 activation by N-terminal cleavage at a predicted PEST cleavage site before relocation to the plasma membrane for zinc influx (Hogstrand et al., 2013).

This was supported by further experimental findings as the far N-terminal region of ZIP6 was not observed at the plasma membrane, even though it was present in the ER (Hogstrand et al., 2013).

This implies that the full-length protein was likely located in the ER, and the cleavage process was required for proper localization of ZIP6 to the plasma membrane. Similarly, ZIP10 has also been shown to undergo proteolytic cleavage at its N-terminus. This was verified by the various band sizes observed when analysed through western blotting (Ehsani et al., 2012). Nevertheless, the significance of this cleavage to protein function remains unclear. Taken together, these findings have reinforced the important role of the N-terminus in ZIP6 and ZIP10 function.

Moreover, ubiquitination is a type of post-translational modification used by the cell to cause protein degradation (Sun et al., 2020)(Chen et al., 2022). In the case of ZIP6, it comprises PEST and ubiquitin sites that are strongly conserved through evolution, indicating their importance. These sites potentially direct ZIP6 towards degradation, resulting in a relatively short half-life of less than one hour for the ZIP6 (Hogstrand et al., 2013). This could explain the observed deficiency in the quantity of recombinant ZIP6 harvested following the transfection process. Therefore, the potential impact of ubiquitin sites in ZIP6 expression and stability remains unclear. Experimental investigation into the effect of the ubiquitin sites on the regulation of ZIP6 function could provide meaningful insights into the mechanisms controlling zinc homeostasis and the associated cellular process.

This chapter will firstly examine the role of N-termini in ZIP6 and ZIP10 by using novel chimeric constructs, wherein the N-terminus has been modified. The use of immunofluorescence and western blot techniques will allow investigation of the effect of these constructs on ZIP6 and ZIP10 localisation and regulation, as compared to their respective wild-type constructs. Subsequently, the downstream effect of altering the N-terminus of ZIP6 and ZIP10 will also be investigated. The final part of this chapter will focus on investigating the impact of ubiquitin sites in ZIP6, using a novel construct wherein all potential ubiquitin sites have been mutated to alanine. These experiments for ubiquitin sites were designed to identify the potential effect of ubiquitination on ZIP6 expression and activation.

5.2 Method

Chimera and mutated ubiquitin constructs were artificially synthesised by Doulix (Venice, Italy) and then confirmed by DNA sequencing. In chimeric ZIP6 and ZIP10 DNA constructs, the first 326 N-terminal amino acid of ZIP6 or the first 408 N-terminal amino acid of ZIP10 was replaced with the first 143 N-terminal amino acid of ZIP7, yielding a chimera that consisted of N-terminus of ZIP7 with transmembrane domains of ZIP6 (noted as ZIP7/ZIP6) or ZIP10 (noted as ZIP7/ZIP10). In a deubiquitinated construct, all potential ubiquitin sites were changed to alanine K467A, K468A, K472A, K456A, K457A, in order to prevent ubiquitination. This novel construct is referred to as ZIP6 Q. Moreover, ZIP7, ZIP6 and ZIP10 Wild Type (WT) were also employed as a control. All constructs have been placed into a plasmid vector (cDNA3.1/V5−TOPO) containing a C-terminal V5 tag that is resistant to ampicillin (**Figure 2.2**). The constructs were then multiplied by introducing them into the JM109 E. coli. The EndoFree Plasmid Maxi Kit (Qiagen) was used to purify the plasmids of chimeric and WT constructs. The purity and concentration of the plasmid DNA was determined using a UV spectrophotometer, which indicated that the OD260/OD280 ratios fell within the acceptable range of 1.8-2.0. This indicates the purity of the DNA. The DNA concentration ranged from 0.94 to 1.92 µg/µL. (**Table 5.1**). For information on the techniques used for transfection (Section2.1.2) and generation of recombinant proteins (2.2), plasmid preparation (Section 2.3), immunofluorescence (Section 2.4), and western blotting (Section 2.5), proximity ligation assays (Section 2.7), Phospho-Kinase Array (Section 2.8) please refer to Chapter 2.

Table 5.1 DNA concentration and OD260/280 ratio of prepared plasmids

Plasmid	DNA concentration µg/µl	OD260/280 Ratio
ZIP7 Wild-Type	1.653	1.897
ZIP6 Wild-Type	1.48	1.89
ZIP10 Wild-Type	1.92	1.89
Chimera ZIP7/ZIP6	1.2	1.86
Chimera ZIP7/ZIP10	0.94	1.88
ZIP6 Q	1.43	1.89

The plasmid DNA was determined with a UV spectrophotometer. OD260/OD280 ratios ranged from 1.8 to 2.0, indicating the purity of the DNAs.

5.3 Results

5.3.1 Verification of chimeric constructs

Exogenous expression of ZIP6 and ZIP10 in cells usually results in very few numbers of cells expressing the recombinant protein (Hogstrand et al., 2013) (Taylor et al., 2016b). This observation is attributed to the ability of ZIP6 and ZIP10 to promote cell detachment. Previously, it has been determined that a short transfection time such as 16-18 hours, will maximise the presence of ZIP6 and ZIP10 transfected cells prior to detachment. Therefore, the MCF-7 cells were initially transfected with the WT ZIP6 and WT ZIP10 for verification and optimisation of transfection time for these constructs. WT ZIP7 were also used as a positive control. The transfection time used for these experiments were 17 and 24 hours.

To optimise the transfection time for WT constructs, immunofluorescence was performed with a V5 antibody. This antibody recognises the C-terminal V5 tag following transfection at 17 and 24 hours. Expectedly, immunofluorescence images showed that the transfection with WT ZIP6 and WT ZIP10 produced few numbers of cells that were positive for V5 in 17 hours (**Figure 5.1 A**) while no transfected cells were detected in 24 hours of transfection (**Figure 5.1 B**) Conversely, cells stained with WT ZIP7 were robustly transfected in both times of transfection (**Figure 5.1 A and B**). These results confirmed that the transfection of cells with ZIP6 and ZIP10 caused cell detachment, leading to lower transfection efficiency, while ZIP7 did not have this effect.

Now, it is intriguing to examine the effects of changing the N-terminus of ZIP6 and ZIP10 on the transfection efficiency of the corresponding recombinant proteins. Interestingly, immunofluorescence images showed that the two chimera constructs were robustly transfected at both transfection times (**Figure 5.2 A and B**), suggesting that modifications to the N-terminus could prevent or perhaps delay the cell detachment observed in the WT ZIP6 and WT ZIP10. This was supported by the representative graph (**Figure 5.2 C**), which showed a high number of transfected cells in all chimeric constructs at both time points. This level of transfection was seen to be comparable to that observed with the WT ZIP7, as determined by positive V5 staining. This suggests that the N-terminus is essential for ZIP6 and ZIP10 activation, and modifications in this region could prevent ZIP6 and ZIP10 from localising at the plasma membrane.

Figure 5.1 The transfection efficiency for WT ZIP transporters

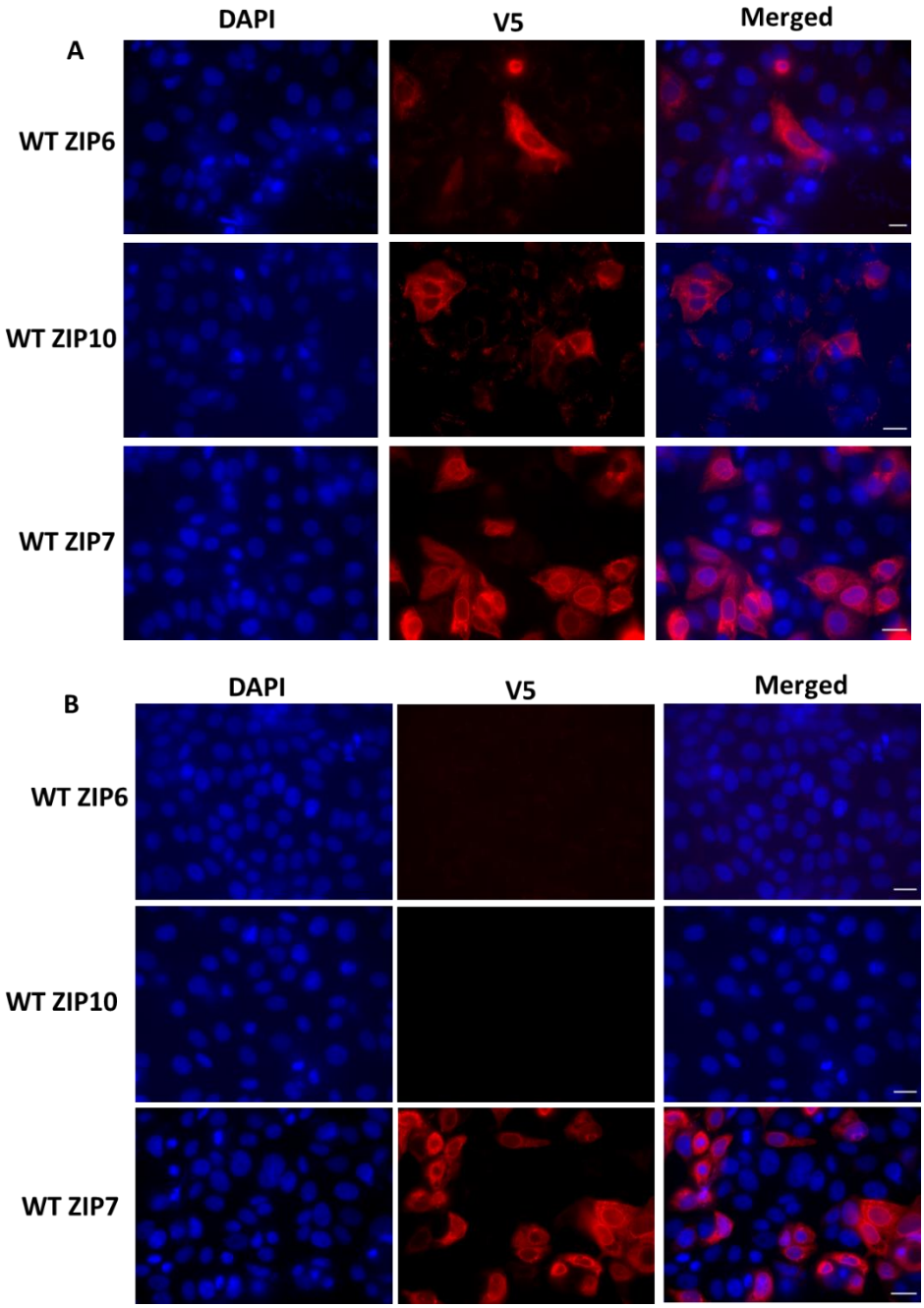

MCF-7 cells were transfected with WT ZIP6, WT ZIP10 and WT ZIP7 constructs for 17 (**A**) and 24 (**B**) hours. The cells were stained for DAPI (blue) and V5 conjugated to Alexa Fluor 594 (Red) and then imaged using a 63x magnification lens on Leica RPE automatic microscope. Scale bar, 10 μm.

Figure 5.2 The transfection efficiency of the chimeric constructs

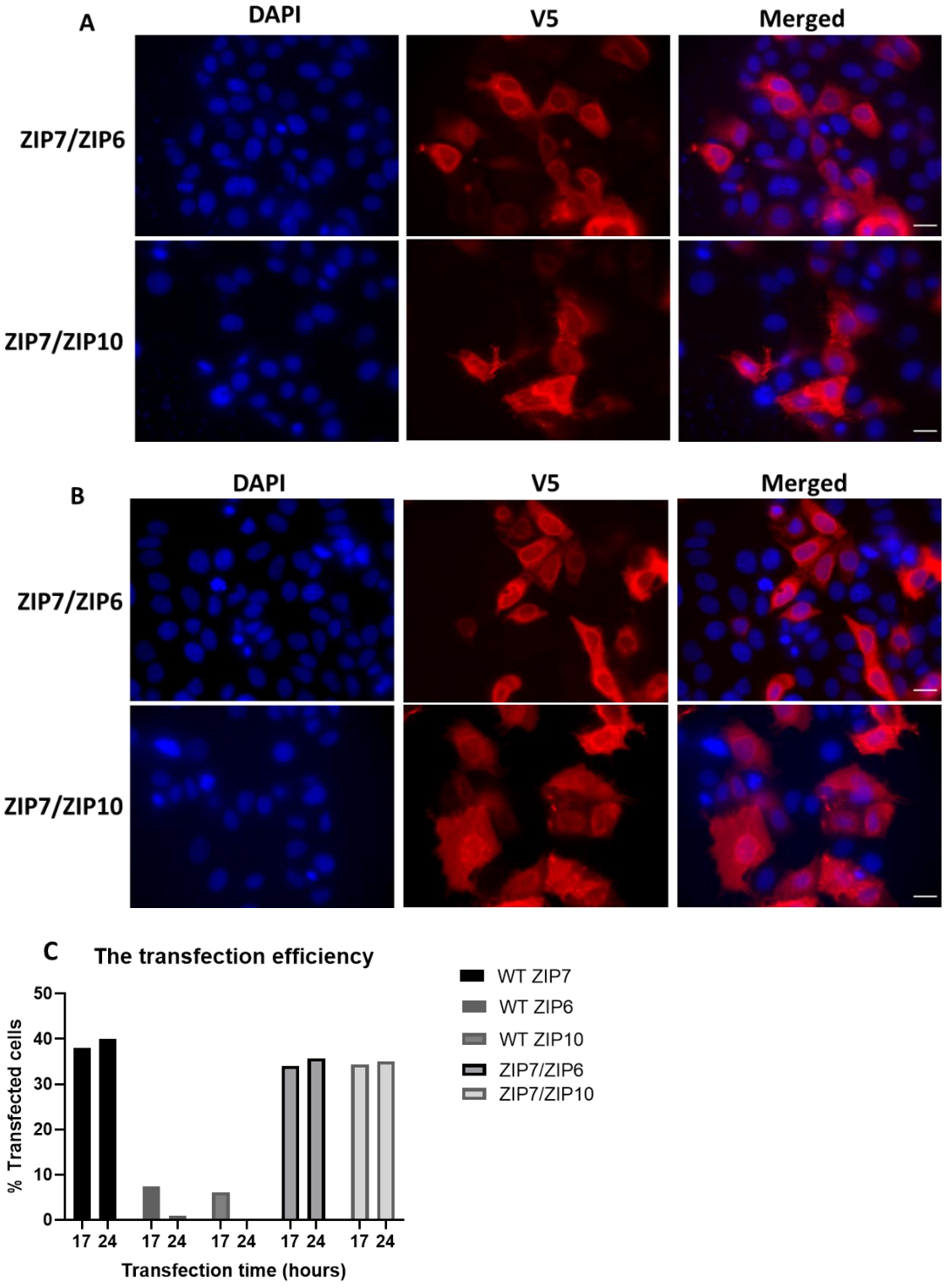

MCF-7 cells were transfected for 17 hours (**A**) and 24 hours (**B**) with chimeras constructed by joining of the N-terminus of ZIP7 with transmembrane domains of ZIP6 (ZIP7/ZIP6) or ZIP10 (ZIP7/ZIP10). The cells were stained for DAPI (blue) and V5 conjugated to Alexa Fluor 594 (red) and then imaged using a 63x magnification lens on Leica RPE automatic microscope. The transfection rates are shown in a bar graph (**C**) as the mean of four represented fields. Scale bar, 10 μm.

5.3.2 Localisation of chimeric constructs

The N-terminus of ZIP6 has been shown to play a role in determining the localization of ZIP6 within the cell (Hogstrand et al., 2013). The ZIP6 pro-protein is located on the ER membrane and remains there until a specific stimulus activates cleavage at the middle of N-terminus region. Once it is activated, ZIP6 moves to the plasma membrane, where it begins to function (Hogstrand et al., 2013). Moreover, ZIP10 has been reported to be cleaved at its N-terminus (Ehsani et al., 2012). However, the significance of this N-terminal cleavage in relation to its localization within the cell remains unclear. Recently, it has been shown that ZIP10 undergoes N-terminal cleavage after being moved to the plasma membrane at the onset of mitosis (Nimmanon et al., 2020). Conversely, ZIP7 does not undergo any N-terminal cleavage as this region in ZIP7 lacks a PEST motif (Taylor et al., 2008)(Taylor et al., 2012). Using the chimeras that combine the N-terminus of ZIP7 with the transmembrane domains of ZIP6 or ZIP10, it would be possible to investigate how these modifications could alter the localisation of ZIP6 or ZIP10. In MCF-7 cells transfected with chimeric constructs, immunofluorescence revealed endoplasmic reticulum staining for ZIP7/ZIP6 at both transfection times, as indicated by positive V5 staining (**Figure 5.3 A**). This staining pattern was observed in both ZIP7 and in pro-protein ZIP6, suggesting a role for the N-terminus in determining ZIP6 localisation. For chimeric ZIP7/ZIP10, the images exhibited a localization pattern that resembles both ER and PM, as judged by positive V5 staining (**Figure 5.3 B**). Additionally, it can be noticed that the ZIP7/ZIP10 chimera also located to the PM lamellipodiae, indicating the modification of the N-terminus in ZIP10 had no effect on its localisation.

To further investigate the localisation of the chimeric constructs, staining with the V5 antibody was performed again under unpermeabilised conditions to confirm their presence on the PM. In this condition, saponin, which is commonly employed to permeabilize cell membranes, was not used. Therefore, in unpermeabilised conditions, the cell membrane remains intact, and the V5 antibody can only identify the recombinant proteins located extracellular or on cell surface. As shown in **figure 5.4 A and B**, the PM located pattern was observed in two chimeric constructs ZIP7/ZIP6 and ZIP7/ZIP10, indicating their ability to migrate to PM at both transfection times.

However, compared to the standard transfection condition shown in **Figure 5.2**, the transfection rate for both constructs was significantly lower, suggesting that the vast majority of the recombinant proteins still reside in the ER. Therefore, it is important to investigate whether the chimeras that have migrated to the PM are functional and capable of transporting zinc.

Figure 5.3 The localisation of Chimeric construct

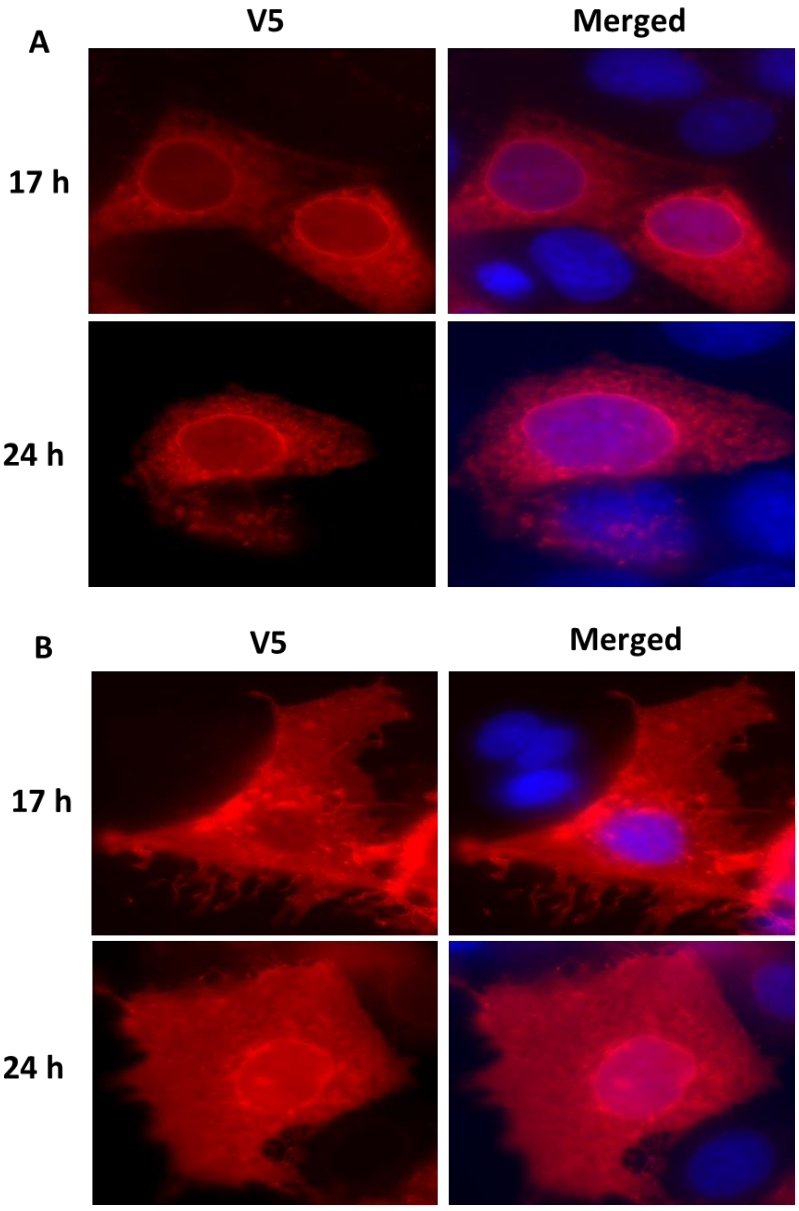

MCF-7 cells were transfected with chimeric constructs ZIP7/ZIP6 (A) and ZIP7/ZIP10 (B) for 17 and 24 hours. An enlarged image of the transfected cells in ZIP7/ZIP6 shows an expression of the recombinant proteins, exhibiting a characteristic ER localisation, similar to the staining pattern observed in both ZIP7 and in pro-protein ZIP6 (**A**). For ZIP7/ZIP10 chimera, the imaged showed both ER and PM localisation for both transfection time (**B**).

Figure 5.4 Localisation of chimeric constructs in unpermeabilised condition

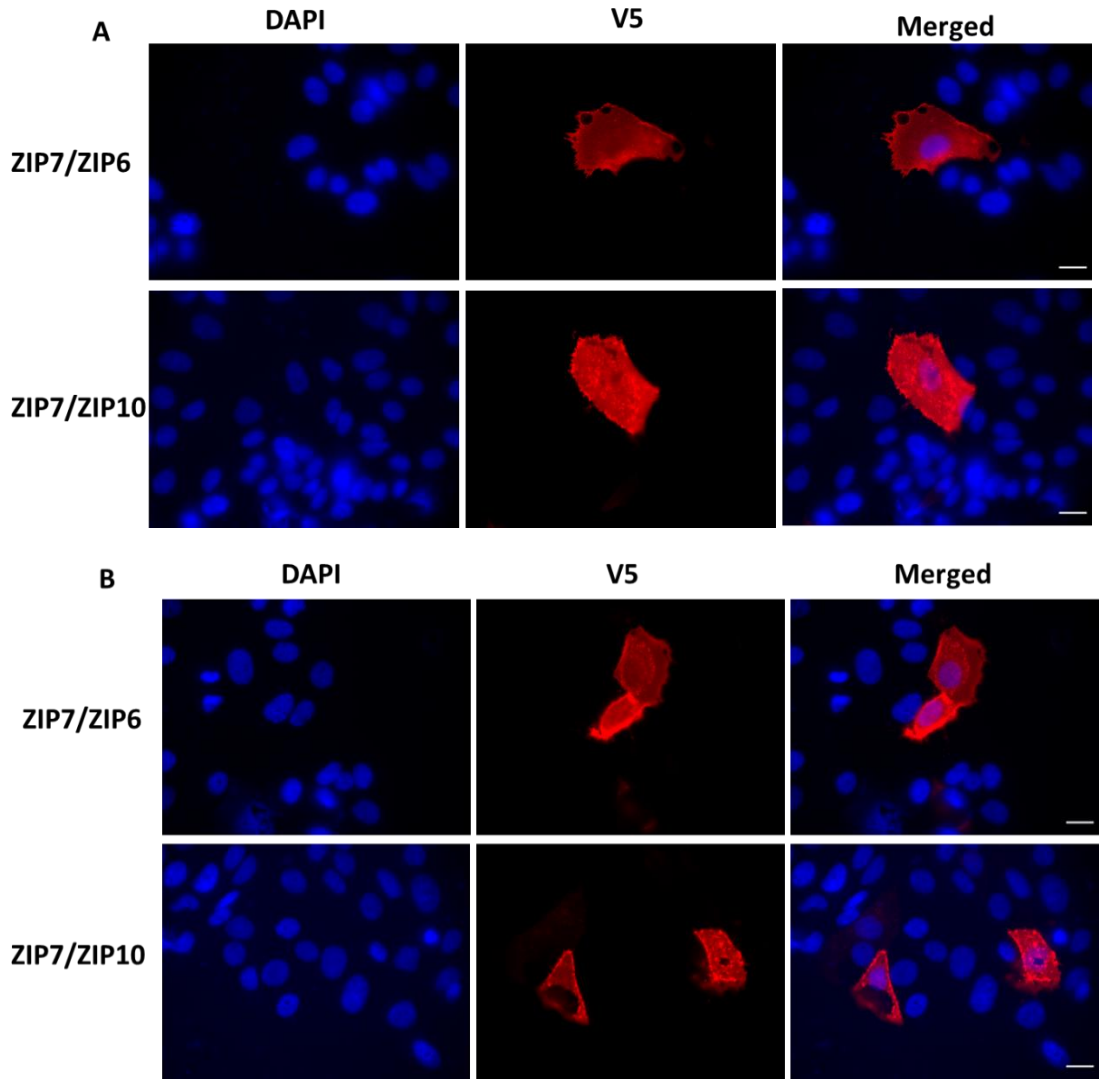

Immunofluorescence of unpermeabilized MCF-7 cells transfected with a chimeric construct ZIP7/ZIP6 and ZIP7/ZIP10 for 17 (**A**) and 24 (**B**) hours. Using a V5 antibody, the images confirmed the PM localisation for both constructs. Scale bar =10µm

5.3.3 Using western blot for verification of chimeric constructs

Exogenous expression of ZIP6 and ZIP10 in cells usually results in very few numbers of cells expressing the recombinant protein (Hogstrand et al., 2013) (Taylor et al., 2016b). This observation is attributed to the ability of ZIP6 and ZIP10 to promote cell detachment. Consequently, previous results obtained through immunofluorescence confirmed this phenomenon, as the number of transfected cells in WT ZIP6 and WT ZIP10 were significantly lower compared with WT ZIP7 or chimeric constructs with a ZIP7 N-terminus. To investigate this further, western blotting using a V5 antibody that recognises the C-terminal V5 tag of the recombinant proteins was performed. MCF-7 cells were transfected with WT ZIPs and the chimeric constructs for 17 or 24 hours. Before the cells were harvested, bright-field microscopy images were captured to observe the appearance of cells prior to collection (**Figure 5.5**). Interestingly, many non-adherent cells were observed in WT ZIP6 and WT ZIP10 transfected dishes. In contrast, dishes with WT ZIP7 or chimeric constructs with a ZIP7 N-terminus predominantly exhibited adherent cells, highlighting that modifying the N-terminus in ZIP6 and ZIP10 could prevent cell detachment. No cell detachment was observed in either untransfected dishes or dishes treated with lipofectamine only (transfection reagent), confirming the cell detachment phenomenon was not a result of MCF-7 cells independently or the transfection process. This finding suggests that the observed differences in cell behaviour are associated with the transfected constructs.

Next, the MCF-7 cells were harvested, samples were lysed and prepared, and subsequently run on a western blot, which was then probed for the V5 tag. The results demonstrated that all constructs with a ZIP7 N-terminus were robustly transfected across both transfection times, while those with a ZIP6 or ZIP10 N-terminus were not, as confirmed by the V5 band (**Figure 5.6 A and B**). This suggests that the detached cells were enriched with ZIP6 and ZIP10, which is why the V5 tag could not recognise these constructs in the adherent cells. Moreover, to investigate the possibility of chimeric constructs being cleaved at their N-terminus, a bioinformatic database was used to estimate their molecular weight. The database estimated the molecular weight for the ZIP7/ZIP6 and ZIP7/ZIP10 to be around 63 KDa and 61 KDa, respectively.

Interestingly, the actual size observed of these chimeric constructs was around 62 KDa and 60 KDa, as calculated using a specialized formula detailed in the methods chapter (Section 2.6).

The table showed a comparison between the estimated and actual sizes of the chimeric constructs, consistent with full length proteins and thereby indicating that no proteolytic cleavage had occurred (**Table 5.2**).

Figure 5.5 ZIP6 and ZIP10 produced more detached cells compared to constructs with a ZIP7 N-terminus

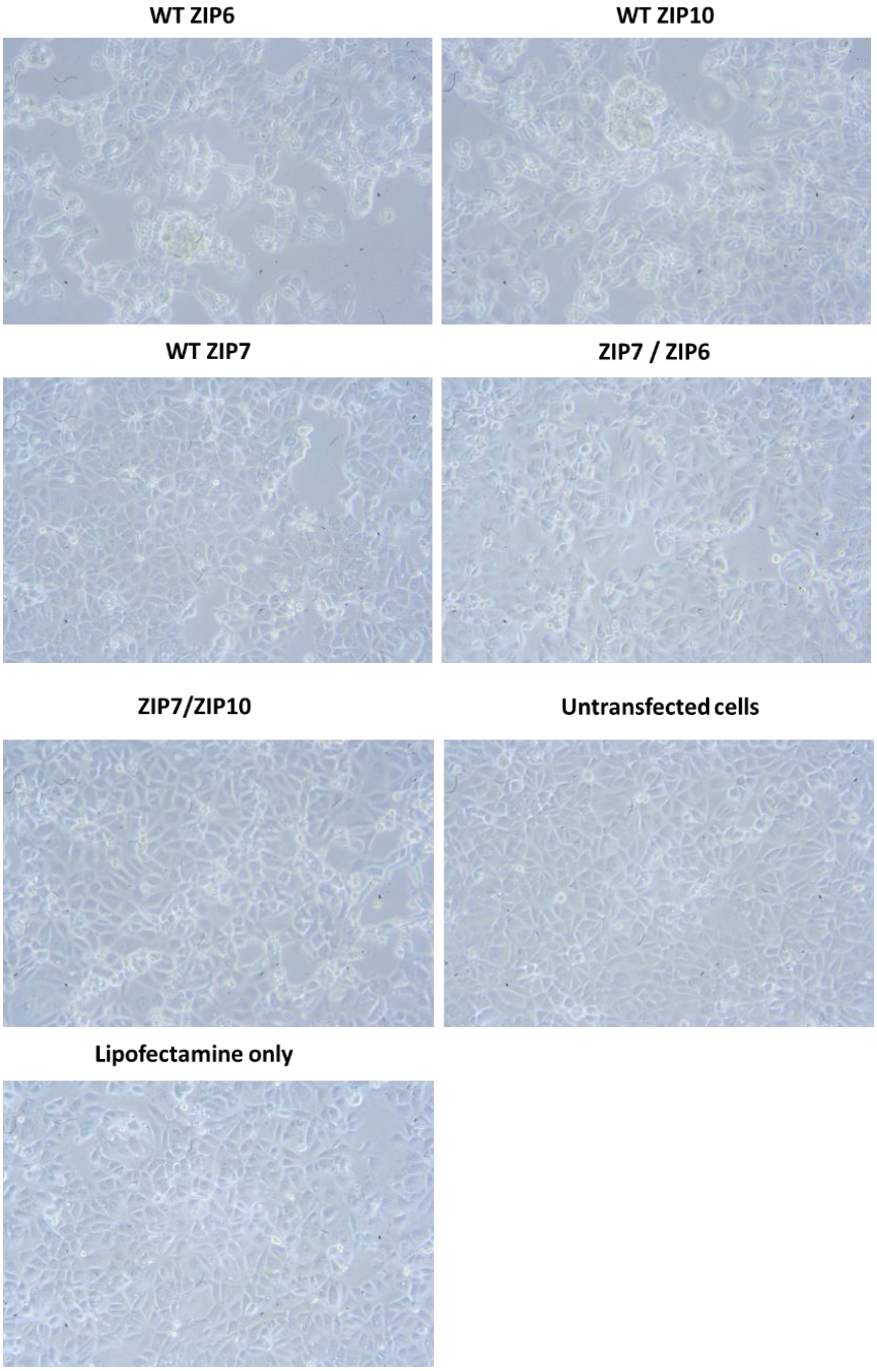

MCF-7 cells transfected with WT ZIP6, WT ZIP10, WT ZIP7 and chimeric constructs with a ZIP7 N-terminus were imaged 17 h after transfection. The cells transfected with ZIP6 and ZIP10 had either detached clumps or detached single round cells, while this observation was not seen in ZIP7 or chimeric constructs with a ZIP7 N-terminus. Untransfected cells and cells with a transfection reagent was also imaged as a negative control.

Figure 5.6 Optimisation of transfection time and molecular weight determination

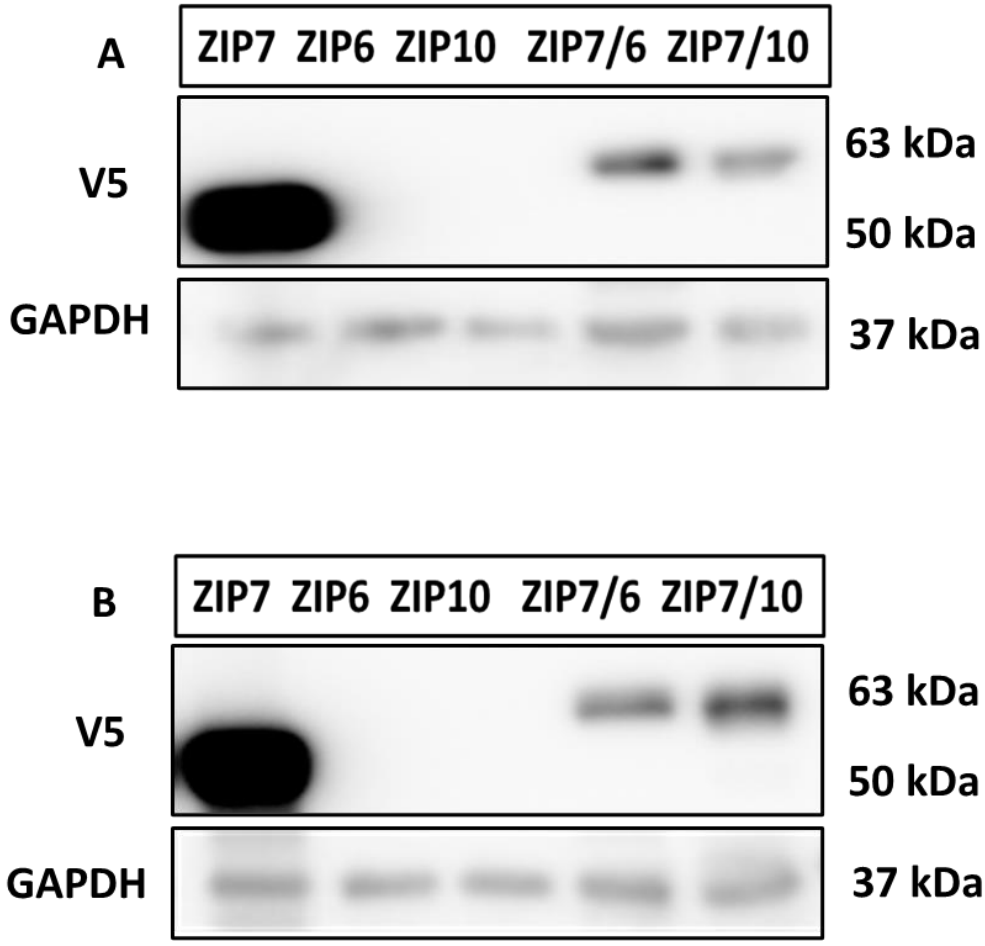

MCF7 cells were transfected with WT ZIP7, WT ZIP6, WT ZIP10 and chimeric constructs with a ZIP7 N-terminus for 17 or and 24 hours. Cells were lysed and subjected to western blotting, with the detection performed using an anti-V5 antibody. Protein bands of V5 (50 for ZIP7 and 63 kDa for chimeras), and GAPDH (37 kDa) were demonstrated, and the data were normalised to GAPDH (n=3).

Table 5.2 Molecular weight determination for chimeric construct

Construct	Estimated	Actual
ZIP7/ ZIP6	63.3 KDa	62.8 KDa
ZIP7/ZIP10	61.78 KDa	60.7 KDa

Numbers represented the molecular weight of protein bands in kDa. The estimated molecular weights for chimera were calculated using the Compute pI/Mw tool (Bjellqvist et al., 1993),based on the molecular weight of the detected bands.

5.3.4 Investigating the role of ZIP6 and ZIP10 N-terminus in cell detachment

Given that ZIP6 and ZIP10 are mainly observed in the non-adherent cells, it is crucial to investigate the role of their N-terminus in these cells by comparing them to the chimeric constructs. To perform this experiment, MCF-7 cells were transfected with WT ZIP7, WT ZIP6, WT ZIP10 and the chimeric constructs with a ZIP7 N-terminus (ZIP7/ZIP6 and ZIP7/ZIP10). At the time of cell harvest, non−adherent cells found in the medium were gathered and pooled together with attached cells and this mixed population of cells, which includes both non-adherent and adherent cells, was referred to as a pooled sample. Moreover, separate samples were also prepared using only adherent cells, which were referred to as adherent cell samples. A V5 antibody was then used to conduct western blotting. As expected, a V5 band was easily detected in WT ZIP7 in both pooled and mainly adherent samples (**Figure 5.7**), confirming the expression of this construct was found in the adherent cells and indicating that no detachment had occurred. Interestingly, in the chimeric constructs featuring a ZIP7 N-terminus, the V5 band was detected in both samples (ZIP7/ZIP6 and ZIP7/ZIP10), with greater intensity observed in the adherent samples (**Figure 5.7**). This result suggests that the transfected cells with these chimeric constructs in adherent samples did not undergo detachment. This finding confirmed that the modifying of the N-terminus of ZIP6 and ZIP10 could prevent cell detachment, thereby highlighting the critical role of the N-terminus of ZIP6 and ZIP10 in activating their respective transporters. Due to the difficulty of detecting a V5 band for WT ZIP6 and WT ZIP10, the blots were developed for a longer time while the rest of the samples were covered by a filter paper. This approach allowed for the bands corresponding to ZIP6 and ZIP10 to be adequately produced and visualized. Eventually, the V5 band for the WT ZIP6 and WT ZIP10 began to emerge. As shown in **Figure 5.7,** the V5 bands for WT ZIP6 and WT ZIP10 appeared at 103 and 105 KDa, respectively.

However, these molecular weights represent the full length of each protein, suggesting the inactivated form. To identify cleaved sites in cells transfected with ZIP6 or ZIP10 in pooled samples, a panel of antibodies that recognises a specific region in the recombinant protein should be utilized. This is important as the V5 tag only recognises the tag on the C-terminus of the recombinant protein.

5.3.5 The role of the N-terminus of ZIP6 and ZIP10 in mediating PLK1 activation

To investigate whether these detached cells in pooled samples were still alive and proliferating, PLK1, which is transcriptionally activated during cell detachment and enhances anoikis resistance (Lin et al., 2011), was investigated (**Figure 5.8**). In WT ZIP7, no bands for pPLK1^{T210} were observed either in pooled or adherent samples, confirming that the cells remained attached, not undergoing any form of detachment. Similarly, the chimeric ZIP7/ZIP6 failed to upregulate the pPLK1^{T210} in both sample types, highlighting that the modifying of the ZIP6 N-terminus could prevent the activation of its corresponding transporter. Moreover, the chimeric ZIP7/ZIP10 showed some pPLK1^{T210} activation in pooled samples while no band was seen in the adherent ones.

Interestingly, cells transfected with WT ZIP6 significantly increased PLK1 in pooled samples, while no band was observed in the adherent ones. This confirmed that the detached cells seen in pooled samples remained alive. When compared to the chimeric with non-cleavable N-terminus (ZIP7/ZIP6), ZIP6 significantly activated pPLK1^{T210}, confirming the role of N-terminus cleavage in ZIP6 activation.

Likewise, ZIP10 transfected cells markedly upregulated pPLK1^{T210} in pooled samples compared to adherent ones. This also confirmed the detached cells in this sample were alive, mirroring the behaviour of ZIP6. In addition, the increased phosphorylation of PLK1 in WT ZIP10 compared with chimeric construct ZIP7/ZIP10 was significant. This highlighted the distinct role of ZIP10 N- terminus in activating its corresponding transporter.

Taken together, these findings highlighted the distinct role of ZIP6 and ZIP10 N-termini in the activation of PLK1, suggesting that modifying this region could prevent cell detachment and subsequent resistance to anoikis.

Figure 5.7 Investigating the role of ZIP6 and ZIP10 N-terminus by using pooled compared with adherent samples.

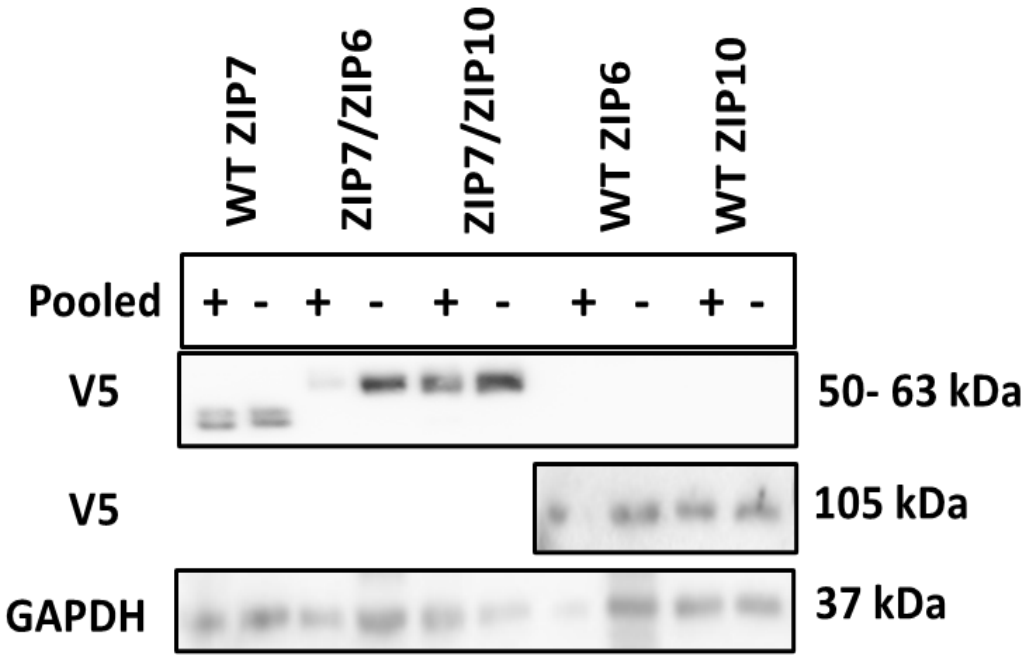

MCF7 cells were transfected with WT ZIP7, chimeric constructs with a ZIP7 N-terminus, WT ZIP6 and WT ZIP10 for 17 hours. Cells were lysed as pooled (+) or adherent (-) and analysed using western blotting with an anti-V5 antibody. The first part of the blot showed the V5 bands for WT ZIP7 and the chimeric constructs. The second part displayed the V5 band for ZIP6 and ZIP10, which were visualised for a longer exposure time. GAPDH was utilised as a loading control (n=3).

Figure 5.8 Modifying the N-terminus of ZIP6 and ZIP10 prevents cell detachment

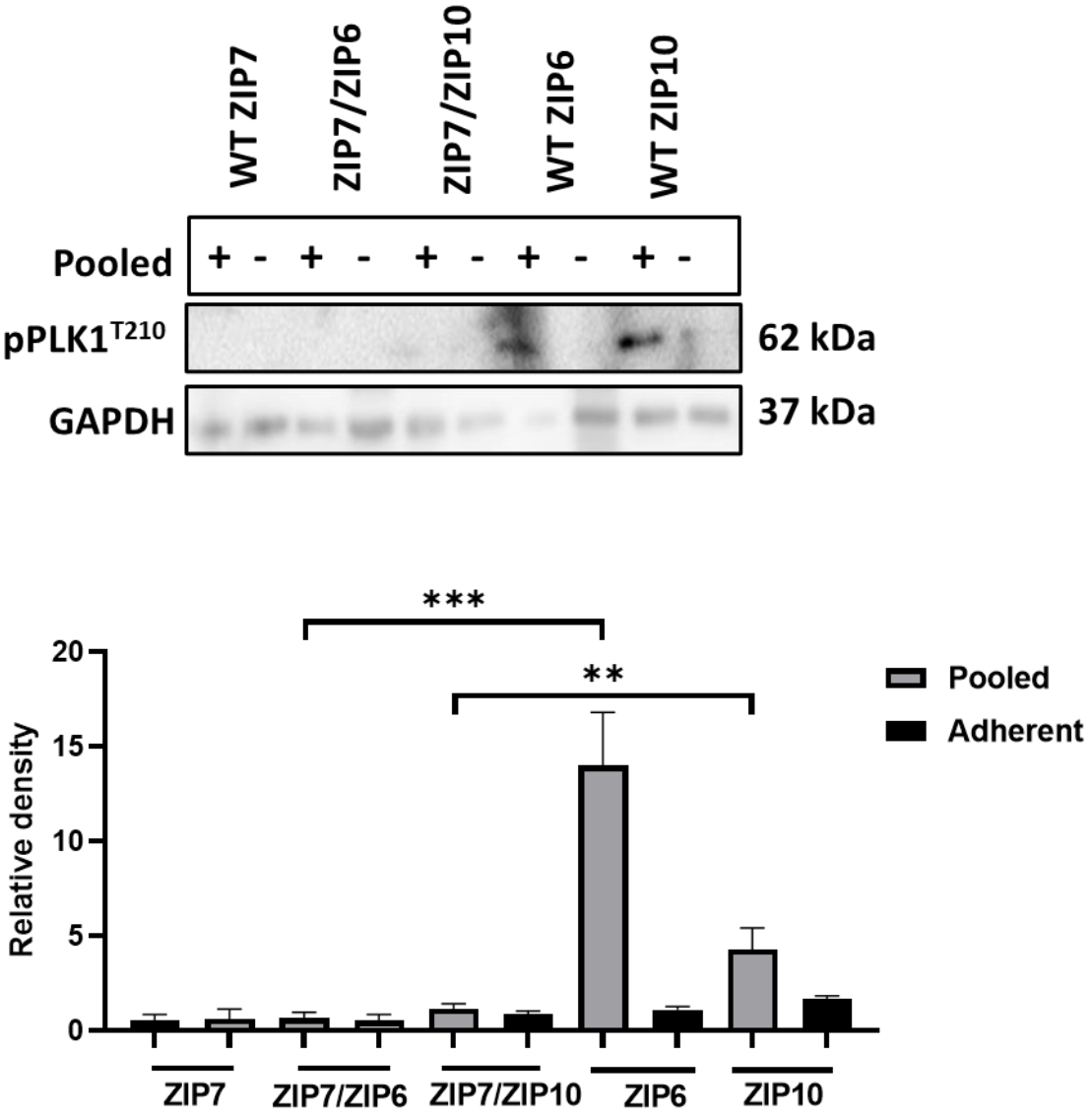

MCF7 cells were transfected with WT ZIP7, chimeric constructs with a ZIP7 N-terminus, WT ZIP6 and WT ZIP10 for 17 hours. Cells were lysed as pooled (+) or adherent (-) and analysed using western blotting with pPLK1^{T210}. The bar graph shows the densitometric data, which has been normalized to GAPDH and illustrated as mean ± standard error (n=3).

5.3.6 Modifying the N-terminus of ZIP6 or ZIP10 reduced the activation of STAT3

ZIP6 and ZIP10 have been identified as a downstream target of STAT3, which is a cancer-promoting transcription factor that is upregulated in many cancers including breast cancer (Yamashita et al., 2004)(Taylor et al., 2016)(Avalle et al., 2017). Moreover, STAT3 has been found to regulate the EMT process which is frequently associated with cancer metastasis (Li and Huang, 2017)(Avalle et al., 2017). Notably, both ZIP6 and ZIP10 have been reported as contributors in driving the EMT and cell migration processes (Hogstrand et al., 2013) (Taylor et al., 2016). These involvements of ZIP6 and ZIP10 are mediated by signalling pathways that are dependent on STAT3. Therefore, to investigate the role of ZIP6 and ZIP10 N-terminus in STAT3 activation, the form of STAT3 (pSTAT3^{S727}) was investigated.

MCF-7 cells were transfected with WT ZIP7, WT ZIP6, WT ZIP10 and chimeric constructs with ZIP7 N-terminus WT ZIP6 (ZIP7/ZIP6) and WT ZIP10 (ZIP7/ZIP10). The cells then were lysed as pooled samples and analysed by western blot (**Figure 5.9**). In WT ZIP7, no detectable band was observed, providing confirmation that the overexpression of ZIP7 did not result in the detachment of cells. Both chimeric constructs ZIP7/ZIP6 and ZIP7/ZIP10 showed a reduction in the presence of phosphorylated STAT3^{S727}. As expected, the WT ZIP6 and WT ZIP10 increased the expression of pSTAT3^{S727}, confirming that the detached cells were enriched with the pSTAT3^{S727}. Notably, cells expressing ZIP6 showed a significant elevation in pSTAT3^{S727} compared with the chimeric construct ZIP7/ZIP6, indicating that modifying the N-terminus could prevent cell detachment. Similarly, ZIP10 showed a significant increase in pSTAT3^{S727} compared with a chimeric construct ZIP7/ZIP10. This implies the ZIP10 N-terminus is required for the activation of ZIP10 transporter. Collectively, these data suggest that the N-terminus of ZIP6 and ZIP10 plays a functional role in stimulating cells to undergo the EMT process, allowing cell detachment.

Figure 5.9 Modifying the N-terminus of ZIP6 or ZIP10 reduced the activation of STAT3

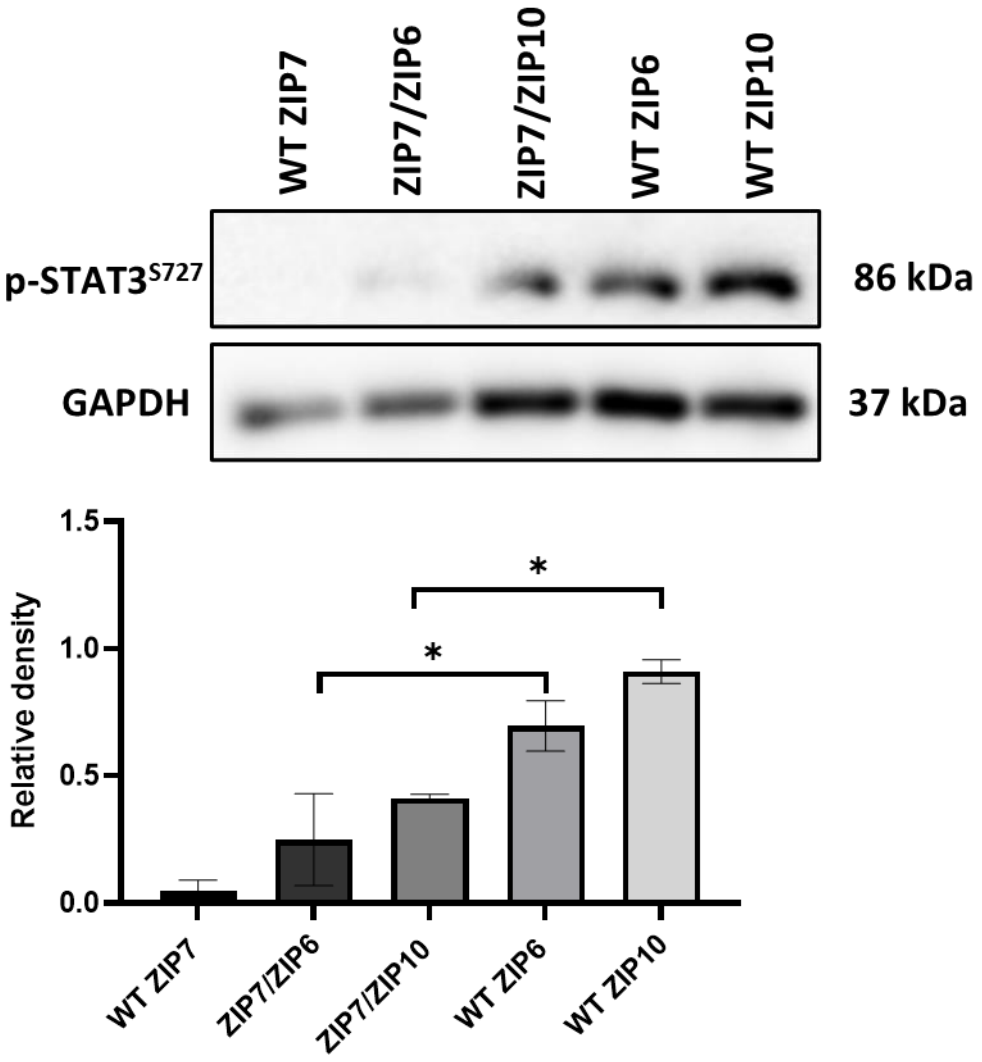

MCF7 cells were transfected with WT ZIP7, chimeric constructs with a ZIP7 N-terminus, WT ZIP6 and WT ZIP10 for 17 hours. Cells were lysed as pooled and analysed using western blotting with pSTAT3^{S727}. The bar graph shows the densitometric data, which has been normalized to GAPDH and illustrated as mean ± standard error (n=3).

5.3.7 N-terminus of ZIP6 and ZIP10 promotes phosphorylation of several protein kinases

To determine the downstream targets of the ZIP6 and ZIP10 N-termini, and to understand how modifications to the N-termini affect these targeted kinases, phosphokinase arrays were used. The phosphokinase array is a high-throughput method that identifies the activation of 37 different cellular kinases simultaneously, along with their specific phosphorylated sites. To perform this, MCF-7 cells were transfected with WT ZIP7, chimeric constructs with a ZIP7 N-terminus, WT ZIP6 and WT ZIP10. The cells were then lysed as pooled samples.

The data from arrays demonstrated that cells transfected with WT ZIP7, ZIP7/ZIP6 and WT ZIP6 showed induced phosphorylation of many kinases (**Figure 5.10 A**). Likewise, this effect on these kinases was also observed in the cells that were transfected with WT ZIP10 compared to those transfected with ZIP7/ZIP10 and WT ZIP7 (**Figure 5.10 B**). The images displayed noticeable spots of phosphorylated kinases including pGSK-3ß^{S9}, pHSP27$^{S78,\ S82}$, pP70^{T389}, pPRAS40^{T246}, pSTAT3^{S727} and HSP60 which are indicated by arrows. However, it is worth noting that three pairs of dark reference points can be found at the top-right, top-left, and bottom-left corners, which are used for alignment.

To evaluate the levels of each kinase, bar graphs were created, presenting the densitometric values of the corresponding duplicate dot pairs for all detected kinases. Kinases that showed a high changed in chimeric construct containing a ZIP7 N-terminus, particularly when compared to WT ZIP6 or ZIP10, were classified as highly activated. This shift highlights the potential effect of the ZIP6 or ZIP10 N-terminus in activating the kinases.

Generally, the arrays data revealed that cells transfected with WT ZIP7, the chimeric ZIP7/ZIP6 construct and WT ZIP6 had markedly induced phosphorylation (>300 density units) of pGSK-3ß^{S9}, pP70^{T389}, and HSP60. Additionally, a mild increase in phosphorylation (100-200 density units) was observed for pHSP27$^{S78,\ S82}$, pPRAS40^{T246} and pSTAT3^{S727} (**Figure 5.11**).

In **Figure 5.12**, the phosphorylation levels of pP70^{T389} and HSP60 were also notably increased (>300 density units) in ZIP10 compared with WT ZIP7 and the chimeric ZIP7/ZIP10 construct. Phosphorylated GSK-3ß^{S9} was found to be highly in both WT ZIP7 and a chimera containing a ZIP7 N-terminus compared with ZIP10.

Phosphorylation levels of pHSP27^{S78,82}, pPRAS40^{T246} and pSTAT3^{S727} showed a mild increase in phosphorylation (100-200 density units) in all samples. To ascertain the impact of ZIP6 and ZIP10 N-termini, the densitometric values of the highly activated kinases were represented in separate bar graphs (**Figure 5.13 A and B**). Most of these kinases such as pHSP27$^{S78, 82}$, pPRAS40^{T246}, pP70^{T389}, pPYK2^{Y402} and HSP60 demonstrated changes in their phosphorylation level when compared to ZIP6 or ZIP10 and the chimeric construct containing a ZIP7 N-terminus. Interestingly, pGSK-3ß^{S9} ,which exhibited a high phosphorylation level, was reported to be phosphorylated by zinc influx from the plasma membrane (Hogstrand et al., 2013) (Taylor et al., 2016). Therefore, it is worth considering this kinase as an activated kinase that needs to be investigated.

Figure 5.10 Investigating the role of N-terminus of ZIP6 and ZIP10 in phosphorylated kinases

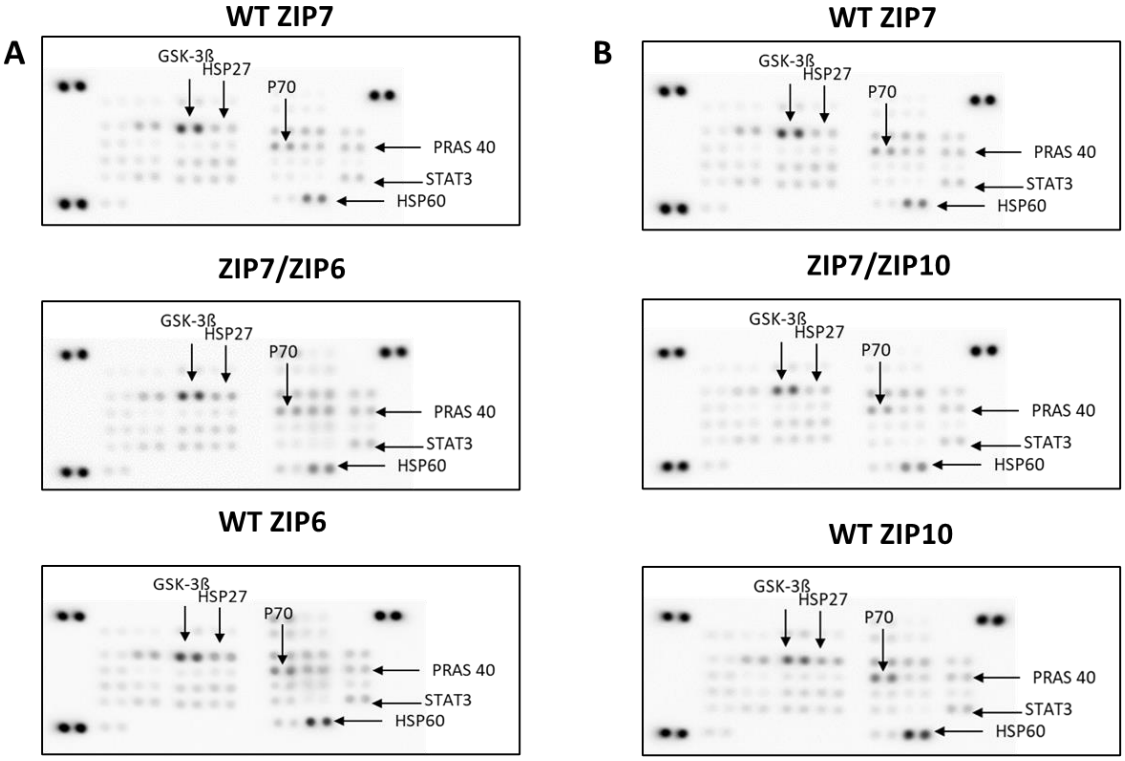

MCF−7 cells were transfected with WT ZIP7, chimeric ZIP7/ZIP6 construct and ZIP6 (**A**). In addition, the cells were transfected with WT ZIP7, chimeric ZIP7/ZIP10 construct and ZIP10 (**B**). The human phospho-kinase antibody arrays (ARY003C; R&D Systems) were used to examine 37 phosphorylated kinases and 2 total proteins. Signals for each kinase appear as a pair of duplicate spots, with three pairs of dark reference at the top-right, top-left, and bottom-left corners, which are used for alignment. The most activated kinases are indicated with black arrows.

Figure 5.11 Densitometric analysis of phospho-kinases arrays in transfected MCF-7 with WT ZIP7 and chimeric construct containing a ZIP7 N-terminus compared with WT ZIP6

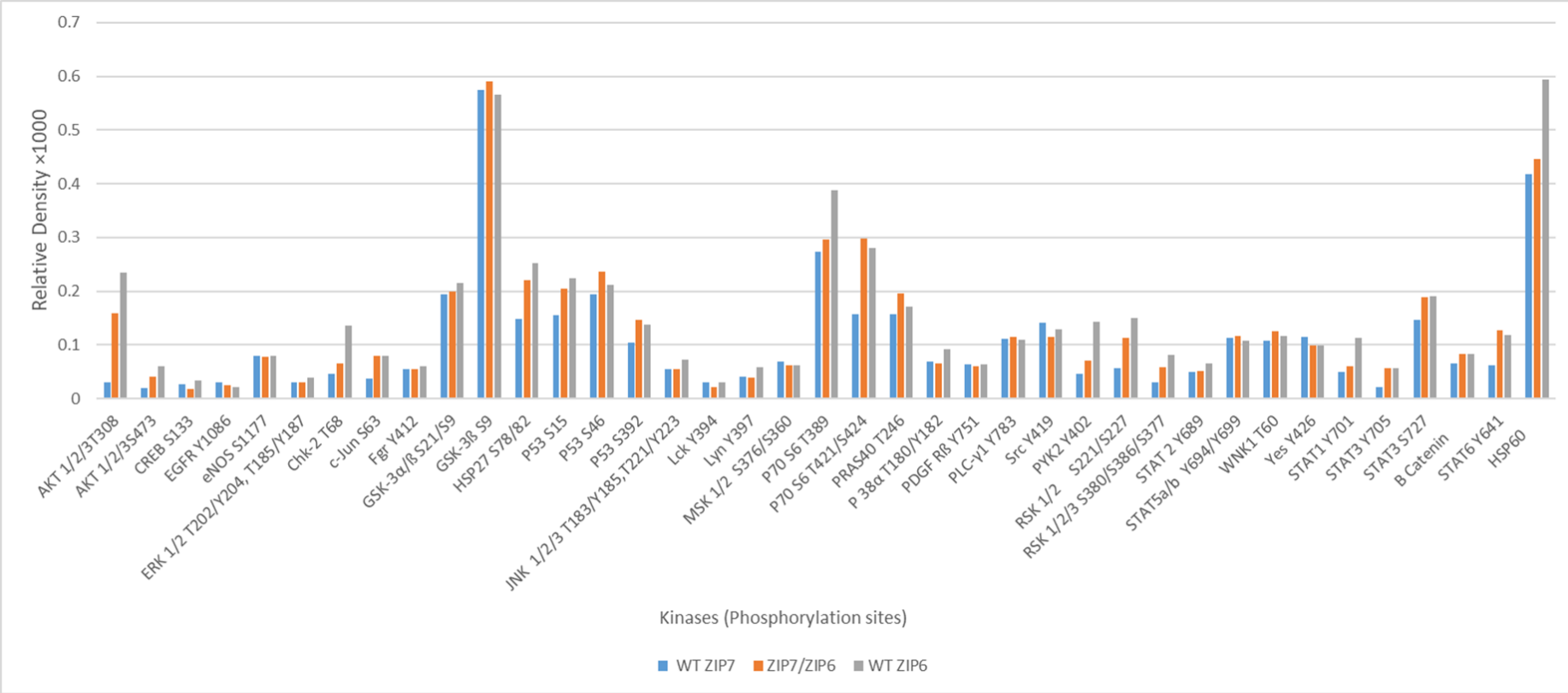

MCF−7 cells were transfected with WT ZIP7, chimeric ZIP7/ZIP6 construct and ZIP6. The phosphorylation of selected kinases at the residues specified beneath the kinase names was identified using the human phospho-kinase antibody arrays (ARY003C; R&D Systems). Normalised data are shown as the average of duplicate dots for each kinase (n=2).

Figure 5.12 Densitometric analysis of phospho-kinases arrays in transfected MCF-7 with WT ZIP7 and chimeric construct containing a ZIP7 N-terminus compared with WT ZIP10

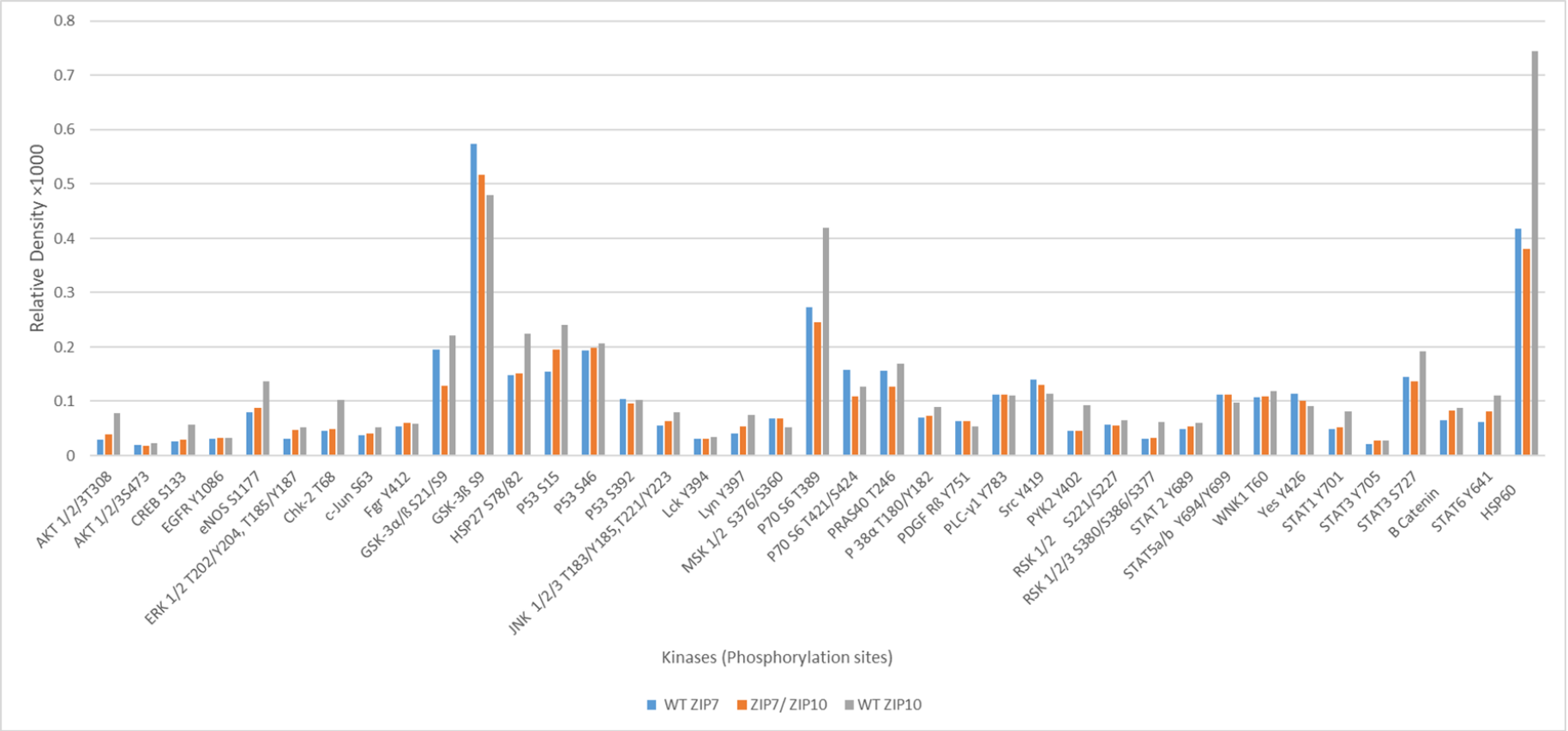

MCF−7 cells were transfected with WT ZIP7, chimeric ZIP7/ZIP10 construct and ZIP10. The phosphorylation of selected kinases at the residues specified beneath the kinase names was identified using the human phospho-kinase antibody arrays (ARY003C; R&D Systems). Normalised data are shown as the average of duplicate dots for each kinase (n=2).

Figure 5.13 The highly activated kinases in ZIP6 and ZIP10 compared with chimeric constructs containing a ZIP7 N-terminus

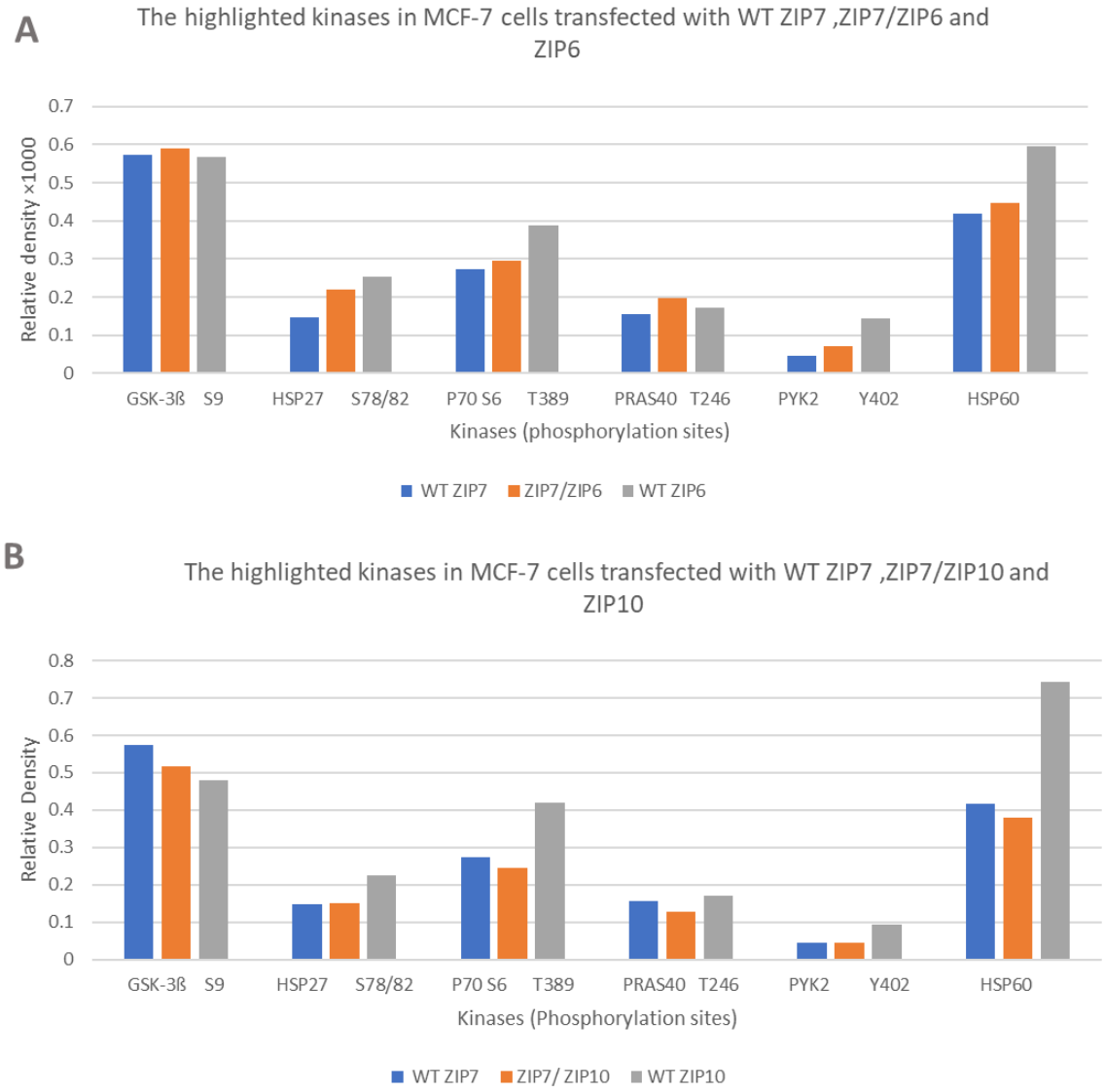

MCF−7 cells were transfected with WT ZIP7, chimeric ZIP7/ZIP6 construct and ZIP6 (**A**). Furthermore, the cells were transfected with WT ZIP7, chimeric ZIP7/ZIP10 construct and ZIP10 (**B**). The phosphorylation of selected kinases at the residues specified beneath the kinase names was identified using the human phospho-kinase antibody arrays (ARY003C; R&D Systems). Normalised data are shown as the average of duplicate dots for each kinase (n=2).

5.3.8 Western blotting confirms kinases activation by N-terminus of ZIP6 and ZIP10 compared with chimeric constructs

The phospho-kinase arrays have been used to point the direction of what downstream kinases are mediated by zinc influx from the plasma membrane. The kinases that exhibited a high change in WT ZIP6 and ZIP10, particularly when compared to chimeric constructs, were classified as highly activated kinases. To confirm the phosphorylation of these kinases due to ZIP6 and ZIP10 overexpression and to evaluate the effect of modifying the N-terminus of these respective transporters, a western blot was performed on cells transfected with WT ZIPs and chimeric constructs. The cells were then lysed as pooled samples and analysed by SDS-PAGE and western blot. The kinases identified by the arrays, which include pGSK-3ß^{S9}, pPYK2^{Y402}, pP70^{T389}, pPRAS40^{T246}, HSP60 and pHSP27^{S78,82}, were then confirmed by western blot.

It has been reported that GSK-3ß undergoes inhibitory phosphorylation on residue S9, mediated by the influx of zinc from the plasma membrane (Hogstrand et al., 2013)(Taylor et al., 2016). When ZIP6 and ZIP10 undergo N-terminal cleavage before and after relocating to the PM, they transport zinc inside the cell, which results in the inactivating GSK-3ß^{S9}, either directly through the impact of zinc, or indirectly via the activation of AKT by zinc (Lee et al., 2009). Therefore, pGSK-3ß^{S9} was evaluated in order to see the effect of modifying the N-terminus of ZIP6 and ZIP10 in this kinase (**Figure 5.14**). In WT ZIP7, the GSK-3ß^{S9} phosphorylation level was barely detectable. This was expected since the ZIP7 transporter was not stimulated with zinc. Interestingly, alteration of N-terminus in ZIP6 and ZIP10 resulted in a significant decrease in pGSK-3ß^{S9}, compared to the level seen with the respective WT transporters. As the results showed, the pGSK-3ß^{S9} level was significantly reduced in the chimeric ZIP7/ZIP6 construct compared to WT ZIP6. A similar effect was also observed with ZIP7/ZIP10 when compared to WT ZIP10. This implies the critical role of the N-termini in both ZIP6 and ZIP10 in transporting zinc and inducing their activity.

Figure 5.14 Modification of N-terminus diminished the effect of GSK-3ß

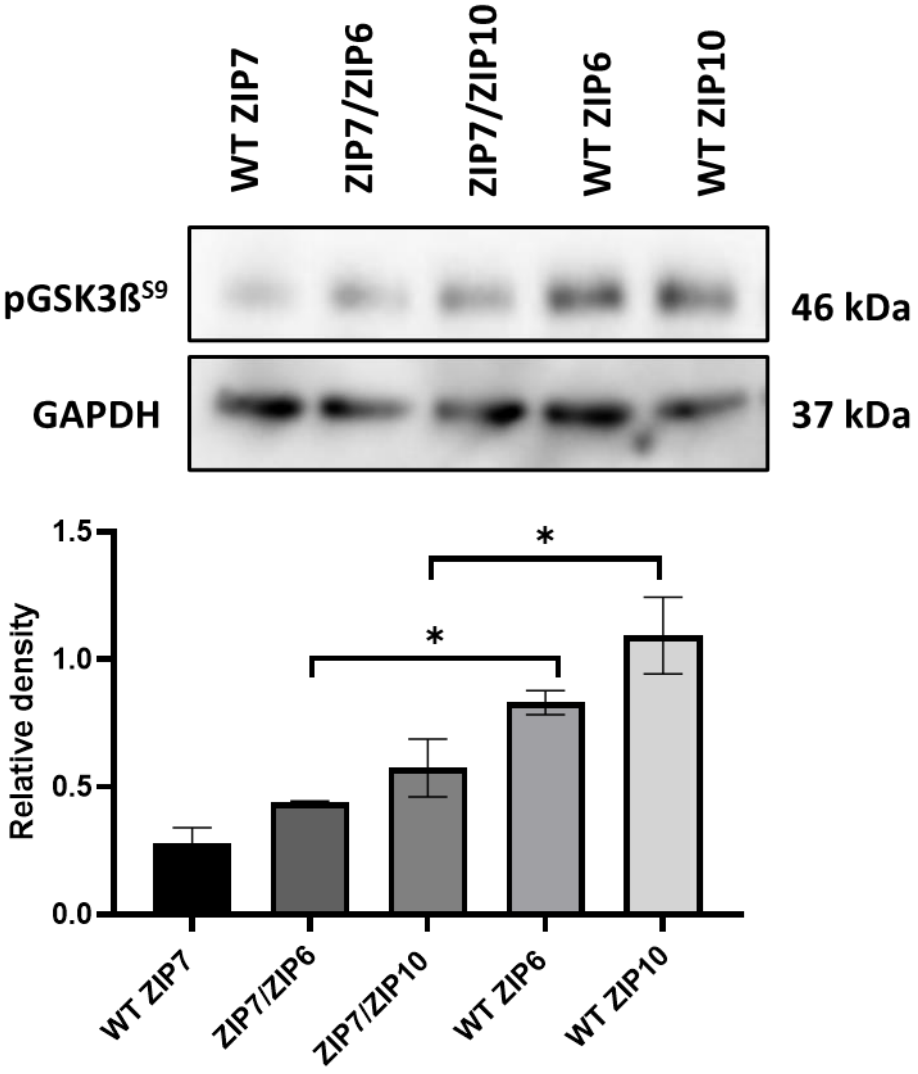

MCF7 cells were transfected with WT ZIP7, chimeric constructs with a ZIP7 N-terminus, WT ZIP6 and WT ZIP10 for 17 hours. Cells were lysed as pooled and analysed using western blotting with pGSK-3ßS9. GAPDH was utilised as a loading control. The bar graph shows the densitometric data, which has been normalized to GAPDH and presented as mean ± standard error (n=3) *p=0.05; **p=0.01; ***p<0.001.

One of the kinases that showed high activation in WT ZIP6 and ZIP10, as revealed by the phospho-kinases array compared to the chimeric constructs was pPyk2^{Y402}. Interestingly, this particular kinase was shown to enhance TGF-β mediated EMT, leading to increased metastasis in breast cancer (Verma et al., 2015).

To investigate the potential effects of the N-terminus in ZIP6 and ZIP10 in activating this kinase, a western blot was performed using MCF-7 cells (**Figure 5.15**).

In WT ZIP7, the activation of pPyk2^{Y402} was observed to be significantly lower compared to the rest of the samples, highlighting that the zinc transporter located on the ER is not primarily responsible for trigging pPyk2^{Y402} activation and, subsequently, inducing EMT. Intriguingly, modification to the N-terminus of ZIP6 and ZIP10 led to a marked reduction in pPyk2^{Y402} activation as the phosphorylation level in chimeric ZIP7/ZIP6 construct was remarkably lower compared with the WT ZIP6. A similar effect was also noticed in the ZIP7/ZIP10 when compared to WT ZIP10. This result indicates that the activation of pPyk2^{Y402} was facilitated by the activated forms of ZIP6 and ZIP10, thereby confirming the role of their N-termini in promoting the activity of their respective transporters.

In order to confirm the results obtained from the array data, MCF-7 cells were probed with pP70 S6^{T389} antibody by western blotting (**Figure 5.16**). P70 S6^{T389} was shown to be activated in WT ZIP7 as compared to its activity WT ZIP6 and WT ZIP10. This activation of pP70 S6^{T389} is not surprising because it has previously been recognized as one of the downstream effectors of the zinc release mediated by ZIP7 (Nimmanon et al., 2017). The WT ZIP6 and WT ZIP10 showed a reduction in the levels of pP70 S6^{T389}. Interestingly, the chimeric ZIP7/ZIP6 construct significantly increased the phosphorylation of P70 S6^{T389} compared with WT ZIP6. Similarly, modification to the N-terminus of ZIP10 (ZIP7/ZIP10) resulted in a substantial increase in the activation of P70 S6^{T389} compared with WT ZIP10. These findings confirm that the P70 S6^{T389} kinase may not be directly affected by zinc transport through the transporters that are located on the PM. The modification of the N-terminus in the chimeric constructs has caused them to act more like the ZIP7 transporter. However, whether the chimeric constructs located on the ER, in the same manner as ZIP7, might be capable of facilitating zinc transport and thus activating this kinase requires further investigation.

Figure 5.15 Modification of N-terminus diminished the effect of Pyk2 activation

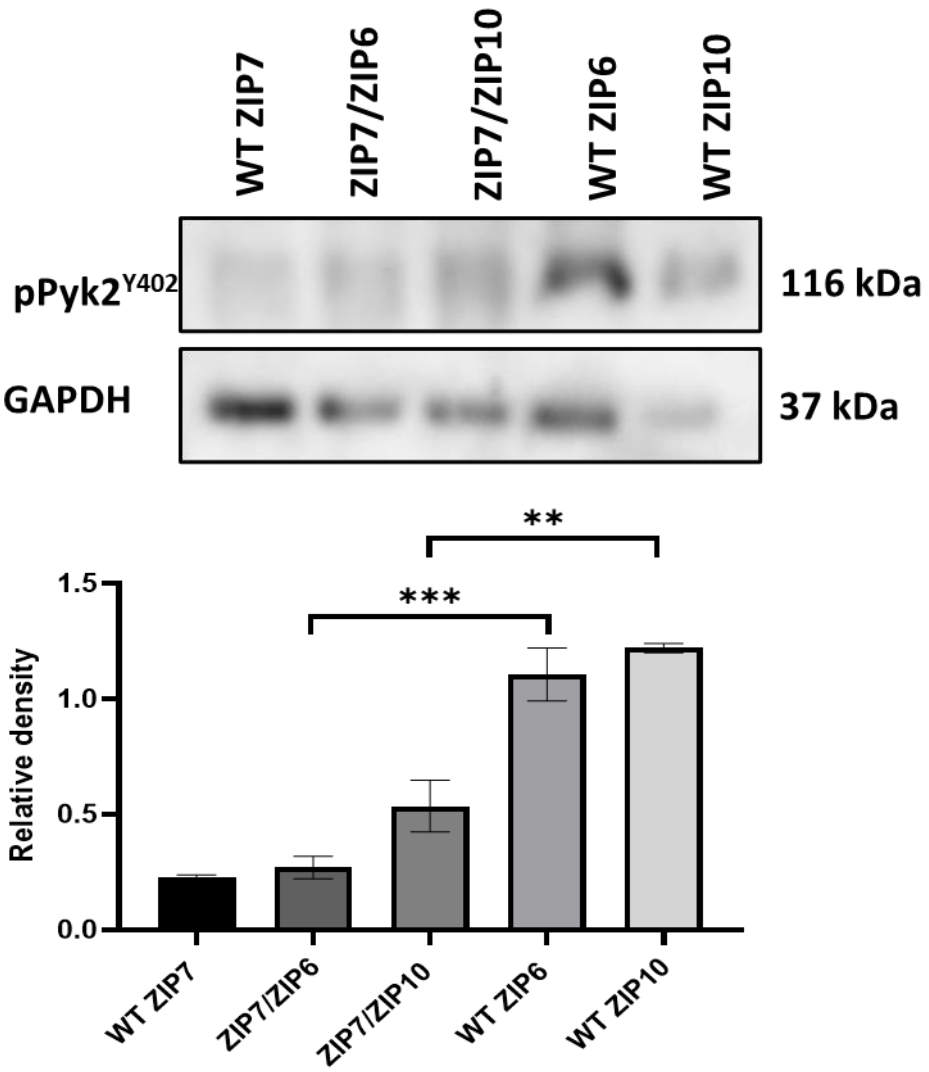

MCF7 cells were transfected with WT ZIP7, chimeric constructs with a ZIP7 N-terminus, WT ZIP6 and WT ZIP10 for 17 hours. Cells were lysed as pooled and analysed using western blotting with pPyk2^{Y402}. GAPDH was utilised as a loading control. The bar graph shows the densitometric data, which has been normalized to GAPDH and illustrated as mean ± standard error (n=3) *p=0.05; **p=0.01; ***p<0.001.

5.16 The role of zinc transporter in the activation of P70 S6 compared with chimeric constructs

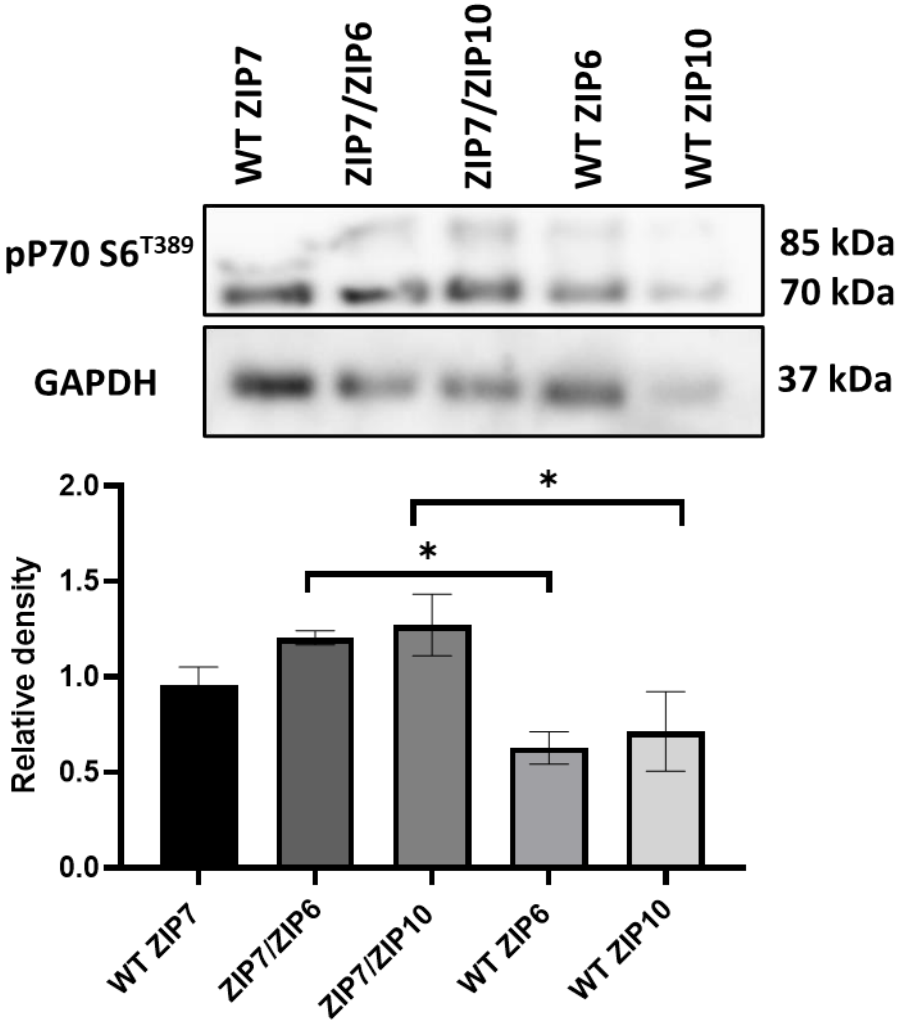

MCF7 cells were transfected with WT ZIP7, chimeric constructs with a ZIP7 N-terminus, WT ZIP6 and WT ZIP10 for 17 hours. Cells were lysed as pooled and analysed using western blotting with pP70 $S6^{T389}$. GAPDH was utilised as a loading control. The bar graph shows the densitometric data, which has been normalized to GAPDH and illustrated as mean ± standard error (n=3) *p=0.05; **p=0.01; ***p<0.001.

PRAS40 was also identified as one of the kinases influenced by the overexpression of ZIP transporters and chimeric constructs, based on phospho-kinase array results. This kinase was recognised as an AKT substrate, known for regulating cell growth and survival (Wiza et al., 2012). To validate this effect, western blotting was performed using pPRAS40^{T246} antibody (**Figure 5.17 A**). In WT ZIP7, the activation of pPRAS40^{T246} was significantly elevated compared to that in ZIP7/ZIP10, WT ZIP6 and ZIP10. Given that PRAS40 is known to be an AKT substrate, this association could potentially explain the observed upregulation of PRAS40 due to the effect of ZIP7. In the chimeric ZIP7/ZIP6 construct, the phosphorylation level was increased compared to WT ZIP6, albeit the rise was not statistically significant. Similarly, the chimeric ZIP7/ZIP10 construct did not show a significant change when it compared with WT ZIP10, meaning that these chimeric constructs may not effectively transport zinc into cytoplasm and subsequently activate this kinase. Both WT ZIP6 and ZIP10 induced low phosphorylation level of pPRAS40^{T246} in comparison to WT ZIP7. These findings indicate that the pPRAS40^{T246} was primarily activated via ZIP7 when it is phosphorylated on the long cytoplasmic loop between TM3-4, as the effect of this kinase was predominantly observed in WT ZIP7.

HSP60 is a heat shock protein that responds to stressful condition and assists in the proper folding of proteins (Cappello et al., 2008). Similar to the effect of ZIP7 on the PRAS40^{T246}, the activation of HSP60 also appeared to depend on the zinc release mediated by ZIP7 (**Figure 5.17 B**). Directly contradicting the phospho-array data, western blotting results showed that the activation of HSP60 was significantly increased in WT ZIP7 compared to all other samples. This suggests that the HSP60 is triggered in response to the zinc release facilitated by ZIP7 activation. Interestingly, both chimeric constructs containing a ZIP7 N-terminus apparently reduced the effect of HSP60, suggesting that these constructs may lack functional capability to transport zinc out of the ER. This confirms the importance of phosphorylation sites in the ZIP7 cytoplasmic loop as a gate keeper to release zinc from the ER. Conversely, neither ZIP6 nor ZIP10 were able to activate HSP60, further substantiating that the HSP60 primarily responds to zinc release mediated by ZIP7. This could indicate that ER stress might occur due to the redistribution of zinc from the ER to the cytoplasm.

Finally, to validate the array results, MCF-7 cells were probed with pHSP27$^{S78/82}$ antibody by western blotting (**Figure 5.17 C**). Cells transfected with WT ZIP7 resulted in an increase in pHSP27$^{S78/82}$ level though it was not significant in comparison to all other samples.

This trend was previously shown in (chapter 4) as a downstream result of ZIP7 activation. In terms of chimera constructs, both showed comparable levels of pHSP27$^{S78/82}$ phosphorylation, which were not statistically significant when compared with their respective WT transporters. Similarly, the activation of pHSP27$^{S78/82}$ resulting from transfection with WT ZIP6 and ZIP10 was nearly identical, with no remarkable change observed. This suggests that these transporters may require additional stimulation to trigger any noticeable effect on this kinase.

In conclusion, these experiments confirmed the vital role of the N-terminus of ZIP6 and ZIP10 in activating their transporters to facilitate zinc influx, which subsequently activate various downstream kinases. Using western blotting, it was found that modification of the N-terminus in ZIP6 and ZIP10 resulted in a remarkable decrease in the phosphorylation of pGSK-3ß^{S9} and pPyk2^{Y402}, compared to WT ZIP6 and WT ZIP10, highlighting the critical role of the N-terminus in activating these kinases. Moreover, the activation of pP70 S6^{T389} was found to be affected by the ZIP7 transporter, rather than by transporter located on the plasma membrane.

Another notable observation includes the activation of PRAS40, which was primarily triggered by ZIP7-mediated zinc release. Finally, an increased activation of stress-responsive protein HSP60 was only observed in WT ZIP7, suggesting potential ER stress due to the redistribution of zinc from the ER to the cytoplasm.

Figure 5.17 Western blot analysis of multiple kinases in response to the effect of ZIP transporters and chimeric constructs

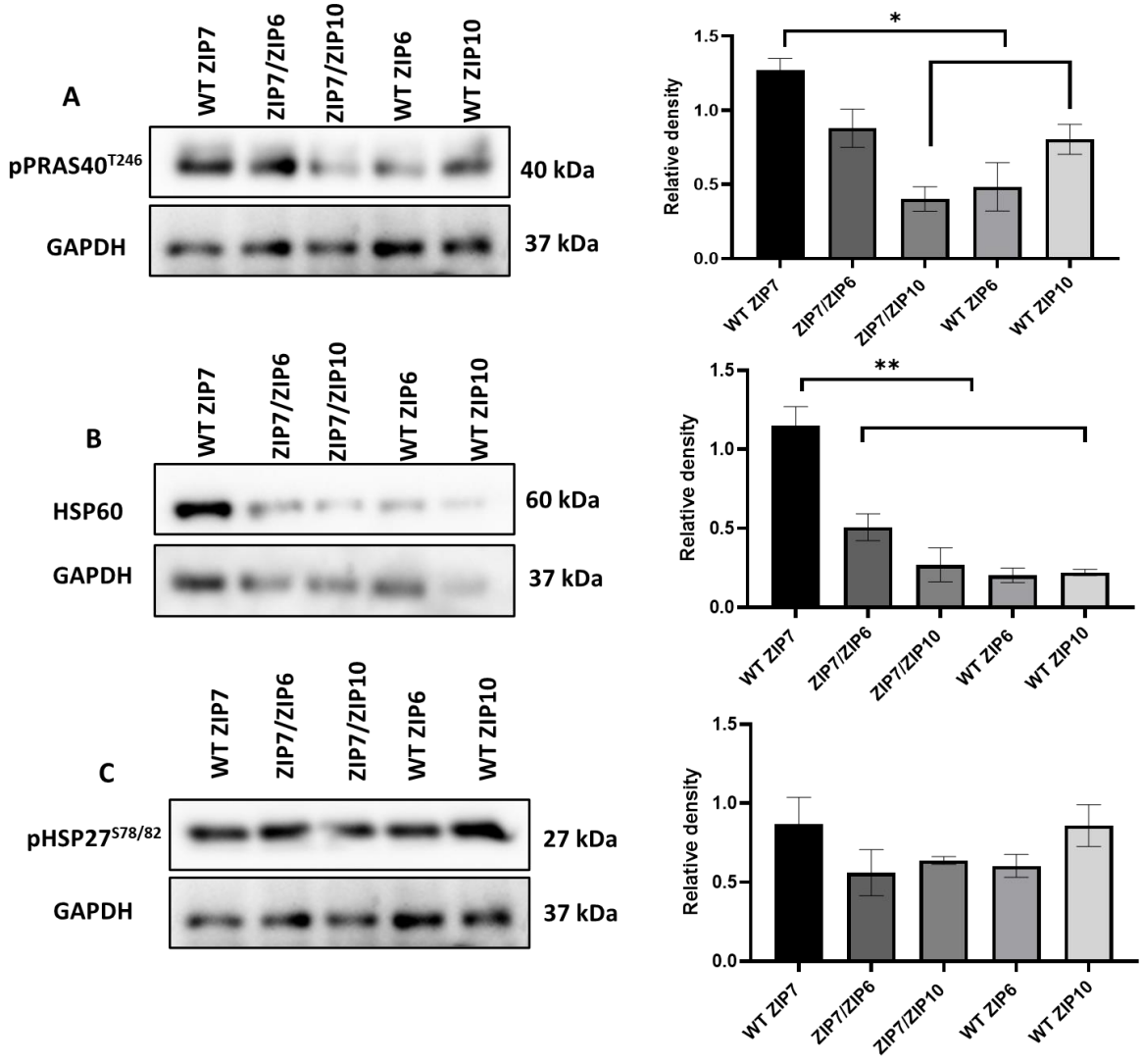

MCF7 cells were transfected with WT ZIP7, chimeric constructs with a ZIP7 N-terminus, WT ZIP6 and WT ZIP10 for 17 hours. Cells were lysed as pooled and analysed using SDS-PAGE and western blotting with pPRAS40^{T246} (**A**), HSP60 (**B**) and pHSP27$^{S78/82}$ (**C**). GAPDH was utilised as a loading control. The bar graph shows the densitometric data, which has been normalized to GAPDH and presented as mean ± standard error (n=3). *p=0.05; **p=0.01; ***p<0.001.

5.3.9 The effect of ubiquitination on ZIP6 function

Ubiquitination is a type of post-translational modification used by the cell to cause protein degradation (Sun et al., 2020)(Chen et al., 2022). In the case of ZIP6, it comprises ubiquitin sites that are strongly conserved through evolution, indicating their importance. These sites potentially direct ZIP6 towards degradation, resulting in a relatively short half-life of less than one hour for the ZIP6. The short half-life is due to the ability of ZIP6 to be degraded once the transporter is no longer useful or to stop cell division when it is not the appropriate time (Hogstrand et al., 2013) (Taylor, 2023). This could explain the observed deficiency in the quantity of recombinant ZIP6 harvested following the transfection process. Therefore, the effect of ubiquitination on the regulating of ZIP6 expression and stability, and its impact on ZIP6 function, was investigated using a mutant with all potential ubiquitin sites changed to alanine K467A, K468A, K472A, K456A, K457A, in order to prevent ubiquitination. This novel construct is referred to as ZIP6 Q.

The five residues of ZIP6, which are located between transmembrane domain 3 and 4, are assumed to undergo ubiquitination, leading to degradation of the protein. To investigate this hypothesis, the impact of mutated residues on ZIP6 degradation was investigated. Initially, MCF-7 cells were transfected with WT ZIP6 and ZIP6 Q for 17 hours. Immunofluorescence was then performed using a V5 antibody, which binds the C−terminal V5 tag of the recombinant protein.

As shown in **figure 5.18,** a limited number of cells were successfully transfected with WT ZIP6, representing about 3 to 5 % of the whole cell population, as determined by V5 staining. This suggests that the protein was degraded following N-terminal cleavage. In a surprising contrast, a significantly higher percentage of successful transfection was observed with ZIP6 Q, with about 37% of the cell population testing positive for V5 antibody as demonstrated in the graph. This observation implies that this mutation mostly abolished ZIP6 degradation, confirmed by the number of transfected cells per field in ZIP6 Q compared with WT ZIP6, as revealed by V5 staining. Thus, the alteration made on these residues seems to be essential for stability of ZIP6 and its expression within the cell.

Figure 5.18 The alteration of ubiquitin sites mostly suppressed ZIP6 degradation

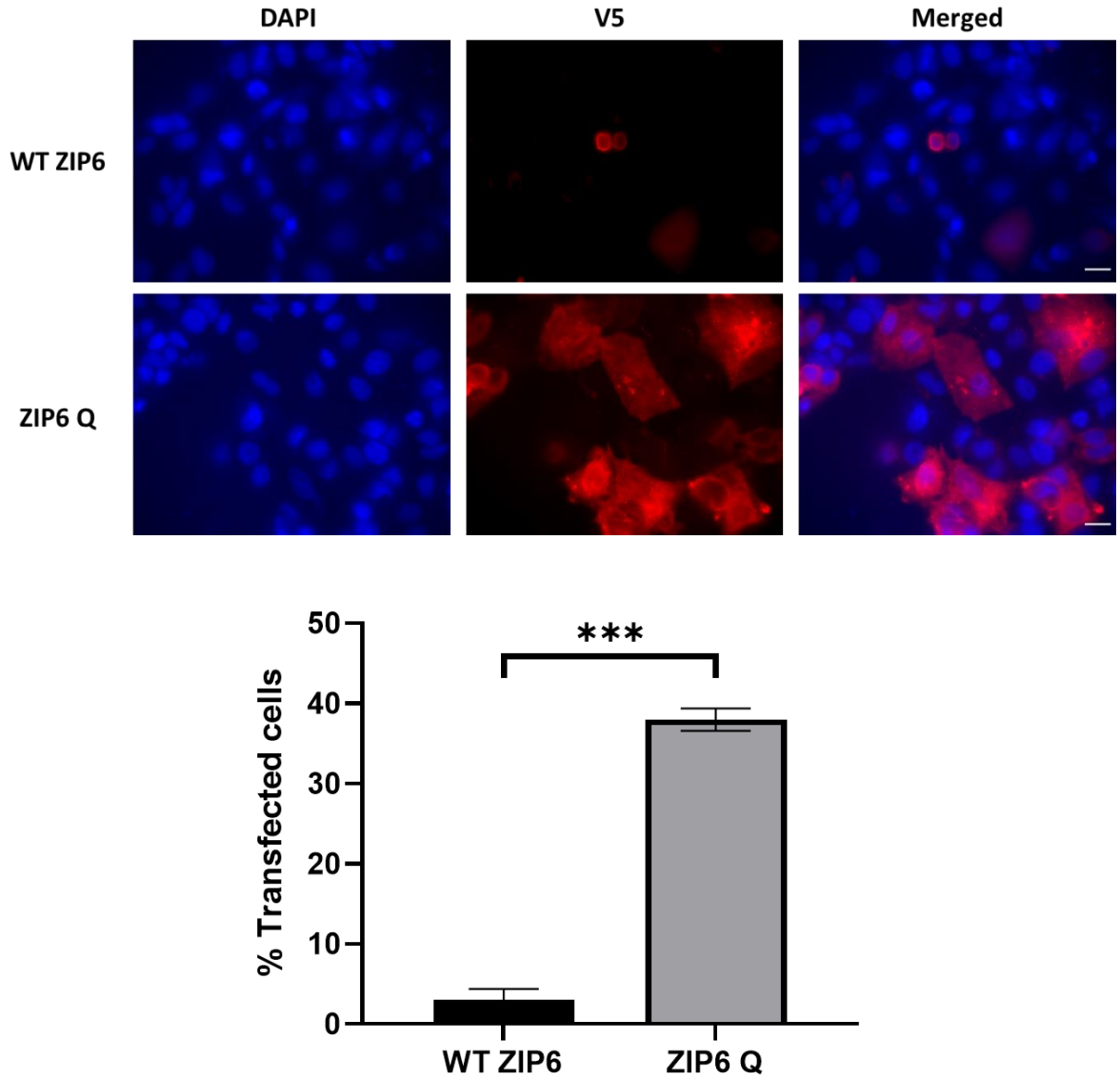

MCF-7 cells were transfected with WT ZIP6 and deubiquitinated ZIP6 (ZIP6 Q) 17 hours. The cells were stained for DAPI (blue) and V5 Alexa Fluor 594 (red), and then imaged using a 63x magnification lens on Leica RPE automatic microscope. The number of transfected cells was counted as cells positive for V5 per the whole cell population (n=3) *p=0.05; **p=0.01; ***p<0.001.

5.3.10 Investigating the effect of ubiquitination on ZIP6 function by using Western blotting

To verify the ZIP6 Q constructs compared with WT ZIP6 and investigate how the alteration on ZIP6 ubiquitin sites affects on its function, western blotting was performed. In these following experiments, the chimeric construct of containing a ZIP7 N-terminus on ZIP6 was used to provide a robust comparison in investigating ZIP6 function. Therefore, MCF-7 cells were transfected with all these constructs for 17 hours. Before the cells were harvested, bright-field microscopy images were captured to observe the appearance of cells prior to collection (**Figure 5.19**). Interestingly, adherent cells were observed in the chimeric ZIP7/ZIP6 construct transfected dishes. In contrast, dishes with WT ZIP6 or ZIP6 Q ZIP7 predominantly exhibited non-adherent cells, highlighting the effect of the N-terminus and ubiquitin sites in stimulating cell detachment. No cells detachment was observed in either untransfected dishes or dishes treated with lipofectamine only (transfection reagent), confirming the cells detachment phenomenon was not a result of MCF-7 cells by itself or the transfection process. This finding suggests that the observed differences in cell behaviour are associated with the transfected constructs.

At the time of cell harvest, non−adherent cells found in the medium were gathered and pooled together with attached cells. This mixed population of cells, which includes both non-adherent and adherent cells, is referred to as a pooled sample. Moreover, separate samples were also prepared using only adherent cells, which were referred to as adherent cell samples. Western blotting was employed using a V5 antibody to recognise the C−terminal V5 tag in the recombinant protein. As can be seen from the **Figure 5.20**, the chimeric ZIP7/ZIP6 was easily detected, demonstrating a band at 63 KDa. This band represented the full length of this construct. This indicates that the chimeric construct did not undergo N-terminal cleavage or degradation. Due to the difficulty of detecting V5 band of ZIP6, the blot was developed for a longer time while the ZIP7/ZIP6 was covered by a filter paper. This approach allowed for the bands corresponding to ZIP6 and ZIP6 Q to be adequately produced and visualized. Eventually, the V5 band for the WT ZIP6 and ZIP6 Q began to emerge. As shown in **Figure 5.20,** the V5 band for ZIP6 appeared only at 73 kDa representing cleaved form of ZIP6. Noteworthy, the low percentage of the recombinant ZIP6 protein has been frequently noticed as a result of proteolytic degradation sites (Taylor et al., 2003).

Interestingly, the amount of the ZIP6 Q was twice as much as in the WT ZIP6 as judged by V5 in pooled and adherent samples. The V5 bands for ZIP Q appeared at 73 kDa and 108 kDa, representing the active form and full length of ZIP6, respectively. This difference between the WT ZIP6 and the mutant constructs of ZIP6 confirms that the ubiquitin residues are important to increase the stability and presence of ZIP6 within the cell.

Figure 5.19 WT ZIP6 and ZIP6 Q produced more detached cells compared to ZIP7/ZIP6

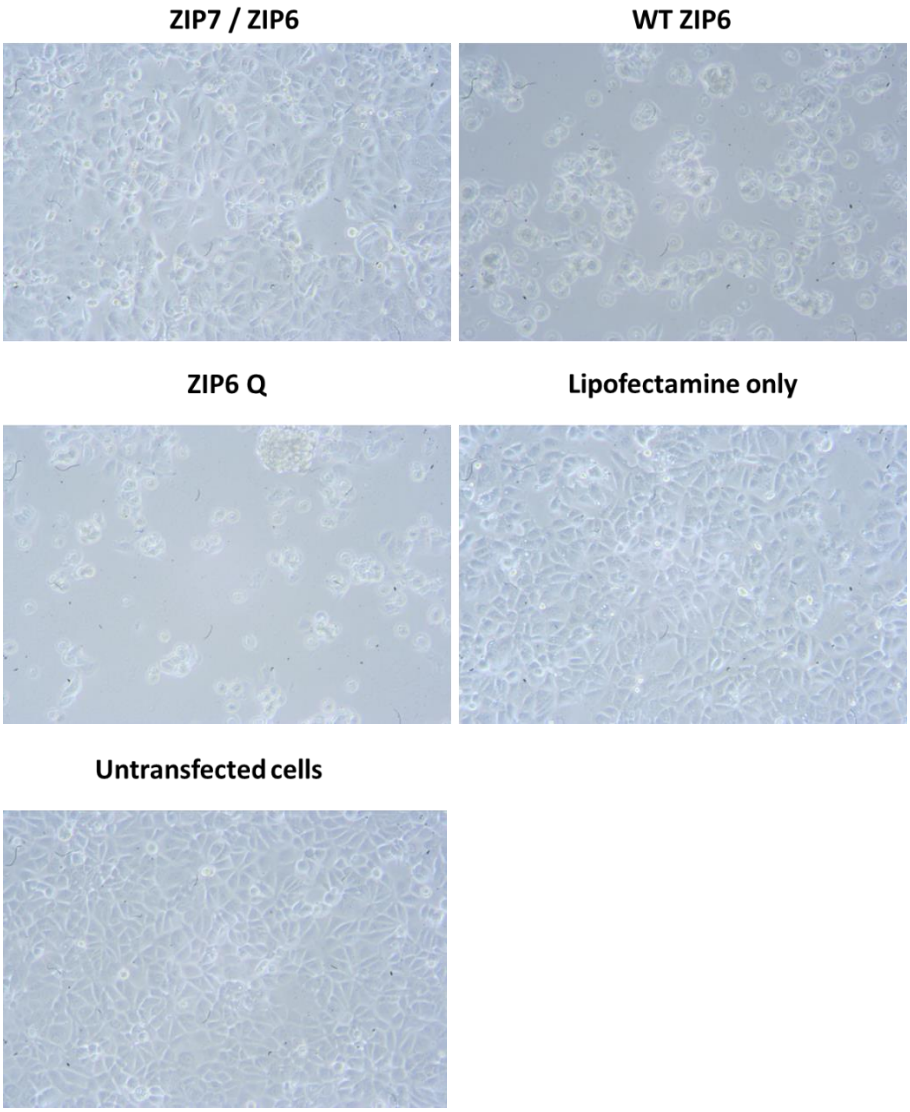

MCF7 cells were transfected with a chimeric construct with a ZIP7 N-terminus (ZIP7/ZIP6), WT ZIP6 and ZIP6 Q for 17 hours. The cells transfected with ZIP6 and ZIP6 Q had either detached clumps or detached single round cells, while this observation was not seen in the chimeric constructs with a ZIP7 N-terminus. Untransfected cells and cells with a transfection reagent lipofectamine was also imaged as a negative control.

5.20 Verifying the construct of mutated ubiquitin sites in ZIP6 by comparing pooled and adherent samples using Western blotting

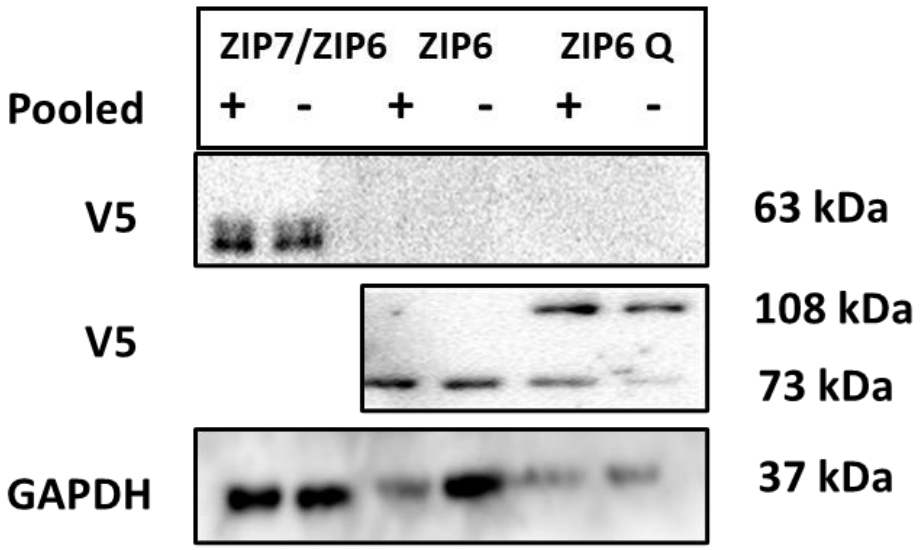

MCF7 cells were transfected with a chimeric construct with a ZIP7 N-terminus (ZIP7/ZIP6), WT ZIP6 and ZIP6 Q for 17 hours. Cells were lysed as pooled or adherent and analysed using western blotting with an anti-V5 antibody. The first part of the blot showed the V5 bands for ZIP7/ZIP6. The second part displayed the V5 band for ZIP6 and ZIP6 Q at different KDa 73 and 108, which were visualised for a long exposure time.

5.3.11 The impact of ubiquitin sites in sustaining the ZIP6 activation.

ZIP6 Q has been shown to have a longer half-life in cells compared to WT ZIP6. It would be intriguing to investigate whether this increased stability of this mutant could affect the functionality of ZIP6, particularly its ability to facilitate cell detachment and confer anoikis resistance. Moreover, having previously demonstrated the upregulation of PLK1 and STAT3 in WT ZIP6 compared to the chimeric ZIP7/ZIP6 construct, it is interesting to investigate the effect of deubiquitinated ZIP6 mutant on this activation. This investigation could provide valuable insights into the role of ubiquitination in regulating ZIP6.

To perform this, MCF-7 cells were transfected with a chimeric ZIP7/ZIP6 construct, WT ZIP6 and ZIP6 Q, and then harvested as pooled and adherent samples. To assess the levels of activated PLK1 and STAT3, the cells were probed with antibodies targeting $pSTAT3^{S727}$ and $pPLK1^{T210}$.

To observe the effect of deubiquitination on pSTAT3^{S727} activation, western blotting results initially revealed that the phosphorylation level of pSTAT3^{S727} was significantly attenuated by the modification of the N-terminus in the chimeric ZIP7/ZIP6 construct in both types of samples (**Figure 5.21 A**). This further confirmed that the N-terminus of ZIP6 is essential for ZIP6 activation. As expected, in WT ZIP6, the activation of pSTAT3^{S727} was observed only in pooled samples, indicating that the activation of pSTAT3^{S727}, as mediated by ZIP6, induced cell detachment. Interestingly, ZIP6 Q dramatically increased the phosphorylation level of pSTAT3^{S727} in pooled samples, while no such increase was observed in adherent samples. This result suggests that deubiquitination can potentiate cells to detach through the activation of pSTAT3^{S727}. The observation also indicates the increased stability of ZIP6 Q can profoundly enhance the activation of ZIP6, meaning that the ubiquitin sites may impact the functionality of ZIP6, particularly regarding its role in promoting cellular detachment.

To investigate whether these detached cells in pooled samples were still alive and proliferating, the activity of PLK1, a protein known to be transcriptionally activated during cell detachment and which promotes anoikis resistance (Lin et al., 2011), was used. In the chimeric ZIP7/ZIP6 constructs, no bands for pPLK1^{T210} were observed either in either pooled or adherent samples, confirming that the most of the cells remained attached, not undergoing any form of detachment (**Figure 5.21 B**). This finding aligns with the observation regarding pSTAT3^{S727} activation. In WT ZIP6, phosphorylation of pPLK1^{T210} was observed only in pooled samples, confirming that the detached cells mediated by the activation of ZIP6 were still alive. Notably, cells transfected with ZIP6 Q significantly upregulated pPLK1^{T210} in pooled samples, while no band was observed in the adherent ones. This confirmed that the detached cells found in pooled samples also remained alive. Moreover, this upregulation of pPLK1^{T210} was significantly increased compared with the level observed in pooled samples transfected with WT ZIP6. This suggests a potentially vital role for ubiquitin sites in sustaining ZIP6 activity, thereby further indicating the effect of deubiquitination on ZIP6 functionality.

Figure 5.21 The impact of ubiquitin sites in sustaining ZIP6 activity

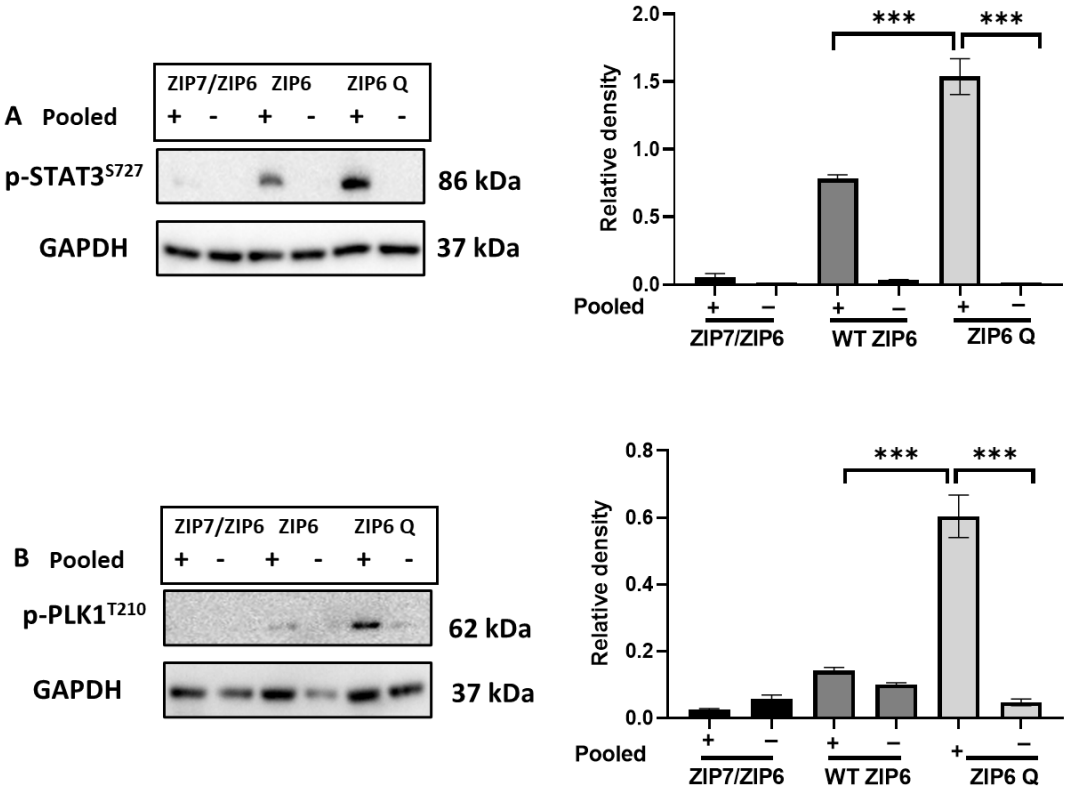

MCF7 cells were transfected with a chimeric construct with a ZIP7 N-terminus (ZIP7/ZIP6), WT ZIP6 and ZIP6 Q for 17 hours. Cells were lysed as pooled and adherent samples, and then analysed using western blotting with pSTAT3^{S727} (**A**) and pPLK1^{T210} (**B**). GAPDH was utilised as a loading control. The bar graph shows the densitometric data, which has been normalized to GAPDH and illustrated as mean ± standard error (n=3) *p=0.05; **p=0.01; ***p<0.001.

5.3.12 The effect of ubiquitin sites in promoting phosphorylation of several protein kinases

To explore the downstream targets of the ubiquitin sites in ZIP6, and to examine how mutated ubiquitin sites affect these targeted kinases, phospho-kinase array was employed. To perform this, MCF-7 cells were transfected with chimeric ZIP7/ZIP6 constructs, WT ZIP6 and ZIP6 Q.

The data from the arrays displayed that cells transfected with all these constructs showed induced phosphorylation of many kinases (**Figure 5.22**). The images display noticeable spots of phosphorylated kinases including pGSK-3ß^{S9}, pHSP27$^{S78, 82}$, pP70 S6^{T389} and HSP60 which are indicated by arrows. However, it is worth noting that three pairs of dark reference points can be found at the top-right, top-left, and bottom-left corners, which are used for alignment.

To evaluate the levels of each kinase, a bar graph was created, presenting the densitometric values of the corresponding duplicate dot pairs for all detected kinases. Kinases that showed a high change in their phosphorylation level (> 200 density units) were classified as highly activated.

Generally, the array data displayed that cells transfected with ZIP7/ZIP6, WT ZIP6 and ZIP6 Q markedly induced phosphorylation (>300 density units) of pGSK-3ß^{S9}, pP70^{T389}, and HSP60. Additionally, a mild increase in phosphorylation (100-200 density units) was observed for pAKT^{T308}, pHSP27$^{S78,\ 82}$, pPRAS40^{T246} and pSTAT3^{S727} (**Figure 5.23**).

To determine the effect of ubiquitin sites on ZIP6 activation, the densitometric values of the highly activated kinases were represented in separate bar graphs (**Figure 5.24**). pGSK-3ß^{S9}, which exhibited a high phosphorylation level, was reported to be phosphorylated by zinc influx from the plasma membrane (Hogstrand et al., 2013) (Taylor et al., 2016). However, given its increased levels across all samples, western blotting was required to probe the differences among them. Phosphorylation levels of pHSP27$^{S78,\ 82}$, pP70^{T389} and pPRAS40^{T246} mainly showed an increase in WT ZIP6 and ZIP6Q as compared to ZIP7/ZIP6, indicating a dominant effect of the N-terminus over the ubiquitin sites on these kinases.

Notably, HSP60 were found to be increased in ZIP6 Q compared to the chimeric construct and WT ZIP6, suggesting a role for ubiquitin sites. HSP60 is known to respond to cellular stress conditions (Lianos et al., 2015). Therefore, sustained activation of ZIP6 attributed to deubiquitinating, might facilitate a greater influx of zinc, thereby leading to cellular stress as a result of zinc dyshomeostasis.

Figure 5.22 Investigating the role of ubiquitin sites in ZIP6 in phosphorylated kinases

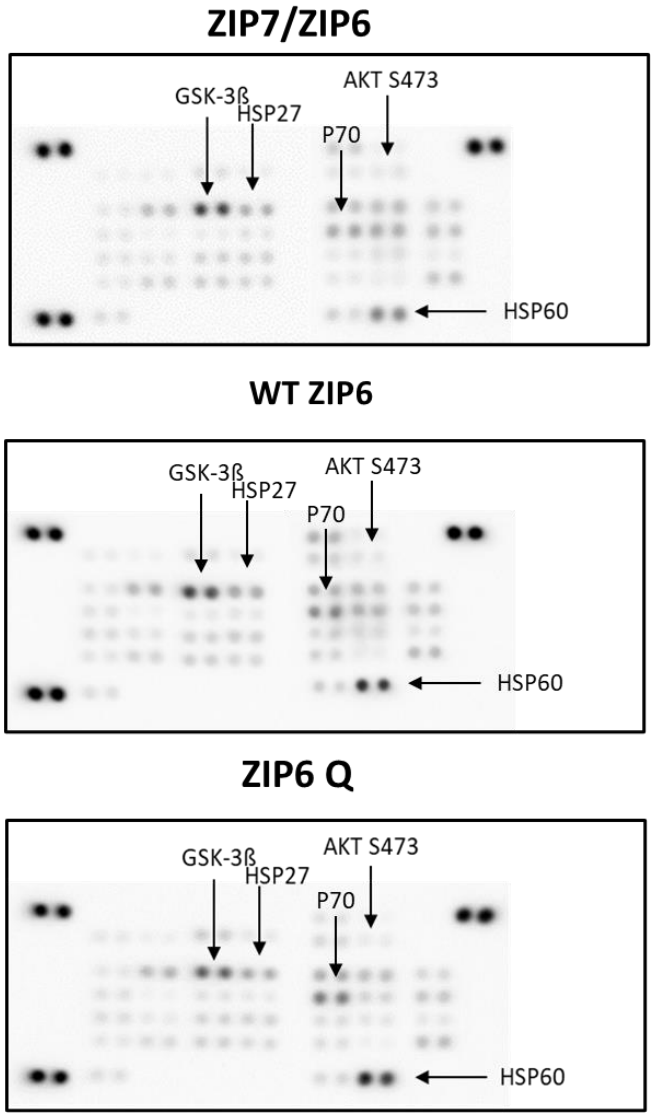

MCF7 cells were transfected with a chimeric construct with a ZIP7 N-terminus (ZIP7/ZIP6), WT ZIP6 and ZIP6 Q for 17 hours. The human phospho-kinase antibody arrays (ARY003C; R&D Systems) were used to examine 37 phosphorylated kinases and 2 total proteins. Signals for each kinase appear as a pair of duplicate spots, with three pairs of dark reference at the top-right, top-left, and bottom-left corners, which are used for alignment.

Figure 5.23 Densitometric analysis of phospho-kinase arrays in transfected MCF-7 cells with ZIP7/ZIP, WT ZIP6 and ZIP6 Q

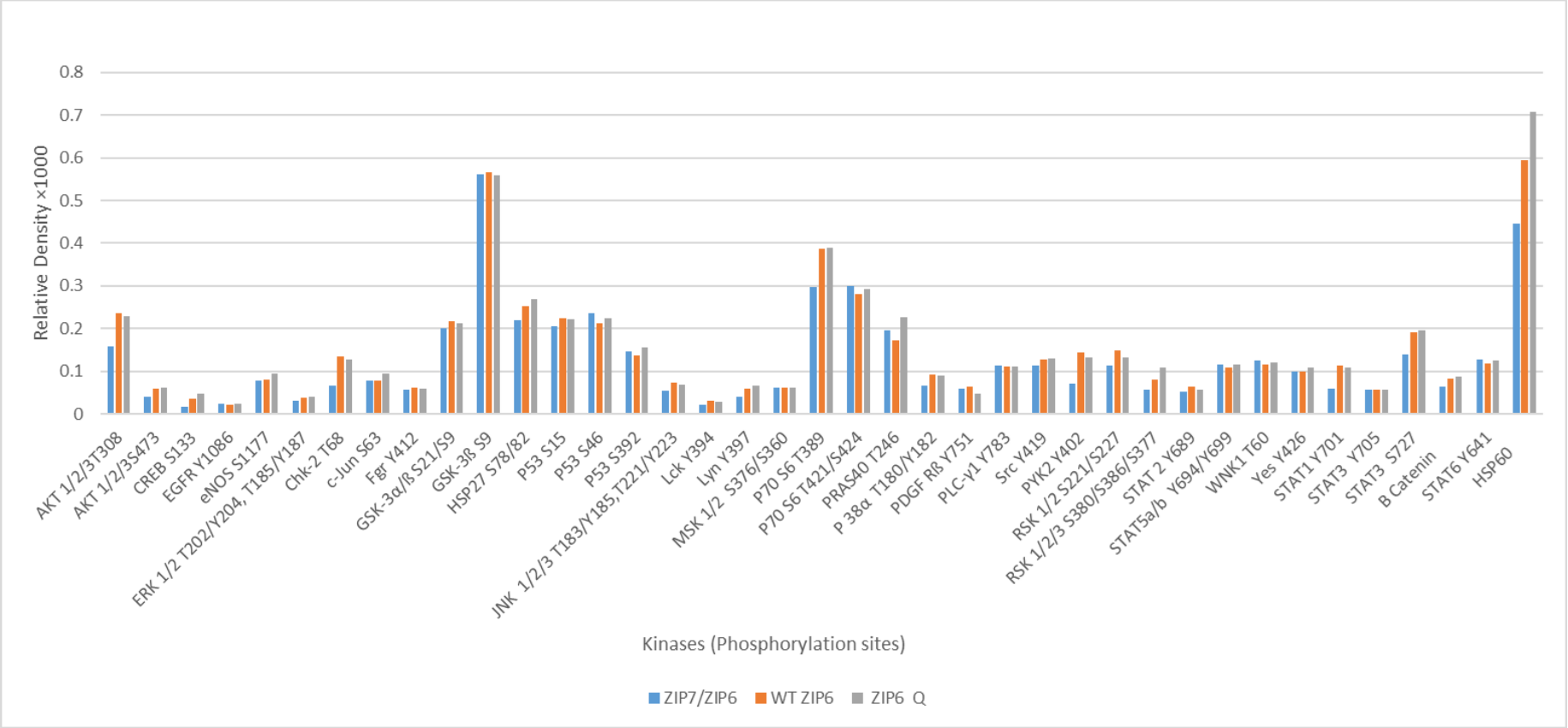

MCF7 cells were transfected with a chimeric construct with a ZIP7 N-terminus (ZIP7/ZIP6), WT ZIP6 and ZIP6 Q for 17 hours. The phosphorylation of selected kinases at the residues specified beneath the kinase names was identified using the human phospho-kinase antibody arrays (ARY003C; R&D Systems). Normalised data are shown as the average of duplicate dots for each kinase (n=2).

Figure 5.24 The highlighted kinases in MCF-7 cells transfected with ZIP7/ZIP6, WT ZIP6 and ZIP6 Q

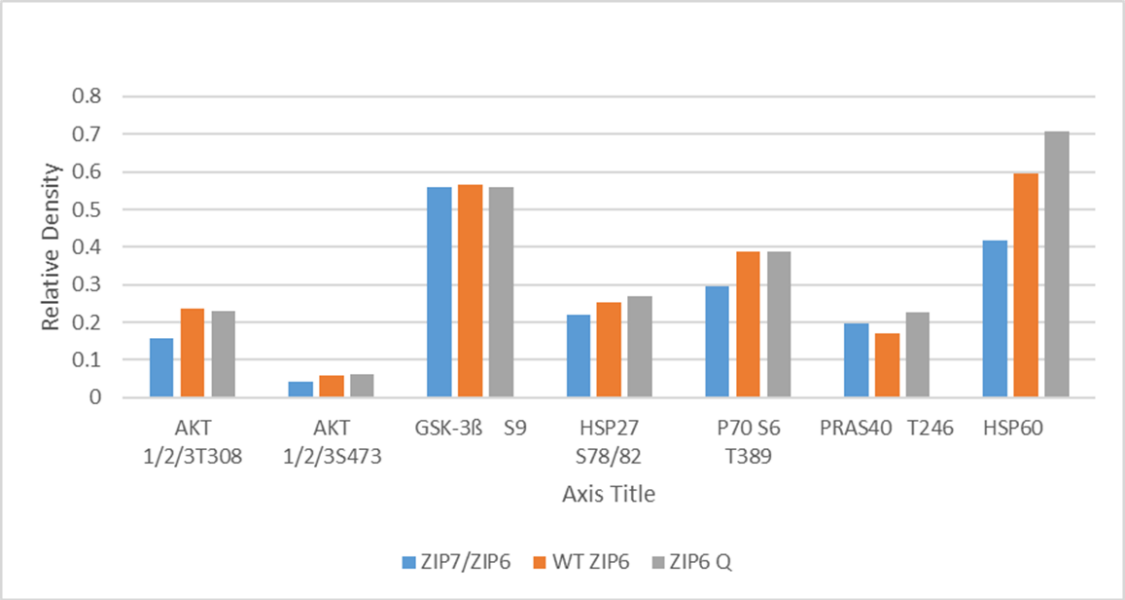

MCF7 cells were transfected with a chimeric construct with a ZIP7 N-terminus (ZIP7/ZIP6), WT ZIP6 and ZIP6 Q for 17 hours. The phosphorylation of selected kinases at the residues specified beneath the kinase names was identified using the human phospho-kinase antibody arrays (ARY003C; R&D Systems). Normalised data are demonstrated as the average of duplicate dots for each kinase (n=2).

5.3.13 Western blotting confirms kinases activation by the effect of ubiquitin sites in ZIP6

The phospho-kinase arrays were used to identify which downstream kinases were activated as a result of the ubiquitination at the sites in ZIP6. To confirm the phosphorylation of these highly activated kinases, a western blot was performed on cells transfected with a chimeric ZIP7/ZIP6 construct, WT ZIP6 and ZIP6 Q. After transfection, the cells then were lysed as pooled and adherent samples and analysed by western blot. Nevertheless, due to time restriction, the kinases confirmed by western blotting were limited to pGSK-3ß^{S9} and pAKT^{S473}.

When ZIP6 undergoes N-terminal cleavage and relocates to the PM, ZIP6 transports zinc into the cell. This zinc influx results in the inactivating pGSK-3ß^{S9} phosphorylation, either directly through the impact of zinc, or indirectly via the activation of AKT by zinc (Hogstrand et al., 2013). The western blotting result showed that the phosphorylation of pGSK-3ß^{S9} significantly decreased in the ZIP6 chimera with a modified N-terminus compared with WT ZIP6 (**Figure 5.25 A**). This provides further confirmation of the critical role of the N-terminus of ZIP6 in transporting zinc and inducing its activity. Moreover, the phosphorylation level of pGSK-3ß^{S9} in pooled and adherent samples appeared to be similar, indicating that no cell detachment had occurred. In WT ZIP6, the phosphorylation level of pGSK-3ß^{S9} was elevated in both pooled and adherent samples. However, an increase was noticed in adherent samples. This might be attributed to the endogenous ZIP6. Interestingly, cells transfected with ZIP6 Q resulted in a significant increase in pGSK-3ß^{S9} in pooled samples compared to the level observed in adherent ones. This observation highlights the effect of mutated ubiquitin sites in ZIP6 in stimulating cells to undergo detachment. Nevertheless, the difference between ZIP6 Q in pooled samples compared with ZIP6 was not significant, consistent with the data revealed by the phospho-kinase array. Therefore, given the phosphorylation of pGSK-3ß^{S9} has been shown to be reliant on preceding AKT activation (Lee et al., 2009), the activation of AKT was examined.

In the chimeric ZIP7/ZIP6 construct, modification of the N-terminus resulted in a significant attenuation in the activation of pAKT^{S473} in pooled samples compared to WT ZIP6 (**Figure 5.25 B**). This not only highlights the role of the ZIP6 N-terminus, but also indicates that the chimeric construct was unable to functionally transport zinc. In WT ZIP6, the phosphorylation level of pAKT^{S473} markedly increased when compared to ZIP7/ZIP6. Interestingly, the mutated ubiquitin sites in ZIP6 effectively increased the activation of pAKT^{S473} in pooled samples compared to the adherent one, indicating more cells were detached due to sustained activation of ZIP6. Additionally, the difference in pAKT^{S473} activation between WT ZIP6 and ZIP6 Q was significant, emphasising the impact of ubiquitin sites in regulating ZIP6 function.

Figure 5.25 The effect of ubiquitin sites in regulating ZIP6 activation

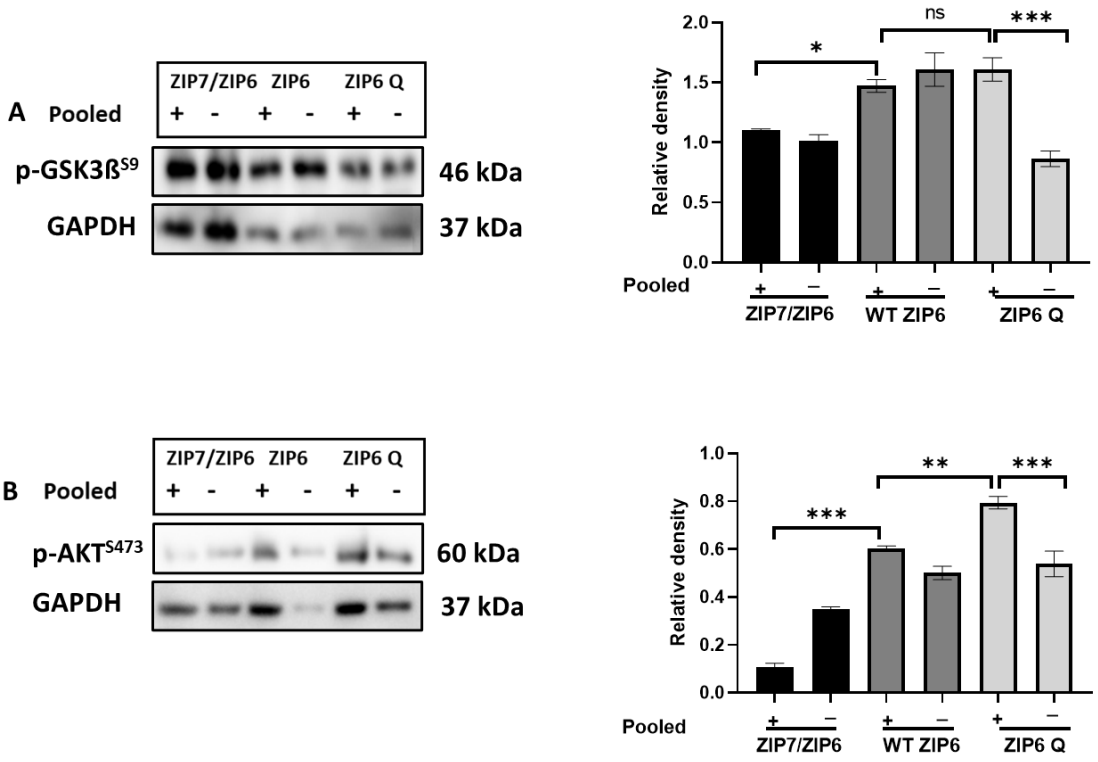

MCF7 cells were transfected with a chimeric construct with a ZIP7 N-terminus (ZIP7/ZIP6), WT ZIP6 and ZIP6 Q for 17 hours. Cells were lysed as pooled and adherent samples, and then analysed using western blotting with pGSK-3ß^{S9}(**A**) and pAKT^{S473} (**B**). GAPDH was utilised as a loading control. The bar graph shows the densitometric data, which has been normalized to GAPDH and illustrated as mean ± standard error (n=3) *p=0.05; **p=0.01; ***p<0.001.

5.4 Chapter summary

This chapter provided insight into the critical role of the ZIP6 and ZIP10 N-termini, employing novel chimeric constructs that replace the N-terminus with a non-cleavable one. The exogenous expression of WT ZIP6 and ZIP10 in cells promotes cell detachment, leading to a lower transfection efficiency. Using an immunofluorescence technique, the chimeric constructs appeared to prevent or delay this cell detachment (**Figure 5.2**), as demonstrated by the high number of transfected cells which were comparable to the WT ZIP7. Moreover, modifying the N-terminus of ZIP6 and ZIP10 showed an alteration in localization, largely restricting the construct to the ER (**Figure 5.3**). A bright-field images showed that the chimeric constructs were effective in preventing cellular detachment, as evidenced by the presence of adherent cells in the images taken with a bright-field microscope, compared to their respective WT constructs (**Figure 5.5**).

Additionally, these detached cells in WT ZIP6 and ZIP10 were examined and found to be alive and proliferating, as indicated by the markers pPLK1^{T210} and pSTAT3^{S727}. These markers suggest that the cells have become resistant to anoikis and were undergoing the process of EMT (**Figure 5.8 and 9**). Furthermore, modifying the ZIP6 and ZIP10 N-termini significantly attenuated the effect of influx zinc by decreasing the phosphorylation level of pGSK-3ß ^{S9}, a kinase that responds rapidly to zinc level. These constructs also diminished the effect of ZIP6 and ZIP10 in triggering cell migration, as supported by the decreased in pPyk2^{Y402} phosphorylation level compared to their respective transporters (**Figure 5.15**). These findings highlight that the distinct N-termini of ZIP6 and ZIP10 play a crucial role in controlling their function and activity.

The final part of this chapter focused on ubiquitination, and how this process impacts on ZIP6 degradation. ZIP6 is subject to degradation, which may explain not only the decreased expression of this protein after transfection but also how the cell prevents cell division being initiated prematurely. By using a novel construct in which all the predicted ubiquitin sites were mutated, immunofluorescence images showed a high number of cells positive for V5 in this recombinant mutant, showing an increased stability and presence in cells compared to WT ZIP6 (**Figure 5.18**). This result confirmed that the ubiquitin sites are primarily responsible for the degradation of ZIP6 and its short half-life.

Moreover, deubiquitinated ZIP6 was found to sustain ZIP6 activation, stimulating more cells to detach and significantly upregulating the activation of pSTAT3^{S727} and pPLK1^{T210} (**Figure 5.21**), kinases that respond to the EMT process and cell migration and have been shown to be activated by ZIP6. These findings imply that the ubiquitination process alters ZIP6 stability and function.

Finally, this chapter presented an exploration of how ZIP6 and ZIP10 are activated within cells by modifying their critical region of their structure. Additionally, this chapter experimentally demonstrated how ZIP6 can be “turned off” or “on” through alterations in its structure. These insights not only help us to understand the mechanism for these transporters but also enable new tools to be discovered for diseases, such as cancer, that are exacerbated by these transporters.

Chapter 6

Discussion

Zinc is the micronutrient with the second highest abundance in the human body, after iron, and it plays a crucial part in the function of various cellular activities (Hara et al., 2017). Zinc is essential for regular cell growth and development. It is linked with over 3,000 enzymes and proteins that play significant roles in the metabolism of carbohydrates, lipids, and proteins. Zinc was found to be the only metal detected in all classes of enzymes (Hambidge, 2000). Moreover, approximately 10 % of the proteins encoded in the human genome need zinc for their appropriate function and structure (Hambidge, 2000)(Health and Prasad, 2013). Therefore, it is unsurprising that zinc is involved in various processes such as cellular signalling, gene expression and membrane function and structure (Cummings and Kovacic, 2009)(Bafaro et al., 2017). Given the importance of zinc for many biological roles, its excess or deficiency can hugely impact human health.

Dysregulation in zinc levels has been recently involved in metabolic disorders (Tuncay et al., 2017) (Adulcikas et al., 2019), immune system defects (Miyai et al., 2014a), neurogenerative disorders (Grubman et al., 2014) and cancer (Taylor et al., 2008) (Sheng et al., 2017). ZIP transporters, which regulate zinc transport, are becoming increasingly associated with these number of human illnesses, including cancer, due to either increases or decreases in their functionality. Therefore, it is vital to further investigate their functional roles in cells to deepen our understanding. Thus, this project has focused on three important zinc transporters (ZIP7, ZIP6 and ZIP10) that are linked to many diseases, including cancer, to understand their functional mechanism in cells. By analysing the amino acid sequences of these transporters, the predicted structure of these transporters was obtained, and new potential phosphorylation sites were discovered (Chapter 3). Moreover, the expression pattern and prognostic value of these transporters in clinical breast cancer samples was evaluated (Chapter 3). The activation of ZIP7-mediated zinc release was further expanded to explore new phosphorylation sites necessary for maximal ZIP7 activation (Chapter 4). The role of ZIP6 and ZIP10 N-termini was further deciphered by determining their vital role in regulating their respective transporters (Chapter 5). Additionally, for the first time, the impact of ubiquitination as post−translational mechanisms of ZIP6 was experimentally investigated (Chapter 5).

The most striking discovery in this project was the identification of additional phosphorylation sites required for maximal ZIP7 activation. Additionally, this project investigated the vital role of ZIP6 and ZIP10 N-termini. Modifying the N-terminus by employing novel chimeric constructs resulted in a significant downregulation in the function of ZIP6 and ZIP10 transporters in cells. These discoveries not only understand the mechanism for these transporters but also enable new tools to be discovered for diseases, such as cancer, that are exacerbated by these transporters.

6.1 The importance of understanding the mechanism of zinc transporters

Zinc is unable to diffuse passively through cell membranes, so cellular zinc homeostasis is maintained through the function of the ZnT family (SLC30A), which acts as zinc efflux transporters, and the ZIP family (SLC39A), which serves as zinc influx transporters (Cummings and Kovacic, 2009)(Bafaro et al., 2017). ZnT transporters are responsible for lowering the level of cytosolic zinc, whereas ZIP transporters facilitate the movement of zinc into the cytoplasm, either from intracellular stores or from outside the cells. ZIP transporters are categorised according to the phylogenetic tree into four subfamilies, including gufA (ZIP11), subfamily I (ZIP9), subfamily II (ZIP1-3), and the LIV−1 subfamily (4-8, 10, and 12-14). Intracellular zinc is maintained by various zinc transporters. For instance, ZnT2 and ZnT4 reduce cytoplasmic zinc levels by depositing zinc within the lysosome. In contrast, ZIP8 increases cytoplasmic zinc levels by releasing zinc from the lysosome (Kimura and Kambe, 2016) (Hara et al., 2017). Similarly, ZIP9 and ZIP13, which are localized to the Golgi apparatus, also contribute to the increase of cytoplasmic zinc by releasing zinc from this compartment into the cytosol (Kambe et al., 2015). However, ZIP7, situated in the endoplasmic reticulum (ER), is the main regulator of intracellular zinc balance (Taylor et al., 2008). It facilitates the release of zinc from the ER into the cytoplasm. It is noteworthy that the ER is considered as a major zinc reservoir within the cell (Chabosseau et al., 2014). ZIP7 has been shown to be phosphorylated at its residues S275 and S276 by protein kinase CK2. Once phosphorylated, it releases zinc into the cytoplasm, thereby activating signalling pathways such as PI3K-AKT, MAPK and mTOR, which are linked to cell survival and proliferation (Taylor et al., 2012)(Nimmanon et al., 2017) (Paul et al., 2020).

Noteworthy, ZIP6 and ZIP10, which are relocated to the plasma membrane after being activated, have each been shown to initiate cell rounding and detachment, leading to the EMT process, by influxing zinc from outside the cell (Hogstrand et al., 2013) (Taylor et al., 2016).

Recently, our group has discovered the essential role of ZIP6 and ZIP10 to form a heteromer, which facilitates zinc influx, subsequently triggering mitosis. The ZIP6/ZIP10 heteromer has to be relocated to the plasma membrane to begin mitosis, a process that requires the cleavage of the N-terminus of ZIP6 (Nimmanon et al., 2020).

In the present study, the relationship between the overexpression of ZIP7, ZIP6, and ZIP10 and the progression of cancer diseases was thoroughly investigated. This investigation aimed to understand how the function of these transporters at a molecular level might translate into effects in a clinical context. This highlights the importance of understanding the mechanisms of these transporters, as such knowledge could pave the way for potential therapeutic interventions.

6.1.1 An elevated expression of ZIP transporters is strongly associated with human breast cancer

Having established the association of ZIP7, ZIP6, and ZIP10 transporters with signalling pathways linked to cancer (Grattan and Freake, 2012)(Saravanan et al., 2022), it is now interesting to explore how these findings translate to the clinical context. Using the GEPIA online tool (Tang et al., 2019), the analysis of patient data revealed substantial and statistically significant elevations in the levels of ZIP7, ZIP6 as well as ZIP4 in tumour samples when compared to corresponding normal breast tissue (**Figure 3.8**). However, ZIP10 exhibited a tendency to increase in tumour samples but the increases observed were not statistically significant. The findings of this study align with the conclusions of the review conducted by (Takatani-Nakase, 2018), demonstrating the importance of the activity of ZIP7, ZIP6 and ZIP10 transporters as a crucial element in breast cancer. It highlights the role of ZIP7 in tamoxifen-resistant breast cancer cells, as well as the roles of ZIP6 and ZIP10 in the invasion and metastasis of breast cancer cells (Takatani-Nakase, 2018). Moreover, the overexpression of ZIP7 was observed experimentally in other different types of cancer such as colorectal cancer (Sheng et al., 2017), cervical cancer (Wei et al., 2017) and lung adenocarcinoma (Zhou et al., 2021).

ZIP7 was also shown to promote multiple growth and proliferation pathways such as AKT which is known to increase cell survival (Chang et al., 2003) and MAPK which is known to drive cell proliferation (Fiore et al., 2017).

Further confirmation of this was achieved through the use of ZIP7 knockdown, which resulted in the suppression of cell growth and initiation of apoptosis in colorectal cancer (Sheng et al., 2017) as well as reduced cell proliferation in cervical cancer (Wei et al., 2017). These findings indicate the crucial role of ZIP7 in cancer and emphasise the importance of understanding its mechanism for potential therapeutic targeting. As CK2 has been shown to regulate ZIP7 activation (Taylor et al., 2012), CK2 inhibitor CX-4945, which has shown potential in inhibiting tumour growth in breast cancer cell lines (Siddiqui-Jain et al., 2010), is currently being used in clinical trials for a novel cancer therapeutic (D'Amore et al., 2020). One possible mechanism of action for CX-4945 could be the inhibition of zinc signalling pathways mediated by ZIP7 activation.

Intriguingly, among the LIV-1 subfamily, ZIP6 levels were found to be the highest in cancer samples. Considering the abnormal growth of cancer cells, the elevated expression of ZIP6 is consistent with its known role in promoting cell division (Nimmanon et al., 2020). Therefore, this elevation could be attributed to the cellular requirement for ZIP6-mediated zinc influx to initiate mitosis. Moreover, the increase of ZIP10 was not significant in cancer compared to normal relative samples. It is worth noting that ZIP10 has been shown to form a heteromer with ZIP6, regulating zinc influx to initiate mitosis (Nimmanon et al., 2020).These findings indicate that ZIP6 might play a more dominant role than ZIP10 in the mechanism of regulating zinc influx to trigger cell division. These observations also suggest that the ZIP transporters can be integrated to perform their cellular functions.

ZIP4 is known to be essential for zinc uptake in a normal state and plays a critical role in the absorption of zinc from the diet in the gut (Kambe and Andrews, 2009). Additionally, mutations in ZIP4 can lead to a rare inherited disorder known as Acrodermatitis Enteropathica, characterized by the inability to absorb zinc, resulting in zinc deficiency (Dufner-Beattie et al., 2003). ZIP4 has been shown to be upregulated when cells are deficient in zinc (Cousins, 2010).

In this context, the high level of ZIP4 observed in breast cancer might be due to zinc deficiency as a direct result of the cancer using more zinc for proliferation.

This is supported by the fact that decreased serum zinc levels have been shown in breast cancer patients (Feng et al., 2020). Interestingly, the upregulation of ZIP4 alongside lower serum zinc levels was recently observed in poorer prognosis in colon cancer (Wu et al., 2020). Moreover, elevated ZIP4 upregulation was linked with a more severe grade of gliomas and shorter overall survival (Lin et al., 2013). This observation could be consistent with those in breast cancer, which showed an elevated of ZIP4, suggesting that cancer cells have a strong requirement for zinc to grow and elevation.

Further examination was performed to investigate the prognostic role of ZIP7 and ZIP6 in breast cancer. The results demonstrated that elevated ZIP7 expression was linked to poor relapse-free survival (RFS) and overall survival (OS). The elevation of ZIP7 appears to be proportional to the severity of the cancer (**Figure 3.9**). These findings were consistent with the studies that showed a role of ZIP7 in driving multiple growth and proliferation pathways in breast cancer cells (Nimmanon et al., 2017). Recently, it has also been demonstrated that ZIP7 is crucial for the survival and proliferation of lung adenocarcinoma (Zhou et al., 2021). Moreover, the poorer relapse-free survival observed in the group of patients treated only with tamoxifen indicates that ZIP7 might develop resistance to tamoxifen, an idea supported by its increased expression in this group. This means that a higher ZIP7 level is consistent with the likelihood of developing resistance due to the upregulation of growth signalling pathways. It is also supported by the study showing an elevation of activated ZIP7 in TamR cells, breast cancer cells associated with resistance and progression (Ziliotto et al., 2019). Notably, the development of resistance to tamoxifen poses a major challenge, often resulting in a more aggressive and altered form of breast cancer (Nicholson and Johnston, 2005). Therefore, ZIP7 could serve as a promising therapeutic target in breast cancer.

In contrast, increased levels of ZIP6 were associated with a better prognosis, as these patients showed significant improvements in both overall survival and relapse-free survival rates (**Figure 3.10**). This data, examining only chemotherapy treated patients, suggests that elevated levels of ZIP6 are associated with lower aggressive cancers.

However, ZIP6 has been shown to mediate zinc influx, driving cell division (Nimmanon et al., 2020). Thus, the observed improvement could be attributed to an increased sensitivity to chemotherapy, which might be due to the accelerated growth rates of tumours exhibiting high ZIP6 levels.

It is noteworthy that the observed elevation in ZIP6, as determined by mRNA expression, correlates with overall survival and relapse-free survival rates without considering protein expression levels. Importantly, the relationship between mRNA expression and protein production is not always linear (Pascal et al., 2008). This discrepancy is likely due to post-translational modifications that affect protein half-life. Therefore, ZIP6 has been identified to possess many ubiquitination sites that are responsible for protein degradation (Hogstrand et al., 2013) (Saravanan et al., 2022). Even if large amounts of ZIP6 are synthesised, they might be immediately degraded through the ubiquitination process. This suggests that mRNA abundance may be a weak indicator of the corresponding protein concentration.

6.2 The involvement of additional residues required for maximal activation of ZIP7

ZIP7, located in the endoplasmic reticulum, is recognised as a primary regulator of intracellular zinc homeostasis (Hogstrand et al., 2009) (Taylor et al., 2012). ZIP7 has been shown to facilitate zinc release from the endoplasmic reticulum - a major store for zinc within the cell, into the cytoplasm (Taylor et al., 2004)(Taylor et al., 2012). In order to release zinc, ZIP7 has been shown to be phosphorylated at residues S275 and S276 by protein kinase CK2 (Taylor et al., 2012). Once phosphorylated, it releases zinc into the cytoplasm, which in turn inhibits protein tyrosine phosphatases and activates signalling pathways such as PI3K-AKT, MAPK and mTOR. These pathways are linked to cell survival and proliferation (Nimmanon et al., 2017)(Sheng et al., 2017)(Adulcikas et al., 2019).

In the previous section, according to the clinical data, ZIP7 was found to be significantly upregulated in breast cancer samples and was strongly associated with poorer patient outcomes. Frequently, breast cancers that are positive for the oestrogen receptor are treated with anti-hormonal therapies. Tamoxifen is the most commonly used anti-oestrogen treatment in these cases (Chang, 2012). However, over time, most cancers develop resistance to tamoxifen and evolve into more aggressive forms. Interestingly, in the model of tamoxifen-resistant cells (TamR), the cells showed a significant increase in ZIP7 as well as a large elevation in the level of intracellular zinc (Ziliotto et al., 2019).

This resistance could be facilitated by ZIP7-mediated zinc release, as zinc is known for its role in inhibiting tyrosine phosphatases (Bellomo et al., 2014), which subsequently activates downstream tyrosine kinases pathways such as EGFR, IGF-1R and Src that promote cell growth(Hutcheson et al., 2003).

In the present study, for the first time, four potential phosphorylation sites in ZIP7 were predicted and experimentally investigated using novel ZIP7 constructs, and the kinases predicted to phosphorylate these sites were also examined. These investigations will help to understand the function of this transporter, which in turn could pave the way for potential therapeutic targeting.

6.2.1 The identification of phosphorylation sites with kinase prediction for ZIP7

Following the discovery that ZIP7 activation is facilitated by CK2-mediated phosphorylation at residues S275 and S276 (Taylor et al., 2012), it was hypothesized that other phosphorylation sites on ZIP7 or other ZIP transporters could play a role in the post-translational regulation of ZIP transporters. Using multiple online databases, ZIP7 was found to have two additional phosphorylation sites (Serine 293 and Threonine 294) located on the cytoplasmic loop between TM3 and TM4 (**Figure 6.1**). Only the residues on this cytoplasmic loop were included due to the presence of a conserved mixed−charged area across ZIP transporters in this region (Taylor et al., 2003). This area on the cytoplasmic loop has been recognised as a likely reactive region, probably interacting with other proteins (Zhu and Karlin, 1996)(Taylor et al., 2004b).

Accordingly, the long cytoplasmic loop in ZIP4 has been found to play a vital role in regulating intracellular zinc levels by modulating ZIP4 concentrations on the plasma membrane, thus this area is critical to sustain zinc homeostasis within the cell (Bafaro et al., 2015). Phosphorylation occurring in this region could be important to this critical function. The hallmarks of cancer consist of ten distinct biological features acquired by cells during their transition from a normal to a neoplastic growth state. These features comprise the acquired capabilities to evade growth suppressors; maintain proliferative signalling; achieve replicative immortality; resist cell death; reprogram cellular metabolism; induce the vasculature; evade immune destruction, genome instability and mutation; promote tumour inflammation; and activate invasion and metastasis (Hanahan, 2022).

Figure 6.1 Prediction of phosphorylation sites in ZIP7

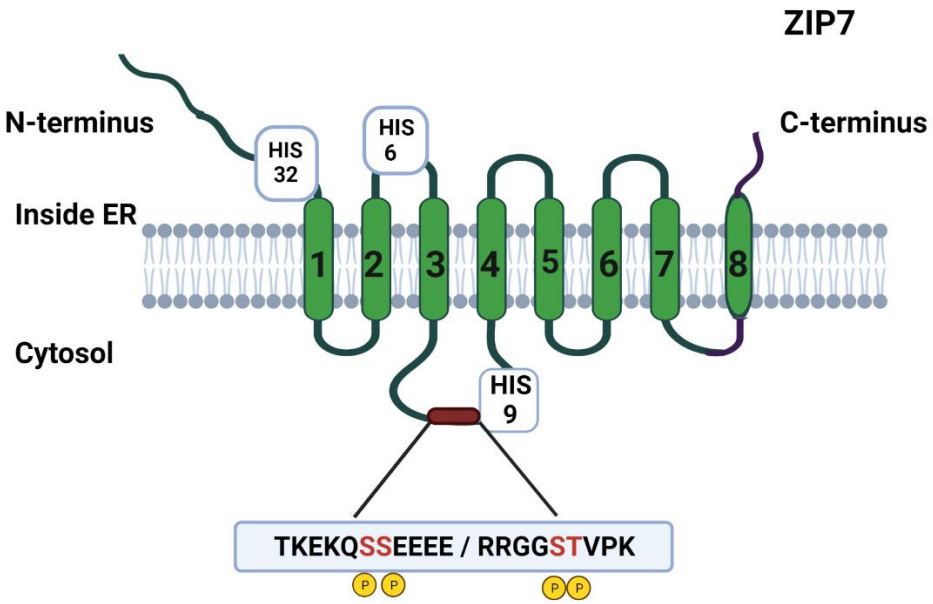

This schematic demonstrates the predicted phosphorylation sites in the ZIP7 transporter. The red colour represents the 275, 276, 293 and 294 residues that undergo phosphorylation. Predicted phosphorylation residues on the loop between TM3 and TM4 of ZIP7 were obtained by using Kinexus, NetPhos-3.1 and PHOSIDA (Gnad et al., 2007).

Interestingly, the predicted kinases for S293 and T294 are MAPKKAPK2-3 and PIM1-3, respectively (**Table 3.2**). These predicted kinases, closely tied to the hallmarks of cancer, have been shown to contribute to several of these hallmarks. Specifically, MAPKAPK2−3 promotes cell migration (Soni et al., 2019b), and PIM1−3, promotes cell proliferation and migration (Chen and Tang, 2019).

Moreover, the close location of phosphorylation sites in ZIP7 suggests that multiple sites might need to be phosphorylated in order to activate this transporter. This proximity indicates that it might also be subjected to hierarchical phosphorylation. This refers to the mechanism whereby the phosphorylation of a protein at a particular site, often termed a 'priming phosphorylation, enables a subsequent phosphorylation on a different residue within the same protein (St-Denis et al., 2015).

For instance, CK2 was shown to be required as a priming kinase for the subsequent ability of GSK-3ß to phosphorylate glycogen synthase on other residues in the process of glucose metabolism (Fiol et al., 1987). Intriguingly, CK2 was experimentally confirmed to phosphorylate ZIP7 at its residues S275 and S276 (Taylor et al., 2012). Thus, it could serve as a priming kinase for the subsequent activation of MAPKAPK2-3 and PIM1-3 which could lead to the phosphorylation of ZIP7 on S293 and T294. This synergetic mechanism of phosphorylation suggests that the use of a CK2 inhibitor would decrease the phosphorylation of S275 and S276, subsequently reducing the phosphorylation of S293 and T294 residues by other kinases.

6.2.2 Confirmation that AKT activation is downstream of ZIP7 activation

When CK2 phosphorylates ZIP7 at S275 and S276 residues, it triggers the release of zinc from cellular stores (Taylor et al., 2012). The released zinc then inhibits protein tyrosine phosphatases and activates cellular serine kinases such as MAPK, mTOR and PI3K-AKT, which together enhance tumour cell growth and motility (Nimmanon et al., 2017). In MCF-7 cells transfected with the WT ZIP7, it has been shown that AKT undergoes phosphorylation on S473 within 5 minutes following zinc treatment (Taylor et al., 2012). The early phosphorylation of ZIP7 on residues S275 and S276, facilitated by CK2 after 2 minutes of zinc treatment, is compatible with the AKT activation (Taylor et al., 2012). Thus, the activation of AKT was recognised as a good indicator of zinc release triggered by ZIP7 from cellular stores.

In the present study, the $pAKT^{S473}$ activation was significantly increased following zinc treatment in WT ZIP7. After stimulation by zinc, WT ZIP7 displayed significantly increased activation of $pAKT^{S473}$ when compared to the ZIP7 mutants AA and T294A, where S275 and S276 and T294A mutated to alanine, suggesting the role of these residues in ZIP7 activation. In the mutant of S293, the attenuation of $pAKT^{S473}$ activation was not significant compared with WT ZIP7. This might suggest that S293 and T294 are not equivalent residues in the activation of ZIP7, seemingly with the latter being more dominant. AKT, also known as protein kinase B, is a serine/threonine protein kinase that plays a crucial role in regulating cell proliferation and cell survival (Chang et al., 2003). It is activated by phosphorylation at the threonine 308 and serine 473 residues, a process triggered by external stimulants like growth factors or insulin.

However, the S473 residue is the most frequently investigated site for AKT phosphorylation, as it has been primarily investigated in the context of cancer (Vivanco and Sawyers, 2002). The activation of AKT has been shown to be linked to the prognosis of breast cancer due to its role in cell proliferation and survival processes (Chang et al., 2003). The activation of $pAKT^{S473}$ has been identified as a direct downstream effector of the zinc release mediated by ZIP7 from cellular stores (Taylor et al., 2012)(Nimmanon et al., 2017), these findings suggest that, similar to S275 and S276, the T294 residue is required for ZIP7 activation.

The close proximity of T294 and S275/S276 residues suggests that ZIP7 might be subject to hierarchical phosphorylation. This refers to the mechanism whereby the phosphorylation of a protein at a particular site, often termed a 'priming' kinase, enables a subsequent phosphorylation to take place on another residue of the same protein. CK2 might also be a primed kinase, phosphorylating a protein only after it has been phosphorylated by another kinase (St-Denis et al., 2015). Here, PIM1-3 could function as the 'priming' kinase, enabling ZIP7 to be subsequently phosphorylated by CK2. This suggests that S294 is initially phosphorylated by PIM1-3, which in turn enables CK2 to phosphorylate S275/S276. Once phosphorylated, the released zinc activities signalling pathways that are linked with cellular growth and survival.

Interestingly, the PIM family of serine/threonine kinases is known for its role in regulating cell survival mechanisms and driving cancer progression and growth (Cen et al., 2014). Furthermore, it is also found to promote breast cancer tumorigenesis (Ren et al., 2018) and its upregulation is associated with poor prognosis (Chen and Tang, 2019). Therefore, PIM1-3 might facilitate their role through the phosphorylation of ZIP7, in conjugation with the hierarchical phosphorylation by CK2. This idea is supported by the finding that most CK2 inhibitors can also effectively inhibit PIM with comparable efficacy (Pagano et al., 2008)(Sarno et al., 2011), suggesting that they share a similar active biological structure. This implies that one possible mechanism of action for CK2 inhibitors is through the inhibition of zinc signalling pathways in ZIP7.

6.2.3 Phosphorylation of ZIP7 by interacting with MAPKAPK2

ZIP7 is known to undergo post-translational modification via phosphorylation, a modification that alters the structural formation of a protein, thereby affecting its ability to interact with multiple proteins within several signalling pathways (Deribe et al., 2010).

ZIP7 has been shown to be phosphorylated at S275 and S276 residues by CK2 within 2 minutes of stimulus, triggering ZIP7 activation and the release of zinc from stores into the cytosol (Taylor et al., 2012). This zinc release subsequently activates multiple signalling pathways that are associated with the prognosis of cancer (Nimmanon et al., 2017). An initial bioinformatic search for the human ZIP7 protein sequence identified potential phosphorylation sites (S293 and T294). These sites are predicted to be phosphorylated by MAPKAPK2-3 and PIM1-3, respectively.

Here, in this study, it was interesting to explore the association between ZIP7 and one of these kinases, especially given that no previous experiments had been performed to confirm this prediction. The choice to initially investigate the MAPKAPK2 kinase was encouraged by the intention to examine the role of S293 residues using a quantitative approach. However, the use of PIM1-3 will be shown at the end of this section.

The protein-protein interaction technique has evidenced the binding of ZIP7 and MAPKAPK2 kinase within 2 minutes of zinc stimulation, in a manner similar to CK2. The involvement of CK2 in ZIP7 transporter activation is a significant finding (Taylor et al., 2012), given its established role in promoting cell survival (Unger et al., 2005). Furthermore, human breast cancer tissues have exhibited an elevation of CK2 (Filhol et al., 2015), suggesting a link between CK2 expression and breast cancer tumorigenesis. Consistent with the role of CK2, MAPKAPK2 kinase is also known to play a vital role in cell progression and proliferation in breast cancer (Juan Wang et al., 2020). MAPKAPK2, downstream substrate of p38 mitogen-activated protein kinase (MAPK), controls various cellular processes including proliferation, cell-cycle progression and metastasis (Li et al., 2003). These insights suggest that MAPKAPK2 might facilitate its role through the phosphorylation on ZIP7 at S293 residue, thereby activating multiple pathways implicated cancer progression. This is an interesting finding because p38 MAPK, the upstream of MAPKAPK2, regulates more than sixty substrates. As such, its direct inhibition could lead to undesirable side effects (Fiore et al., 2017) (Soni et al., 2019b). Therefore, the strategy of targeting ZIP7 through its kinase MAPKAPK2 might serve as a beneficial therapeutic approach for modulating tumour progression. This approach could provide a more selective way of regulating the specific cellular processes implicated in cancer development.

6.2.4 Using a novel ZIP7 construct to confirm the role of additional residues in ZIP7 activation

The previous section demonstrated the involvement of S293 and T294 residues in ZIP7 activation by using mutants in which each residue had individually mutated. To further investigate the role of these residues, along with S275/S276, in maximal activation of ZIP7, a novel ZIP7 construct was created in which all four residues were mutated in the same construct. This construct was named the 4A mutant (consisting of S275A, S276A, S293A and T294A).

Additionally, new constructs of WT ZIP7 and S275A/S276A (AA) were also created. All these desired constructs were artificially synthesised by Doulix (Venice, Italy). Artificial gene synthesis was recruited as an alternative to site-directed mutagenesis; hence it can create mutations specifically at any wanted residues (Hsu et al., 2014).

In the present study, all these new constructs were synthesised without a histidine tag (His-Tag). The first investigation, therefore, was to examine the impact of the His-Tag on zinc transport ability. The results confirmed that the absence of the His-Tag provides a more distinct differentiation between the WT and AA mutant following zinc treatment, suggesting that the His-tag may in fact have bound zinc and lessened the true effect. Many recombinant proteins have been modified to add His-Tag into their DNA for stability and purification purposes (Carson et al., 2007). However, histidine has a high affinity for zinc, and it has been reported that it has a role in zinc transport activity (Zhang et al., 2019). One of the unique characterisations of ZIP transporters, particularly those belonging to the LIV-1 subfamily, is the presence of histidine-rich regions at their N-terminus and long cytoplasmic loop between TM3 and TM4. These regions are thought to be a zinc-binding domain of ZIP transporters (Taylor et al., 2003). Therefore, the ZIP7 construct containing the His-Tag may bind to zinc in the endoplasmic reticulum and delay it from being released to the cytoplasm.

This result further supports the idea that the presence of a His-tag could alter the structure and function of a protein of interest, particularly those with high metal affinity (Booth et al., 2018). It is possible, therefore, that removing the His-Tag could result in a recombinant protein that exhibits activity or functionality comparable to that of the native protein. Hence, the constructs without a His-Tag were used for all the following experiments.

6.2.5 The stimulatory effect of the S293 and T294 residues on ZIP7-mediated zinc release

When CK2 phosphorylates ZIP7 at S275 and S276 residues, it triggers the release of zinc from cellular stores (Taylor et al., 2012). The released zinc then activates cellular serine kinases such as MAPK, mTOR and PI3K-AKT, which together enhance tumour cell growth and motility (Nimmanon et al., 2017). Previous results showed the involvement of two additional residues (S293 and T294) in ZIP7 activation as these residues had been individually mutated compared to WT and S275A/S276A. The activation was assessed using AKT, as it is recognised as an indicator of the downstream effector of zinc release mediated by ZIP7 (Taylor et al., 2012).

In the present study, the role of these residues will be investigated using a novel construct in which all four residues (S275, S276, S293 and T294) were mutated in the same construct (4A). The WT and S275A/S276A (AA) were also used for comparison. The current study found that the 4A construct was effectively attenuated the impact of ZIP7 activation, showing significantly decreased $pAKT^{S473}$ activation compared to the WT and AA. This result supports the earlier observation, which showed the stimulatory role of these additional residues along with S275 and S276. Interestingly, a previous study showed that the band for total ZIP7 and the phosphorylated form of ZIP7 was 40 and 48 KDa, respectively (Nimmanon et al., 2017). It is believed that phosphorylation at the S275 and S276 sites on ZIP7 results in a 4 KDa increase in size - a phenomenon previously observed when two serine sites within a protein molecule are phosphorylated (Bin et al., 2011). The 8 KDa difference in size between the phosphorylated ZIP7 band and the total ZIP7 band adds further support to this result. It suggests the existence of additional phosphorylation sites in ZIP7, beyond the S275 and S276 residues. Therefore, the difference in size could be attributed to the simultaneous phosphorylation at S293 and T294 residues, which supports the finding from the present study. Collectively, these findings confirmed the role of these additional two residues in the maximal activation of ZIP7. It can thus be suggested that the ZIP7 undergo phosphorylation by several kinases along with CK2. Using a bioinformatics database, ZIP7 was predicted to be phosphorylated by MAPKAPK2 and PIM1-3 at S293 and T294, respectively. This was confirmed for MAPKAPK2 to be associated with ZIP7, indicating its role in phosphorylating ZIP7. Taken together, these findings further our understanding of how the ZIP7 protein is activated, which may provide useful insights into how this protein transporter functions.

6.2.6 The binding of ZIP7 with predicted kinases MAPKAPK2 and PIM1

ZIP7 was discovered to be regulated by CK2 phosphorylation on serine residues 275/276 (Taylor et al., 2012). This phosphorylation has been shown to be essential for ZIP7 to transport zinc and activate signalling pathways are associated with cell survival and proliferation (Nimmanon et al., 2017). Bioinformatic analysis of the predicted kinases for ZIP7 identified that additional serine and threonine sites might be phosphorylated by MAPKAPK2 and PIM1 at S293 and T294 residues, respectively. Furthermore, previous results confirmed the role of these two residues in the maximal activation of ZIP7 as judged by AKT activation. However, the predicted kinases that phosphorylate these additional residues have not been experimentally investigated. Therefore, the present study aimed to investigate the binding of these kinases with ZIP7 and their subsequent impact on zinc transport. CK2 is recognized as a central regulator of several proteins and pathways (Unger et al., 2005). Its high prevalence in cancer cells has been noted, suggesting its substantial role in the progression of tumour development (Trembley et al., 2009). In particular, it was observed that an elevated expression of CK2 in the mammary glands was associated with a higher risk of metastasis in breast cancer, serving as an indicator of poor prognosis (Giusiano et al., 2011).

Here, in the present study, CK2 was found to be associated transiently with ZIP7 following extracellular zinc stimulation. The most important finding was the ability of the ZIP7 mutation (4A) to prevent this association, confirming the involvement of all four residues in regulating ZIP7. These results are consistent with a previous study which observed the physical interaction of CK2 with ZIP7 (Taylor et al., 2012). Additionally, CK2 has been shown to be involved zinc homeostasis in breast cancer. It has been found that knockdown of CK2α subunit substantially decreased the zinc level in breast cancer (Zaman et al., 2019), indicating its role through the phosphorylation of ZIP7. An initial bioinformatic search for the human ZIP7 protein sequence identified potential phosphorylation sites (S293 and T294). These sites are predicted to be phosphorylated by MAPKAPK2-3 and PIM1-3, respectively. Interestingly, these predicted kinases are involved in regulating cell survival mechanisms and contribute to cancer progression and growth. In particular, both kinases are recognized for playing a vital role in cell progression and proliferation in breast cancer (Juan Wang et al., 2020)(Chen and Tang, 2019).

For the first time, in the study, MAPKAPK2 and PIM1 were both observed to be physically associated with WT ZIP7 following external zinc stimulation. Interestingly, these kinases failed to associate with the ZIP7 4A mutant, suggesting that all four residues are essential for maximal activation of ZIP7. These observations were comparable with those seen with CK2, suggesting there is a more prominent role for ZIP7 in cell growth through the MAPKAPK2 and PIM1 signalling pathways.

MAPKAPK2, a downstream substrate of p38 MAPK, is associated with cancer development and metastasis (Li et al., 2003). MAPKAPK2 promotes head and neck squamous cell carcinoma progression (Soni et al., 2019b), colorectal cancer development (Phinney et al., 2018) and breast cancer progression (Murali et al., 2018). Meanwhile, PIM, the family of serine/threonine kinases, is known for its role in regulating cell survival mechanisms and driving cancer progression and growth (Cen et al., 2014). PIM1 is known to promote multiple myeloma (Chen et al., 2011), breast cancer (Ren et al., 2018) and prostate cancer (Luszczak et al., 2020). The roles of both MAPKAPK2 and PIM1 in carcinogenesis suggest that they are promising new therapeutic targets for cancer treatment. Consequently, ZIP7 might be among the substrates of these kinases, contributing to the cancer-promoting effects associated with MAPKAPK2 and PIM1. Their regulation might be facilitated through the activation of ZIP7 in hierarchical phosphorylation process involving CK2. Given that CK2 is known for its role in a hierarchical phosphorylation (St-Denis et al., 2015), the initial phosphorylation of S275/S276 by CK2 may be the trigger for the phosphorylation of S293 and T294 by MAPKAPK2 and PIM1, respectively. As this activation of ZIP7 requires phosphorylation all these three kinases, this understanding provides a potential novel strategy to indirectly target ZIP7.

6.2.7 Mutation of four ZIP7 residues effectively reduced the activity of kinase signalling pathways induced by ZIP7 activation

ZIP7, located in the endoplasmic reticulum (ER), plays a crucial role in transporting zinc from t to the cytoplasm (Taylor et al., 2012). The distinct localisation of ZIP7 in the ER enables it to play a crucial role in maintaining intracellular zinc levels. Recently, it has been shown that complete loss of ZIP7 in cell lines results in a reduction in cytoplasmic zinc, as quantified by mass spectrometry (Woodruff et al., 2018).

This vital role for maintaining intracellular zinc can significantly impact growth factor signalling (Taylor et al., 2003)(Hogstrand et al., 2009), confirming the important role of ZIP7 in signalling pathways. ZIP7 has previously been linked to cancer progression, as it has been shown to stimulate pathways such as PI3K-AKT, MAPK and mTOR, which are essential for cell growth and survival (Nimmanon et al., 2017).

In the present study, the role of essential ZIP7 residues in regulating the activity of cellular signalling pathways were investigated. Using phospho-kinase arrays and western blot have confirmed the activation of GSK-3ß, HSP27 and ERK1/2, which was further enhanced by zinc treatment. Interestingly, the activity of these kinases was effectively reduced in a 4A construct in which all four residues had been mutated to alanine. This reduction was significant compared to WT and S275/S276 mutant, confirming the role of all four residues in regulating the zinc function of ZIP7. ZIP7 activation resulted in the release of zinc into the cytoplasm, which in turn inhibits tyrosine phosphatase, leading to an extended activation of tyrosine kinases (Hogstrand et al., 2009). It has been also found to stimulate pathways such as MAPK, PI3K-AKT, and mTOR, which are essential for cell proliferation (Nimmanon et al., 2017). Moreover, the release of zinc facilitated by ZIP7 has been identified as driving the aggressive tendencies of tamoxifen-resistant breast cancer cells. This associates ZIP7 with the process through which breast cancer cells develop resistance to tamoxifen (Ziliotto et al., 2019).

Here, the mutation of all four residues in ZIP7 reduced the GSK-3ß kinase that has been shown to be phosphorylated as result of ZIP7-medited zinc release (Nimmanon et al., 2017). GSK-3ß (glycogen synthase kinase 3 beta) is a serine/threonine protein kinase, which plays a significant role in various signalling pathways. Phosphorylation of GSK-3ß promotes cell proliferation and cell differentiation (Xu et al., 2009). Moreover, phosphorylated GSK-3ß is linked to various diseases, including cancers, and often results in resistance to treatments like chemotherapy and radiotherapy (Shimura, 2011). The phosphorylation of GSK-3ß has been shown to be induced directly through zinc (Ilouz et al., 2002) or indirectly through the action of AKT (Lee et al., 2009), another kinase activated in response to zinc.

However, a recent study has shown that GSK-3ß was phosphorylated 10 minutes following zinc treatment compared with AKT which was phosphorylated after 5 minutes (Nimmanon et al., 2017), suggesting that GSK-3ß phosphorylation may depend on preceding AKT activation. Therefore, a reduction in the phosphorylation level of GSK-3ß through the mutation of ZIP7 makes this transporter a promising therapeutic approach.

Another activated kinase induced by ZIP7 activation, and significantly inhibited by ZIP7 mutation, was HSP27. HSP27, also known as Heat Shock Protein 27, is recognised for its tumorigenic and metastatic roles (Taylor and Benjamin, 2005). The overexpression of phosphorylated levels of HSP27 contributes to the cancer progression by enhancing tumour formation and resistance to treatment (Lianos et al., 2015)(Tanaka et al., 2018). Interestingly, HSP27 is known to be a substrate of the p38/MAPKAPK2 pathway. As such, the phosphorylation of HSP27, which relies on p38/MAPKAPK2, has been shown in the progression of ovarian cancer (Pavan et al., 2014), colorectal cancer (Henriques et al., 2018) and more recently, breast cancer (Juan Wang et al., 2020). It is noteworthy that MAPKAPK2 was shown to phosphorylate ZIP7; therefore, the phosphorylation of HSP27 might be induced through ZIP7-mediated zinc release. These findings elucidate how HSP27 is phosphorylated in cancer cells, suggesting that ZIP7 could be a promising therapeutic target.

Finally, ZIP7 activation has been shown to increase the activation of ERK1/2, another kinase, which has been previously linked with decreased survival rates in clinical breast cancer cases (Frogne et al., 2009). Recently, mutations in the ERK1/2 pathway have been found as one of the key factors contributing to endocrine resistance (Smith et al., 2021). ERK1/2 has been identified as a main downstream of ZIP7-mediated zinc release (Nimmanon et al., 2017), further confirming the significant role of ZIP7 activation in the progression of endocrine resistance. Interestingly, the current study found the ZIP7 4A mutant effectively reduced the activation of ERK1/2. This reduction was significantly observed in comparison with S275A/276A, confirming the role of all four residues in the maximal activation of ZIP7.

In conclusion, all these findings support the discovery of ZIP7-mediated zinc release in driving signalling pathways which have been implicated in cancer growth. In this study, for the first time, it has been demonstrated that mutating all four residues in ZIP7 successfully inhibits the kinases implicated in cancer growth and proliferation, thus confirming the functioning mechanism of the ZIP7 transporter. The current study postulated that phosphorylation of ZIP7 at S275/S276/S293 and T294 residues mediates the activation of several kinases related to cancer proliferation and survival (**Figure 6.2**). This discovery showed that ZIP7 can be activated through phosphorylation by multiple kinases. Therefore, targeting ZIP7-mediated zinc release with a kinase inhibitor cocktail emerges as a promising approach in cancer therapy.

Figure 6.2 Downstream signalling pathways of maximal ZIP7 activation

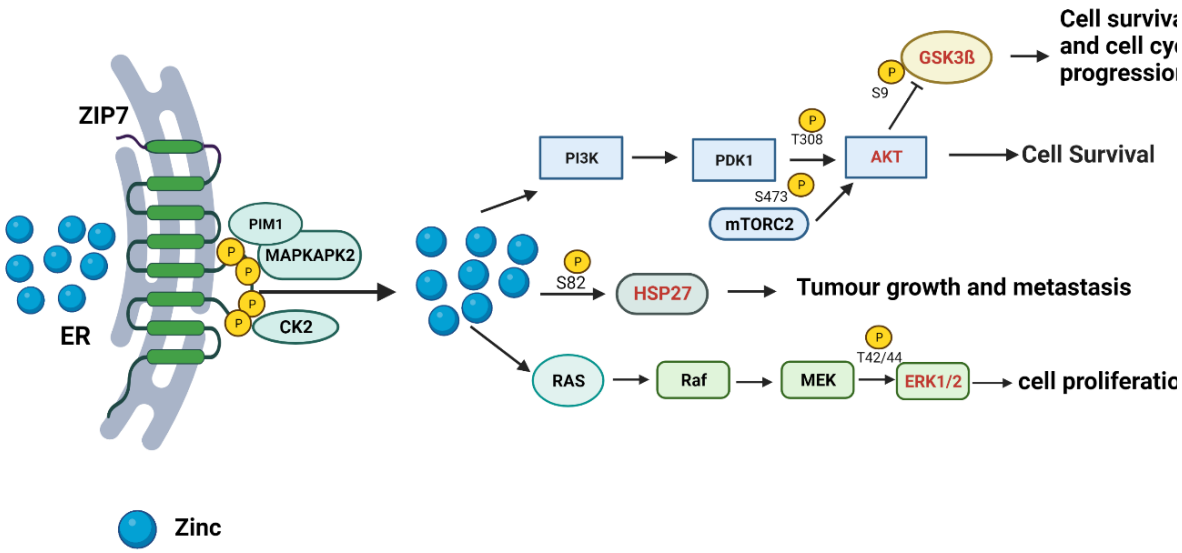

ZIP7 is activated by CK2 at S275/S276, MAPKAPK2 at S293 and PIM1 at T294 phosphorylation in the long intracellular loop between TM3 and TM4. This phosphorylation of ZIP7 triggers the release of zinc from the ER into the cytosol, which in turn activates several downstream signalling pathways known to play a part in the development of cancer. Key kinases that are activated by the zinc release mediated by ZIP7 are indicated in red colour.

6.3 The essential role of ZIP6 and ZIP10 N-termini in regulating their functional activity

ZIP6 and ZIP10, two close homologues within the LIV-1 subfamily, are zinc transporters that have been independently implicated in various types of cancer including breast cancer (Jones et al., 2022). ZIP6 and ZIP10 have been found to be associated with aggressive breast cancer and its spread to the lymph nodes (Takatani-Nakase et al., 2022)(Saravanan et al., 2022). Their implications in cancer metastasis are supported by the fact that both zinc transporters have separately been known to initiate cell rounding and detachment, leading to the epithelial mesenchymal transition (EMT) process (Hogstrand et al., 2013)(Taylor et al., 2016). ZIP6 and ZIP10 have been shown to undergo N-terminal cleavage, which suggests an integral aspect of their functional activity. Once on the plasma membrane, ZIP6 and ZIP10 can transport zinc and induce their activity (Nimmanon et al., 2020), highlighting the important role of the N-terminus in regulating their localisation and activity.

In this present study, the potential phosphorylation sites in ZIP6 and ZIP10 were initially identified, and the kinases predicted to phosphorylate these sites were also determined. Moreover, the role of the N-terminus in ZIP6 and ZIP10 was investigated by employing novel constructs that contain modified N-termini compared with their respective transporters.

6.3.1 The identification of phosphorylation site with kinase prediction for ZIP6

In ZIP6, the analysis of phosphorylation sites recognised multiple potential serine and tyrosine sites on the long cytoplasmic loop between TM3 and TM4 (**Figure 6.3**). It is noteworthy that several residues, each having only one record citing mass spectrometry data, were excluded as they may be false ‘hits’. Therefore, the analysis resulted in the selection of five residues with the highest number of predictions according to PhosphoSite Plus (Hornbeck et al., 2015) (**Table 3.2**). Among the residues identified was serine 471 (3 records), which is predicted to be phosphorylated by PKA family of kinases. Interestingly, this family of PKA is known to be upregulated in cases of breast cancer with a poor prognosis and demonstrates a heightened tolerance to anti-estrogen therapy (H. Zhang et al., 2020). Recently, PKA activation was demonstrated to correlate with breast cancer metastasis (Paul et al., 2020). This could suggest that the role of the activated PKA family might be facilitated by ZIP6.

Unexpectedly, the analysis predicted several potential tyrosine phosphorylation sites, previously unexplored in zinc transporters. The potential tyrosine phosphorylation sites were Y528 and Y531, in the ZIP6 sequence, with the highest number of records citing mass spectrometry data (126 and 65 records, respectively). This suggests that phosphorylation could occur at these sites. The Y528 and Y531 residues are predicted to be phosphorylated by the Src family of kinases, a family of kinases associated with cell cycle progression and migration (Parsons and Parsons, 2004). Importantly, tyrosine phosphorylation plays a vital role in cell invasion and metastasis (Benvenuti and Comoglio, 2006), potentially indicating its significance for ZIP6 function. This data could indicate a mechanism of ZIP6 regulation. It is noteworthy that zinc has been found to inhibit tyrosine phosphatases (Bellomo et al., 2014), resulting in an inability to deactivate various tyrosine kinase signalling pathways. Therefore, if ZIP6 is activated by tyrosine phosphorylation, zinc influx due to ZIP6 activation would inhibit tyrosine phosphatases essential for deactivation of ZIP6. This would lead to prolonged ZIP6 activation, resulting in further zinc influx.

This continual cycle of events, in which kinases stimulate zinc signalling activation, reveals how ZIP6 may regulate its own activity. This speculation might also apply to ZIP10, as it has been predicted to have tyrosine phosphorylation sites. This speculation of the presence of zinc can stimulate further zinc intake from extracellular space into the cell is similar to well-established process in cellular biology involving calcium ions (Endo, 2009). In this process, the influx of calcium from outside the cells or from cellular stores can trigger further calcium release, a process known as calcium-induced calcium release (CICR). This occurs when calcium binds to specific receptors - like the ryanodine receptor on the membrane of the endoplasmic or sarcoplasmic reticulum (Endo, 2009). From the time zinc was recognized as a second messenger in cells (Yamasaki et al., 2007) there has been increasing evidence suggesting similarity between the roles of zinc and calcium across various cellular signalling pathways. Along with Src, EGFR has also been predicted to phosphorylate these tyrosine sites. Therefore, it would be intriguing to investigate Src and EGFR in future work by using kinase inhibitor or perhaps a recombinant phospho-ablative mutant.

Figure 6.3 Prediction of phosphorylation sites in ZIP6

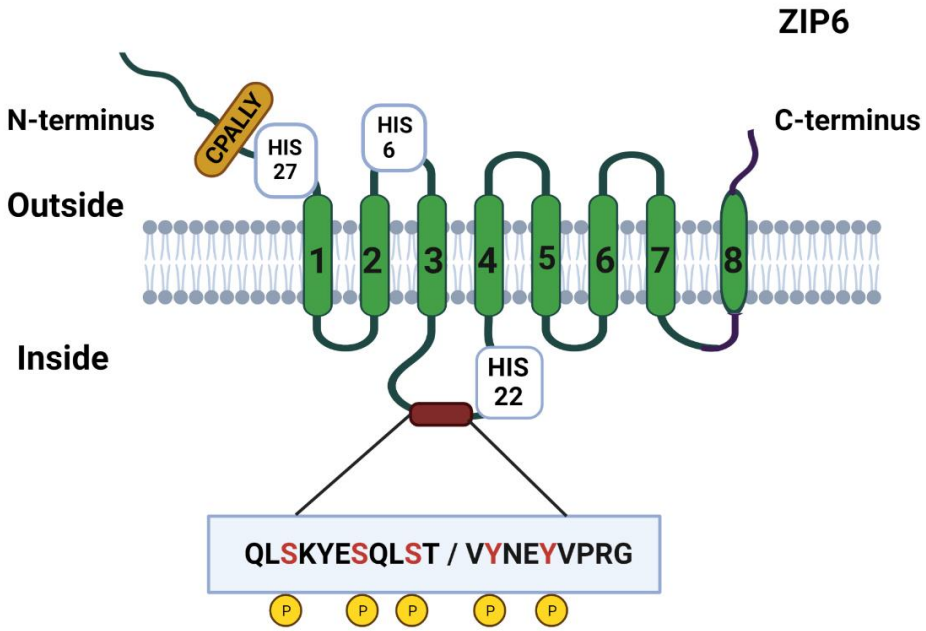

This schematic demonstrates the predicted phosphorylation sites in the ZIP6 transporter. The red colour represents only the serine 471,475 and 478, and tyrosine 528 and 531 residues, all of which are highlighted in this section and have a high probability of undergoing phosphorylation. Each residue that has only one record citing mass spectrometry data was excluded, as they may represent false hits. Predicted phosphorylation residues on the loop between TM3 and TM4 of ZIP6 were obtained by using Kinexus, NetPhos-3.1 and PHOSIDA (Gnad et al., 2007).

6.3.2 The identification of phosphorylation site with kinase prediction for ZIP10

10 potential phosphorylation sites were identified in ZIP10 between TM3 and TM4 in the long cytoplasmic loop (**Figure 6.4**). Intriguingly, several kinases known for their role in mitosis and cell migration, such as PLK1, PIM and CDK1, were predicted to phosphorylate ZIP10. This finding is interesting as it aligns with prior studies indicating a dual function for ZIP10: as a homodimer, it stimulates cell migration (Taylor et al., 2016), while forming a heterodimer with ZIP6 it initiates mitosis (Nimmanon et al., 2020). For instance, PLK1 has been found to be associated with several cancers, such as colorectal, renal and breast cancer (Fu and Wen, 2017). Additionally, PLK1 has shown direct involvement in tumour progression, as its overexpression has been observed to be associated with increased motility and invasiveness in prostate cancer (Wu et al., 2016). Therefore, the regulation of these different processes might potentially involve the phosphorylation of ZIP10 by different kinases.

Moreover, the prediction of phosphorylation of ZIP10 on two neighbouring residues, namely S539 and T540, mirrors the observations seen in ZIP7 at S275 and S276 sites as well as in ZIP6 at the S478 and T479 sites. This is further evidence of the shared characteristics among ZIP7, ZIP6, and ZIP10, zinc transporters that are extensively investigated due to their links with cancer. In addition, similar to ZIP7 and ZIP6, CK2 was predicted to phosphorylate ZIP10 at multiple sites. This is important due to the vital role of CK2 in promoting cell survival (Trembley et al., 2010) and its overexpression in breast cancer (Zaman et al., 2019). Zinc also promotes cell survival (MacDonald, 2000), and maybe this major role of zinc is manifested by CK2. Conversely, CK2 is known to drive cell survival and maybe it does this be activating ZIP7 to release zinc. This was supported by the observations made when using a CK2 inhibitor to prevent the association of CK2 with ZIP7, subsequently affecting the signalling pathways of ZIP7-mediated zinc release (Taylor et al., 2012). Indeed, inhibition of CK2 has been also demonstrated to induce cell death in a breast cancer cell line that is resistant to antiestrogens (Yde et al., 2007). This suggests that the CK2 inhibitor would potentially be beneficial as a cancer therapeutic, and its mechanism of action might be through the inhibition of signalling pathways in these zinc transporters.

Figure 6.4 Prediction of phosphorylation sites in ZIP10

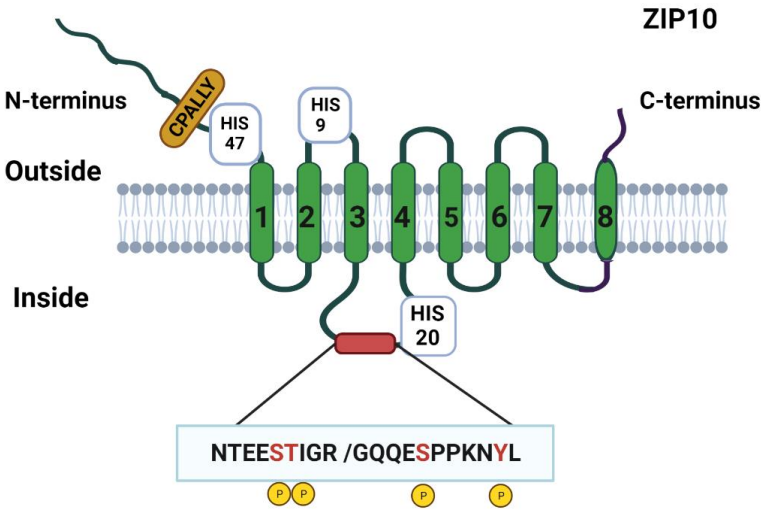

This schematic demonstrates the predicted phosphorylation sites in the ZIP10 transporter. The red colour represents the serine 539, threonine 540, serine 591 and tyrosine 596 residues, all of which are highlighted in this section and have a high probability of undergoing phosphorylation. However, additional predicted phosphorylation sites are indicated in Table 3.2. Predicted phosphorylation residues on the loop between TM3 and TM4 of ZIP10 were obtained by using Kinexus, NetPhos-3.1 and PHOSIDA (Gnad et al., 2007).

6.3.3 Modification of the N-terminus alters the localisation of ZIP6 and ZIP10 transporters

The behaviour of ZIP6 and ZIP10 transporters has consistently differed from other transporters within the LIV-1 subfamily, particularly because both transporters play a vital role in promoting migration via cell rounding and detachment (Taylor et al., 2016). Therefore, exogenous expression of ZIP6 and ZIP10 in cells usually results in very few numbers of cells expressing the recombinant protein, due to the cells having detached from the dish before harvesting. Interestingly, the present study found that modifying the N-terminus of ZIP6 and ZIP10 produced efficiently transfected cells, suggesting that this modification prevents the cells from detaching. This is further supported by white-light images showing that cells transfected with ZIP7/ZIP6 and ZIP7/ZIP10 constructs remained adherent, in contrast to the cells transfected with WT ZIP6 and WT ZIP10, which appeared to be detached. What was surprising is that the localisation of these constructs has been observed on the endoplasmic reticulum, confirming that the change of the N-terminus prevents the ZIP6 and ZIP10 transporters from relocating to the plasma membrane.

Moreover, western blot results showed non-cleaved bands for chimera constructs, as the estimated bands for full-length size were comparable to the observed ones. ZIP6 and ZIP10 contain a highly predicted PEST site at their N-terminus (**Figure 3.6**). The PEST cleavage site is an amino acid sequence associated with having a short half-life (Rogers et al., 1986). This correlates with the observation of an inability to identify the far N-terminal region of ZIP6 at the plasma membrane, even though it was detectable in the ER (Hogstrand et al., 2013). The relevance of this cleavage has been suggested as a requirement for ZIP6 to relocate to the plasma membrane and initiate cell rounding and detachment. Similarly, ZIP10 was shown to be cleaved at its N-terminus as validated by different band sizes analysed by western blotting (Ehsani et al., 2012). However, the role of this cleavage has still been uncertain for ZIP10. The role of N-terminal cleavage in transporter regulation has also been observed in ZIP4 (Kambe and Andrews, 2009). This transporter, located in the plasma membrane and upregulated during zinc deficiency, has been reported to undergo proteolytic cleavage at its N-terminus. During periods of zinc deficiency, only the transmembrane domains are identifiable on the plasma membrane (Cui et al., 2014)(Zhang et al., 2019), indicating that N-terminal cleavage is a response to zinc availability.

However, this cleavage does not result in the relocation of the ZIP4 transporter. Furthermore, a transporter can be relocated in response to metal availability without being cleaved. For instance, the copper uptake transporter (CTR1), which is located in the plasma membrane, has been reported to be internalized in response to elevated extracellular copper levels to reduce the rate of copper entry (Molloy and Kaplan, 2009). This internalization serves to protect against copper toxicity. Once extracellular copper returns to normal levels, the CTR1 transporter is relocated to the plasma membrane (Clifford et al., 2016). Interestingly, the findings of this study confirmed that modification of the N-terminus prevents ZIP6 and ZIP10 from being cleaved and relocated to the plasma membrane. Thus, the necessity for cleavage to enable relocation to the plasma membrane appears to be a unique mechanism for ZIP6 and ZIP10 transporters. These confirm the role of the N-terminus in regulating localisation of ZIP6 and ZIP10 and the impact of that on their function.

6.3.4 Modifying the N-terminus of ZIP6 or ZIP10 reduced the activation of PLK1 and STAT3

The ability of ZIP6 and ZIP10 to promote cell migration of breast cancer cells was associated with a rise in the number of detached cells. These cells, enriched with either ZIP6 or ZIP10, remained alive and proliferating, indicating a resistance to anoikis (Hogstrand et al., 2013) (Taylor et al., 2016). Human polo-like kinase 1 (PLK1), a highly conserved serine/threonine kinase, has been noted to be upregulated in various solid tumours including prostate cancer (Weichert et al., 2004), ovarian cancer (Takai et al., 2001) and breast cancer (Wolff et al., 2000). PLK1 overexpression has been associated with its anti-apoptotic function and contribution to cell survival and proliferation (Takai et al., 2005) (Zhang et al., 2012). Its activation has been demonstrated during cell detachment and resistance to anoikis in cancer cells (Lin et al., 2011). PLK1 is also recognized as indispensable for activating the complex between cyclin B and CDK1, a crucial step needed for the initiation of mitosis (Winkles and Alberts, 2005). Interestingly, the present study found that modification of the N-terminus in ZIP6 and ZIP10 led to a significant reduction in PLK1 activation compared to the WT transporters. This finding suggests a critical role for this region in ZIP6 and ZIP10 in promoting cell detachment, leading to resistance to anoikis. In esophageal squamous cell carcinoma (ESCC), detachment of cells has been observed to trigger the upregulation of PLK1 (Lin et al., 2011).

In contrast, the depletion or inhibition of PLK1 restored the sensitivity of cells to anoikis (Liu and Erikson, 2003) (Lin et al., 2011). It seems possible that this association between PLK1 and cell detachment leading to resistance to anoikis might be regulated by ZIP6 and ZIP10-mediated zinc influx. This is supported by the fact that cell detachment triggered by ZIP6 and ZIP10 have been observed viable and actively proliferating (Hogstrand et al., 2013)(Taylor et al., 2016). Moreover, PLK1 was predicted to phosphorylate ZIP10 (**Table 3.2)**. However, further investigation is required to determine whether this phosphorylation is necessary for ZIP10 activation, zinc transport, and the subsequent initiation of cell detachment. Collectively, these findings confirm the critical role of N-terminus in regulating cell detachment and anoikis resistance through upregulation of PLK1.

Despite this being the first evidence for the implication of zinc transporters in PLK activation, there is an increasing number of studies demonstrating that overexpression of PLK1 causes cells to acquire mesenchymal features from epithelial cells, a process known as EMT (Wu et al., 2016) (Ferrarotto et al., 2016) (Fu and Wen, 2017). EMT is a crucial mechanism of tumour progression and metastasis, and enables cancer cells to avoid anoikis (Tiwari et al., 2012). Indeed, there are other molecules, such as STAT3, that the regulate EMT process particularly in breast cancer cells (Li and Huang, 2017) (Kim et al., 2019). These findings suggest that PLK1 and STAT3 are important for the EMT process, as reciprocal activation contributing to cell survival has been observed (Zhang et al., 2012). Notably, ZIP6 and ZIP10 transporters have been demonstrated to control EMT during gastrulation in zebrafish (Yamashita et al., 2004) and in cancer cells through the activation of STAT3 (Hogstrand et al., 2013) (Taylor et al., 2016).

Remarkably, the current study found that the modifying of the N-terminus in ZIP6 and ZIP10 led to the downregulation of STAT3. These results suggest that this aspect of the transporters plays a crucial role in their ability to regulate the EMT process. These results match those observed in an earlier study showing the role of the N-terminus of prions in the mechanism of cell adhesion and detachment, which leads to EMT by binding to NCAM1 (Brethour et al., 2017).

The prion protein was discovered to have evolved from the LIV-1 subfamily of ZIP transporters and as such the N-terminus bears a close resemblance to both ZIP6 and ZIP10 (Schmitt-Ulms et al., 2009). Interestingly, the prion protein was also observed to undergo N-terminus proteolytic cleavage under zinc-deficient conditions in order to transport zinc into cells, similar to that shown for ZIP6 and ZIP10 (Ehsani et al., 2012). Given that the shape of the N-terminus of ZIP6 and ZIP10 resembles prions, the N-terminus of ZIP6 and ZIP10 can also bind to NCAM1, facilitating the influx of zinc to initiate cell detachment and EMT. Taken together, these findings confirm the importance of the N-terminus in ZIP6 and ZIP10 for their functional roles.

6.3.5 Modification of N-terminus diminished the effect of ZIP6 and ZIP10 in cell migration

ZIP6 and ZIP10 have been associated with invasive breast cancer and its metastasis to lymph nodes (Kagara et al., 2007a) (Grattan and Freake, 2012). These transporters have been shown to be involved in the EMT process, a STAT3-dependent mechanism. The influx of zinc through ZIP6 and ZIP10 results in inhibition of GSK-3β (either directly or indirectly via the stimulation of AKT) leading to the nuclear translocation of Snail. Snail, which is a transcription factor, diminishes the production of the adhesion molecule E-cadherin, leading to the EMT process (Tiwari et al., 2012) (Hogstrand et al., 2013).

Interestingly, in cells transfected with chimera constructs where the N-termini of ZIP6 and ZIP10 were modified, GSK-3ß was not phosphorylated compared with the action of WT ZIP6 and ZIP10. This finding suggests that this region in ZIP6 and ZIP10 transporters is required for zinc transport. Moreover, Pyk2, a non-receptor tyrosine kinase, was also downregulated in the chimera constructs compared to the respective transporters. Notably, Pyk2 regulates multiple signalling pathways that control cell growth, survival and migration (Sun et al., 2008) and plays a functional role in the EMT process in human mammary cells (Verma et al., 2015).

Both the inactivation of GSK-3ß and the upregulation of Pyk2 are involved in EMT, a crucial mechanism of tumour metastasis (Li and Huang, 2017) (Verma et al., 2015). These kinases might be implicated in EMT due to the zinc influx mediated by ZIP6 and ZIP10. Both transporters need to be N-terminally cleaved before and after relocating to the plasma membrane.

Once on the plasma membrane, influxed zinc may bind to the juxtamembrane region in ZIP6 and ZIP10, due to the abundance of histidine residues in that area. Given that ZIP6 and ZIP10 have an abundance of histidine residues compared to other LIV-1 subfamily (Kambe et al., 2021), this zinc binding might inhibit GSK-3β and activate Pyk2, resulting in cell detachment and the EMT process. This process was inhibited when the N-terminus was modified, indicating the critical role for this region in ZIP6 and ZIP10 functionality. Understanding this mechanism for ZIP transporters suggests that the N-terminus region could be a novel target for mitigating cancer migration in therapy.

6.3.6 Response of HSP60 protein to the intracellular zinc

The location of zinc transporters appears to be crucial in defining their function. For instance, ZIP7 is located in the endoplasmic reticulum and is responsible for releasing zinc from this compartment into the cytoplasm after being phosphorylated (Taylor et al., 2012). The released zinc then activates signalling pathways linked to cell growth and proliferation (Nimmanon et al., 2017). Conversely, when ZIP6 and ZIP10 become activated, they relocate to the plasma membrane, allowing zinc to influx and mediate the EMT process (Taylor et al., 2016) or mitoses (Nimmanon et al., 2020).

In the present study, WT of ZIP7, ZIP6 and ZIP10, as well as chimeric constructs, were investigated with several protein kinases. Interestingly, upregulation of HSP60 was only noticed in WT ZIP7. This was a fascinating finding since HSP60 is a heat shock protein that responds to stressful conditions and assists in the proper folding of proteins (Cappello et al., 2008). Its upregulation has been linked to several diseases including cancer (Lianos et al., 2015). Thus, the unique location of ZIP7 on the ER allows it to release zinc from this compartment after being phosphorylated. Therefore, the exclusive upregulation of HSP60 observed in WT ZIP7 might be due to endoplasmic reticulum stress as a result of zinc depletion from the ER.

ZIP7 has been associated with ER stress events in two distinct ways. Firstly, the elimination of ZIP7 in human cells leads to significantly reduced levels of zinc in the cytoplasm, impaired cell proliferation, and activation of ER stress (Woodruff et al., 2018). In contrast, in hyperglycemic cardiomyocytes a substantial redistribution of cellular zinc was noted, characterized by an elevation in cytosolic zinc and a corresponding decrease in ER zinc. This depended on the phosphorylation of ZIP7 (Tuncay et al., 2017).

This is an interesting finding because the chimera constructs were also observed to be located in the ER, and no upregulation of HSP60 was noticed. This suggests that, without phosphorylation, these constructs could not functionally transport zinc.

Given that the ER contains a relatively high concentration of zinc (Chabosseau et al., 2014), and ZIP7 serves as an essential 'gate-keeper' for zinc release from the ER and is responsible for zinc homeostasis (Taylor et al., 2012b), these findings suggest that ZIP7 is essential for endoplasmic reticulum function. It also emphasises the importance of post-translational modifications in determining the location and activity of zinc transporters.

In conclusion, this section focused on the role of the N-terminus of ZIP6 and ZIP10 in cancer progression, particularly in breast cancer. These transporters have been associated with invasive breast cancer and its metastasis to lymph nodes. They have been shown to facilitate a process called epithelial mesenchymal transition (EMT), which is critical for cancer metastasis (**Figure 6.5**). This thesis demonstrates for the first time that the N-terminal region of these transporters is essential for their localization and function within cells.

Chimera constructs were created in which the N-termini of ZIP6 and ZIP10 were modified. This modification prevented the transporters from relocating to the plasma membrane and initiating cell detachment, a first step in EMT (**Figure 6.5**). They were instead localized in the endoplasmic reticulum, a change that effectively impeded their functional activity. These results confirm the role of the N-terminus in regulating the localization and function of ZIP6 and ZIP10 transporters.

In these constructs, the modification also resulted in reduced cell migration, suggesting the importance of this region in zinc transport and the regulation of the EMT process. Understanding the functional mechanism of the N-terminal cleavage in ZIP transporters could offer new therapeutic strategies for mitigating cancer metastasis.

Figure 6.5 Modification of N-terminus diminishes the activation effect of ZIP6 and ZIP10

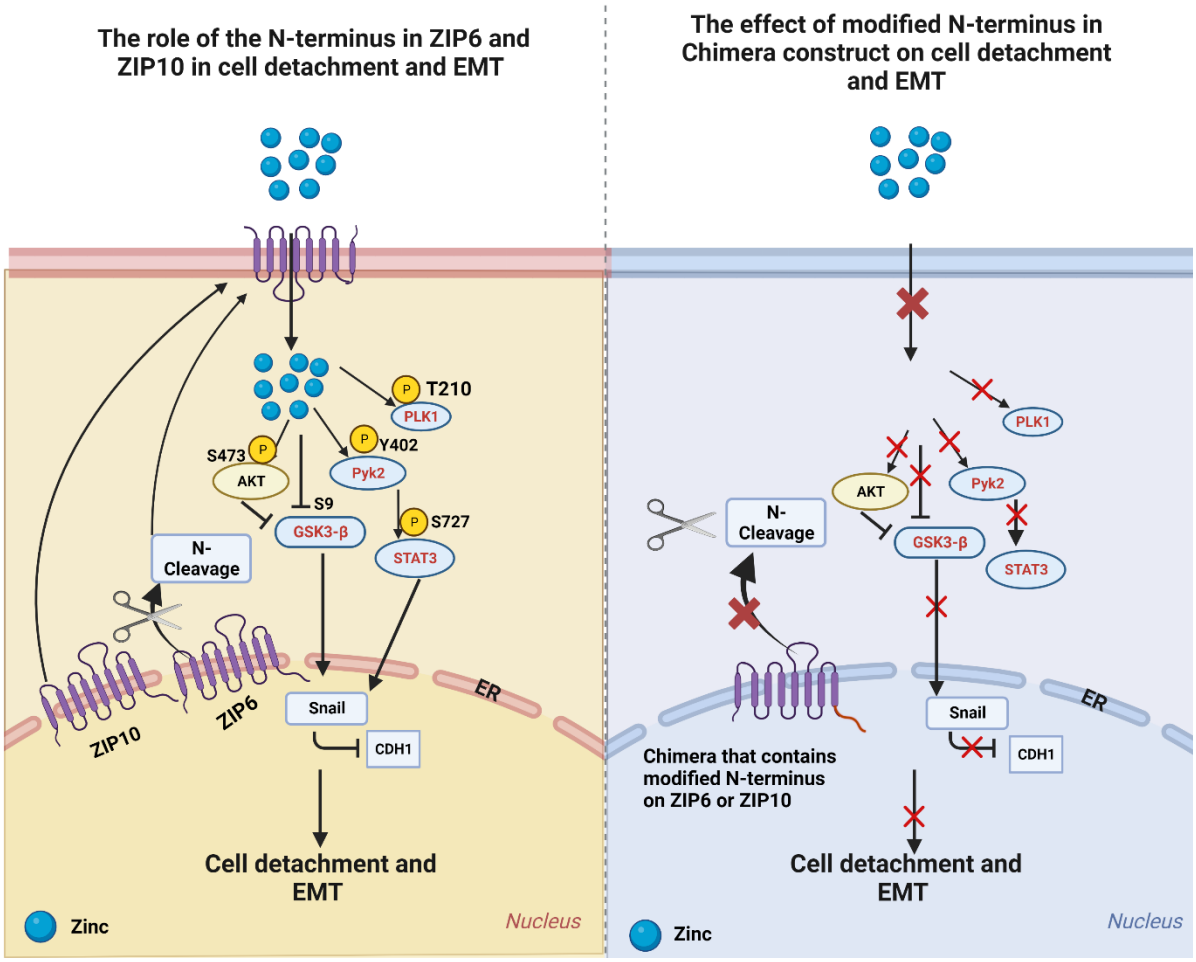

ZIP6 and ZIP10 are initially produced as a pro-protein within the endoplasmic reticulum, where it undergoes proteolytic cleavage before and being relocated to the plasma membrane. The transport of zinc triggered by ZIP6 and ZIP10 can lead to the suppression of GSK-3ß, either through a direct mechanism or through the activation of AKT, which is also activated by zinc. This suppression of GSK-3ß causes Snail to remain in the nucleus, where it serves to repress E-cadherin, consequently leading to cell detachment and EMT. This mechanism is inhibited when the N-terminus in ZIP6 or ZIP10 is modified, as demonstrated in the right diagram.

6.4 The effect of ubiquitination on ZIP6 function

Ubiquitination is a post-translational modification of proteins that plays a vital role in maintaining normal homeostasis and contributing to diseases (Kona et al., 2013). The process of ubiquitination involves the covalent attachment of ubiquitin (Ub) to lysine residues of a target protein, recognising target proteins for proteasome degradation (**Figure 1.10**) (Mansour, 2018)(Sun et al., 2020).

The formation of a Ub conjugate needs the presence of three enzymes: an E1 ubiquitin-activating enzyme, an E2 ubiquitin-conjugating enzyme, and an E3 ubiquitin ligase (Sun et al., 2020). The result of this reaction is the attachment of a single molecule of ubiquitin to a target protein, referred to as monoubiquitination. Further attachment of multiple ubiquitin molecules makes ubiquitin chains, referred to as polyubiquitination. This polyubiquitination then triggers the degradation of the target protein by serving as a signal for recognition by the 26S proteasome (Yao and Cohen, 2002)(Song and Rape, 2008). This process is extremely controlled, with the ability to have significant impacts on various cellular pathways during both cell survival and death (Yao and Cohen, 2002).

Similar to other post-translational modifications, the ubiquitination process can be reversed by the deubiquitinating enzyme (DUB) family (Song and Rape, 2008). When DUBs fail to remove ubiquitin from proteins that have already interacted with the 26S proteasome, it disrupts the functioning of the proteasome and therefore affects the homeostasis of cells (Sun et al., 2020)(Chen et al., 2022). Therefore, ubiquitination and deubiquitination have been observed to be dysregulated in various types of diseases including cancers (Sun et al., 2020).

In zinc transporters, ZIP6 has been shown to have multiple ubiquitin sites that are linked with the low expression and instability of the protein (Hogstrand et al., 2013). In the present study, the effect of ubiquitination on the regulating of ZIP6 expression and stability, and its impact on ZIP6 function was investigated by employing a novel construct with all ubiquitin sites changed to alanine in order to prevent ubiquitination.

6.4.1 The role of ubiquitination in regulating ZIP6 expression

Typically, exogenous expression of ZIP6 in cells results in very few cells expressing the recombinant protein (Hogstrand et al., 2013). The short half-life is due to the ability of ZIP6 to be degraded once the transporter is no longer useful. Interestingly, in the present study, inhibiting ubiquitination sites resulted in an increased presence of ZIP6 protein, as determined by the efficiency of transfected cells compared to WT ZIP6. This observation confirms the role of ubiquitination in ZIP6 degradation.

In mineral transportation, ubiquitination acts as a key mechanism, enabling trace elements to adapt to their environment for homeostatic iron transport regulation. ZIP14, while primarily known as a zinc transporter (Lichten and Cousins, 2009), is also identified as an iron transporter (Nam et al., 2013). In cases of iron deficiency, ZIP14 is observed to be ubiquitinated and degraded, with its levels increasing in response to iron supplementation (Hennigar and McClung, 2016). This elucidates how iron is redirected from storage tissues during iron deficiency, thus enhancing the accessibility of iron for its required functions. Given that ZIP6 is highly regulated by the cell, its short half-life could be attributed to degradation via ubiquitination when cellular conditions are not conducive to migration or mitosis. This explains why endogenous ZIP6 was induced by mitotic agents such as nocodazole (Nimmanon et al., 2020), making ZIP6 easier to identify in laboratory culture. Therefore, the present findings suggest that the deubiquitinated ZIP6 mutant could be employed as a novel construct to investigate ZIP6 function due to its prolonged expression.

6.4.2 The impact of ubiquitin sites in sustaining ZIP6 activation

Inhibiting the ubiquitin sites in ZIP6 resulted in extended expression of the transporter. Interestingly, the inhibition of ubiquitination, which increased the instability of ZIP6, also affected its function. PLK1 and STAT3 have been shown to be involved in cell migration and the EMT process (Lin et al., 2011)(Li and Huang, 2017). In the present study, the activation of these kinases was significantly upregulated in the construct where ubiquitin was inhibited, compared with WT ZIP6. Here, it has been demonstrated that when ZIP6 degradation was inhibited, an increased amount of ZIP6 was observed. This excess ZIP6 allowed for increased zinc influx, leading to sustained activation of EMT markers. These observations confirm that the inhibition of ubiquitination could lead to sustained ZIP6 activation.

The function of ZIP transporters can be highly regulated in cells. For instance, ZIP4 is required for enterocytes to import zinc from the diet (Dufner-Beattie et al., 2003). ZIP4 has been found to be degraded through ubiquitination at higher levels of zinc concentrations, which results in a decrease in the uptake of zinc mediated by ZIP4 (Mao et al., 2007). Therefore, this mechanism regulates the influx of zinc into the cell and failure of ubiquitination can lead to zinc dyshomeostasis.

In the case of ZIP6, observations from this study suggest that if ZIP6 were ubiquitinated, it would control the levels of ZIP6 in the cell and, consequently, the amount of zinc transported into the cell. In contrast, when ubiquitination of ZIP6 is inhibited, this might prevent degradation of ZIP6, potentially leading to its overaccumulation or recycling back to the plasma membrane, and potentially sustaining the function of ZIP6. This hypothesis is supported by the significant upregulation of STAT3 and PLK1 kinases linked to cancer metastasis observed in the construct where ubiquitination sites were inhibited (**Figure 6.6**).

There are other examples of the role of ubiquitination altering cell properties to encourage cancer. Previous studies have demonstrated that when Snail fails to be degraded by ubiquitination, it drives tumorigenesis and cancer metastasis through EMT (Wu et al., 2009)(Thompson et al., 2021). Snail, a transcriptional repressor of E-cadherin, is normally ubiquitinated and targeted for degradation by the ubiquitin protein complex known as $SCF^{\beta TrCP}$ (Becker et al., 2007). Inhibiting the interaction between Snail and $SCF^{\beta TrCP}$ prevents its degradation and increases Snail levels, thereby repressing E-cadherin expression and driving EMT, a crucial process for cellular migration and cancer metastasis (Thompson et al., 2021).

Interestingly, the inhibition of GSK-3ß has also been reported to inhibit Snail degradation as a result of zinc influx mediated by ZIP6 (Hogstrand et al., 2013). The association between Snail and GSK-3ß could be explained by ZIP6 hyperactivity resulting in increased zinc influx. This, in turn, leads to the GSK-3β inhibition/Snail activation/E-cadherin loss pathway, driving EMT and cell migration.

In conclusion, this study has demonstrated for the first time the effect of ubiquitin sites on ZIP6 expression and function. This discovery revealed how the ubiquitin sites are essential for 'turning off' ZIP6. Therefore, these findings suggest that targeting the ubiquitin pathway—by enhancing ubiquitination which targets ZIP6 for degradation—could serve as a novel strategy for ZIP6 intervention.

Figure 6.6 The impact of ubiquitin sites in sustaining ZIP6 activation

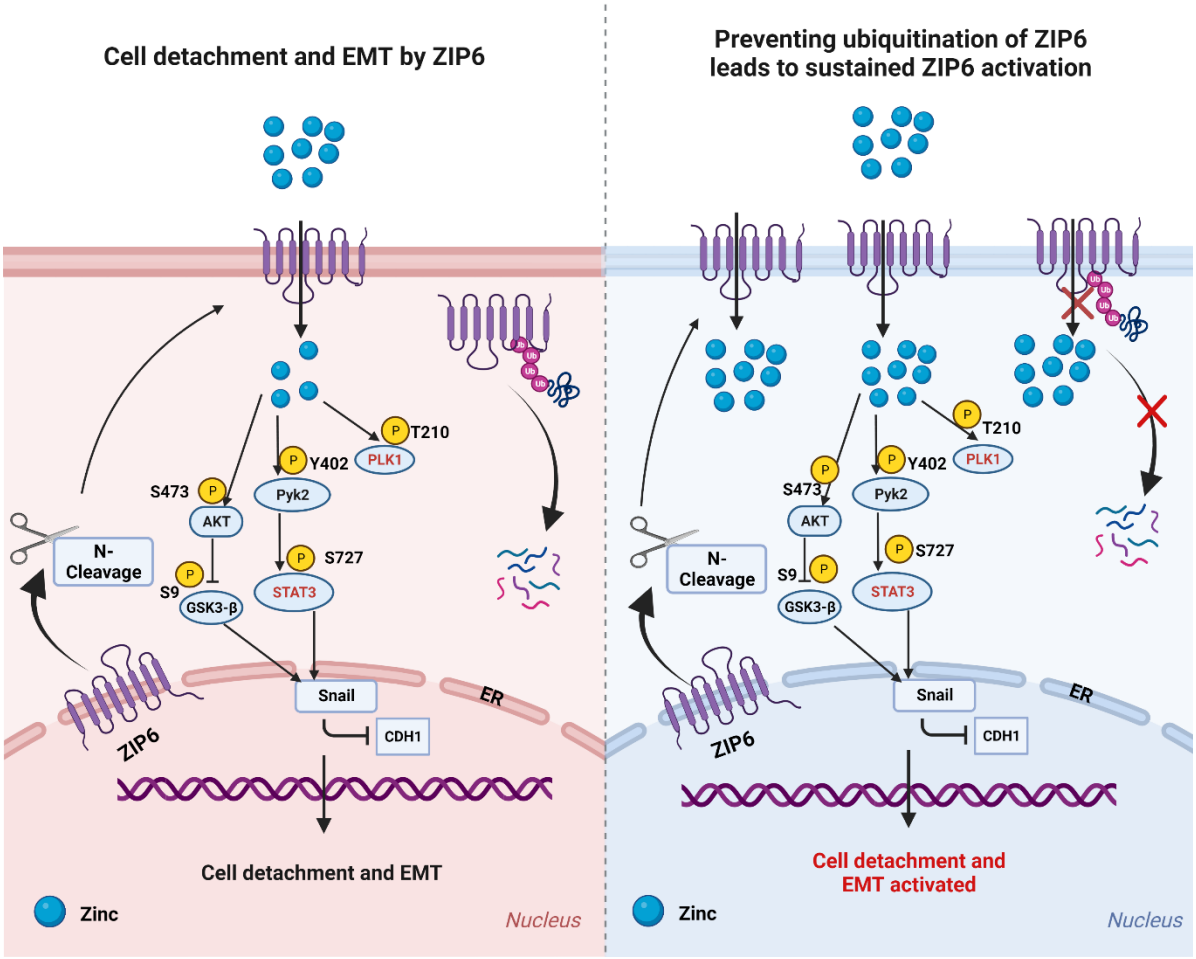

This schematic demonstrates the activation of ZIP6, leading to an influx of zinc and the activation of several markers related to cell detachment and the EMT process. ZIP6 is then subjected to ubiquitination and degradation, as shown in the left diagram. When ZIP6 degradation is inhibited, an increased amount of ZIP6 is observed. This excess ZIP6 allows for increased zinc influx, leading to sustained activation of EMT markers as shown in the right diagram.

6.5 Future work

The current study has unveiled novel phosphorylation sites indispensable for achieving the maximal activation of ZIP7. Furthermore, it was revealed that the N-terminal cleavage of ZIP6 and ZIP10 is critical for activating these transporters. Notably, this study also demonstrated that ZIP6 undergoes degradation through ubiquitination. Despite these significant discoveries, further work is necessary to fully understand the functional implications of these findings.

For ZIP7, the intracellular zinc concentration in cells transfected with a novel 4A construct needs to be measured and compared with the wild type. This can be accomplished using a selective indicator with a high affinity for zinc binding, such as FluoZin™-3.

For ZIP6 and ZIP10, several predicted tyrosine phosphorylation sites have been cited frequently in mass spectrometry data. No one has shown that ZIP transporters are phosphorylated on a tyrosine, yet they are known to activate Src, EGFR and other well-known tyrosine kinases which are also known to be activated by zinc. Therefore, these sites are required to be experimentally investigated.

Moreover, given the similarity between these transporters and the prion protein, it is worth noting that early research found presenilin plays a role in the transcription process of the cellular prion protein (Vincent et al., 2009). It would be interesting to use a presenilin inhibitor to disrupt the N-terminal cleavage of ZIP6 and ZIP10 to decipher whether presenilin is involved in the N-terminal cleavage.

Finally, to determine the impact of endogenous ZIP6 and ZIP10 interacting with chimera constructs, it would be beneficial to use cell lines that lack ZIP6, such as NMuMG ZIP6, and compare them with MCF-7.

Chapter 7

References

Adulcikas, J., Norouzi, S., Bretag, L., Sohal, S.S., Myers, S., 2018. The zinc transporter SLC39A7 (ZIP7) harbours a highly-conserved histidine-rich N-terminal region that potentially contributes to zinc homeostasis in the endoplasmic reticulum. Comput. Biol. Med. 100, 196–202. https://doi.org/10.1016/j.compbiomed.2018.07.007

Adulcikas, J., Sonda, S., Norouzi, S., Sohal, S.S., Myers, S., 2019. Targeting the zinc transporter ZIP7 in the treatment of insulin resistance and type 2 diabetes. Nutrients 11. https://doi.org/10.3390/nu11020408

Andreini, C., Bertini, I., 2012. A bioinformatics view of zinc enzymes. J. Inorg. Biochem. 111, 150–156. https://doi.org/10.1016/j.jinorgbio.2011.11.020

Ardito, F., Giuliani, M., Perrone, D., Troiano, G., Muzio, L. Lo, 2017. The crucial role of protein phosphorylation in cell signalingand its use as targeted therapy (Review). Int. J. Mol. Med. 40, 271–280. https://doi.org/10.3892/ijmm.2017.3036

Artimo, P., Jonnalagedda, M., Arnold, K., Baratin, D., Csardi, G., De Castro, E., Duvaud, S., Flegel, V., Fortier, A., Gasteiger, E., Grosdidier, A., Hernandez, C., Ioannidis, V., Kuznetsov, D., Liechti, R., Moretti, S., Mostaguir, K., Redaschi, N., Rossier, G., Xenarios, I., Stockinger, H., 2012. ExPASy: SIB bioinformatics resource portal. Nucleic Acids Res. 40, 597–603. https://doi.org/10.1093/nar/gks400

Avalle, L., Camporeale, A., Camperi, A., Poli, V., 2017. STAT3 in cancer: A double edged sword. Cytokine 98, 42–50. https://doi.org/10.1016/j.cyto.2017.03.018

Bafaro, E., Liu, Y., Xu, Y., Dempski, R.E., 2017. The emerging role of zinc transporters in cellular homeostasis and cancer. Signal Transduct. Target. Ther. 2, 1–12. https://doi.org/10.1038/sigtrans.2017.29

Bafaro, E.M., Antala, S., Nguyen, T.V., Dzul, S.P., Doyon, B., Stemmler, T.L., Dempski, R.E., 2015. The large intracellular loop of hZIP4 is an intrinsically disordered zinc binding domain. Metallomics 7, 1319–1330. https://doi.org/10.1039/c5mt00066a

Barnett, J.P., Blindauer, C.A., Kassaar, O., Khazaipoul, S., Martin, E.M., Sadler, P.J., Stewart, A.J., 2013. Allosteric modulation of zinc speciation by fatty acids. Biochim. Biophys. Acta - Gen. Subj. 1830, 5456–5464. https://doi.org/10.1016/j.bbagen.2013.05.028

Becker, K.F., Rosivatz, E., Blechschmidt, K., Kremmer, E., Sarbia, M., Höfler, H., 2007. Analysis of the E-cadherin repressor snail in primary human cancers. Cells Tissues Organs 185, 204–212. https://doi.org/10.1159/000101321

Bellomo, E., Massarotti, A., Hogstrand, C., Maret, W., 2014. Zinc ions modulate protein tyrosine phosphatase 1B activity. Metallomics 6, 1229–1239. https://doi.org/10.1039/c4mt00086b

Benvenuti, S., Comoglio, P.M., 2006. The MET Receptor Tyrosine Kinase in Invasion and Metastasis. J. Cell. Physiol. 211(3), 736–747. https://doi.org/10.1002/JCP

Bhullar, K.S., Lagarón, N.O., McGowan, E.M., Parmar, I., Jha, A., Hubbard, B.P., Rupasinghe, H.P.V., 2018. Kinase-targeted cancer therapies: Progress,

challenges and future directions. Mol. Cancer 17, 1–20. https://doi.org/10.1186/s12943-018-0804-2

Bin, B.H., Fukada, T., Hosaka, T., Yamasaki, S., Ohashi, W., Hojyo, S., Miyai, T., Nishida, K., Yokoyama, S., Hirano, T., 2011. Biochemical characterization of human ZIP13 protein: A homo-dimerized zinc transporter involved in the spondylocheiro dysplastic Ehlers-Danlos syndrome. J. Biol. Chem. 286, 40255–40265. https://doi.org/10.1074/jbc.M111.256784

Bitirim, C. V., 2021. The role of zinc transporter proteins as predictive and prognostic biomarkers of hepatocellular cancer. PeerJ 9. https://doi.org/10.7717/peerj.12314

Bjellqvist, B., Hughes, G.J., Pasquali, C., Paquet, N., Ravier, F., Sanchez, J. -C, Frutiger, S., Hochstrasser, D., 1993. The focusing positions of polypeptides in immobilized pH gradients can be predicted from their amino acid sequences. Electrophoresis 14, 1023–1031. https://doi.org/10.1002/elps.11501401163

Booth, W.T., Schlachter, C.R., Pote, S., Ussin, N., Mank, N.J., Klapper, V., Offermann, L.R., Tang, C., Hurlburt, B.K., Chruszcz, M., 2018. Impact of an N-terminal polyhistidine tag on protein thermal stability. ACS Omega 3, 760–768. https://doi.org/10.1021/acsomega.7b01598

Bowers, K., Srai, S.K.S., 2018. The trafficking of metal ion transporters of the Zrt- and Irt-like protein family. Traffic 19, 813–822. https://doi.org/10.1111/tra.12602

Brethour, D., Mehrabian, M., Williams, D., Wang, X., Ghodrati, F., Ehsani, S., Rubie, E.A., Woodgett, J.R., Sevalle, J., Xi, Z., Rogaeva, E., Schmitt-Ulms, G., 2017. A ZIP6-ZIP10 heteromer controls NCAM1 phosphorylation and integration into focal adhesion complexes during epithelial-to-mesenchymal transition. Sci. Rep. 7, 1–19. https://doi.org/10.1038/srep40313

Bulldan, A., Bartsch, J.W., Konrad, L., Scheiner-Bobis, G., 2018. ZIP9 but not the androgen receptor mediates testosterone-induced migratory activity of metastatic prostate cancer cells. Biochim. Biophys. Acta - Mol. Cell Res. 1865, 1857–1868. https://doi.org/10.1016/j.bbamcr.2018.09.004

Cappello, F., De Macario, E.C., Marasà, L., Zummo, G., Macario, A.J.L., 2008. Hsp60 expression, new locations, functions and perspectives for cancer diagnosis and therapy. Cancer Biol. Ther. 7, 801–809. https://doi.org/10.4161/cbt.7.6.6281

Carson, M., Johnson, D.H., McDonald, H., Brouillette, C., DeLucas, L.J., 2007. His-tag impact on structure. Acta Crystallogr. Sect. D Biol. Crystallogr. 63, 295–301. https://doi.org/10.1107/S0907444906052024

Cen, B., Xiong, Y., Song, J.H., Mahajan, S., DuPont, R., McEachern, K., DeAngelo, D.J., Cortes, J.E., Minden, M.D., Ebens, A., Mims, A., LaRue, A.C., Kraft, A.S., 2014. The Pim-1 Protein Kinase Is an Important Regulator of MET Receptor Tyrosine Kinase Levels and Signaling. Mol. Cell. Biol. 34, 2517–2532. https://doi.org/10.1128/mcb.00147-14

Chabosseau, P., Tuncay, E., Meur, G., Bellomo, E.A., Hessels, A., Hughes, S., Johnson, P.R.V., Bugliani, M., Marchetti, P., Turan, B., Lyon, A.R., Merkx, M., Rutter, G.A., 2014. Mitochondrial and ER-targeted eCALWY probes reveal high

levels of free Zn2+. ACS Chem. Biol. 9, 2111–2120. https://doi.org/10.1021/cb5004064

Chang, F., Lee, J.T., Navolanic, P.M., Steelman, L.S., Shelton, J.G., Blalock, W.L., Franklin, R.A., McCubrey, J.A., 2003. Involvement of PI3K/Akt pathway in cell cycle progression, apoptosis, and neoplastic transformation: A target for cancer chemotherapy. Leukemia 17, 590–603. https://doi.org/10.1038/sj.leu.2402824

Chang, M., 2012. Tamoxifen resistance in breast cancer. Biomol. Ther. 20, 256–267. https://doi.org/10.4062/biomolther.2012.20.3.256

Chasapis, C.T., Spiliopoulou, C.A., Loutsidou, A.C., Stefanidou, M.E., 2012. Zinc and human health: An update. Arch. Toxicol. 86, 521–534. https://doi.org/10.1007/s00204-011-0775-1

Chen, J., Tang, G., 2019. PIM-1 kinase: A potential biomarker of triple-negative breast cancer. Onco. Targets. Ther. 12, 6267–6273. https://doi.org/10.2147/OTT.S212752

Chen, L., Kashina, A., 2021. Post-translational Modifications of the Protein Termini. Front. Cell Dev. Biol. 9, 1–14. https://doi.org/10.3389/fcell.2021.719590

Chen, L.S., Redkar, S., Taverna, P., Cortes, J.E., Gandhi, V., 2011. Mechanisms of cytotoxicity to Pim kinase inhibitor, SGI-1776, in acute myeloid leukemia. Blood 118, 693–702. https://doi.org/10.1182/blood-2010-12-323022

Chen, Z., Bullock, A.N., Es, R., Ring, E., 2022. Ubiquitin ligases: guardians of mammalian development 0123456789. https://doi.org/10.1038/s41580-021-00448-5

Cheng, X., Wang, J., Liu, C., Jiang, T., Yang, N., Liu, D., Zhao, H., Xu, Z., 2021. Zinc transporter SLC39A13/ZIP13 facilitates the metastasis of human ovarian cancer cells via activating Src/FAK signaling pathway. J. Exp. Clin. Cancer Res. 40, 1–15. https://doi.org/10.1186/s13046-021-01999-3

Chimienti, F., Seve, M., Richard, S., Mathieu, J., Favier, A., 2001. Role of cellular zinc in programmed cell death: Temporal relationship between zinc depletion, activation of caspases, and cleavage of Sp family transcription factors. Biochem. Pharmacol. 62, 51–62. https://doi.org/10.1016/S0006-2952(01)00624-4

Clifford, R.J., Maryon, E.B., Kaplan, J.H., 2016. Dynamic internalization and recycling of a metal ion transporter: Cu homeostasis and CTR1, the human Cu+ uptake system. J. Cell Sci. 129, 1711–1721. https://doi.org/10.1242/jcs.173351

Colvin, R.A., Holmes, W.R., Fontaine, C.P., Maret, W., 2010. Cytosolic zinc buffering and muffling: Their role in intracellular zinc homeostasis. Metallomics 2, 306–317. https://doi.org/10.1039/b926662c

Cousins, R.J., 2010. Gastrointestinal factors influencing zinc absorption and homeostasis. Int. J. Vitam. Nutr. Res. 80, 243–248. https://doi.org/10.1024/0300-9831/a000030

Cui, X., Zhang, Y., Yang, J., Sun, X., Hagan, J.P., Guha, S., Li, M., 2014. ZIP4 confers resistance to zinc deficiency-induced apoptosis in pancreatic cancer. Cell Cycle 13, 1180–1186. https://doi.org/10.4161/cc.28111

Cummings, J.E., Kovacic, J.P., 2009. The ubiquitous role of zinc in health and disease: State-of-the-Art Review. J. Vet. Emerg. Crit. Care 19, 215–240. https://doi.org/10.1111/j.1476-4431.2009.00418.x

D'Amore, C., Borgo, C., Sarno, S., Salvi, M., 2020. Role of CK2 inhibitor CX-4945 in anti-cancer combination therapy – potential clinical relevance. Cell. Oncol. 43, 1003–1016. https://doi.org/10.1007/s13402-020-00566-w

Dereeper, A., Guignon, V., Blanc, G., Audic, S., Buffet, S., Chevenet, F., Dufayard, J.F., Guindon, S., Lefort, V., Lescot, M., Claverie, J.M., Gascuel, O., 2008. Phylogeny.fr: robust phylogenetic analysis for the non-specialist. Nucleic Acids Res. 36, 465–469. https://doi.org/10.1093/nar/gkn180

Deribe, Y.L., Pawson, T., Dikic, I., 2010. Post-translational modifications in signal integration. Nat. Struct. Mol. Biol. 17, 666–672. https://doi.org/10.1038/nsmb.1842

Ding, B., Lou, W., Xu, L., Li, R., Fan, W., 2019. Analysis the prognostic values of solute carrier (SLC) family 39 genes in gastric cancer. Am. J. Transl. Res. 11, 486–498.

Dinkel, H., Chica, C., Via, A., Gould, C.M., Jensen, L.J., Gibson, T.J., Diella, F., 2011. Phospho.ELM: A database of phosphorylation sites-update 2011. Nucleic Acids Res. 39, 261–267. https://doi.org/10.1093/nar/gkq1104

Dufner-Beattie, J., Wang, F., Kuo, Y.M., Gitschier, J., Eide, D., Andrews, G.K., 2003. The acrodermatitis enteropathica gene ZIP4 encodes a tissue-specific, zinc-regulated zinc transporter in mice. J. Biol. Chem. 278, 33474–33481. https://doi.org/10.1074/jbc.M305000200

Ehsani, S., Salehzadeh, A., Huo, H., Reginold, W., Pocanschi, C.L., Ren, H., Wang, H., So, K., Sato, C., Mehrabian, M., Strome, R., Trimble, W.S., Hazrati, L.N., Rogaeva, E., Westaway, D., Carlson, G.A., Schmitt-Ulms, G., 2012. LIV-1 ZIP ectodomain shedding in prion-infected mice resembles cellular response to transition metal starvation. J. Mol. Biol. 422, 556–574. https://doi.org/10.1016/j.jmb.2012.06.003

Endo, M., 2009. Calcium-induced calcium release in skeletal muscle. Physiol. Rev. 89, 1153–1176. https://doi.org/10.1152/physrev.00040.2008

Farquharson, M.J., Al-Ebraheem, A., Geraki, K., Leek, R., Jubb, A., Harris, A.L., 2009. Zinc presence in invasive ductal carcinoma of the breast and its correlation with oestrogen receptor status. Phys. Med. Biol. 54, 4213–4223. https://doi.org/10.1088/0031-9155/54/13/016

Feng, Y., Zeng, J.W., Ma, Q., Zhang, S., Tang, J., Feng, J.F., 2020. Serum copper and zinc levels in breast cancer: A meta-analysis. J. Trace Elem. Med. Biol. 62, 126629. https://doi.org/10.1016/j.jtemb.2020.126629

Fernald, K., Kurokawa, M., 2013. Evading apoptosis in cancer. Trends Cell Biol. 23, 620–633. https://doi.org/10.1016/j.tcb.2013.07.006

Ferrarotto, R., Goonatilake, R., Yoo, S.Y., Tong, P., Giri, U., Peng, S., Minna, J., Girard, L., Wang, Y., Wang, L., Li, L., Diao, L., Peng, D.H., Gibbons, D.L., Glisson, B.S., Heymach, J. V., Wang, J., Byers, L.A., Johnson, F.M., 2016.

Epithelial-mesenchymal transition predicts polo-like kinase 1 inhibitor-mediated apoptosis in non-small cell lung cancer. Clin. Cancer Res. 22, 1674–1686. https://doi.org/10.1158/1078-0432.CCR-14-2890

Filhol, O., Giacosa, S., Wallez, Y., Cochet, C., 2015. Protein kinase CK2 in breast cancer: The CK2β regulatory subunit takes center stage in epithelial plasticity. Cell. Mol. Life Sci. 72, 3305–3322. https://doi.org/10.1007/s00018-015-1929-8

Fiol, C.J., Mahrenholz, A.M., Wang, Y., Roeske, R.W., Roach, P.J., 1987. Formation of protein kinase recognition sites by covalent modification of the substrate. Molecular mechanism for the synergistic action of casein kinase II and glycogen synthase kinase 3. J. Biol. Chem. 262, 14042–14048. https://doi.org/10.1016/s0021-9258(18)47901-x

Fiore, M., Forli, S., Manetti, F., 2017. Targeting Mitogen-activated Protein Kinase-activated Protein Kinase 2 (MAPKAPK2, MK2): Medicinal Chemistry Efforts to Lead Small Molecule Inhibitors to Clinical Trials. Physiol. Behav. 176, 139–148. https://doi.org/10.1053/j.gastro.2016.08.014.CagY

Fong, L.Y., Jing, R., Smalley, K.J., Wang, Z.X., Taccioli, C., Fan, S., Chen, H., Alder, H., Huebner, K., Farber, J.L., Fiehn, O., Croce, C.M., 2018. Human-like hyperplastic prostate with low ZIP1 induced solely by Zn deficiency in rats. Proc. Natl. Acad. Sci. U. S. A. 115, E11091–E11100. https://doi.org/10.1073/pnas.1813956115

Frogne, T., Benjaminsen, R. V., Sonne-Hansen, K., Sorensen, B.S., Nexo, E., Laenkholm, A.V., Rasmussen, L.M., Riese, D.J., De Cremoux, P., Stenvang, J., Lykkesfeldt, A.E., 2009. Activation of ErbB3, EGFR and Erk is essential for growth of human breast cancer cell lines with acquired resistance to fulvestrant. Breast Cancer Res. Treat. 114, 263–275. https://doi.org/10.1007/s10549-008-0011-8

Fu, Z., Wen, D., 2017. The emerging role of polo-like kinase 1 in epithelial-mesenchymal transition and tumor metastasis. Cancers (Basel). 9, 1–15. https://doi.org/10.3390/cancers9100131

Fuhs, S.R., Hunter, T., 2017. pHisphorylation: the emergence of histidine phosphorylation as a reversible regulatory modification. Curr. Opin. Cell Biol. 45, 8–16. https://doi.org/10.1016/j.ceb.2016.12.010

Fukada, T., Kambe, T., 2014. Zinc signals in cellular functions and disorders, Springer 4. https://doi.org/10.1007/978-4-431-55114-0

Fukada, T., Yamasaki, S., Nishida, K., Murakami, M., Hirano, T., 2011. Zinc homeostasis and signaling in health and diseases. J. Biol. Inorg. Chem. 16, 1123–1134. https://doi.org/10.1007/s00775-011-0797-4

Gartmann, L., Wex, T., Grüngreiff, K., Reinhold, D., Kalinski, T., Malfertheiner, P., Schütte, K., 2018. Expression of zinc transporters ZIP4, ZIP14 and ZnT9 in hepatic carcinogenesis—An immunohistochemical study. J. Trace Elem. Med. Biol. 49, 35–42. https://doi.org/10.1016/j.jtemb.2018.04.034

Giusiano, S., Cochet, C., Filhol, O., Duchemin-Pelletier, E., Secq, V., Bonnier, P., Carcopino, X., Boubli, L., Birnbaum, D., Garcia, S., Iovanna, J., Charpin, C., 2011. Protein kinase CK2α subunit over-expression correlates with metastatic

risk in breast carcinomas: Quantitative immunohistochemistry in tissue microarrays. Eur. J. Cancer 47, 792–801. https://doi.org/10.1016/j.ejca.2010.11.028

Gnad, F., Ren, S., Cox, J., Olsen, J. V., Macek, B., Oroshi, M., Mann, M., 2007. PHOSIDA (phosphorylation site database): Management, structural and evolutionary investigation, and prediction of phosphosites. Genome Biol. 8. https://doi.org/10.1186/gb-2007-8-11-r250

Grattan, B.J., Freake, H.C., 2012. Zinc and Cancer: Implications for LIV-1 in Breast Cancer. Nutrients 4, 648–675. https://doi.org/10.3390/nu4070648

Grubman, A., Lidgerwood, G.E., Duncan, C., Bica, L., Tan, J.L., Parker, S.J., Caragounis, A., Meyerowitz, J., Volitakis, I., Moujalled, D., Liddell, J.R., Hickey, J.L., Horne, M., Longmuir, S., Koistinaho, J., Donnelly, P.S., Crouch, P.J., Tammen, I., White, A.R., Kanninen, K.M., 2014. Deregulation of subcellular biometal homeostasis through loss of the metal transporter, Zip7, in a childhood neurodegenerative disorder. Acta Neuropathol. Commun. 2, 1–14. https://doi.org/10.1186/2051-5960-2-25

Guerinot, M. Lou, 2000. <Guerinot - 2000 - The ZIP family of metal transporters(2).pdf> 1465, 190–198.

Gumulec, J., Masarik, M., Adam, V., Eckschlager, T., Provaznik, I., Kizek, R., 2014. Serum and tissue zinc in epithelial malignancies: A meta-analysis. PLoS One 9. https://doi.org/10.1371/journal.pone.0099790

Győrffy, B., 2021. Survival analysis across the entire transcriptome identifies biomarkers with the highest prognostic power in breast cancer. Comput. Struct. Biotechnol. J. 19, 4101–4109. https://doi.org/10.1016/j.csbj.2021.07.014

Haase, H., Beyersmann, D., 2002. Intracellular zinc distribution and transport in C6 rat glioma cells. Biochem. Biophys. Res. Commun. 296, 923–928. https://doi.org/10.1016/S0006-291X(02)02017-X

Haase, H., Rink, L., 2014. Zinc signals and immune function. BioFactors 40, 27–40. https://doi.org/10.1002/biof.1114

Hambidge, K.M., Krebs, N.F., 2007. Zinc Deficiency: A Special Challenge. J. Nutr. 137, 1101–1105. https://doi.org/10.1093/jn/137.4.1101

Hambidge, K.M., Miller, L. V., Westcott, J.E., Krebs, N.F., 2008. Dietary reference intakes for zinc may require adjustment for phytate intake based upon model predictions. J. Nutr. 138, 2363–2366. https://doi.org/10.3945/jn.108.093823

Hambidge, M., 2000. Zinc and Health: Current status and future directions. J. Nutr. 130, 1344S-1349S.

Hanahan, D., 2022. Hallmarks of Cancer: New Dimensions. Cancer Discov. 12, 31–46. https://doi.org/10.1158/2159-8290.CD-21-1059

Hara, T., Takeda, T. aki, Takagishi, T., Fukue, K., Kambe, T., Fukada, T., 2017. Physiological roles of zinc transporters: molecular and genetic importance in zinc homeostasis. J. Physiol. Sci. 67, 283–301. https://doi.org/10.1007/s12576-017-0521-4

Hara, T., Yoshigai, E., Ohashi, T., Fukada, T., 2022. Zinc transporters as potential therapeutic targets: An updated review. J. Pharmacol. Sci. 148, 221–228. https://doi.org/10.1016/j.jphs.2021.11.007

Health, H., Prasad, A.S., 2013. Discovery of Human Zinc De fi ciency : Its Impact on 176–190. https://doi.org/10.3945/an.112.003210.176

Hennigar, S.R., Kelleher, S.L., 2012. Zinc networks: The cell-specific compartmentalization of zinc for specialized functions. Biol. Chem. 393, 565–578. https://doi.org/10.1515/hsz-2012-0128

Hennigar, S.R., McClung, J.P., 2016. Homeostatic regulation of trace mineral transport by ubiquitination of membrane transporters. Nutr. Rev. 74, 59–67. https://doi.org/10.1093/nutrit/nuv060

Henriques, A., Koliaraki, V., Kollias, G., 2018. Mesenchymal MAPKAPK2/HSP27 drives intestinal carcinogenesis. Proc. Natl. Acad. Sci. U. S. A. 115, E5546–E5555. https://doi.org/10.1073/pnas.1805683115

Hogstrand, C., Kille, P., Ackland, M.L., Hiscox, S., Taylor, K.M., 2013. A mechanism for epithelial-mesenchymal transition and anoikis resistance in breast cancer triggered by zinc channel ZIP6 and STAT3 (signal transducer and activator of transcription 3). Biochem. J. 455, 229–237. https://doi.org/10.1042/BJ20130483

Hogstrand, C., Kille, P., Nicholson, R.I., Taylor, K.M., 2009. Zinc transporters and cancer: a potential role for ZIP7 as a hub for tyrosine kinase activation. Trends Mol. Med. 15, 101–111. https://doi.org/10.1016/j.molmed.2009.01.004

Hooper, N.M., 1994. T---- 354, 0–5.

Hornbeck, P. V., Zhang, B., Murray, B., Kornhauser, J.M., Latham, V., Skrzypek, E., 2015. PhosphoSitePlus, 2014: Mutations, PTMs and recalibrations. Nucleic Acids Res. 43, D512–D520. https://doi.org/10.1093/nar/gku1267

Hotz, C., Lowe, N.M., Araya, M., Brown, K.H., 2003. Assessment of the Trace Element Status of Individuals and Populations: The Example of Zinc and Copper. J. Nutr. 133, 1563S-1568S. https://doi.org/10.1093/jn/133.5.1563s

Hsu, P.D., Lander, E.S., Zhang, F., 2014. Development and applications of CRISPR-Cas9 for genome engineering. Cell 157, 1262–1278. https://doi.org/10.1016/j.cell.2014.05.010

Humphrey, S.J., James, D.E., Mann, M., 2015. Protein Phosphorylation: A Major Switch Mechanism for Metabolic Regulation. Trends Endocrinol. Metab. 26, 676–687. https://doi.org/10.1016/j.tem.2015.09.013

Hutcheson, I.R., Knowlden, J.M., Madden, T., Barrow, D., Gee, J.M.W., Wakeling, A.E., Nicholson, R.I., 2003. Oestrogen receptor-mediated modulation of the EGFR / MAPK pathway in tamoxifen-resistant MCF-7 cells 81–93.

Ilouz, R., Kaidanovich, O., Gurwitz, D., Eldar-Finkelman, H., 2002. Inhibition of glycogen synthase kinase-3β by bivalent zinc ions: Insight into the insulin-mimetic action of zinc. Biochem. Biophys. Res. Commun. 295, 102–106. https://doi.org/10.1016/S0006-291X(02)00636-8

Jeong, J., Eide, D.J., 2013. The SLC39 family of zinc transporters. Mol. Aspects

Med. 34, 612–619. https://doi.org/10.1016/j.mam.2012.05.011

Jin, H., Liu, P., Wu, Y., Meng, X., Wu, M., Han, J., Tan, X., 2018. Exosomal zinc transporter ZIP4 promotes cancer growth and is a novel diagnostic biomarker for pancreatic cancer. Cancer Sci. 109, 2946–2956. https://doi.org/10.1111/cas.13737

Johnston, S.R.D., 2010. New strategies in estrogen receptor-positive breast cancer. Clin. Cancer Res. 16, 1979–1987. https://doi.org/10.1158/1078-0432.CCR-09-1823

Jones, S., Farr, G., Nimmanon, T., Ziliotto, S., Gee, J.M.W., Taylor, K.M., 2022. The importance of targeting signalling mechanisms of the SLC39A family of zinc transporters to inhibit endocrine resistant breast cancer. Explor. Target. Anti-tumor Ther. 3, 224–239. https://doi.org/10.37349/etat.2022.00080

Kagara, N., Tanaka, N., Noguchi, S., Hirano, T., 2007a. Zinc and its transporter ZIP10 are involved in invasive behavior of breast cancer cells. Cancer Sci. 98, 692–697. https://doi.org/10.1111/j.1349-7006.2007.00446.x

Kagara, N., Tanaka, N., Noguchi, S., Hirano, T., 2007b. Zinc and its transporter ZIP10 are involved in invasive behavior of breast cancer cells. Cancer Sci. 98, 692–697. https://doi.org/10.1111/j.1349-7006.2007.00446.x

Kambe, T., Andrews, G.K., 2009. Novel Proteolytic Processing of the Ectodomain of the Zinc Transporter ZIP4 (SLC39A4) during Zinc Deficiency Is Inhibited by Acrodermatitis Enteropathica Mutations. Mol. Cell. Biol. 29, 129–139. https://doi.org/10.1128/mcb.00963-08

Kambe, T., Taylor, K.M., Fu, D., 2021. Zinc transporters and their functional integration in mammalian cells. J. Biol. Chem. 296, 100320. https://doi.org/10.1016/J.JBC.2021.100320

Kambe, T., Tsuji, T., Hashimoto, A., Itsumura, N., 2015. The physiological, biochemical, and molecular roles of zinc transporters in zinc homeostasis and metabolism. Physiol. Rev. 95, 749–784. https://doi.org/10.1152/physrev.00035.2014

Kim, M.S., Lee, H.S., Kim, Y.J., Lee, D.Y., Kang, S.G., Jin, W., 2019. MEST induces Twist-1-mediated EMT through STAT3 activation in breast cancers. Cell Death Differ. 26, 2594–2606. https://doi.org/10.1038/s41418-019-0322-9

Kimura, T., Kambe, T., 2016. The functions of metallothionein and ZIP and ZnT transporters: An overview and perspective. Int. J. Mol. Sci. 17, 10–12. https://doi.org/10.3390/ijms17030336

Koen, E.J., Collier, A.B., 2010. The basics of epithelial-mesenchymal transition. Phys. Plasmas To be subm, 1420–1428. https://doi.org/10.1172/JCI39104.1420

Kona, F.R., Buac, D., Dou, Q.P., 2013. Ubiquitin. Brenner's Encycl. Genet. Second Ed. 4, 242–245. https://doi.org/10.1016/B978-0-12-374984-0.01599-0

Krebs, N.F., 2000. Overview of Zinc Absorption and Excretion in the Human Gastrointestinal Tract. J. Nutr. 130, 1374S-1377S. https://doi.org/10.1093/jn/130.5.1374s

Krężel, A., Maret, W., 2021. The Bioinorganic Chemistry of Mammalian Metallothioneins. Chem. Rev. 121, 14594–14648. https://doi.org/10.1021/acs.chemrev.1c00371

Larkin, M.A., Blackshields, G., Brown, N.P., Chenna, R., Mcgettigan, P.A., McWilliam, H., Valentin, F., Wallace, I.M., Wilm, A., Lopez, R., Thompson, J.D., Gibson, T.J., Higgins, D.G., 2007. Clustal W and Clustal X version 2.0. Bioinformatics 23, 2947–2948. https://doi.org/10.1093/bioinformatics/btm404

Lee, S.R., Chanoit, G., McIntosh, R., Zvara, D.A., Xu, Z., 2009. Molecular mechanism underlying Akt activation in zinc-induced cardioprotection. Am. J. Physiol. - Hear. Circ. Physiol. 297, 569–575. https://doi.org/10.1152/ajpheart.00293.2009

Li, B., Huang, C., 2017. Regulation of EMT by STAT3 in gastrointestinal cancer (Review). Int. J. Oncol. 50, 753–767. https://doi.org/10.3892/ijo.2017.3846

Li, Y., Inoki, K., Vacratsis, P., Guan, K.L., 2003. The p38 and MK2 kinase cascade phosphorylates tuberin, the tuberous sclerosis 2 gene product, and enhances its interaction with 14-3-3. J. Biol. Chem. 278, 13663–13671. https://doi.org/10.1074/jbc.M300862200

Lianos, G.D., Alexiou, G.A., Mangano, Alberto, Mangano, Alessandro, Rausei, S., Boni, L., Dionigi, G., Roukos, D.H., 2015. The role of heat shock proteins in cancer. Cancer Lett. 360, 114–118. https://doi.org/10.1016/j.canlet.2015.02.026

Lichten, L.A., Cousins, R.J., 2009. Mammalian Zinc Transporters: Nutritional and Physiologic Regulation. Annu. Rev. Nutr. 29, 153–176. https://doi.org/10.1146/annurev-nutr-033009-083312

Lin, D.C., Zhang, Y., Pan, Q.J., Yang, H., Shi, Z.Z., Xie, Z.H., Wang, B.S., Hao, J.J., Zhang, T.T., Xu, X., Zhan, Q.M., Wang, M.R., 2011. PLK1 is transcriptionally activated by NF-κB during cell detachment and enhances anoikis resistance through inhibiting β-catenin degradation in esophageal squamous cell carcinoma. Clin. Cancer Res. 17, 4285–4295. https://doi.org/10.1158/1078-0432.CCR-10-3236

Lin, Y., Chen, Y., Wang, Y., Yang, J., Zhu, V.F., Liu, Y., Cui, X., Chen, L., Yan, W., Jiang, T., Hergenroeder, G.W., Fletcher, S.A., Levine, J.M., Kim, D.H., Tandon, N., Zhu, J.J., Li, M., 2013. ZIP4 is a novel molecular marker for glioma. Neuro. Oncol. 15, 1008–1016. https://doi.org/10.1093/neuonc/not042

Liu, X., Erikson, R.L., 2003. Polo-like kinase (Plk)1 depletion induces apoptosis in cancer cells. Proc. Natl. Acad. Sci. U. S. A. 100, 5789–5794. https://doi.org/10.1073/pnas.1031523100

Liu, Y., Batchuluun, B., Ho, L., Zhu, D., Prentice, K.J., Bhattacharjee, A., Zhang, M., Pourasgari, F., Hardy, A.B., Taylor, K.M., Gaisano, H., Dai, F.F., Wheeler, M.B., 2015. Characterization of zinc influx transporters (ZIPs) in pancreatic β cells: Roles in regulating cytosolic zinc homeostasis and insulin secretion. J. Biol. Chem. 290, 18757–18769. https://doi.org/10.1074/jbc.M115.640524

Luszczak, S., Kumar, C., Sathyadevan, V.K., Simpson, B.S., Gately, K.A., Whitaker, H.C., Heavey, S., 2020. PIM kinase inhibition: co-targeted therapeutic approaches in prostate cancer. Signal Transduct. Target. Ther. 5.

https://doi.org/10.1038/s41392-020-0109-y

MacDonald, R.S., 2000. Zinc and Health : Current Status and Future Directions The Antioxidant Properties of Zinc 1 , 2. J. Nutr. 130, 1488–1492.

Mansour, M.A., 2018. Ubiquitination: Friend and foe in cancer. Int. J. Biochem. Cell Biol. 101, 80–93. https://doi.org/10.1016/j.biocel.2018.06.001

Mao, X., Kim, B.E., Wang, F., Eide, D.J., Petris, M.J., 2007. A histidine-rich cluster mediates the ubiquitination and degradation of the human zinc transporter, hZIP4, and protects against zinc cytotoxicity. J. Biol. Chem. 282, 6992–7000. https://doi.org/10.1074/jbc.M610552200

Maret, W., 2017. Zinc in cellular regulation: The nature and significance of “zinc signals.” Int. J. Mol. Sci. 18. https://doi.org/10.3390/ijms18112285

Maret, W., 2008. Metallothionein redox biology in the cytoprotective and cytotoxic functions of zinc. Exp. Gerontol. 43, 363–369. https://doi.org/10.1016/j.exger.2007.11.005

Maret, W., 2003. Oxidative Stress Mediated by Trace Elements Cellular Zinc and Redox States Converge in the. J. Nutr 133, 1460–1462.

Maret, W., Sandstead, H.H., 2006. Zinc requirements and the risks and benefits of zinc supplementation. J. Trace Elem. Med. Biol. 20, 3–18. https://doi.org/10.1016/j.jtemb.2006.01.006

Maywald, M., Rink, L., 2022. Zinc in Human Health and Infectious Diseases. Biomolecules 12. https://doi.org/10.3390/biom12121748

McClelland, R.A., Manning, D.L., Gee, J.M.W., Willsher, P., Robertson, J.F.R., Ellis, I.O., Blamey, R.W., Nicholson, R.I., 1998. Oestrogen-regulated genes in breast cancer: Association of pLIV1 with response to endocrine therapy. Br. J. Cancer 77, 1653–1656. https://doi.org/10.1038/bjc.1998.271

Mei, Z., Yan, P., Wang, Y., Liu, S., He, F., 2018. Knockdown of zinc transporter ZIP8 expression inhibits neuroblastoma progression and metastasis in vitro. Mol. Med. Rep. 18, 477–485. https://doi.org/10.3892/mmr.2018.8944

Meyer, R.D., Srinivasan, S., Singh, A.J., Mahoney, J.E., Gharahassanlou, K.R., Rahimi, N., 2011. PEST Motif Serine and Tyrosine Phosphorylation Controls Vascular Endothelial Growth Factor Receptor 2 Stability and Downregulation. Mol. Cell. Biol. 31, 2010–2025. https://doi.org/10.1128/mcb.01006-10

Miyai, T., Hojyo, S., Ikawa, T., Kawamura, M., Irié, T., Ogura, H., Hijikata, A., Bin, B.H., Yasuda, T., Kitamura, H., Nakayama, M., Ohara, O., Yoshida, H., Koseki, H., Mishima, K., Fukada, T., 2014a. Zinc transporter SLC39A10/ZIP10 facilitates antiapoptotic signaling during early B-cell development. Proc. Natl. Acad. Sci. U. S. A. 111, 11780–11785. https://doi.org/10.1073/pnas.1323549111

Miyai, T., Hojyo, S., Ikawa, T., Kawamura, M., Irié, T., Ogura, H., Hijikata, A., Bin, B.H., Yasuda, T., Kitamura, H., Nakayama, M., Ohara, O., Yoshida, H., Koseki, H., Mishima, K., Fukada, T., 2014b. Zinc transporter SLC39A10/ZIP10 facilitates antiapoptotic signaling during early B-cell development. Proc. Natl. Acad. Sci. U. S. A. 111, 11780–11785. https://doi.org/10.1073/pnas.1323549111

Molloy, S.A., Kaplan, J.H., 2009. Copper-dependent recycling of hCTR1, the human high affinity copper transporter. J. Biol. Chem. 284, 29704–29713. https://doi.org/10.1074/jbc.M109.000166

Murakami, M., Hirano, T., 2008. Intracellular zinc homeostasis and zinc signaling. Cancer Sci. 99, 1515–1522. https://doi.org/10.1111/j.1349-7006.2008.00854.x

Murali, B., Ren, Q., Luo, X., Faget, D. V., Wang, C., Johnson, R.M., Gruosso, T., Flanagan, K.C., Fu, Y., Leahy, K., Alspach, E., Su, X., Ross, M.H., Burnette, B., Weilbaecher, K.N., Park, M., Mbalaviele, G., Monahan, J.B., Stewart, S.A., 2018. Inhibition of the stromal p38MAPK/MK2 pathway limits breast cancer metastases and chemotherapy-induced bone loss. Cancer Res. 78, 5618–5630. https://doi.org/10.1158/0008-5472.CAN-18-0234

Nam, H., Wang, C.Y., Zhang, L., Zhang, W., Hojyo, S., Fukada, T., Knutson, M.D., 2013. ZIP14 and DMT1 in the liver, pancreas, and heart are differentially regulated by iron deficiency and overload: Implications for tissue ironuptake in iron-related disorders. Haematologica 98, 1049–1057. https://doi.org/10.3324/haematol.2012.072314

Nicholson, R.I., Johnston, S.R., 2005. Endocrine therapy - Current benefits and limitations. Breast Cancer Res. Treat. 93. https://doi.org/10.1007/s10549-005-9036-4

Nimmanon, T., Ziliotto, S., Morris, S., Flanagan, L., Taylor, K.M., 2017. Phosphorylation of zinc channel ZIP7 drives MAPK, PI3K and mTOR growth and proliferation signalling. Metallomics 9, 471–481. https://doi.org/10.1039/c6mt00286b

Nimmanon, T., Ziliotto, S., Ogle, O., Burt, A., Gee, J.M.W., Andrews, G.K., Kille, P., Hogstrand, C., Maret, W., Taylor, K.M., 2020. The ZIP6/ZIP10 heteromer is essential for the zinc-mediated trigger of mitosis. Cell. Mol. Life Sci. https://doi.org/10.1007/s00018-020-03616-6

Nishito, Y., Kambe, T., 2019. Zinc transporter 1 (ZNT1) expression on the cell surface is elaborately controlled by cellular zinc levels. J. Biol. Chem. 294, 15686–15697. https://doi.org/10.1074/jbc.RA119.010227

Ohashi, K., Nagata, Y., Wada, E., Zammit, P.S., Shiozuka, M., Matsuda, R., 2015. Zinc promotes proliferation and activation of myogenic cells via the PI3K/Akt and ERK signaling cascade. Exp. Cell Res. 333, 228–237. https://doi.org/10.1016/j.yexcr.2015.03.003

Östman, A., Hellberg, C., Böhmer, F.D., 2006. Protein-tyrosine phosphatases and cancer. Nat. Rev. Cancer 6, 307–320. https://doi.org/10.1038/nrc1837

Pagano, M.A., Bain, J., Kazimierczuk, Z., Sarno, S., Ruzzene, M., Di Maira, G., Elliott, M., Orzeszko, A., Cozza, G., Meggio, F., Pinna, L.A., 2008. The selectivity of inhibitors of protein kinase CK2: An update. Biochem. J. 415, 353–365. https://doi.org/10.1042/BJ20080309

Parsons, S.J., Parsons, J.T., 2004. Src family kinases, key regulators of signal transduction. Oncogene 23, 7906–7909. https://doi.org/10.1038/sj.onc.1208160

Pascal, L.E., True, L.D., Campbell, D.S., Deutsch, E.W., Risk, M., Coleman, I.M.,

Eichner, L.J., Nelson, P.S., Liu, A.Y., 2008. Correlation of mRNA and protein levels: Cell type-specific gene expression of cluster designation antigens in the prostate. BMC Genomics 9, 1–13. https://doi.org/10.1186/1471-2164-9-246

Paul, M.R., Pan, T.C., Pant, D.K., Shih, N.N.C., Chen, Y., Harvey, K.L., Solomon, A., Lieberman, D., Morrissette, J.J.D., Soucier-Ernst, D., Goodman, N.G., Stavropoulos, S.W., Maxwell, K.N., Clark, C., Belka, G.K., Feldman, M., DeMichele, A., Chodosh, L.A., 2020. Genomic landscape of metastatic breast cancer identifies preferentially dysregulated pathways and targets. J. Clin. Invest. 140, 4252–4265. https://doi.org/10.1172/JCI129941

Pavan, S., Musiani, D., Torchiaro, E., Migliardi, G., Gai, M., Di Cunto, F., Erriquez, J., Olivero, M., Di Renzo, M.F., 2014. HSP27 is required for invasion and metastasis triggered by hepatocyte growth factor. Int. J. Cancer 134, 1289–1299. https://doi.org/10.1002/ijc.28464

Phinney, B.B., Ray, A.L., Peretti, A.S., Jerman, S.J., Grim, C., Pinchuk, I. V., Beswick, E.J., 2018. MK2 regulates macrophage chemokine activity and recruitment to promote colon tumor growth. Front. Immunol. 9, 1–12. https://doi.org/10.3389/fimmu.2018.01857

Pinter, T.B.J., Stillman, M.J., 2014. The zinc balance: Competitive zinc metalation of carbonic anhydrase and metallothionein 1A. Biochemistry 53, 6276–6285. https://doi.org/10.1021/bi5008673

Prasad, A.S., Halsted, J.A., Nadimi, M., 1961. Syndrome of iron deficiency anemia, hepatosplenomegaly, hypogonadism, dwarfism and geophagia. Am. J. Med. 31, 532–546. https://doi.org/10.1016/0002-9343(61)90137-1

Qin, Y., Miranda, J.G., Stoddard, C.I., Dean, K.M., Galati, D.F., Palmer, A.E., 2013. Direct comparison of a genetically encoded sensor and small molecule indicator: Implications for quantification of cytosolic Zn2+. ACS Chem. Biol. 8, 2366–2371. https://doi.org/10.1021/cb4003859

Ren, C., Yang, T., Qiao, P., Wang, L., Han, X., Lv, S., Sun, Y., Liu, Z., Du, Y., Yu, Z., 2018. PIM2 interacts with tristetraprolin and promotes breast cancer tumorigenesis. Mol. Oncol. 12, 690–704. https://doi.org/10.1002/1878-0261.12192

Renty B Franklin, L.C.C., 2014. Evidence that Human Prostate Cancer is a ZIP1-Deficient Malignancy that could be Effectively Treated with a Zinc Ionophore (Clioquinol) Approach. Chemother. Open Access 04. https://doi.org/10.4172/2167-7700.1000152

Rogers, L.D., Overall, C.M.C., 2013. Proteolytic post-translational modification of proteins: Proteomic tools and methodology. Mol. Cell. Proteomics 12, 3532–3542. https://doi.org/10.1074/mcp.M113.031310

Rogers, S., Wells, R., Rechsteiner, M., 1986. Amino acid sequences common to rapidly degraded proteins: The PEST hypothesis. Science (80-.). 234, 364–368. https://doi.org/10.1126/science.2876518

Roskoski, R., 2019. Targeting ERK1/2 protein-serine/threonine kinases in human cancers. Pharmacol. Res. 142, 151–168. https://doi.org/10.1016/j.phrs.2019.01.039

Ruff, K.M., Pappu, R. V., 2021. AlphaFold and Implications for Intrinsically Disordered Proteins. J. Mol. Biol. 433, 167208. https://doi.org/10.1016/j.jmb.2021.167208

Rusch, P., Hirner, A. V., Schmitz, O., Kimmig, R., Hoffmann, O., Diel, M., 2021. Zinc distribution within breast cancer tissue of different intrinsic subtypes. Arch. Gynecol. Obstet. 303, 195–205. https://doi.org/10.1007/s00404-020-05789-8

Saravanan, R., Balasubramanian, V., Swaroop Balamurugan, S.S., Ezhil, I., Afnaan, Z., John, J., Sundaram, S., Gouthaman, S., Pakala, S.B., Rayala, S.K., Venkatraman, G., 2022. Zinc transporter LIV1: A promising cell surface target for triple negative breast cancer. J. Cell. Physiol. https://doi.org/10.1002/jcp.30880

Sarno, S., Papinutto, E., Franchin, C., Bain, J., Elliott, M., Meggio, F., Kazimierczuk, Z., Orzeszko, A., Zanotti, G., Battistutta, R., A. Pinna, L., 2011. ATP Site-Directed Inhibitors of Protein Kinase CK2: An Update. Curr. Top. Med. Chem. 11, 1340–1351. https://doi.org/10.2174/156802611795589638

Schmitt-Ulms, G., Ehsani, S., Watts, J.C., Westaway, D., Wille, H., 2009. Evolutionary descent of prion genes from the ZIP family of metal Ion transporters. PLoS One 4. https://doi.org/10.1371/journal.pone.0007208

Sheng, N., Yan, L., You, W., Tan, G., Gong, J., Chen, H., Yang, Y., Hu, L., Wang, Z., 2017. Knockdown of SLC39A7 inhibits cell growth and induces apoptosis in human colorectal cancer cells. Acta Biochim. Biophys. Sin. (Shanghai). 49, 926–934. https://doi.org/10.1093/abbs/gmx094

Shimura, T., 2011. Acquired Radioresistance of Cancer and the AKT/GSK3β/cyclin D1 Overexpression Cycle. J. Radiat. Res. 52, 539–544. https://doi.org/10.1269/jrr.11098

Siddiqui-Jain, A., Drygin, D., Streiner, N., Chua, P., Pierre, F., O'Brien, S.E., Bliesath, J., Omori, M., Huser, N., Ho, C., Proffitt, C., Schwaebe, M.K., Ryckman, D.M., Rice, W.G., Anderes, K., 2010. CX-4945, an orally bioavailable selective inhibitor of protein kinase CK2, inhibits prosurvival and angiogenic signaling and exhibits antitumor efficacy. Cancer Res. 70, 10288–10298. https://doi.org/10.1158/0008-5472.CAN-10-1893

Sievers, F., Higgins, D.G., 2018. Clustal Omega for making accurate alignments of many protein sequences. Protein Sci. 27, 135–145. https://doi.org/10.1002/pro.3290

Silva, V.C., Cassimeris, L., 2013. Stathmin and microtubules regulate mitotic entry in HeLa cells by controlling activation of both Aurora kinase A and Plk1. Mol. Biol. Cell 24, 3819–3831. https://doi.org/10.1091/mbc.E13-02-0108

Smith, A.E., Ferraro, E., Safonov, A., Morales, C.B., Lahuerta, E.J.A., Li, Q., Kulick, A., Ross, D., Solit, D.B., de Stanchina, E., Reis-Filho, J., Rosen, N., Arribas, J., Razavi, P., Chandarlapaty, S., 2021. HER2 + breast cancers evade anti-HER2 therapy via a switch in driver pathway. Nat. Commun. 12, 1–10. https://doi.org/10.1038/s41467-021-27093-y

Song, L., Rape, M., 2008. Reverse the curse-the role of deubiquitination in cell cycle control. Curr. Opin. Cell Biol. 20, 156–163.

https://doi.org/10.1016/j.ceb.2008.01.012

Song, Y., Leonard, S.W., Traber, M.G., Ho, E., 2009. Zinc deficiency affects DNA damage, oxidative stress, antioxidant defenses, and DNA repair in rats. J. Nutr. 139, 1626–1631. https://doi.org/10.3945/jn.109.106369

Soni, S., Anand, P., Padwad, Y.S., 2019a. MAPKAPK2 : the master regulator of RNA- binding proteins modulates transcript stability and tumor progression 1, 1–18.

Soni, S., Saroch, M.K., Chander, B., Tirpude, N.V., Padwad, Y.S., 2019b. MAPKAPK2 plays a crucial role in the progression of head and neck squamous cell carcinoma by regulating transcript stability. J. Exp. Clin. Cancer Res. 38, 1–13. https://doi.org/10.1186/s13046-019-1167-2

St-Denis, N., Gabriel, M., Turowec, J.P., Gloor, G.B., Li, S.S.C., Gingras, A.C., Litchfield, D.W., 2015. Systematic investigation of hierarchical phosphorylation by protein kinase CK2. J. Proteomics 118, 49–62. https://doi.org/10.1016/j.jprot.2014.10.020

Sun, C.K., Man, K., Ng, K.T., Ho, J.W., Lim, Z.X., Cheng, Q., Lo, C.M., Poon, R.T., Fan, S.T., 2008. Proline-rich tyrosine kinase 2 (Pyk2) promotes proliferation and invasiveness of hepatocellular carcinoma cells through c-Src/ERK activation. Carcinogenesis 29, 2096–2105. https://doi.org/10.1093/carcin/bgn203

Sun, T., Liu, Z., Yang, Q., 2020. The role of ubiquitination and deubiquitination in cancer metabolism. Mol. Cancer 19, 1–19. https://doi.org/10.1186/s12943-020-01262-x

Takagishi, T., Hara, T., Fukada, T., 2017. Recent Advances in the Role of SLC39A/ZIP Zinc Transporters In Vivo. Int. J. Mol. Sci. 18, 1–21. https://doi.org/10.3390/ijms18122708

Takai, N., Hamanaka, R., Yoshimatsu, J., Miyakawa, I., 2005. Polo-like kinases (Plks) and cancer. Oncogene 24, 287–291. https://doi.org/10.1038/sj.onc.1208272

Takai, N., Miyazaki, T., Fujisawa, K., Nasu, K., Hamanaka, R., Miyakawa, I., 2001. Expression of polo-like kinase in ovarian cancer is associated with histological grade and clinical stage. Cancer Lett. 164, 41–49. https://doi.org/10.1016/S0304-3835(00)00703-5

Takatani-Nakase, T., 2018. Zinc transporters and the progression of breast cancers. Biol. Pharm. Bull. 41, 1517–1522. https://doi.org/10.1248/bpb.b18-00086

Takatani-Nakase, T., Matsui, C., Sakitani, M., Nakase, I., 2022. ZIP6-centered zinc regulatory and malignant characteristics of breast cancer cells. Met. Res.

Takatani-Nakase, T., Matsui, C., Takahashi, K., 2016. Role of the LIV-1 subfamily of zinc transporters in the development and progression of breast cancers: A mini review. Biomed. Res. Clin. Pract. 1, 71–75. https://doi.org/10.15761/brcp.1000114

Tanaka, T., Iino, M., Goto, K., 2018. Sec6 enhances cell migration and suppresses apoptosis by elevating the phosphorylation of p38 MAPK, MK2, and HSP27. Cell. Signal. 49, 1–16. https://doi.org/10.1016/j.cellsig.2018.04.009

Tang, Z., Kang, B., Li, C., Chen, T., Zhang, Z., 2019. GEPIA2: an enhanced web server for large-scale expression profiling and interactive analysis. Nucleic Acids Res. 47, W556–W560. https://doi.org/10.1093/nar/gkz430

Taylor, K.M., 2023. The LIV-1 Subfamily of Zinc Transporters: From Origins to Present Day Discoveries. Int. J. Mol. Sci. 24. https://doi.org/10.3390/ijms24021255

Taylor, K.M., Hiscox, S., Nicholson, R.I., 2004a. Zinc transporter LIV-1: A link between cellular development and cancer progression. Trends Endocrinol. Metab. 15, 461–463. https://doi.org/10.1016/j.tem.2004.10.003

Taylor, K.M., Hiscox, S., Nicholson, R.I., Hogstrand, C., Kille, P., 2012a. Cell biology: Protein kinase CK2 triggers cytosolic zinc signaling pathways by phosphorylation of zinc channel ZIP7. Sci. Signal. 5, 1–10. https://doi.org/10.1126/scisignal.2002585

Taylor, K.M., Kille, P., Hogstrand, C., 2012b. Protein kinase CK2 opens the gate for zinc signaling. Cell Cycle 11, 1863–1864. https://doi.org/10.4161/cc.20414

Taylor, K.M., Morgan, H.E., Johnson, A., Hadley, L.J., Nicholson, R.I., 2003. Structure-function analysis of LIV-1, the breast cancer-associated protein that belongs to a new subfamily of zinc transporters. Biochem. J. 375, 51–59. https://doi.org/10.1042/BJ20030478

Taylor, K.M., Morgan, H.E., Johnson, A., Nicholson, R.I., 2004b. Structure-function analysis of HKE4, a member of the new LIV-1 subfamily of zinc transporters. Biochem. J. 377, 131–139. https://doi.org/10.1042/BJ20031183

Taylor, K.M., Morgan, H.E., Smart, K., Pumford, Sara, 2007. The Emerging Role of the LIV-1 Subfamily of Zinc Transporters in Breast Cancer. Mol. Med. 8, 125–133. https://doi.org/10.2119/2007

Taylor, K.M., Muraina, I.A., Brethour, D., Nimmanon, T., Ziliotto, S., Kille, P., Hogstrand, C., 2016. Zinc transporter ZIP10 forms a heteromer with ZIP6 which regulates embryonic development and cell migration. Biochem. J. 473, 2531–2544. https://doi.org/10.1042/BCJ20160388

Taylor, K.M., Vichova, P., Jordan, N., Hiscox, S., Hendley, R., Nicholson, R.I., 2008. ZIP7-mediated intracellular zinc transport contributes to aberrant growth factor signaling in antihormone-resistant breast cancer cells. Endocrinology 149, 4912–4920. https://doi.org/10.1210/en.2008-0351

Taylor, R.P., Benjamin, I.J., 2005. Small heat shock proteins: A new classification scheme in mammals. J. Mol. Cell. Cardiol. 38, 433–444. https://doi.org/10.1016/j.yjmcc.2004.12.014

Thompson, L.L., Rutherford, K.A., Lepage, C.C., McManus, K.J., 2021. The SCF complex is essential to maintain genome and chromosome stability. Int. J. Mol. Sci. 22. https://doi.org/10.3390/ijms22168544

Tiwari, N., Gheldof, A., Tatari, M., Christofori, G., 2012. EMT as the ultimate survival mechanism of cancer cells. Semin. Cancer Biol. 22, 194–207. https://doi.org/10.1016/j.semcancer.2012.02.013

Tozlu, S., Girault, I., Vacher, S., Vendrell, J., Andrieu, C., Spyratos, F., Cohen, P.,

Lidereau, R., Bieche, I., 2006. Identification of novel genes that co-cluster with estrogen receptor alpha in breast tumor biopsy specimens, using a large-scale real-time reverse transcription-PCR approach. Endocr. Relat. Cancer 13, 1109–1120. https://doi.org/10.1677/erc.1.01120

Trembley, J.H., Chen, Z., Unger, G., Slaton, J., Kren, B.T., Van Waes, C., Ahmed, K., 2010. Emergence of protein kinase CK2 as a key target in cancer therapy. BioFactors 36, 187–195. https://doi.org/10.1002/biof.96

Trembley, J.H., Wang, G., Unger, G., Slaton, J., Ahmed, K., 2009. CK2: A key player in cancer biology. Cell. Mol. Life Sci. 66, 1858–1867. https://doi.org/10.1007/s00018-009-9154-y

Tuncay, E., Bitirim, V.C., Durak, A., Carrat, G.R.J., Taylor, K.M., Rutter, G.A., Turan, B., 2017. Hyperglycemia-induced changes in ZIP7 and ZnT7 expression cause Zn2+ release from the sarco(endo)plasmic reticulum and mediate ER stress in the heart. Diabetes 66, 1346–1358. https://doi.org/10.2337/db16-1099

Unger, G., Davis, A., Slaton, J., Ahmed, K., 2005. Protein Kinase CK2 as Regulator of Cell Survival: Implications for Cancer Therapy. Curr. Cancer Drug Targets 4, 77–84. https://doi.org/10.2174/1568009043481687

Unno, J., Masamune, A., Hamada, S., Shimosegawa, T., 2014. The zinc transporter LIV-1 is a novel regulator of stemness in pancreatic cancer cells. Scand. J. Gastroenterol. 49, 215–221. https://doi.org/10.3109/00365521.2013.865075

Verma, N., Keinan, O., Selitrennik, M., Karn, T., Filipits, M., Lev, S., 2015. PYK2 sustains endosomal-derived receptor signalling and enhances epithelial-to-mesenchymal transition. Nat. Commun. 6. https://doi.org/10.1038/ncomms7064

Vincent, B., Sunyach, C., Orzechowski, H.D., St George-Hyslop, P., Checler, F., 2009. p53-Dependent transcriptional control of cellular prion by presenilins. J. Neurosci. 29, 6752–6760. https://doi.org/10.1523/JNEUROSCI.0789-09.2009

Vivanco, I., Sawyers, C.L., 2002. The phosphatidylinositol 3-kinase-AKT pathway in humancancer. Nat. Rev. Cancer 2, 489–501. https://doi.org/10.1038/nrc839

Wang, Juan, Wang, G., Cheng, D., Huang, S., Chang, A., Tan, X., Wang, Q., Zhao, S., Wu, D., Liu, A.T., Yang, S., Xiang, R., Sun, P., 2020. Her2 promotes early dissemination of breast cancer by suppressing the p38-MK2-Hsp27 pathway that is targetable by Wip1 inhibition. Oncogene 39, 6313–6326. https://doi.org/10.1038/s41388-020-01437-2

Wang, Jie, Zhao, H., Xu, Z., Cheng, X., 2020. Zinc dysregulation in cancers and its potential as a therapeutic target. Cancer Biol. Med. 17, 612–625. https://doi.org/10.20892/j.issn.2095-3941.2020.0106

Wei, Y., Dong, J., Li, F., Wei, Z., Tian, Y., 2017. Original article : KNOCKDOWN OF SLC39A7 SUPPRESSES CELL PROLIFERATION , 1165–1176.

Weichert, W., Schmidt, M., Gekeler, V., Denkert, C., Stephan, C., Jung, K., Loening, S., Dietel, M., Kristiansen, G., 2004. Polo-like kinase 1 is overexpressed in prostate cancer and linked to higher tumor grades. Prostate 60, 240–245. https://doi.org/10.1002/pros.20050

Winkles, J.A., Alberts, G.F., 2005. Differential regulation of polo-like kinase 1, 2, 3,

and 4 gene expression in mammalian cells and tissues. Oncogene 24, 260–266. https://doi.org/10.1038/sj.onc.1208219

Wiza, C., Nascimento, E.B.M., Ouwens, D.M., 2012. Role of PRAS40 in Akt and mTOR signaling in health and disease. Am. J. Physiol. - Endocrinol. Metab. 302, 1453–1460. https://doi.org/10.1152/ajpendo.00660.2011

Wolff, G., Hildenbrand, R., Schwar, C., Grobholz, R., Kaufmann, M., Stutte, H.J., Strebhardt, K., Bleyl, U., 2000. Polo-like kinase: A novel marker of proliferation: Correlation with estrogen-receptor expression in human breast cancer. Pathol. Res. Pract. 196, 753–759. https://doi.org/10.1016/S0344-0338(00)80107-7

Woodruff, G., Bouwkamp, C.G., De Vrij, F.M., Lovenberg, T., Bonaventure, P., Kushner, S.A., Harrington, A.W., 2018. The zinc transporter SLC39A7 (ZIP7) is essential for regulation of cytosolic zinc levels s. Mol. Pharmacol. 94, 1092–1100. https://doi.org/10.1124/mol.118.112557

Wu, J., Ivanov, A.I., Fisher, P.B., Fu, Z., 2016. Polo-like kinase 1 induces epithelial-to-mesenchymal transition and promotes epithelial cell motility by activating CRAF/ERK signaling. Elife 5, 1–25. https://doi.org/10.7554/eLife.10734

Wu, L., Chaffee, K.G., Parker, A.S., Sicotte, H., Petersen, G.M., 2015. Zinc transporter genes and urological cancers: integrated analysis suggests a role for ZIP11 in bladder cancer. Tumor Biol. 36, 7431–7437. https://doi.org/10.1007/s13277-015-3459-2

Wu, X., Wu, H., Liu, L., Qiang, G., Zhu, J., 2020. Serum zinc level and tissue ZIP4 expression are related to the prognosis of patients with stages I-III colon cancer. Transl. Cancer Res. 9, 5585–5594. https://doi.org/10.21037/tcr-20-2571

Wu, Y., Mark Evers, B., Zhou, B.P., 2009. Small C-terminal domain phosphatase enhances snail activity through dephosphorylation. J. Biol. Chem. 284, 640–648. https://doi.org/10.1074/jbc.M806916200

Xu, C., Kim, N.G., Gumbiner, B.M., 2009. Regulation of protein stability by GSK3 mediated phosphorylation. Cell Cycle 8, 4032–4039. https://doi.org/10.4161/cc.8.24.10111

Xu, H., Zhou, J., Lin, S., Deng, W., Zhang, Y., Xue, Y., 2017. PLMD: An updated data resource of protein lysine modifications. J. Genet. Genomics 44, 243–250. https://doi.org/10.1016/j.jgg.2017.03.007

Yamasaki, S., Sakata-Sogawa, K., Hasegawa, A., Suzuki, T., Kabu, K., Sato, E., Kurosaki, T., Yamashita, S., Tokunaga, M., Nishida, K., Hirano, T., 2007. Zinc is a novel intracellular second messenger. J. Cell Biol. 177, 637–645. https://doi.org/10.1083/jcb.200702081

Yamashita, S., Miyagi, C., Fukada, T., Kagara, H., Che, Y.S., Hirano, T., 2004. Zinc transporter LIV1 controls epithelial-mesenchymal transition in zebrafish gastrula organizer. Nature 429, 298–302. https://doi.org/10.1038/nature02545

Yang, J., Zhang, Y., Cui, X., Yao, W., Yu, X., Cen, P., E. Hodges, S., E. Fisher, W., C. Brunicardi, F., Chen, C., Yao, Q., Li, M., 2013. Gene Profile Identifies Zinc Transporters Differentially Expressed in Normal Human Organs and Human Pancreatic Cancer. Curr. Mol. Med. 13, 401–409.

https://doi.org/10.2174/156652413805076786

Yang, T., Ren, C., Qiao, P., Han, X., Wang, L., Lv, S., Sun, Y., Liu, Z., Du, Y., Yu, Z., 2018. PIM2-mediated phosphorylation of hexokinase 2 is critical for tumor growth and paclitaxel resistance in breast cancer. Oncogene 37, 5997–6009. https://doi.org/10.1038/s41388-018-0386-x

Yao, T., Cohen, R.E., 2002. A cryptic protease couples deubiquitination and degradation by the proteasome. Nature 419, 403–407. https://doi.org/10.1038/nature01071

Yde, C.W., Frogne, T., Lykkesfeldt, A.E., Fichtner, I., Issinger, O.G., Stenvang, J., 2007. Induction of cell death in antiestrogen resistant human breast cancer cells by the protein kinase CK2 inhibitor DMAT. Cancer Lett. 256, 229–237. https://doi.org/10.1016/j.canlet.2007.06.010

Yu, Zhen, Yu, Ze, Chen, Z.B., Yang, L., Ma, M.J., Lu, S.N., Wang, C.S., Teng, C.B., Nie, Y.Z., 2019. Zinc chelator TPEN induces pancreatic cancer cell death through causing oxidative stress and inhibiting cell autophagy. J. Cell. Physiol. 234, 20648–20661. https://doi.org/10.1002/jcp.28670

Yuan, N., Wang, Y.H., Li, K.J., Zhao, Y., Hu, X., Mao, L., Zhao, W.J., Lian, H.Z., Zheng, W.J., 2012. Effects of exogenous zinc on the cellular zinc distribution and cell cycle of A549 cells. Biosci. Biotechnol. Biochem. 76, 2014–2020. https://doi.org/10.1271/bbb.120216

Zaman, M.S., Johnson, A.J., Petersingham, G., Muench, G.W., Dong, Q., Wu, M.J., 2019. Protein kinase CK2 is involved in zinc homeostasis in breast and prostate cancer cells. BioMetals 0123456789. https://doi.org/10.1007/s10534-019-00218-z

Zhang, H., Kong, Q., Wang, J., Jiang, Y., Hua, H., 2020. Complex roles of cAMP–PKA–CREB signaling in cancer. Exp. Hematol. Oncol. 9, 1–13. https://doi.org/10.1186/s40164-020-00191-1

Zhang, T., Kuliyev, E., Sui, D., Hu, J., 2019. The histidine-rich loop in the extracellular domain of ZIP4 binds zinc and plays a role in zinc transport. Biochem. J. 476, 1791–1803. https://doi.org/10.1042/BCJ20190108

Zhang, Y., Bai, J., Si, W., Yuan, S., Li, Y., Chen, X., 2020. SLC39A7, regulated by miR-139-5p, induces cell proliferation, migration and inhibits apoptosis in gastric cancer via Akt/mTOR signaling pathway. Biosci. Rep. 0, 1–9. https://doi.org/10.1042/bsr20200041

Zhang, Y., Du, X., Wang, C., Lin, D., Ruan, X., Feng, Y., Huo, Y., Peng, H., Cui, J., Zhang, T., Wang, Y., Zhang, H., Zhan, Q., Wang, M., 2012. Reciprocal activation between PLK1 and Stat3 contributes to survival and proliferation of esophageal cancer cells. Gastroenterology 142, 521-530.e3. https://doi.org/10.1053/j.gastro.2011.11.023

Zhou, H., Zhu, Y., Qi, H., Liang, L., Wu, H., Yuan, J., Hu, Q., 2021. Evaluation of the prognostic values of solute carrier (SLC) family 39 genes for patients with lung adenocarcinoma. Aging (Albany. NY). 13, 5312–5331. https://doi.org/10.18632/aging.202452

Zhu, Z.Y., Karlin, S., 1996. Clusters of charged residues in protein three-dimensional structures. Proc. Natl. Acad. Sci. U. S. A. 93, 8350–8355. https://doi.org/10.1073/pnas.93.16.8350

Ziliotto, S., Gee, J.M.W., Ellis, I.O., Green, A.R., Finlay, P., Gobbato, A., Taylor, K.M., 2019. Activated zinc transporter ZIP7 as an indicator of anti-hormone resistance in breast cancer. Metallomics 11, 1579–1592. https://doi.org/10.1039/c9mt00136k